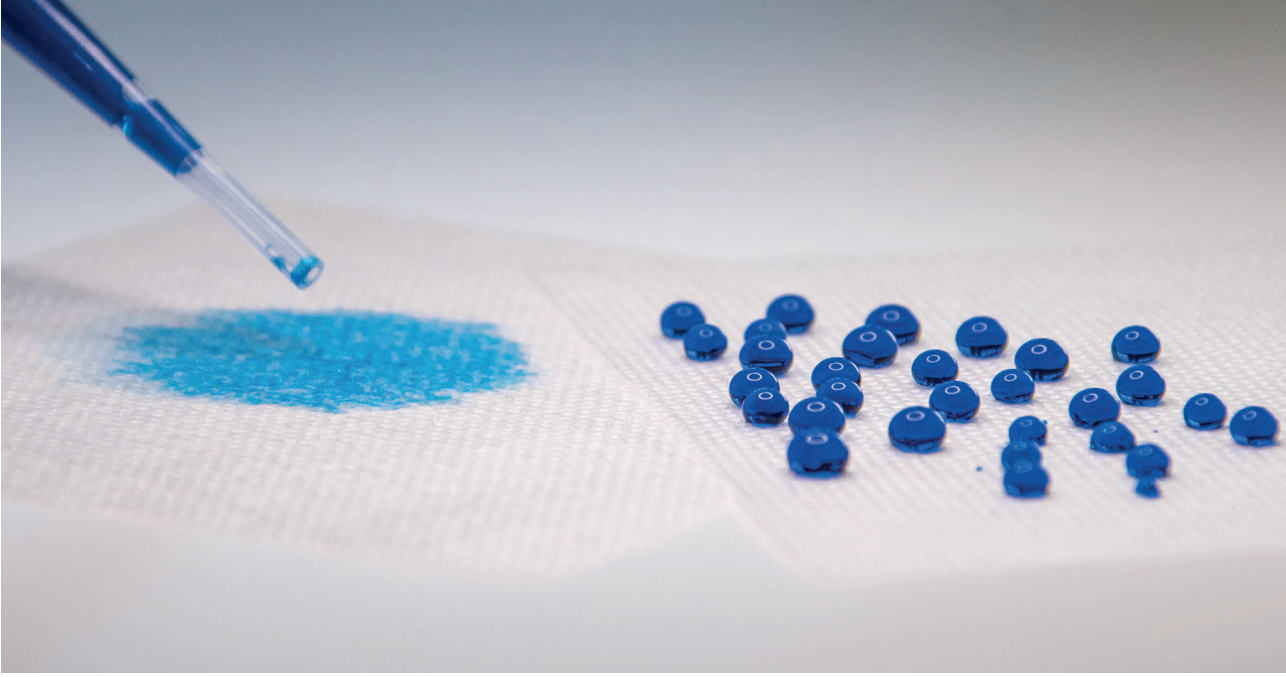

FAU Forschungen, Reihe B, Medizin, Naturwissenschaft, Technik 34

Franz J. Lanyi

Modification of Interfacial Properties of Polypropylene Fibers using Hydrophilic Melt Additives – Interactions with Crystallization

FAU UNIVERSITY PRESS

Franz J. Lanyi

Modification of Interfacial Properties of Polypropylene Fibers using Hydrophilic Melt Additives - Interactions with Crystallization

FAU Forschungen, Reihe B
Medizin, Naturwissenschaft, Technik
Band 34

Herausgeber der Reihe:
Wissenschaftlicher Beirat der FAU University Press

Franz J. Lanyi

Modification of Interfacial Properties of Polypropylene Fibers using Hydrophilic Melt Additives – Interactions with Crystallization

Erlangen
FAU University Press
2020

Bibliografische Information der Deutschen Nationalbibliothek:
Die Deutsche Nationalbibliothek verzeichnet diese Publikation in der Deutschen Nationalbibliografie; detaillierte bibliografische Daten sind im Internet über http://dnb.d-nb.de abrufbar.

Bitte zitieren als
Lanyi, Franz J. 2020. Modification of Interfacial Properties of Polypropylene Fibers using Hydrophilic Melt Additives - Interactions with Crystallization. FAU Forschungen, Reihe B, Medizin, Naturwissenschaft, Technik Band 34. Erlangen: FAU University Press.
DOI: 10.25593/978-3-96147-361-8.

Der vollständige Inhalt des Buchs ist als PDF über den OPUS-Server der Friedrich-Alexander-Universität Erlangen-Nürnberg abrufbar:
https://opus4.kobv.de/opus4-fau/home

Coverfoto: Fabian Theisz

Verlag und Auslieferung:
FAU University Press, Universitätsstraße 4, 91054 Erlangen

Druck: docupoint GmbH

ISBN: 978-3-96147- 360-1 (Druckausgabe)
eISBN: 978-3-96147- 361-8 (Online-Ausgabe)
ISSN: 2198-8102
DOI: 10.25593/978-3-96147-361-8

Modification of Interfacial Properties of Polypropylene Fibers using Hydrophilic Melt Additives - Interactions with Crystallization

Der Technischen Fakultät
der Friedrich-Alexander-Universität
Erlangen-Nürnberg

zur
Erlangung des Doktorgrades Dr.-Ing.

vorgelegt von

Franz J. Lanyi, M.Sc.

aus Erlangen

Als Dissertation genehmigt
von der Technischen Fakultät
der Friedrich-Alexander-Universität Erlangen-Nürnberg

Tag der mündlichen Prüfung:	30.07.2020
Vorsitzender des Promotionsorgans:	Prof. Dr.-Ing. habil. Andreas P. Fröba
Gutachter:	Prof. Dr. rer. nat. habil. Dirk W. Schubert
	Prof. Dr. Rainer Adelung

Gewidmet meiner Mutter Marita.

Abstract

Melt additives are low molar mass molecules which are added to polymers during processing. If the molecules migrate to the surface, the properties of the polymer surface can be tailored. Therefore, melt additives offer an easy to implement method to hydrophilize hydrophobic polymers, such as polypropylene. For reproducible product quality, it is necessary to control and understand the complex migration process, influenced by diffusion, surface segregation, miscibility or polymer morphology.

Various commercially available surfactants (ethoxylated alcohols, PEO-PPO-block copolymers, sorbitan esters) are investigated to determine which requirements have to be met by molecules to be utilized as hydrophilic melt additives. In order to correlate polymer morphology and additive migration, a method was developed which determines the degree of crystallinity and the additive concentration at the surface and in the bulk of samples using Fourier-transform infrared spectroscopy (FTIR).

It is demonstrated, that the hydrophilization of the surface is a function of the additive surface concentration and the ability of the additive to enable wetting. Ethoxylated alcohols with a low molar mass, a long hydrophobic and a short hydrophilic part of the surfactant impart the highest hydrophilicity. Novel models for structure formation during injection molding, film casting and fiber spinning are developed using a combination of X-ray diffraction (XRD) and FTIR. The migration of additives with varying molecular architectures was determined over a period of 1000 hours and described using a semiempirical migration equation. Coefficients characterizing the kinetics and thermodynamics of migration are described as a function of the most relevant process parameters and the associated change in polymer morphology. The experiments revealed that migration depends on the packing density of polymer chains given by molecular orientation and (post-)crystallization of the polymer. Besides polymer morphology, the miscibility and molecular dimensions of the additive as well as the storage conditions after production (time and temperature) affect migration.

Within the scope of the work, permanent and durable melt additives for polypropylene as well as methods for the selective activation of hydrophilicity were found.

Acknowledgments

Like many other extensive projects, this work would not have been possible without the help of many people. It was a pleasure for me to work together with these people and to be accompanied on the way to a doctorate.

First of all I would like to thank Prof. Dr. rer. nat. habil. Dirk W. Schubert for the excellent supervision of this work as well as the possibility and the confidence placed in me to develop freely on a scientific level. Many thanks for the opportunity to present my research results at international and national conferences. Furthermore, I thank him for approaches to solving problems that at first seemed unsolvable - because if it was easy, someone would have done it already.

My thanks also go to Prof. Dr. Rainer Adelung from the University of Kiel for preparing the second review of this work.

In particular, I would like to thank Dr. Torsten Lindner as well as Dr. Jan Claussen, Dr. Gueltekin Erdem, Dr. Nathan Whitely, Dr. Olaf Isele, Dr. Holger Beruda, Barbara Hede and Brian Udengaard for their excellent cooperation in the project and their highly competent support.

I would like to thank Dr. Joachim Kaschta for scientific discussions and countless helpful ideas.

I thank my colleagues and friends Jonas Daenicke, Tim Höhnemann, Karsten Leucker and Andreas Ziegmann for numerous ideas, both ingenious and uningenious discussions as well as their patience with me. It was a privilege to share an office with them for five years.

I would like to thank the previous and next generation of doctoral students for scientific discussions and great teamwork during my time at the institute. It was a pleasure to work with and learn from them.

A very special thanks goes to my assistant scientists, bachelor and master students: Stefan Schrüfer, Tobias Bayer, Nicolai Wenzke, Annika Kleebauer, Linda Rockmann, Manuel Sopper, Julian Kattinger and Khushdeep Sharma. Without the endless hours of experimentation and their motivated work, this thesis would have been far from comprehensive.

I thank all technical staff of the institute of polymer materials. Special thanks are due to Harald Rost, Marko Heyder and Alfred Frey for their competent help, for their creative suggestions and for the construction and maintenance of numerous devices and experimental setups. I thank Jenny Reiser for her

support in sample preparation and FTIR measurements and Inge Herzer for carrying out the DSC and GPC measurements. Thanks to Brigitte Saigge and Alexandra Müller for organizing my administrative chaos and thanks to Susanne Michler, who was very helpful in organizing the materials.

Furthermore I would like to thank the FAU mechanics and electronics workshop, especially Stefan Ossege, Michael Miller and Erich Meyer for the implementation of simple, amateurish sketches and rough ideas to functioning components of the spinning line.

I thank Tobias Rejek for his support with the spin coating experiments.

I express my gratitude to Dr. Steffen Neumeier and Lisa Freund as well as Dr. Jochen Schmidt and Maximilian Dechet for their support and competent help with all XRD measurements.

I want to acknowledge Dr. Yvonne Reimann and Dr. Marten Gernot von Croda for their support in obtaining the additives.

I thank my mother Marita from the bottom of my heart for the opportunity of my education and her devoted support, without which I would not be where I am now.

Last but not least, I thank my beloved girlfriend Nora for her dedicated encouragement during every minute of my doctorate.

Table of Contents

1 Introduction

Polypropylene (PP) is the second most commonly manufactured polymer after polyethylene (PE) and is mainly used for the production of flexible packaging materials, such as films or bags, as well as for fibers and nonwovens [1]. In 2016, 56 million tons of polypropylene were produced worldwide [2] of which about 10 million tons were processed in Europe [1]. Due to the predominant application of polypropylene in the manufacture of medical and hygiene products, it is the most commonly used plastic for fiber products with a market share of around 50 % [3, 4]. This is primarily due to its outstanding chemical resistance, good mechanical properties and low density at low cost. The inert and hydrophobic surface of polypropylene is advantageous for many purposes. However, for applications in the hygiene sector (e.g. for wipes or diapers) or for filter and absorption materials, a hydrophilic surface is often desired.

Hydrophilization of the surface is achieved in most cases by surface treatment with a spin finish [5–7], but it can also be obtained by corona treatments [8, 9] or the grafting of functional groups to the matrix polymer [10, 11]. These procedures all suffer from certain disadvantages. When coating the surface, the surface properties are changed by spraying on a wetting agent. The additional processing step has to be integrated into the production line and requires supplementary energy. Due to the surface tension of the spin finish, the coatings tend to agglomerate to large droplets, resulting in a non-uniform distribution on the surface. The fixation of the spin finish works mainly by adhesion forces. It is therefore assumed that the coating can be easily removed by abrasion, in contact with other liquids or during further processing of the fibers (e.g. in the thermal bonding process). The use of melt additives allows to avoid these disadvantages.

Melt additives are molecules with functional groups useful for the application, which are added to the polymer in small amounts (1-2 %) before or during the process and dispersed in the matrix polymer. The additive may accumulate on the surface as a function of time and thus modify its properties. This enrichment process is called migration and can be caused by spontaneous segregation towards the surface, by diffusion or by shear phenomena.

It is therefore apparent that there is a technological demand for the development of novel melt additives for the hydrophilization of polypropylene. To date, surprisingly little literature has been published on this topic. Datla's

doctoral thesis [12] on hydrophilic melt additives was followed by two further publications [13, 14] which cover the use of surfactants with different molecular structures and functional groups (e.g. ethoxylated alcohols and nonylphenols) for the hydrophilization of polypropylene. It has been shown that it is possible to make polypropylene surfaces wettable with the aid of melt additives. In Datla's work it is assumed that the greatest influence on the hydrophilization of the surface is the chemical structure of the additive. Various additives with different functional groups were tested under constant process conditions and the hydrophilization potential was evaluated. Due to processing under constant conditions, it was not possible to generate a fundamental understanding of the migration behavior of the additives as a function of the production parameters, the resulting matrix morphology and the chemical architecture of the additives. Further publications are limited to patent literature or partial aspects of the field of research. To date, the use of ethoxylated alcohols [14–18], organosilicones [19, 20] and polyethylene glycols with different structure [16, 21] has been investigated.

One reason for the small number of publications is the high complexity and interdisciplinarity of the research field, since the analysis of melt additives ranges from the selection of additives with suitable functional groups to their processing and the characterization of migration behavior and performance of the final products. For this reason, there are only publications that cover certain aspects of the topic, such as the diffusion of low molar mass additives in polypropylene [22–24], the development of morphology in injection molded specimen [25], fibers [26–28] and films [29], or the adsorption of additives to polypropylene surfaces [30, 31]. However, there is no comprehensive study that covers all the above-mentioned aspects. In addition to the already discussed economic relevance of the field of research, it is therefore of considerable scientific importance.

Based on the current state of the literature, the aim of this work is the development of hydrophilic melt additives for polypropylene, which can be used for fibers and nonwovens, but also for films and injection molded parts. The focus is on the correlation of the chemical structure of the additive and the hydrophilization potential as well as the migration behavior. Furthermore, the influence of the morphology (e.g. crystallinity in surface and bulk, crystal phases and orientation of polymer chains) of the polymer matrix as a function of the production process and the processing parameters on the migration behavior is investigated (Figure 1.1).

In the first part of the thesis, a comprehensive set of different commercially available surfactants, which consist of a hydrophilic and hydrophobic molecule

part, is selected as potential melt additives. The additives differ in their functional groups and their chemical architecture. It is assumed that the hydrophilic part of the molecule can be used for tailoring the wetting properties, while the hydrophobic part is beneficial for anchoring the molecule to the substrate and improving processability. After a fundamental characterization of the thermal and molecular properties, the additives are tested for their suitability as surface coatings and as melt additives for the hydrophilization of nonwovens in simplified preliminary studies. Subsequently, the additives with the best performance are selected in order to reduce the number of samples for the following studies.

In the second part of the thesis, a method for tracking the degree of crystallinity of the matrix polymer and the surface enrichment of the additives is developed by combining X-ray diffraction (XRD) and Fourier-transform infrared spectroscopy (FTIR). This provides the possibility to correlate the morphology development during production and storage with the migration behavior. Injection molded plates, stretched and unstretched cast films, single fibers and thermally bonded nonwovens are produced by changing the process-specific parameters. The degree of stretching is increased from process to process and the surface enrichment of the additives is analyzed as a function of time. Furthermore, the influence of the molecular structure of the matrix polymer and nucleating agents on morphology formation and migration behavior is investigated. The focus of the second part of the work is to examine the influence of the main process parameters on the morphology development of the matrix polymer and the influence of the morphology development on the migration behavior of the additive. The best performing additives are produced under typical industrial conditions and tested in practice. Subsequently, novel methods for the subsequent and local activation of hydrophilization are developed. The determination of the basic mechanisms how melt additives work or how they migrate to the surface depending on the matrix morphology will contribute to a more economical use and development of the technology in general.

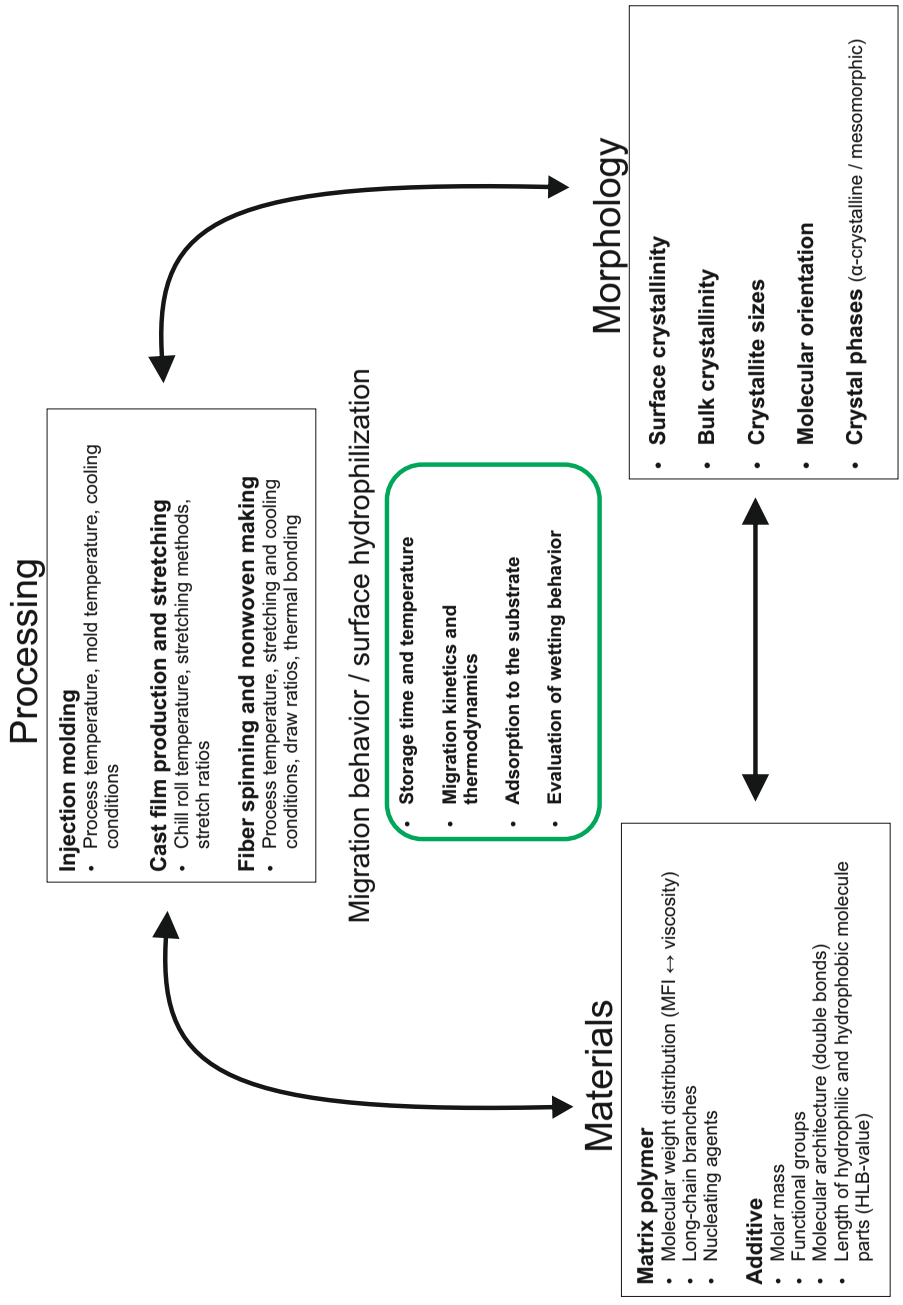

Figure 1.1: Main factors influencing the migration and wetting behavior of melt additives in polymers.

2 Fundamentals and state of the art

2.1 Polypropylene and methods to hydrophilize polypropylene

Polypropylene (PP) is the second most commonly used standard polymer after polyethylene. Due to its good processability, it is used in many relevant processes such as injection molding, film blowing or casting and fiber spinning. It is applied, for example, as a packaging material, in vehicle construction for vehicle interiors, in electrical engineering for housings or sheathings or in the manufacture of fibers and nonwovens for the production of hygiene articles, medical products, geotextiles or carpets [1, 3, 4]. This broad application is mainly due to the properties that are advantageous for many industrial sectors. The most important characteristics are:

- Low density of 0.9 g cm^{-3} for light weight construction
- High thermal stability due to a melting point of above 160 °C and low thermal degradation during processing
- High chemical and environmental stress cracking resistance
- Excellent mechanical properties

Due to the low raw material costs and the good processability of the material, polypropylene is the most frequently used material for the production of spunbond nonwovens [4]. Linear, isotactic polypropylenes with a melt flow index (MFI) of 12 - 60 g 10 min^{-1} and a rather narrow molecular weight distribution (polydispersity of 3 - 6) are usually used for the production of spunbond nonwovens [32]. For the production of technical fibers lower melt flow indizes in the range of 3 - 5 g 10 min^{-1} are used while for the production of meltblown fibers higher melt flow indizes up to 1200 g 10 min^{-1} are utilized [33]. Fiber grade polypropylenes are usually produced using metallocene catalysts.

2.1.1 Polypropylene surface properties and modification methods

For many applications, e.g. in the food industry, as well as for post-treatment processes such as coating, printing or bonding of components, the surface properties of the plastic are of utmost importance. Due to the non-polar chemical structure, the polypropylene surface is highly hydrophobic and difficult to wet with water. This is reflected in a water contact angle of 90 - 110 °

and a surface energy of 28 - 33 mJ m^{-2} [34–36]. While the hydrophobic surface is useful for many applications, a hydrophilic surface is often required for medical and hygiene products or filter media.

2.1.1.1 Surface coatings

The currently most frequently used process for hydrophilizing textiles or fibers is the coating of the surface with wetting agents. An aqueous dispersion (also called lubricant or spin finish) containing the wetting agent is applied to the substrate in a thin layer by spraying or rolling. This process ensures that the additive is applied only on the surface and therefore does not alter the bulk properties of the material. Furthermore it offers a very effective and easy to implement method to immediately hydrophilize a surface.

However, the coating of polymers has some major disadvantages. The wetting agents are usually water-soluble and only applied directly to the surface. They are therefore only anchored to the surface by physical adhesion and easy to wash off. The wetting agents thus get into the washing water and reduce its surface tension, leading to hydrophobization of the surface. In addition, the applied coatings can be transferred on contact with non-hydrophilized layers and thus hydrophilize regions that should actually be water-repellent. Especially in the case of textiles, the coalescence of drops from the spin finish due to their high surface tension and the high porosity of the textiles can lead to an uneven coating of the substrate.

Commercially available products are marketed and patented by Cognis under the trademark Aquasoft® [7]. Schill and Seilacher have a coating product called Silastol in their portfolio and patented substances for the hydrophilic finishing of polypropylene [5, 6].

2.1.1.2 Plasma, corona and flame treatment

When treating a surface with plasma, corona discharge or a gas flame, polymer molecules on the surface of the substrate can be oxidized by free radicalization. The treatment results in the formation of C-OH, COOH, C-O-C, epoxy or ester groups on the surface which alter the surface energy and lead to a better wettability of the substrate.

The advantages of an oxidation of the surface are the rapid treatment as well as the simple implementation of the process. However, variations in ambient temperature or humidity can cause large variations in the process and the associated uniformity of surface treatment. A major disadvantage of these processes is the poor long-term stability of the hydrophilization

due to restructuring of the surface and the reaction of the functional groups which were formed during the treatment [8, 9]. It is also reported that the use of plasma treatments can cause damage to the polypropylene surface (etching and voids) [34]. Furthermore, the use of corona treatments may cause cross-linking or degradation of polymer chains, resulting in poorer sealability [37].

2.1.1.3 Hydrophilic melt additives

An alternative to the surface treatment methods discussed above is the incorporation of hydrophilic additives into the melt. The additives should initially be distributed evenly in the melt and accumulate on the surface after the finished product has cooled down. The time-dependent surface enrichment (also called migration) is strongly dependent on the environmental and production conditions and is discussed in detail in chapter 2.3.

By adding the wetting agent to the process, no further production step is necessary, making the treatment very efficient and easy to implement. Furthermore, a permanent and durable as well as uniform hydrophilization might be achieved by the use of melt additives. It is assumed that the additive chains anchor to the polypropylene surface as a result of the necessary migration step. A controlled migration would allow to hydrophilize only certain parts of the nonwoven during a subsequent activation step. Therefore, the use of melt additives is a potential solution to avoid the disadvantages of the established processes for the hydrophilization of polypropylene surfaces. However, since usually not all of the additive migrates to the surface, an increased additive usage is expected compared to conventional procedures. In addition, the migration can be difficult to control and predict due to the various parameters influencing migration.

For the hydrophilization of polypropylene with melt additives there are already commercially available solutions. Some of the chemical structures which can be used as a hydrophilic melt additive are protected by patents. In the academic field there are so far only a few studies dealing with the hydrophilization of polypropylene by means of melt additives. In the following, publications on the hydrophilization of polypropylene using melt additives are discussed.

The structure most commonly used in patent literature for the hydrophilization of polypropylene is a mixture of various ethoxylated alcohols of structure CH_3-CH_2-$(CH_2$-$CH_2)_m$-CH_2CH_2-$(OCH_2CH_2)_n$-OH where m is between 9 and 35 and n between 1 and 10 [17–19, 38]. Masterbatches consisting of these molecules were first sold by Ciba under the trademark Irgasurf® and then by

Techmer PM under the trade name Techsurf. Further additive groups, which are used for the hydrophilization of the surface, are organosilicones [19, 20, 39], polyethylene glycols [21], fatty acid monoglycerides [19, 40] or alkoxylated alkyl phenols [41]. Another hydrophilic masterbatch for polypropylene with unknown composition is sold by Polyvel under the trade name VW-351.

In the field of academic research there are only a few publications on the subject of hydrophilic melt additives for polypropylene, especially when it comes to application-relevant melt additives for fibers, nonwovens or films. This is probably due to the high experimental effort involved in the development of melt additives and the complexity of the research field. Datla contributed a PhD thesis [12] on the topic of hydrophilic melt additives as well as two papers [13, 14] which cover the use of ethoxylated alcohols, ethoxylated fatty amines, nonylphenols, glycerol mono stearates and polyethylene glycol for the hydrophilization of polypropylene. Although it has been demonstrated that it is possible to hydrophilize the polypropylene surface with ethoxylated alcohols, there are no experiments which led to a fundamental understanding of the hydrophilization behavior with regard to the chemical structure as well as the migration kinetics and thermodynamics of the additives depending on the production parameters.

2.1.2 Applications of hydrophilic polypropylene

Although the poor wettability of polypropylene is essential for many applications, there are applications where the low price as well as the thermal and mechanical properties of polypropylene would be desirable, but the application requires a hydrophilic surface. The following is an overview of possible applications of hydrophilic polypropylene:

Hygiene products
: Water-permeable nonwovens are used in diapers (incontinence articles or baby diapers) or feminine hygiene products [42].

Disposable absorbent products and wipes
: The cleaning performance of wipes can be significantly improved by a hydrophilic surface[43–45].

Wettability of staple fibers with water based binder systems
: Carded fibers are often bonded with water-based binders. Hydrophilic coatings are applied to the surface of the fibers to enhance the wettability with the binder.

Hydrophilic membranes
Water-permeable membranes are important for media filtration in many industries. For example, coalescence filters for separating water from exhaust gases could be manufactured from polypropylene nonwovens [46].

Battery seperators
Hydrophilic separators made of polyolefins are used especially for nickel accumulators to separate the electrodes [47, 48].

Improvements for coatability of products
The coating of polypropylene surfaces by water-based coating systems would be improved by a hydrophilic surface.

Antifog materials
In the food industry, polyolefin films are frequently used for food packaging. These films can appear cloudy due to fog formation on the surface caused by evaporated water. A hydrophilic surface leads to a film formation of the water whereby the surface appears clear again [49].

Antistatic materials
Due to the strong non-polarity of polypropylene, it tends to become electrostatically charged. A hydrophilic surface can form a thin film of moisture on the polymer surface which dissipates charges.

2.2 Crystallization and morphology development in polypropylene

The crystalline phase of polypropylene can be present in the mesomorphic or α-, β- or γ-crystalline form, depending on the processing, especially the cooling conditions. The β- and γ-crystalline structure are metastable and require special nucleating agents and cooling conditions [50] which are not applied in this thesis. Only the α-crystalline phase (also called α-monoclinic form) and the mesomorphic (also called smectic) phase are of higher interest and will be discussed in this chapter with regard to their structural properties, formation and transformation. In general, the α-crystalline structure is the predominant and most stable structure while the mesomorphic crystal structure is metastable. The mesomorphic phase requires rapid supercooling of the melt and can subsequently transform into the α-crystalline structure upon heat input.

So far the structure of strongly cooled PP is not completely explained in literature and generally described as a kind of paracrystal [51], microcrystal [52] or

as a molecular state of order between the amorphous and the α-crystalline phase [53]. It is assumed that it consists of bundles of parallel chains that form the same conformation as the α-monoclinic phase [54], but show conformational errors along the chain [55]. In the mesomorphic phase, the distant order exists only along the polymer chain axis, which leads to greater disorder in the lateral packing density. This suggests a less dense crystal and a higher permeability compared to the α-crystalline form.

The mesomorphic phase is formed at cooling rates of several 100 to 1000 °C s^{-1}, when crystallized isothermally between 0 and 30 °C [56, 57] or cooled with very high rates from the melt [58–60]. In the fiber spinning process, the mesomorphic phase can develop at low take-up speeds [26, 58] or high extrusion temperatures combined with moderate take-off velocities [61]. In the production of cast films, the mesomorphic phase is formed at a chill roll temperature of 20 - 30 °C and below [24]. The α-monoclinic phase is formed at cooling rates lower than 100 °C s^{-1} [62, 63] and is usually found in films which were cast onto a non-cooled chill roll [24], slowly cooled PP products or heat treated samples. Due to shear-induced crystallization, the α-crystalline morphology is also found samples which were stretched during cooling [58]. In the case of industrially manufactured polypropylene products, the non-uniform cooling conditions during the process can result in the simultaneous presence of mesomorphic and α-crystalline structure. For example, injection molded parts show a mesomorphic structure on the rapidly cooled surface layer while they are α-crystalline in the core [25, 64].

Although the mesomorphic phase is stable at room temperature, the transformation into the α-crystalline phase begins at relatively low temperatures of 50 - 80 °C [65, 66]. It is not fully understood if the transition is accompanied by a partial melting of the local crystal order and subsequent nucleation [67] or whether it is a solid state transformation [52, 68].

2.3 (Surface) migration of additives in polymers

In this thesis, the migration of additives is defined as the preferred surface enrichment of the low molar mass component in a polymer blend depending on time and other environmental factors. The migration of additives has been an extensively studied phenomenon for decades. However, due to the complexity and various interconnected parameters influencing migration, there is no comprehensive theory describing the behavior of low molar mass additives in a polymer as well as the kinetic and thermodynamic boundary conditions that affect migration to the surface.

In the following chapter, the main factors influencing migration will be briefly discussed on the basis of available literature. The influence of surface tension, the influence of the molar mass of the components on entropy-driven separation and the role of miscibility of the individual components is explained in detail in chapter 2.3.1.

Storage temperature and environmental properties

The influence of temperature on the enrichment of additives at the surface is a well understood and often discussed phenomenon. There is usually a consensus that an elevated temperature promotes and accelerates surface migration if the additive migrates to the surface at all. The improved migration is mostly explained by the increase of the diffusion coefficient with increasing temperature [69–71].

Usually the migration efficiency increases monotonously with increasing temperature until degradation processes or melting of the matrix change the boundary conditions of the investigated system. However, Wakabayashi et al. [72] report critical temperatures where erucamide in polypropylene suddenly no longer migrated. This phenomenon is attributed to the immobilization of additives as a result of increased miscibility at high temperatures. The same effect was observed by Shuler et al. [22] and explained by a migration of erucamide back into the core from a temperature of 55 °C.

Another aspect that is often overlooked when studying environmental factors is the (air) humidity. The influence of humidity has not yet been explicitly tested for the migration behavior of hydrophilizing additives. However, there are studies by Bergbreiter and Srinivas [73] that investigated the migration of polyethylene glycol inside a polyethylene matrix to a polymer/glass interface and a study by Lee and and Archer [74] that investigated the migration of a polystyrene-b-poly(dimethyl siloxane) block copolymer in a polystyrene matrix to a polymer/aluminum interface. Both studies report significantly different kinetics compared to a migration towards a regular polymer/air interface due to a different interfacial energy. A similar study has been published by Chen et al. [75] where polypropylene-graft-poly(methyl methacrylate) was blended with polypropylene and the surface enrichment was studied. It was shown that the additive is migrating much better towards a steel interface (approx. 700 - 1000 mJ m^{-2}) compared to a polyimide (44 mJ m^{-2}) or a PTFE interface (18 mJ m^{-2}). This means a high surface energy interface is favoring a stronger migration and enrichment of the additive towards the surface. For this reason, strong changes in the interface due to wetting with water

(e.g. during washing or steaming with water vapor) or a small change due to fluctuations in air humidity may cause a change in migration behavior.

Polymer matrix morphology and processing

Polypropylene is a semicrystalline polymer which consists of amorphous and crystalline regions. The crystallites are not permeable for additives, which is why they represent a migration barrier. Additive molecules can only dissolve and accumulate in the amorphous regions of the polymer [76–78]. For this reason, the morphology of the polymer, plays an important role for migration phenomena. The term morphology is used as a generic term for the structural arrangement of polymer chains (i.e. the degree of crystallinity, orientation and crystal phases) in the matrix polymer and is represented by the packing density of the polymer chains. Maghsoud et al. [79] have shown that a lower crystallinity of the polymer correlates with an improved additive migration. A very similar study was conducted by Alin et al. [80] revealing similar phenomena for antioxidants in polypropylene. In processes in which high draw ratios occur during production (fiber spinning, film production), strong orientation of amorphous and crystalline regions is found. These regions are more densely packed and therefore more difficult for additive molecules to permeate, which in turn leads to a reduced migration if the orientation is perpendicular to the direction of migration [76, 81, 82]. Orientation and crystallinity can be controlled by polymer matrix selection or by processing. Since for many processes the material selection can only be changed slightly due to the properties of the end product, the possibilities to influence the polymer morphology are often limited to the processing or the introduction of additives such as nucleating agents. In the case of fiber spinning, the polymer morphology can be changed by cooling and drawing conditions, process temperatures or the calendering process.

Molecular characteristics of the additive

Melt additives are usually comparatively short-chained oligomers which are specially adapted to the extrusion and general processing of polymers. The influence of additive structure on migration behavior is also a highly discussed field in the literature.

Saleem et al. [83] investigated the influence of size and shape of different molecules on diffusion in an LDPE matrix. It was found that the diffusion coefficient decreases with increasing penetrant size. In the absence of structural effects (e.g. double bonds, branching), a linear relationship between the logarithm of the diffusion coefficient and the molar volume of the additive was

found. In addition, it was shown that linear molecules have a higher mobility compared to rigid and unsymmetrical molecules. In a study by Asfour [84] a linear relationship between the diffusion coefficient and the size of n-alkenes in a LDPE film was demonstrated. A study by Földes and Szigeti-Erdei [85] concluded that the migration rate of sorbitol esters into PE is dependent on the size of the molecule. A linear releationship between the relative chain length of additive molecules and the additive amount that migrates to the surface was found. Llop et al. investigated the use of various ethoxylated alcohols to suppress the uncontrolled migration of the slip agent erucamide [86]. Strong differences in migration behavior depending on the molecular architecture of the additive were detected. However, detailed correlations between the molecular structure of the additive and the migration behavior were not found. The migration behavior of ethoxylated alcohols to hydrophilize polypropylene surfaces was also investigated by Datla et al. [14]. While differences in the wettability of the polypropylene surface were attributed to differences in migration behavior, no relationship was established between molecular architecture and migration behavior.

In summary, the molar volume is one of the main factors influencing migration kinetics with regard to the additive structure. The larger the molecule, the greater the resistance for the molecule to migrate to the surface and therefore the lower the coefficient of diffusion. The molar volume depends on properties such as branching, the chain length or the molar mass of the additive or the molecular shape in general. Furthermore, the flexibility of the molecule has to be taken into account.

A second factor that significantly influences the migration to the surface is the chemical composition of the additive. This has an influence on the miscibility as well as the surface tension. The influence of these two parameters is explained in more detail in the following chapters.

2.3.1 Surface segregation of additives

The thermodynamic boundary conditions, which promote or restrict the migration of additives to the surface are discussed controversially and contradictorily in the literature. In the following chapter, the main factors are reviewed using examples from the literature.

2.3.1.1 Influence of the surface tension of the individual components

In many publications the main reason given for the enrichment of a component on the surface is the difference in the surface energy of the single components.

The component with the lower surface energy accumulates on the surface in order to minimize the interfacial free energy of the system.

Lee and Archer conducted a study [74] in which PS-PDMS block copolymers were blended with pure polystyrene. The enrichment of the additive at the surface was explained by a difference in surface tension but also attributed to a difference in the molar mass of the two components. The difference in surface tension between PS-PDMS (14 - 18 mJ m^{-2}) and pure PS (32 - 36 mJ m^{-2}) was large enough for factors such as the molar mass of the matrix polymer to affect migration, but not to alter the main surface component. Jones et al. [87] investigated the surface enrichment of a blend from deuterated polystyrene and protonated polystyrene. It was found via forward recoil elastic scattering and dynamic secondary ion mass spectroscopy that the deuterated polystyrene enriches the surface. The effect was attributed to the difference in surface energy as the lower polarizability of the C-Deuterium bond compared to the C-H bond is leading to a decreased surface energy of the deuterated polystyrene. An influence of the molar mass was excluded because the molar mass of the protonated polystyrene used as matrix polymer was varied over a wide range (670 000 - 1800 000 kg mol^{-1}) and in all cases the deuterated polystyrene migrates to the surface. In a study by Bhatia et al. [88] in which blends of polystyrene and poly(vinyl methyl ether) (PVME) were investigated, it was found that PVME accumulates at the surface. Furthermore, it was shown that the enrichment of PVME at the surface increases with the molar mass of the polystyrene. The lower surface tension (21.9 mJ m^{-2}) of PVME compared to PS (29.7 mJ m^{-2}) is reported as the driving force for the preferred surface enrichment of the PVME. Similar results have been found by Pan et al. for the same system [89].

Assuming that the difference in surface tension is the only reason for segregation of the additive, it would hardly be possible to develop hydrophilic melt additives for polypropylene. Due to the very low surface energy of polypropylene (30 mJ m^{-2}) and the comparatively high surface energy of conventional hydrophilic molecules (42 mJ m^{-2} for PEO), the thermodynamic boundary conditions would prevent the melt additive from migrating to the surface. If molecules have functional groups with significantly different surface energies, as it is the case with surfactants, the part with the lower surface energy is considered to align towards surface while the part with the higher energy depletes from the surface [90, 91].

Although the theory may help to predict which substance will show a preference to accumulate at the surface, there are many studies in which the higher

surface energy component migrates to the surface, especially if it has a much lower molar mass compared to the other component [92, 93].

2.3.1.2 Influence of the molar mass of the individual components

If the surface energy of the individual components in a blend is the same or very similar, the low molar mass component usually accumulates on the surface. Tanaka et al. studied the surface enrichment of blends of low molar mass PMMA and high molar mass PS via X-ray photoelectron spectroscopy and scanning force microscopy [92]. It was found that PMMA migrates to the surface despite the higher surface energy of 44.3 mJ m^{-2} compared to PS (40.9 mJ m^{-2}). A study by Lee and Archer [93] investigated the migration of a PS-b-PMMA block copolymer additive in a PS matrix by varying the matrix molar mass. It was found that the additive migrates to the surface if the molar mass of the matrix is significantly higher than the additive molar mass. If the molar mass of the additive is higher than the matrix molar mass, desaturation of the additive at the surface is observed. The migration mechanism was mainly attributed to the chain end entropy.

If the polymer is exposed to shear forces in the process, the low molar mass component of the blend will usually accumulate at the surface. This effect has mainly been shown for polymer solutions [93, 94].

In summary, there is a superposition of two phenomena: On the one hand, components with a higher surface energy tend to migrate from the surface towards the bulk phase. The lower surface free energy component is enriched at the surface to minimize the polymer-air interface energy. On the other hand, low molar mass components migrate to the surface because they experience a lower conformational entropy penalty of long chains for staying near the interface compared to high molar mass components [95]. It is assumed that the component with the lower surface energy enriches the surface. However, if the components have a significantly different molar mass (as it is the case with melt additives in a polymer matrix), the low molar mass additive might migrate to the surface for entropical reasons, especially if the blend is exposed to high shear forces during production.

2.3.2 Miscibility and solubility

In the literature there are conflicting perspectives on the influence of solubility on the migration of additives in polymers. There are two completely different and contradictory models. The first model assumes that the permeability of a small molecule in a matrix results from the product of the diffusion coefficient

and the solubility of the molecule in the matrix. A two-step solution-diffusion-mechanism is considered. First, the additive molecule is dissolved from the polymer. Then, the molecule can permeate the matrix by diffusion. Accordingly, permeability P is the product of diffusivity (or the diffusion coefficient) D and solubility S [96]:

$$P = D \cdot S \tag{2.1}$$

The disadvantage of this model is the discrepancy to experiments which show a strong surface segregation in completely immiscible blends. According to the model, molecules in non-miscible blends should not be mobile and therefore not be able to enrich the surface over time. On the basis of these considerations it is assumed that in the case of larger additives other diffusion mechanisms are present, since the solution-diffusion model is frequently used for gas diffusion or diffusion in membranes.

The second model considers that only the additive which is not miscible with the matrix, i.e. the undissolved volume, can migrate to the surface. The mechanisms behind this theory are often not explained in detail and are mostly attributed to the formation of gradients due to phase separation [97].

Experiments have shown that the time in which an antioxidant remains effective in a polymer matrix depends on the ratio S^2/D. This means that an antioxidant is most effective if it has a high solubility S in the matrix and at the same time a diffusion coefficient D which is as low as possible [85]. A study by Pan et al. [89] showed that the extent of surface enrichment of PVME in a PS/PVME mixture is highest in thermally induced phase-separated mixtures and lowest in miscible mixtures. Wakabayashi et al. [72] investigated the migration behavior of erucamide and behenamide in polypropylene as a function of storage temperature. It has been found that erucamide only migrates to the surface up to a critical storage temperature, while behenamide migrates well even at high temperatures. The critical storage temperature of the erucamide was attributed to an increased solubility of erucamide, which severely restricts migration. Since behenamide is significantly less soluble than erucamide, it can migrate to the surface even at high temperatures. Another study Wakabayashi et al. concludes that the immobilization of the additives is a result of self association of the additive molecules at higher storage temperatures [98]. Clark et al. [99] studied the surface enrichment of PCL/PVC blends with different mixing ratios. It was found that miscible blends do not show the preferred surface enrichment of a specific component,

while immiscible blends show an enrichment of PCL on the surface. For high PCL concentrations it was found that the PVC enriches the surface.

Assuming that miscibility plays a crucial role in additive migration, the Flory-Huggins theory can provide guidance for the selection of suitable additives as it is a practical tool to describe the thermodynamic properties of a molten polymer blend. The theory describes Gibbs free energy of mixing ΔG_m of a binary blend system:

$$\frac{\Delta G_m}{RT} = \frac{\phi}{N_1}\ln\phi + \frac{(1-\phi)}{N_2}\ln(1-\phi) + \chi_{1,2}\phi(1-\phi) \qquad (2.2)$$

where ϕ is the volume fraction of the polymer, N_1 and N_2 are the number of repeating units of the polymer and the additive, respectively and $\chi_{1,2}$ is the Flory-Huggins interaction parameter between polymer and additive [100, 101]. The first two logarithmic terms of equation 2.2 describe the entropy of mixing of the blend and favor mixing while the last term describes the interaction between polymer and additive and disfavors mixing. The Flory-Huggins parameter is a measure of the compatibility of the components and can be estimated from the Hildebrand solubility parameters δ_1 and δ_2 as $\chi_{1,2}$ is proportional to the square of the difference of the two Hildebrand parameters [102]. Accordingly, polymer and additive become more miscible with increasing similarity. Additives which are chemically very similar to the polymer and have low molar masses should be highly miscible with the polymer and vice versa.

Studies that report a migration of completely miscible and immiscible additives indicate that both models do not fully reflect reality. Thomas and O'Malley showed [103] that in the poorly miscible system PEO / PS the PS component (which has the lower surface tension) migrates to the surface. On the other hand, surface segregation was also observed for blends of poly(vinylidene fluoride-co-hexafluoro-acetone) with poly(butyl acrylate) which are completely miscible at room temperature[97].

In summary, a phase separation for the migration of additives seems to be preferred, since an increased solubility of the additive usually implies that no more migration takes place. However, counterexamples of miscible blends have shown that they can also tend to enrich a component on the surface.

2.3.3 Diffusion

Diffusion refers to the movement of molecules from regions of high concentration to regions of low concentration and is considered one of the main reasons for surface migration. It is assumed that the migration of low molar mass additives can be described by Fick's second law of diffusion [79]:

$$\frac{\partial c}{\partial t} = D\frac{\partial^2 c}{\partial x^2} \tag{2.3}$$

where c is the concentration, t is the time, D is the coefficient of diffusion and x is the 1-dimensional position of a molecule. This equation is used to describe the time-dependent change of a concentration profile as a result of diffusion. The diffusion coefficient D is used to calculate the transport due to the random movement of the molecules and thus provides a measure to describe the kinetics of diffusion. For the case of diffusion of additives in polymers, the diffusion coefficient depends on the temperature, the morphology and nature of the polymer (crystallinity, free volume, orientation) and the concentration, size and shape of the diffusing molecule [76, 83]. It is assumed that the diffusing molecule moves exclusively through amorphous regions and cannot permeate crystallites [78]. The diffusion coefficient increases:

- with increasing temperature [69, 104, 105]
- with decreasing molar mass and molecular size [69, 84]
- with decreasing polymer crystallinity [79, 80]
- with increasing free volume in the polymer [83, 104, 106, 107]

These postulates thus represent the starting point for controlling the migration behavior, since they can be systematically changed by the selection of the matrix polymer, the processing parameters and the storage conditions.

Fieldson and Barbari have shown that it is possible to characterize the diffusion of a penetrant into a polymer using attenuated total reflection Fourier-transform infrared spectroscopy (ATR-FTIR) [108]. A similar approach has also been shown by Guo et al. [109]. Starting from classical diffusion laws, which are already applied in sorption kinetics, an equation was derived which describes the diffusion as a function of the absorption of specific bands in the FTIR spectrum. The equation is analogous to the mass uptake equation used in gravimetric sorption experiments, with the difference that the Fickian concentration profile is substituted into the exponential profile of the

evanescent wave in the ATR-FTIR experiment before it is integrated. The resulting equation is:

$$ln\left(1-\frac{A_t}{A_\infty}\right)=ln\left(\frac{4}{\pi}\right)-\frac{D\pi^2}{4L^2}t \tag{2.4}$$

where A_t is the absorbance of the specific band at a given time t, A_∞ is the absorbance of the specific band after infinitely long time, D is the diffusion coefficient and L is half the thickness of the measured sample. Figure 2.1 shows a schematic illustration of this experiment. Further derivations to this equation can be found in the appendix A.1.1.

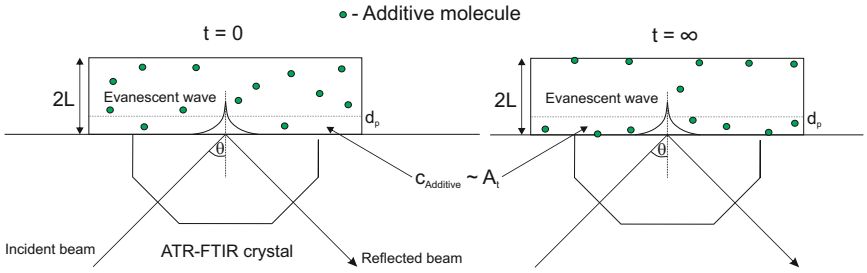

Figure 2.1: Sketch to illustrate the experimental setup used to detect the additive concentration over time via ATR-FTIR. The left side shows the boundary conditions at the beginning of the experiment, the right side shows the additive distribution after infinitely long storage time.

Equation 2.4 is not significantly depending on the penetration depth d_p of the evanescent wave, if the requirements:

$$4\left(\frac{1}{d_p}\right)^2 \gg \frac{\pi^2}{4L^2} \tag{2.5}$$

and

$$1 \gg e^{-2\frac{L}{d_p}} \tag{2.6}$$

are met. Equation 2.4 is analogous to the long-time solution of Fick's second law of diffusion (equation 2.3) and can be used if only limited data is available at $A_t/A_\infty \leq 0.5$ which is the case in most of the experiments conducted in this thesis.

Assuming that the absorption of a specific band in the FTIR spectrum is proportional to the concentration c (see also chapter 4.2.3.1) of an additive, equation 2.4 can be rearranged to:

$$c_{\text{surface}}(t) = c_{\infty} \cdot \left(1 - \frac{4}{\pi} e^{-\left(\frac{t}{\tau_{\text{Migration}}} \right)} \right) \tag{2.7}$$

where

$$\tau_{\text{Migration}} = \frac{4L^2}{D\pi^2} \tag{2.8}$$

$\tau_{\text{Migration}}$ is the characteristic time after approximately 63 % of the additive have migrated to the surface and c_0 and c_∞ are the surface concentration after no and infinitely long time have passed, respectively. This equation has the advantage that, in contrast to parameters from the sorption experiments, it provides comparable results for the maximum surface enrichment of the different experiments in this thesis. In addition, $\tau_{\text{Migration}}$ is an easily comparable characteristic time, which describes the time necessary for the enrichment of the surface and is reciprocally proportional to the diffusion coefficient D and thus also a measure of the diffusion rate.

An exponential parameter b was introduced to improve the adjustability of the fit function to the experimental data. The value for b was usually between 0.4 and 1 and, unless otherwise described, set to 0.5, as this value provided the best fitting results and allowed comparability of the single experiments. Further considerations on exponent b can be found in appendix A.1.1. The term $4 / \pi$ was excluded from the equation for simplification. The result is the semiempirical equation 2.9 which was used for fitting all migration experiments performed in this work. Due to the experimental scattering of the migration data, both equation 2.7 and equation 2.9 yield very similar results, with equation 2.9 offering the highest fitting flexibility and direct accessibility of relevant parameters.

$$c_{\text{surface}}(t) = c_0 + (c_{\infty} - c_0) \cdot \left(1 - e^{-\left(\frac{t}{\tau_{\text{Migration}}} \right)^b} \right) \tag{2.9}$$

A similar equation has been proposed by Long and Richman to describe diffusion behavior of vapors in glass polymers [110]. In cases where surface enrichment is accompanied by surface desaturation due to additive degradation or other phenomena, the equation can be extended with a second exponential function describing surface desaturation:

$$c_{\text{surface}}(t) = c_0 + (c_\infty - c_0)\cdot \underbrace{\left(1 - e^{-\left(\frac{t}{\tau_{\text{Migration}}}\right)^{0.5}}\right)}_{\text{Migration term}} \cdot \underbrace{\left(e^{-\left(\frac{t}{\tau_{\text{Degradation}}}\right)^{c}}\right)}_{\text{Degradation term}} \tag{2.10}$$

where $\tau_{\text{Degradation}}$ is the characteristic time constant for the degradation describing the rate of degradation, and c is an adjustable variable normally set to 2, unless otherwise specified, to adjust the fitting function to the experimental data. Figure 2.2 shows the three types of migration that usually occurred in this work.

Type 1 is pure migration. The external boundary conditions indicate that it is thermodynamically more favorable for the additive molecules to enrich the polymer-air interface than to stay inside the matrix. The migration is not superimposed by desaturation effects which reduce the concentration at the surface. Therefore the surface concentration of the additive reaches a plateau value after a certain time. This migration type is the preferred one. In the mathematical description using equation 2.10, $\tau_{Degradation}$ is infinitely large.

Type 2 is the non-existent migration where two different cases can be distinguished. On the one hand, migration to the surface can be thermodynamically inhibited. This means that it is not the most thermodynamically favorable state for the additive molecule to accumulate at the polymer-air interface. This can be caused, for example, by a very high solubility of the additive inside the polymer matrix. On the other hand, the migration of the molecule can be kinetically inhibited, i.e. the migration to the surface may occur in principle, but the time until the additive migrates to the surface significantly exceeds the experimental measurement range. This is the case, for example, with molecules that are too large and therefore migrate much more slowly than small molecules. In this case the diffusion coefficient can be increased by increasing the temperature to accelerate the migration to the surface. In the

description using equation 2.10, both $\tau_{\text{Migration}}$ and $\tau_{\text{Degradation}}$ are infinitely large.

If the (storage) temperature is increased until the additive is thermally degraded, type 3 results: The migration is superimposed by degradation. The exponential functions used to describe degradation and migration overlap. Degradation is usually slower than migration, which is why $\tau_{\text{Migration}}$ is smaller than $\tau_{\text{Degradation}}$. The superposition results in a maximum, which is commonly reached after a few hours.

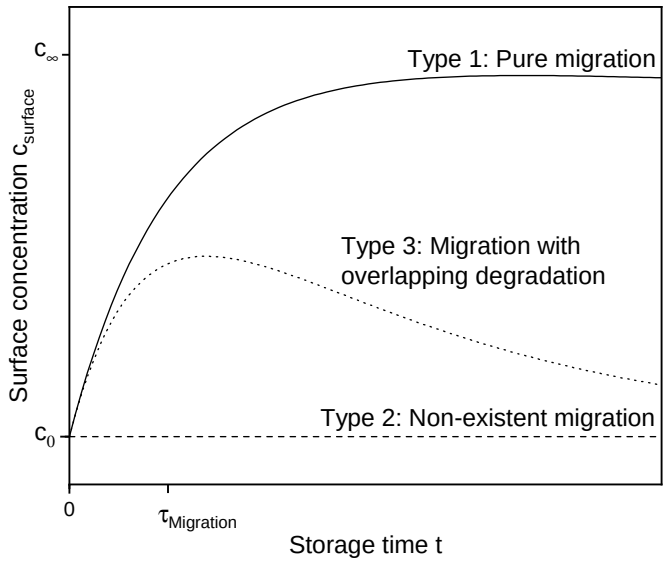

Figure 2.2: Visualization of three types of migration occurring in this thesis that can be described by equation 2.10.

2.3.4 Surface modification of polyolefins with melt additives

The introduction of melt additives into polyolefins is an already well investigated field for some additive types. One of the most commonly utilized additives is erucamide which is used as slip agent to reduce the coefficient of friction of the matrix polymer, to reduce the friction of bottle caps [111, 112] or to generate a softer feel of the final product in general. The use as a migrating slip agent has been extensively studied in polypropylene [22, 72, 98, 113–115] and polyethylene [22, 86, 116–119].

When using antioxidants, it is desired that the additive remains in the polymer matrix and does not migrate in order to achieve the highest possible effectiveness of the antioxidant. The associated studies often concentrate

on restricting the migration of additives [80]. Another field in which the migration properties of low molar mass additives have been investigated is food science. The studies mainly focus on the migration behavior of process additives from packaging polymers into food during microwaving [120, 121].

Antistatics and antifog agents are fields that are closely related to hydrophilic melt additives due to their similar mechanism of action since the additive molecule migrates to the surface and makes it wettable. This allows a thin water film to form on the surface, which either reduces triboelectrically induced voltages (antistatics) or prevents surface haze due to water vapor formation (antifog) [122]. This application is often utilized for films which are especially used in the food industry.

The use of melt additives for the wetting of substrates has been investigated for the utilization of fibers and nonwovens in hygiene applications mainly in an industrial context [19, 42, 123]. Datla investigated the effectiveness of ethoxylated alcohols, nonyl phenol ethoxylates and glycerol monostearates as melt additives in films and fibers with respect to their chemical structure and functional groups [12–14]. Other studies focus on the use of polyethylene glycol (PEG) [16, 124] or polysorbates [122].

The diffusion or migration of additives to the surface is a widely studied field and it has been well understood which parameters are the main factors influencing migration. However, a fundamental understanding of the migration process is still lacking due to the high degree of complexity of the overlapping mechanisms. This thesis examines the main parameters discussed in this chapter and attempts to develop a comprehensive theory for the migration of additives depending on the polymer matrix morphology and processing conditions.

3 Motivation, aims and strategy of this work

This chapter discusses the relevance of this work, its main objectives and the strategy to achieve them.

Polypropylene is the most frequently used polymer for the production of nonwovens, but is also utilized in film production as well as injection molding and is therefore of great economic importance. This is mainly due to the low raw material cost and the useful properties for many purposes. Although the hydrophobic surface of PP is essential for many purposes, hydrophilization of the surface would open up further areas of application. Hydrophilization techniques currently used in the industrial processing of polypropylene, such as coating with wetting agents or corona treatments, have disadvantages which could be avoided by using melt additives which migrate to the surface. The understanding of the function and migration of melt additives may be transferred to other applications, such as surface active melt additives which reduce the coefficient of friction, in order to produce softer nonwovens. The migration of melt additives is highly complex and depends on many factors such as the morphology of the matrix polymer (i.e. the degree of crystallinity, orientation and crystal phases), the chemical structure of the melt additives or the environmental conditions during storage (see chapter 2). So far, only partial aspects of this field of research have been investigated, which is why a comprehensive study of the migration of low molar mass additives in polymers is also interesting from an academic point of view. Based on the literature search from chapter 2, the following general objectives are defined for this work:

- Develop an understanding which requirements have to be met by molecules in order to function as a hydrophilic melt additive for polypropylene
- Understand how the process parameters in the spunbond, cast film and injection molding process affect the morphology development in polypropylene
- Correlate the morphology and the storage conditions with migration phenomena of additives as a function of their chemical architecture
- Develop hydrophilic melt additives for polypropylene, which avoid the disadvantages of currently established processes for surface hydrophilization

In order to achieve these objectives, methods are developed which are able to track the migration of additives to the surface and the polymer matrix morphology during and after the production. The methods are based on the use of Fourier-transform infrared spectroscopy (FTIR) because it allows the degree of crystallinity and the concentration of additives to be determined quickly and non-destructively, both on the surface and in the bulk. An extensive selection of different commercially available potential melt additive types (ethoxylated alcohols, PEO-PPO-block-copolymers, sorbitan esters) is selected based on a literature and patent research. The additives are characterized by thermal analysis with regard to degradation, miscibility and melting behavior.

In simplified preliminary tests, the processability, the adhesion to the surface and the hydrophilization behavior of the molecules are examined in order to evaluate their suitability as melt additives. For more detailed migration experiments, the selection of additives is limited to the best performing molecules, which differ only in their molecular architecture, in order to significantly reduce the test matrix.

The morphology development in polypropylene during injection molding, film casting fiber spinning is characterized depending on relevant process parameters. The degree of stretching and thus the extent of polymer orientation is increased from process to process. The findings are transfered from one process to another in order generate comprehensive models for structure formation during processing. In subsequent experiments, the additives are applied in the characterized processes. The surface enrichment of the additives is tracked over a period of one month and described as a function of the matrix morphology, the process and storage conditions. Finally, nonwovens are produced under industrially relevant conditions to evaluate the suitability of the best performing melt additives for commercial products. The focus is on avoiding the previous disadvantages of the current hydrophilization processes, such as permanence and durability, as well as the subsequent activation of the melt additive using hot air and steam.

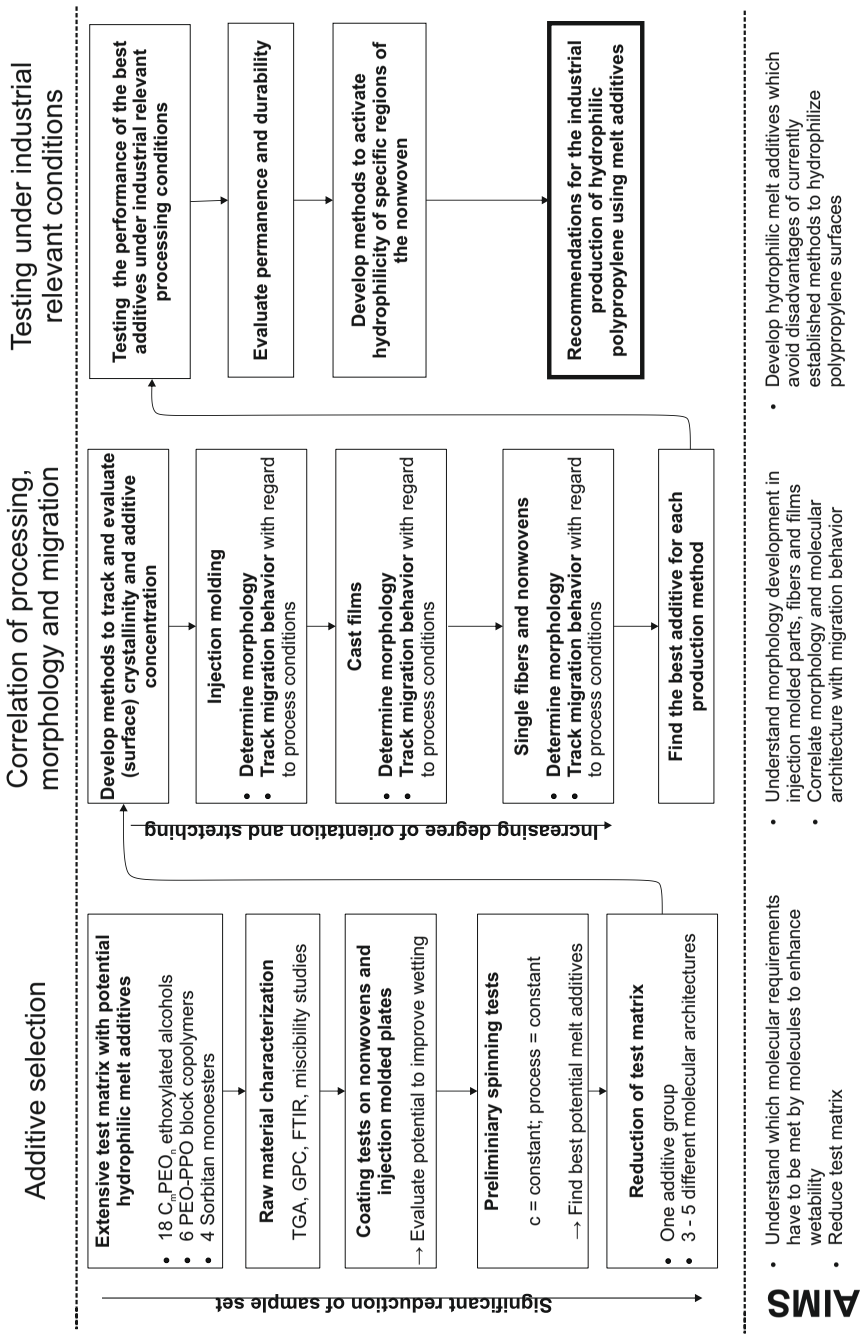

Figure 3.1: Flowchart illustrating the aims and strategy of this thesis.

4 Experimental

This chapter deals with sample preparation, the characterization methods used and the development and validation of novel measurement methods.

4.1 Sample preparation

4.1.1 Masterbatch preparation and melt blending

Masterbatch extrusion

Since larger quantities of additives are required for most of the experiments and the additives can not be added in pure form to the available production lines, the additives were compounded into a masterbatch. To produce the masterbatch, 20 wt% of the additive was premixed with 1 wt% Irgafos 168 (stabilizer) and 79 wt% polypropylene in a tumble mixer for 20 minutes. The mixture was then fed via a volumetric feeder into a co-rotating twin screw extruder (LSM34Gl, Leistritz). Extrusion was carried out at a screw speed of 30 rpm and a temperature of 180 °C. The residence time in the extruder was about 180 seconds. The strand was extruded onto a conveyor belt and cooled with compressed air, as the cooling in a water bath can lead to the release of the additive from the masterbatch into the cooling water. After cooling, the extruded strand was granulated and packed airtight.

Laboratory kneader

If smaller quantities of the additive were required (e.g. to prepare the calibration samples for the FTIR measurements) or if the additive was only available in the liquid state at room temperature and dosing into the extruder was therefore not possible, a laboratory kneader (Haake Polydrive, Thermo Electron GmbH) was used for masterbatch production. Therefore, a volume of 55 cm^3 consisting of 20 wt% of the additive, 1 wt% of Irgafos 168 and 79 wt% of the additive was weighed. The pure polymer was melted at 180 °C for 2 minutes at a rotational speed of 10 rpm. After 2 minutes the stabilizer was added and the speed was increased to 60 rpm to obtain a uniform polymer melt. After a further 3 minutes, the additive was added to the melt and kneaded for 5 minutes, resulting in a total process time of 10 minutes. After kneading, the blend was cooled on a sheet metal, granulated with a Wanner C13.20sv mill and packed airtight.

4.1.2 Fiber spinning and nonwoven production

Single fibers and nonwovens were produced on a pilot spinning line for spunbond nonwovens which consists of an advanced version of a monofilament line which was developed at the institute for polymer materials in cooperation with Fourné Maschinenbau and described in detail by Kunzelmann in his PhD thesis [32]. In order to keep the influence of external climatic conditions as low as possible, the spinning line is located in a separate room, which is tempered to 20 °C and a relative humidity between 40 and 60 % which is considered as optimal spinning conditions according to Fourné [125]. A schematical sketch of the pilot fiber spinning machine can be seen in figure 4.1.

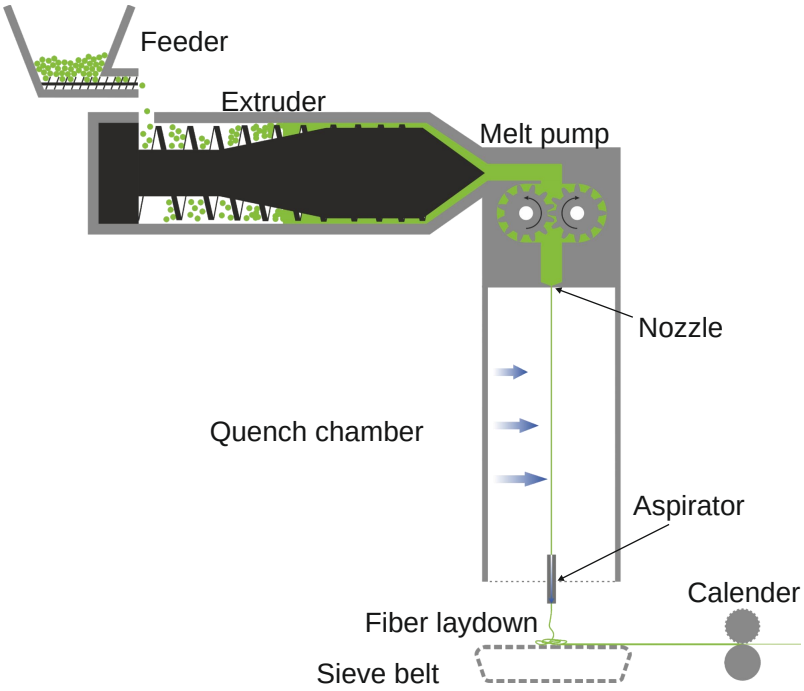

Figure 4.1: Schematic sketch of the pilot fiber spinning line used in this work for the production of single fibers and nonwovens.

The extrusion part of the line consists of a twin-screw extruder (Eurolab 16, Thermofisher Scientific) which is equipped with a feeding system (Brabender). Compared to a single-screw extruder, which is normally used in fiber spinning plants, a twin-screw extruder ensures better mixing and compounding of additives and the matrix polymer. The extruder can operate at a maximum temperature of 300 °C which is sufficient for most commercially available

spinnable polymers. Compared to conventional pilot spinning plants, which are usually operated with throughputs of more than 50 kg h^{-1}, the entire plant is operated in a rather low throughput range between 0.1 and 1 kg h^{-1}. This allows to investigate developmental additives that are only available in doses of several hundred grams.

The twin-screw extruder is connected to the spinning head via a melt line which consists of a static mixing element for further homogenization of the melt, temperature and pressure sensors for process monitoring and control of the feeder unit via a PID controller as well as a gear pump (Mahr GmbH) to ensure a homogeneous volume flow. The spinning head ends in the nozzle package, which takes over the actual thread formation. The nozzle head mainly consists of static mixing parts that ensure a constant and homogeneous polymer flow to the nozzle, a filter disc with a mesh size of 40 µm and the nozzle itself. The nozzle can be replaced according to the requirements of the spinning trial. All experiments were conducted using an eight-nozzle spinning head, each capillary having a diameter of 300 µm and a length to diameter ratio of 2.

After extrusion, the molten fiber is cooled in a quench chamber and stretched aerodynamically using an aspirator. The effective length of the chamber is 150 cm with a width of 15 cm. The cooling of the fiber is realized by blowing air onto the fiber surface from the backside. The cooling profile of the chamber can be adjusted via an air guide panel using six set screws to adjust the panel. The blowing air is provided by an electronically adjustable medium pressure fan which can be adjusted to a maximum volume flow of 900 m^3 min^{-1}. The blowing air can furthermore be dehydrated and cooled down to -8 °C using a recooling plant (Stulz) or heated up to up to 50 °C via an air heating system (G. Maier).

Below the quench chamber, four aspirators (A.I.R. Components) are mounted on an adjustable track system to control the fiber laydown. The aspirators can be switched on individually and are fed with up to 5 bar of compressed air to enable the aerodynamic drawing of the fibers. The aspirators were arranged in a trapezoidal shape, which led to a uniform fiber laydown over approximately 20 cm in width. The fibers are layed down on a sieve belt which is equipped with a Huycon LX127 belt and two vacuum vents which provide a total suction volume of 2000 m^3 h^{-1} to hinder the single fibers from being blown off the belt. The speed of the sieve belt was adjusted to meet the desired base weight of the nonwoven. After the fibers have been laid down on the sieve belt, a laboratory calender (GK 300 L, Saueressig) equipped with a patterned and a smooth roll is used for thermal bonding. If calender patterns other than those

available on the laboratory calender were required, a calender press which was developed in-house, was used. The press consists of a modified injection mold, which is equipped with individually heatable plates. The press was placed in a hot press for applying the necessary pressure for calendering. In order to calender the single fibers, they were taken off the screening belt using a frame and placed in the press. An illustration of the calender press can be found in appendix A.2.1.

An overview of the standard spinning conditions used for most spinning trials can be found in table 4.1. The spinning conditions are highly comparable to industrial spinning conditions.

Table 4.1: Standard spinning conditions used for most spinning experiments performed in this thesis.

	Setting
Process temperature	250 °C
Residence time	10 min
Die	8 holes with diameter of 300 µm
Effective spinning length	1.5 m
Quench chamber conditioning	12 °C at 60 % rel. humidity
Haul-off speed	2000 - 3000 m min^{-1}
Aspirator air pressure	2.5 bar
Fiber diameter	15 - 18 µm
Base weight	20 g m^{-2}
Calendering line pressure	80 N mm^{-1}
Calendering temperature	145 °C (patterned roll) / 120 °C (smooth roll)
Calender pattern	(882 x 524) µm ellipses, 18.1 % area

4.1.3 Cast film extrusion and film stretching

Films were produced on a pilot line for the production of cast films (LSM 34 GI, Leistritz). The line is equipped with a counter-rotating twin screw extruder and a rectangular slot die. The melt flow index of the polypropylene mainly

used in this work is designed for the use in the spunbonding process (MFI = 25 g 10 min^{-1}). Polymers designed for the extrusion of cast films generally have significantly lower melt flow indices. Compared to an industrial process, the production temperature had to be lowered significantly in order to enable a stable and reproducible process. Cast film extrusion was performed at a process temperature of 190 °C while the temperature of the chill roll was maintained at 22 - 24 °C. The additive masterbatch and matrix polymer were premixed in a drum mixer for 10 minutes before being added to the process. After extrusion, the cast films were cooled on a water-cooled chill roll (Göttfert) and then wound up. Cast films were wound at a speed of 10 m min^{-1}, resulting in a draw ratio of about 11. All post-treatments discussed in this work were performed directly after extrusion (maximum 2 hours after extrusion) to eliminate migration effects during storage before post-treatment.

The cast films were hot-stretched using a biaxial stretching device (Brückner Maschinenbau). In this process, an (85 x 85) mm piece of film is clamped with the aid of jaws, heated via hot air and stretched in the hot state. The film is heated to 140 °C for 40 seconds and stretched with a stretching speed of 70 mm s^{-1} to a predetermined ratio either uniaxially or biaxially.

The films were cold stretched uniaxially using a standard tensile testing machine (Z050, Zwick), as it was not able to apply sufficient force to stretch the films in the cold state using the biaxial stretching device. For stretching using the tensile testing device, pieces of cast film measuring (100 x 50) mm were cut out and stretched at a speed of 10 mm min^{-1}. Faster stretching speeds led to premature failure of the film specimen.

4.1.4 Injection molding

Injection molded plates were produced on an Arburg 320 S Allrounder injection molding machine. The temperature of the extruder was set to 200 °C, the feed zone was tempered to 150 °C and the injection flow rate was 60 cm^3 s^{-1}. The holding pressure of 200 bar was held for 15 s. The switchover point was determined in a path-controlled manner. An injection mold was used for the production of 2 plates each measuring (2 x 58 x 58) mm. During the production under standard conditions, the mold was tempered to 40 °C. The injection molded parts were cooled in the mold with a residual cooling time of 6 s, resulting in a total cooling time of 21 s.

4.1.5 Spin coating of injection molded plates

To coat substrates with the additives, the additives had to be dissolved using an appropriate solvent. The additives were dissolved in ethanol because it evaporates quickly and, unlike conventional solvents such as toluene, is harmless to health. For the preparation of the solution, 0.5 g of the respective additive was added to 50 mL ethanol and stirred for at least 4 hours on a stirring plate at room temperature to dissolve the additive completely. After stirring, all solutions appeared clear except those containing sorbitan monoesters and long chained ethoxylated alcohols, probably because of the poor solubility due to the high molar mass of the additives.

Spincoating of injection molded plates and silicon wafers was performed on a WS-650MZ-23 NPP spin coating device (Laurell Technologies Corporation). Before the spin coating process, the substrates were cleaned with isopropanol. The following process parameters were used as they led to a reproducible application of additive layers with a thickness of approximately 30 - 50 nm:

- Rotation time t_{rot} = 45 s
- Rotational speed ω = 2000 rpm
- Acceleration a = 1000 rpm s^{-1}
- Dosing volume V = 1 mL
- Concentration of additive in solution c = 0.5 g · 50 mL^{-1}

4.1.6 Coating of nonwovens

The solution for coating the nonwovens was prepared as described in chapter 4.1.5. The concentration of the coating solution was reduced to 0.278 wt% in order to achieve an additive application of 0.2 wt% with the application of 2 mL of the solution to the nonwoven. Samples with a size of (10 x 10) cm were cut from a polypropylene nonwoven with a base weight of 22 g m^{-2} and placed on a plastic dish. Then, 2 mL of the additive solution was uniformly applied to the nonwovens using a pipette. The solvent was then evaporated under a laboratory fume hood.

4.2 Characterization methods

4.2.1 Wetting tests

4.2.1.1 Contact angle measurements

Contact angle measurements were performed using the sessile drop method on an OCA 30 contact angle measuring device (dataphysics). A droplet with a volume of 4 mL was placed on the surface to be characterized using a needle with an inner diameter of 0.26 mm. The drop was irradiated from one side with a light source and on the other side the drop shape was recorded using a camera. The contact angle was evaluated using the Young-Laplace method. The drop shape was automatically detected and fitted using the program SCA 20 (dataphysics). The placement of the drop and the recording of the drop image were automated in order to obtain a reproducible time of approximately 3 seconds between the placement of the drop on the surface and the actual measurement of the contact angle. Unless otherwise stated, distilled water with a surface tension of 72 mN m^{-1} was used as the measuring liquid. 7 - 10 contact angle measurements were conducted per specimen and the mean and standard deviation were reported.

4.2.1.2 Liquid strike-through test

The strike-through test determines the time it takes a defined fluid to fully penetrate a sample of nonwoven fabric placed on a reference absorption pad. Strike-through experiments were performed according to EDANA standard NWSP 070.3.R0 (15) and DIN EN ISO 90736-8:1998. Two (10 x 10) cm nonwoven sheets were placed on five sheets of filter paper (Ahlstrom grade 989). The stack was placed under a strike-through plate which has a defined star nozzle. 5 mL of a test liquid was discharged at a defined rate of 25 mL / 3.5 s into the star nozzle and the time until the entire liquid has penetrated into the filter paper was measured using 2 electrodes which are short-circuited as long as there is a liquid inside the nozzle. Five measurements were performed per sample set and mean and standard deviation were reported. In the case of hydrophilized nonwovens, simulated urine was used as the test liquid. Simulated urine consists of 0.9 wt% sodium chloride and distilled water and has a surface tension of (70 $\pm$ 2) mN m^{-1}. Further information on the test setup can be found in the relevant standard.

Since the production of nonwovens at the institute represents an abstraction of the industrial process, it was examined whether the wettability of nonwovens, which were produced at the pilot plant described in chapter 4.1.2 and an industrial spinning line (Reicofil R3), is comparable. The experimental setup

used in this thesis for measuring the strike-through time was developed and manufactured in-house. Therefore, the comparability of the measurement results from the self-developed experimental setup and those of a commercially available strike-through tester (Lister AC, Lenzing) had to be ensured. Figure 4.2 shows that the wettability of nonwovens produced on the pilot plant is comparable to that of nonwovens produced on an industrial setup. Furthermore, the transferability of the measurement results from the experimental setup which was developed in-house to a standard measuring instrument is given.

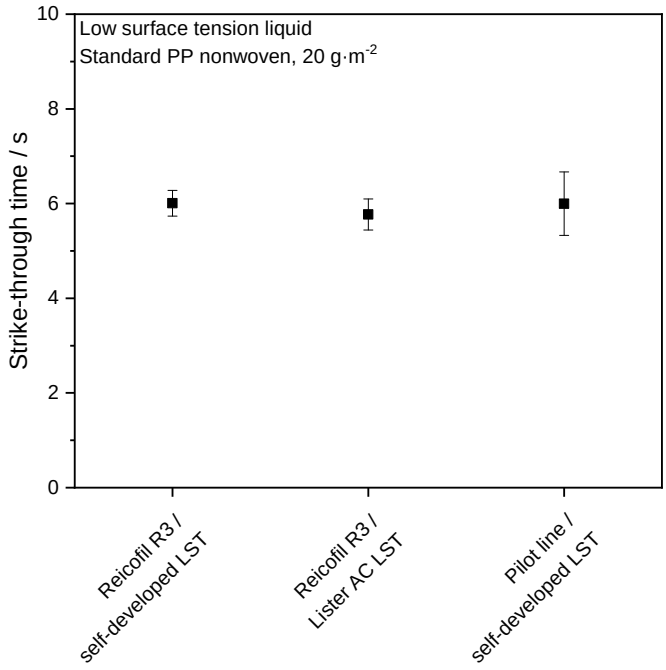

Figure 4.2: Comparison of strike-through data from nonwovens produced on a Reicofil R3 and the institute's pilot line. The data was measured with a self-developed liquid strike-through tester (LST) and a Lenzing Lister AC. Each point represents the mean value and standard deviation of 5 individual measurements. Since the simulated urine does not permeate pure polypropylene nonwovens, a low surface tension liquid was used, which consists of 0.9 wt% sodium chloride, 0.042 wt% Triton-X 100 and distilled water and has a surface tension of 32 mN m^{-1}.

4.2.1.3 Qualitative wetting tests

The quantitative and comparable evaluation of wettable and non-wettable fibers is only possible to a limited extent, since tests for hydrophilicity are usually based on absorption of water or strike-through tests which cannot

be carried out with hydrophobic substrates. Furthermore, a contact angle measurement on thin fibers can only be performed with high experimental effort due to the sample's geometry. For this reason, a qualitative evaluation was conducted to describe the wetting behavior of fibers and nonwovens in six main groups and thus compare both hydrophilic and hydrophobic samples. For this purpose, about 2 grams of fibers or nonwovens were placed in a Petri dish. A syringe was used to apply 5 mL of distilled water and the wetting behavior was determined visually. The evaluation criteria can be found in table 4.2.

Table 4.2: Qualitative evaluation of the wetting behavior of fibers in nonwovens in six groups from very good (1) to very bad (6). Reduction of the contact angle was evaluated by eye.

Evaluation	Qualitative description of wetting behavior
1	Rapid absorption, fast and uniform wetting, no capillary pressure needed for wetting.
2	Rapid wetting, moderate absorption, no capillary pressure needed for wetting.
3	Moderate absorption, reduced contact angle, capillary pressure needed for wetting.
4	Unequal wetting behavior, reduced contact angle, high capillary pressure needed for wetting.
5	Slightly reduced contact angle.
6	No absorption, water running off sample, no changes compared to pure PP.

4.2.1.4 Testing methods for durability

In the continuous use of hydrophilized nonwovens and their end products, the permanence and durability of the samples play a significant role.

Durability is defined as the non-existent transfer of the additive from the sample into water. This property is important because many end products consist of different nonwoven layers with varying wetting properties (e.g. diapers, feminine hygiene articles). If a surface-active additive significantly reduces the wetting properties of water in use, hydrophobic layers may become permeable and the function of the product may be impaired.

To test the durability, about 2 - 2.5 grams of the nonwoven samples (ten (10 x 10) cm sheets of a 20 - 25 g m^{-2} nonwoven) were placed in a tea strainer and put into 250 mL of distilled water for 300 seconds. In order to ensure the exchange of liquids, the washing water was stirred at 500 rpm with the aid of a stirring fish. After washing, the nonwovens were drained and dried under a fume hood. The washing water was collected for further experiments.

The nonwovens were measured before washing and after drying using FTIR to determine whether the surface concentration of the additive changed as a result of the washing process. For an application-oriented test, it was tested

whether the washing water passes through pure polypropylene nonwovens with a base weight of 27 g m^{-2} in a strike-through test. If no measurable transfer of the additive into the washing solution was found, the additive is evaluated as "durable".

4.2.1.5 Testing methods for permanence

Permanence is defined as the non-existent transfer of the surface-active additive to adjacent (nonwoven) layers which do not have an additive on the surface. This property is also of the highest relevance for practical applications. If the additive present on the surface of the substrate is transferred during storage, hydrophobic layers of the final product can be hydrophilized and the function of the product can be severely impaired.

To test the permanence, stacks of nonwoven sheets with a size of (10 x 10) cm were stored in alternating layers of nonwovens with and without the additive. A weight of 1 kg and a contact area of (10 x 10) cm is placed on the stack resulting in an applied pressure of approximately 980 Pa. The stack was stored at 20 °C, 40 °C and 60 °C for 30 days. After storage, the surface of the nonwoven without an additive was measured using FTIR to determine if the additive was transfered in a detectable amount to the surface of the nonwoven. Furthermore, strike-through tests of the nonwovens without an additive were performed to test whether the wetting properties of the nonwoven have been altered significantly.

4.2.2 X-Ray diffraction (XRD)

X-ray diffraction measurements used for the calibration of the FTIR method to determine the crystallinity (see also chapter 4.2.3.4) were performed on a Philips theta-theta goniometer with CuKα radiation between 5 - 40° with an increment of 0.01°, each step being measured for 10 seconds. X-ray diffraction measurements used for the structure determination of films, fibers and injection molded plates were performed on an AXS D8 Advance diffractometer (Bruker) in Bragg-Brentano geometry which was equipped with a VANTEC-1 detector and a Ni filter. Diffractograms were collected using CuKα radiation between 10 - 50° with an increment of 0.014°, each step being measured for 1 second.

Prior to evaluation, the background of the data was adjusted using the program EVA (Bruker) with a correction parameter of 0.025. In the XRD measurement, the degree of crystallinity of polymers is determined by the ratio of the peaks

which are proportional to the crystalline part and the total area under the curve (Equation 4.1) [126].

$$X_C = \frac{A_{\text{crystalline}}}{A_{\text{crystalline}} + A_{\text{amorphous}}} \tag{4.1}$$

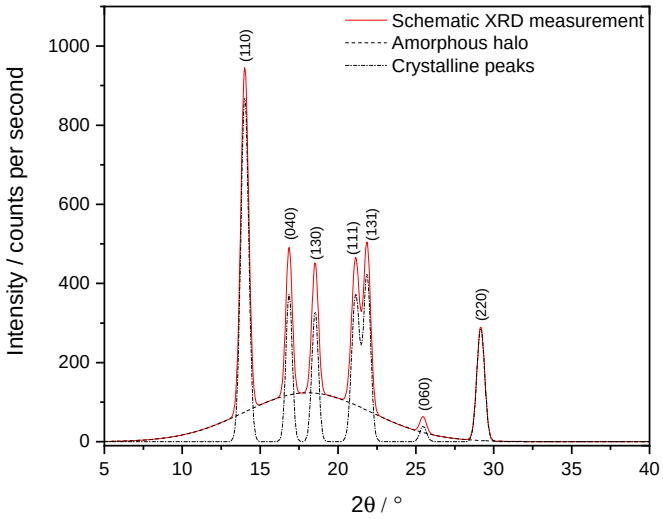

Figure 4.3: Schematic XRD measurement of isotactic polypropylene with separated amorphous halo and crystalline peaks.

The amount of crystalline and amorphous phases of the samples was determined by a fitting procedure consisting of a linear combination of Gaussian peak functions (equation 4.2) for the crystalline phases and a Bigaussian peak function (equation 4.3) for the amorphous phase.

$$\text{Intensity}(2\theta) = \frac{A \cdot e^{\frac{-4\ln(2)(2\theta - \theta_c)^2}{w^2}}}{w \cdot \sqrt{\frac{\pi}{4\ln(2)}}} \tag{4.2}$$

$$\begin{aligned} \text{Intensity}(2\theta) &= h \cdot e^{-0.5\left(\frac{2\theta - \theta_c}{w_1}\right)^2} \text{ for } (2\theta < \theta_c) \text{ and} \\ \text{Intensity}(2\theta) &= h \cdot e^{-0.5\left(\frac{2\theta - \theta_c}{w_2}\right)^2} \text{ for } (2\theta \geq \theta_c) \end{aligned} \tag{4.3}$$

The sample with the highest degree of crystallinity was evaluated first as the crystalline peaks and the amorphous halo were most pronounced for this sample. All parameters which describe the shape of the amorphous halo of the sample with the highest crystallinity (width w_1 and w_2, θ_c), except the peak height h, were kept fixed and used for all the other samples. A typical measurement and its fitting function can be seen in Figure 4.4. The coefficient of determination R^2 was between 0.948 and 0.983 for all evaluated samples, which led to a typical error in the dermination of the crystallinity of about 1 %, which is in good agreement to other publications [127]. Other evaluation methods, e.g. the use of a simple Gaussian peak function for the amorphous halo or the simultaneous adjustment of all parameters over the whole sample set (as described in a publication by Carrubba et al.[128]), yielded very comparable fitting results and calibration curves. The method for determining the degree of crystallinity has been published in [129, 130].

Reflections at 2θ = 14.1°, 16.9°, 18.6°, 21.2°, 22.1°, 25.5° and 28.5 were assigned to the α-monoclinic phase and reflections at 2θ = 14.5° and 21° were assigned to the mesomorphic phase. A β-phase was not considered as peaks which correlate with the β-phase were not found in the investigated samples. In addition, the β-phase is usually not formed in fiber grade polypropylenes or without special nucleating agents that promote the formation of the β-phase [66].

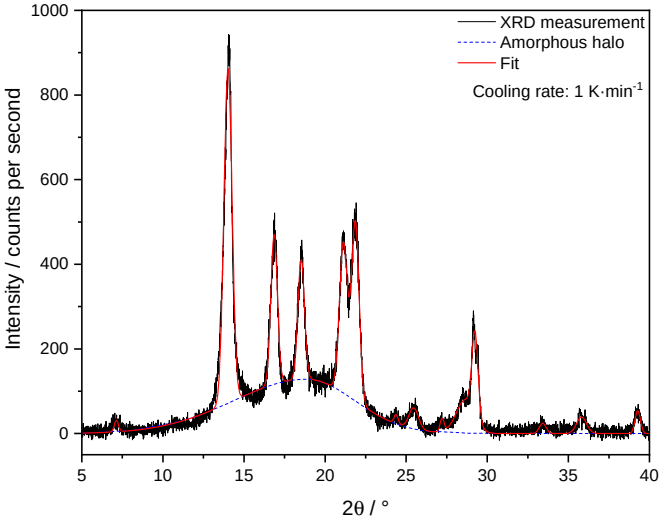

Figure 4.4: XRD measurement of polypropylene cooled with 1 K min $^{-1}$ from 200 °C to 20 °C.

4.2.3 Fourier-transform infrared spectroscopy (FTIR)

FTIR measurements (attenuated total reflection (ATR) and transmission) were performed on a Nicolet 6700 FTIR spectrometer (Thermo scientific) at a temperature of 23 °C. Each measurement was an average of 32 scans at a resolution of 4.0 cm^{-1} in a wave number range from 4000 - 650 cm^{-1}. Each specimen was measured at three different locations to ensure reproducibility throughout the sample set. Background spectra were recorded before the start of the measurements and after no more than 30 minutes or as required (high CO_2 or H_2O peaks). In the case of ATR measurements, the crystal was thoroughly cleaned with isopropanol to prevent carry-over from previous experiments after each measurement.

ATR-FTIR measurements were performed using a single bounce germanium or diamond crystal, each having an angle of reflection θ of 42 °. For a refractive index of $n_{Diamond}$ = 2.4 and $n_{Polypropylene}$ = 1.49 equation 4.4 [131] gives a penetration depth d_p of 2.55 µm at a wave number of 980 cm^{-1}. Accordingly, a penetration depth of 0.7 µm results for the germanium crystal with a refractive index of $n_{Germanium}$ of 4.0. The penetration depth of both crystals is considered as a near-surface region. An illustration of the ATR-FTIR setup with corresponding parameters is shown in figure 4.5.

$$d_p(\lambda)\,[\mu m] = \frac{10^4 \cdot \lambda\,[nm]}{2n_{\text{crystal}} \cdot \pi \cdot \sqrt{sin^2(\theta) - \left(\frac{n_{\text{sample}}}{n_{\text{crystal}}}\right)^2}} \tag{4.4}$$

ATR measurements were corrected for penetration depth throughout the spectrum according to equation 4.4. Subsequently, the baseline was corrected for peaks resulting from water vapor and carbon dioxide. All corrections were performed using the program OMNIC 9 (Thermo Scientific). No further sample preparation was necessary to measure fibers, films, bulk material or nonwovens in ATR mode.

For the transmission measurement of (bulk material) samples, the production of melt films was necessary, since bulk samples are usually too thick to be permeable by FTIR radiation. The melt films were produced with a Graseby Specac hydraulic hot press utilizing an A-ring, which is used for the production of films with an average thickness of 15 - 20 µm. To produce the melt films, 25 mg of the polymer was weighed and placed between two aluminium foils. The sample was then melted at a temperature of 175 °C and pressed with a weight of 5000 kg for 2 minutes. After pressing, the melt film was cooled in a

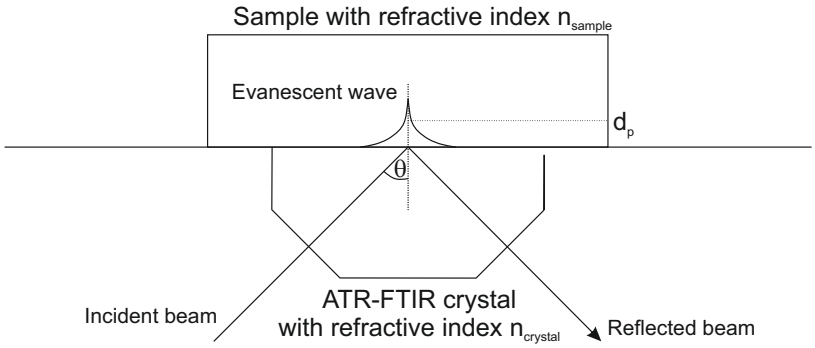

Figure 4.5: Schematic representation of the ATR-FTIR setup with the parameters used in equation 4.4.

water-cooled mold for 10 minutes. For transmission measurements of single fibers, 5 - 10 mg of the fibers were compressed under vacuum with a mass of 7000 kg for 2m̃inutes at 20 °C using a hydraulic press. This resulted in chips with a typical thickness of 10 - 15 µm, which were thin enough to be measured in transmission mode.

4.2.3.1 Determination of additive contents and the degree of crystallinity

FTIR measurements can be used to quantitatively determine the additive contents in polymer blends [132] or the degree of crystallinity of polymers [133–135] after an appropriate calibration procedure. The determination of additive concentrations using FTIR has the advantage that it is a fast and non-destructive method which allows the detection of additives on the surface as well as in the volume of the sample. Furthermore, compared to conventional methods, no extraction of the additive is necessary and therefore multiple measurements of the same sample are possible. The technique is based on the Beer-Lambert law, where the extinction E at a certain wave number λ (reciprocal of the wavelength) is defined as

$$E(\lambda) = \epsilon \cdot c \cdot d_p \tag{4.5}$$

where ϵ is the coefficient of extinction, which is usually determined via a calibration procedure, c is the concentration of the substance which shall be detected and d_p is the thickness (in transmission mode) or the penetration depth (in ATR mode) of the radiated sample.

In a two component system made from substance A and B, the equation can be expressed as:

$$E(\lambda) = \epsilon_A(\lambda) \cdot c_A \cdot d_p + \epsilon_B(\lambda) \cdot c_B \cdot d_p \tag{4.6}$$

If the penetration depth d_p is constant over the entire spectrum, d_p eliminated by forming a ratio of the area or height of two independent peaks at the wave numbers λ_1 and λ_2:

$$\frac{E_1(\lambda_1)}{E_2(\lambda_2)} = \frac{\epsilon_A(\lambda_1) \cdot c_A \cdot d_p + \epsilon_B(\lambda_1) \cdot c_B \cdot d_p}{\epsilon_A(\lambda_2) \cdot c_A \cdot d_p + \epsilon_B(\lambda_2) \cdot c_B \cdot d_p} \tag{4.7}$$

Since in a two-component system the amounts of c_A and c_B add up to one, the equation can be further simplified. After combination of the different specific extinction coefficients at a certain wave number to a correction factor k, equation 4.8 is obtained.

$$\begin{aligned} \frac{E_1(\lambda_1)}{E_2(\lambda_2)} &= \frac{\epsilon_A(\lambda_1) \cdot c_A + \epsilon_B(\lambda_1) \cdot (1 - c_A)}{\epsilon_A(\lambda_2) \cdot c_A + \epsilon_B(\lambda_2) \cdot (1 - c_A)} \\ &= k_1 \cdot c_A + k_2 \cdot (1 - c_A) \\ &= k \cdot c_A + b \end{aligned} \tag{4.8}$$

From equation 4.8 it can be concluded that the peak ratio is proportional to the concentration. This means that the peak ratio can also serve as a semi-quantitative measure of the (surface) concentration of an additive without the need for a calibration procedure. Since many different additives were used in this study and a special calibration for each additive would be very time-consuming, only the peak ratio was used if the additive was not studied in detail.

It has been shown that the peak ratio of two independent peaks and a correction factor k can be used to describe the content of a substance. Since the amounts of amorphous and crystalline phases in a semi-crystalline polymer also add up to one, this method can be easily transferred to determine the degree of crystallinity X_C of a polymer (equation 4.9).

$$\frac{E_1(\lambda_1)}{E_2(\lambda_2)} = k \cdot X_C + b \tag{4.9}$$

The methods for determining k to determine the degree of crystallinity and the additive concentration are explained in the following chapters. The general procedure for determining the degree of crystallinity using FTIR has been described in [129].

4.2.3.2 Calibration procedure for the determination of additive contents

This work focuses on the influence of different process parameters and storage conditions on the migration behavior of various additives. This chapter shows the procedure for calibrating the FTIR method using the additive $C_{18}PEO_2$, since this additive was most frequently used in this work. The calibration procedure for other additives would be analogous and can be transferred to other additive systems. The calibration requires a comprehensive set of polymer-additive blends covering the full range of expected concentration ranges. Furthermore, most additives are expected to migrate to the surface and thus show a concentration gradient towards the surface. For this reason, surface sensitive ATR-FTIR measurements are not suitable for calibration and melt films have to be prepared for measurement in transmission. The blend production was performed using a laboratory kneader and is described in detail in chapter 4.1.1. Melt films were prepared according to the procedure described in chapter 4.2.3.

Blends of the polypropylene Moplen HP561R and 0; 0.5; 1; 2; 5 and 10 wt% of the additive $C_{18}PEO_2$ were prepared, respectively. Higher concentrations led to poorly reproducible results due to the strong segregation behavior of the additive and the matrix polymer. In order to ensure that the determination of the additive concentration is not dependent on the molar mass of the polypropylene grade used, samples with a higher molar mass (Sabic 505p) and a lower molar mass (Borealis HL712FB) polypropylene were prepared. Two melt films were produced per blend, which were each measured at 3 different locations in transmission using the method described in chapter 4.2.3.

For each measurement a peak ratio was determined analogous to equation 4.8. Therefore, a linear baseline from an average height of 918 cm^{-1} to 928 cm^{-1} to an average height of 1310 cm^{-1} to 1311 cm^{-1} was drawn. This baseline lays slightly above the real baseline, especially in the case of transmission measurements. However, this effect is not as pronounced in ATR measurements and leads to

the most reproducible results across all sample geometries used. Particularly with fibers or very rough samples, strong scattering phenomena may occur due to the large surface area, causing the baseline to be strongly curved. This in turn leads to the determination of exaggerated additive concentrations in fibers if a different baseline is used. The extinction E_1 resulting from the additive is defined as the area between the baseline and the curve from 1122 cm^{-1} to 1227 cm^{-1}. This peak results from stretching vibrations of a C-O group, which is characteristic for the PEO part of the surfactant and does not occur in the polypropylene. The extinction E_2, which depends only on the penetration depth, is defined as the maximum height of the peak between a wave number of 960 to 980 cm^{-1} and the baseline. The band at 973 cm^{-1} is a characteristic band for isotactic segments in polypropylene and therefore often used as an internal reference for the penetration depth in FTIR measurements of polypropylene [23, 136, 137]. The procedure for determining E_1 and E_2 is illustrated in figure 4.7.

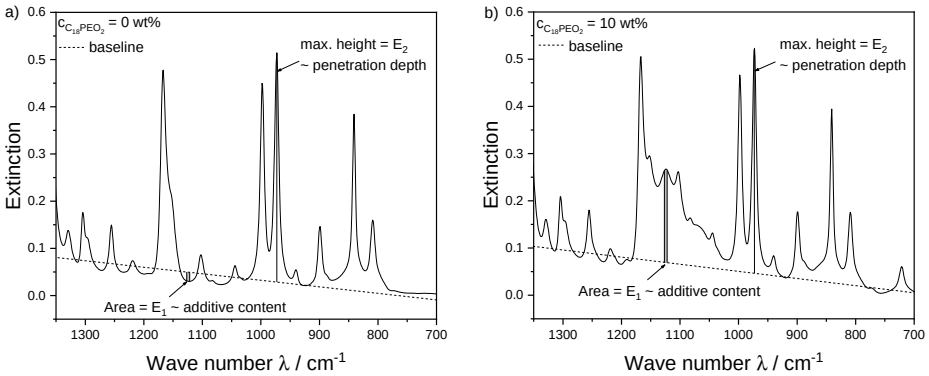

Figure 4.6: Procedure for obtaining E_1 and E_2 from data measured via FTIR. Although the baseline overestimates the real baseline, it provided the most reproducible calibration results, especially for highly scattering samples measured in ATR mode. Figure (a) shows a sample without any $C_{18}PEO_2$ added, figure (b) shows a sample with 10 wt% $C_{18}PEO_2$.

The initial concentration is then plotted over the peak ratio E_1/E_2 and fitted linearly (figure 4.7 (a)). The resulting calibration line is:

$$c_{C_{18}PEO_2}\left(\frac{E_1(1122\ \mathrm{cm}^{-1})}{E_2(973\ \mathrm{cm}^{-1})}\right) = 0.94 + 4.46 \cdot \frac{E_1}{E_2} \qquad (4.10)$$

Equation 4.10 allows to directly determine the concentration of $C_{18}PEO_2$ by calculating the peak ratio. Figure 4.7 (b) shows that the method has a

relative error of less than 10%. This is due to experimental scattering and the segregation of additive and polymer during calibration sample preparation.

a)

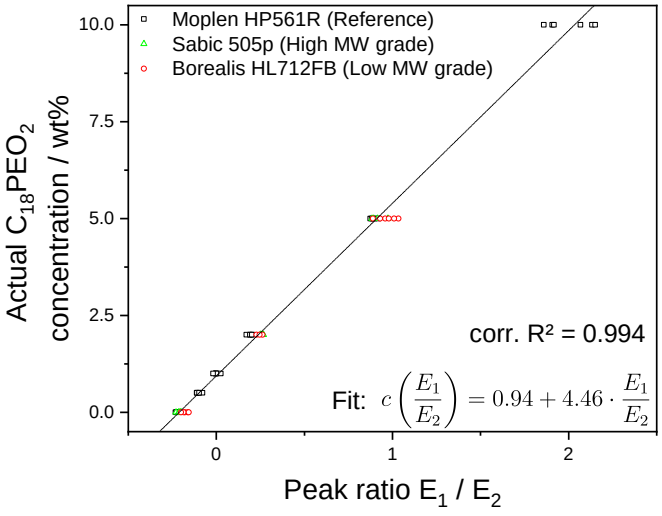

b)

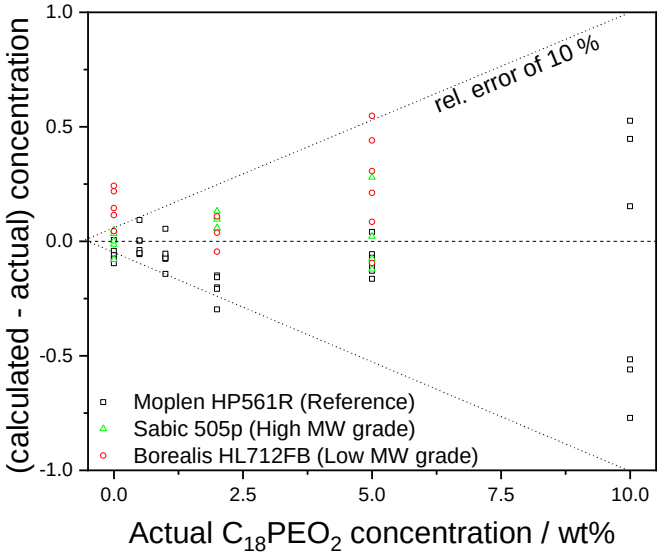

Figure 4.7: Calibration curve (a) and difference between actual and calibrated values (b) for the calibration of the FTIR method using $C_{18}PEO_2$ as an additive.

4.2.3.3 Method validation

To verify the transferability of the near-surface concentration of the additive determined by FTIR to the wetting behavior of fibers and plates, the wetting behavior of samples with different surface concentrations of $C_{18}PEO_2$ was evaluated.

Figure 4.8 illustrates that both the contact angle and the wettability of the fibers correlate with the surface concentration. If there is no decteable amount of additive on the surface, the wetting behavior does not change compared to pure polypropylene. From a surface concentration of about (1.5 ± 0.5) wt% of $C_{18}PEO_2$, the contact angle of plates decreases and fibers become much more wettable. From a concentration of approximately 3 wt%, all substrates were excellently wettable. Although FTIR cannot be used to determine the alignment of additives on the surface or the exact concentration directly on the surface at a penetration depth of a few Å, it offers a practical tool for evaluating the migration behavior of (hydrophilic melt) additives.

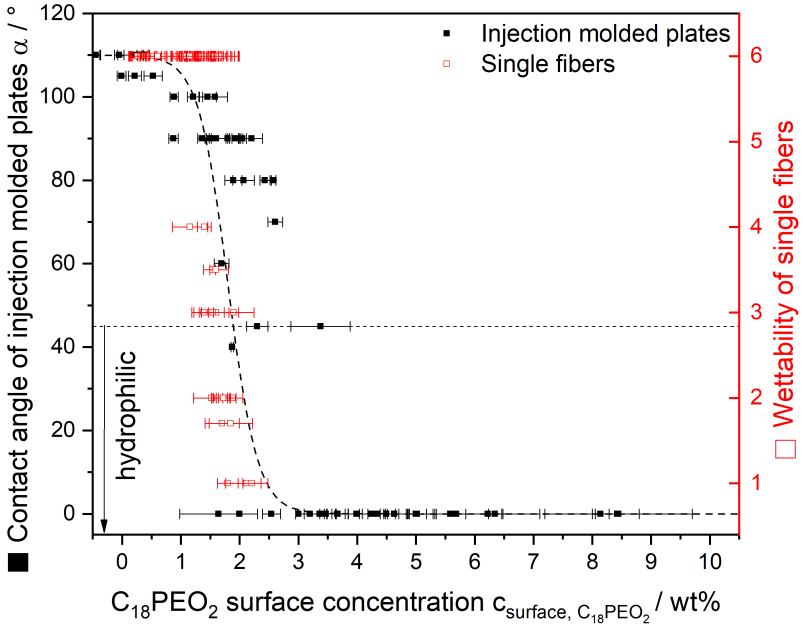

Figure 4.8: Contact angle of injection molded plates and wettability of single fibers as a function of the $C_{18}PEO_2$ surface concentration to illustrate that the surface concentration determined by FTIR correlates with the wettability of the substrate. Surface concentration determined via FTIR using a diamond crystal with a penetration depth d_p of 2.55 µm. The dotted line in the figure is drawn to guide the eye.

4.2.3.4 Calibration procedure for the determination of the crystallinity

This chapter covers the calibration procedure for determining the degree of crystallinity using FTIR. In order to obtain a reliable calibration curve, it was necessary to use samples covering the entire range of achievable degrees of crystallinity from 40 - 60 % [78] in an isotactic polypropylene. For this purpose, calibration samples were punched out of films with a uniform thickness and cooled under well defined conditions. The uniform sample geometry allowed homogeneous cooling conditions and therefore keep the crystallinity gradient over the sample profile as low as possible.

The polypropylene films were produced using a hot press (LaboPress 200 T, Vogt Maschinenbau GmbH) at a temperature of 240 °C to yield films with an area of (8 x 8) cm and a uniform thickness of approximately 280 µm. The material was heated for 1 minute without any pressure, for 2 minutes with a pressure of 10 bar and for 2 minutes with a pressure of 200 bar, respectively. The resulting films were cooled between two ceramic plates to obtain an even surface structure. Samples with a diameter of 4 mm were punched out of these films and placed in differential scanning calorimeter (DSC) pans (Tzero aluminium, TA instruments). The use of other DSC pans resulted in samples with a strong crystallinity gradient accross the profile.

The calibration samples were heated to 200 °C, held for 5 minutes at 200 °C and then cooled using various methods. Low cooling rates (1 K min^{-1} and 20 K min^{-1}) were achieved by controlled cooling programs using a DSC (DSC Q 2000, TA Instruments). High cooling rates were achieved by heating the DSC pans to 200 °C in a hot air oven and cooling them in a salt-water-ice mixture, resulting in cooling rates of approximately 3500 K min^{-1} (estimated according to an approach by Böckh and Wetzel[138]). The samples were prepared with and without stirring and with and without subsequent tempering for 60 minutes at elevated temperatures of 50 °C and 80 °C, respectively. An overview of all calibration samples and their manufacturing processes can be found in table 4.3.

The general method for determining the degree of crystallinity using FTIR measurements has already been described in chapter 4.2.3.1. Comparable techniques for determining the degree of crystallinity using FTIR spectroscopy have been published by Burfield et al.[133], Huy et al.[134] or Kilic et al.[135].

To determine the degree of crystallinity, the ratio of the peak height of the peak at 998 cm^{-1} h_{998} and the peak height of the peak at 973 cm^{-1} h_{973} is formed. The peak at 998 cm^{-1} corresponds to the crystalline phase in polypropylene.

Table 4.3: Overview of all samples used to calibrate the method to determine the degree of crystallinity via FTIR.

Sample ID	Cooling method	Cooling rate
1	Salt-ice-water + stirring	≈ 3500 K min^{-1}
2	Salt-ice-water	≈ < 3500 K min^{-1}
3	Salt-ice-water + 50 °C annealing	≈ < 3500 K min^{-1}
4	Salt-ice-water + 80 °C annealing	≈ < 3500 K min^{-1}
5	DSC	20 K min^{-1}
6	DSC	1 K min^{-1}

The height of this peak increases linearly with the degree of crystallinity [133, 139, 140]. Since the α and β crystal phases in polypropylene have similar spectra, the peak height h_{998} can therefore be regarded as a measure of the total crystallinity of the sample and does not have to be subdivided into individual crystal phase fractions. The peak at 973 cm^{-1} correlates linearly with the penetration depth of the IR radiation and is not dependent on the degree of crystallinity [23, 136, 137]. Therefore the ratio of the maximum peak heights of the peak at 998 cm^{-1} h_{998} and 973 cm^{-1} h_{973} is regarded as a linear proportional measure for the degree of crystallinity X_C (equation 4.11).

$$\frac{h_{998}(998\ \mathrm{cm}^{-1})}{h_{973}(973\ \mathrm{cm}^{-1})} = k \cdot X_C + b \tag{4.11}$$

The peak height of both peaks was determined by first drawing a linear baseline through the data points at 1025 cm^{-1} and 950 cm^{-1}. The maximum height between the signal and the baseline was then measured in the range of 960 cm^{-1} and 985 cm^{-1} (for the peak at 973 cm^{-1}) and in the range of 985 cm^{-1} and 1005 cm^{-1} (for the peak at 998 cm^{-1}). Figure 4.9 shows a section of the FTIR spectrum of a rapidly cooled sample that should have a low crystallinity and a spectrum of a sample that was slowly cooled and therefore should have a high crystallinity.

Since an XRD measurement took about 10 hours, it had to be verified that no changes in the degree of crystallinity occurred during the measurement due to relaxation or recrystallization phenomena of metastable crystal phases. Figure 4.10 shows the peak ratio h_{998}/h_{973} which is proportional to the degree of crystallinity and thus illustrates the recrystallization behavior of a rapidly

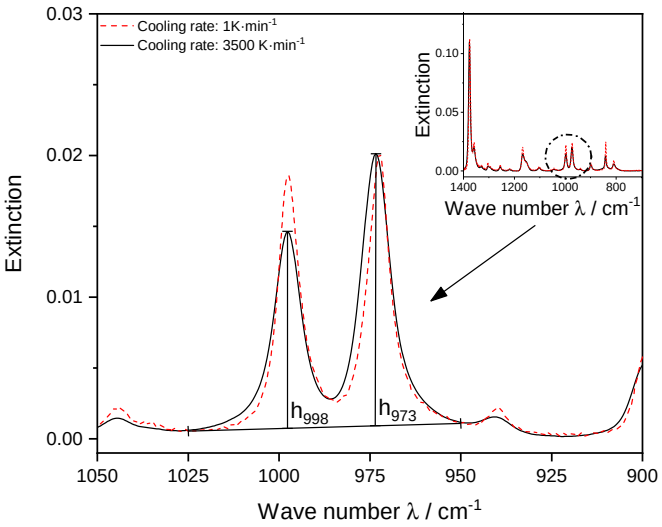

Figure 4.9: FTIR measurement of a rapidly and a slowly cooled polypropylene sample used to calibrate the method to determine the degree of crystallinity using FTIR.

cooled sample from the calibration set. Usually the samples showed slight relaxation phenomena immediately after production and the crystallinity did not change after a storage time of 24 hours. All samples were measured using FTIR immediately after production and 1, 2 and 3 days after manufacture to obtain information from two different penetration depths and to ensure that the degree of crystallinity did not change during storage. It was verified that all samples of the calibration sample set were free of crystallinity gradients (see also figure A.3, appendix A.2.2).

Two days after sample preparation, XRD measurements were performed to determine the crystallinity of the samples from the calibration set according to the procedure described in chapter 4.2.2. By plotting the crystallinity determined by XRD over the peak ratio h_{998}/h_{973} determined by FTIR measurements, a calibration line can be obtained by a linear fit through the origin (figure 4.11). The slope of this line can now be utilized to determine the degree of crystallinity of polypropylene samples:

$$X_C = (61.4 \pm 1.1)\% \cdot \frac{h_{998}}{h_{973}} \tag{4.12}$$

The value k = 61.4 % is in rather good agreement with the value of 56 % published by Huy et al. [134]. In Huy's work, the method was calibrated using differential scanning calorimetry. Since no heat of fusion is mentioned which

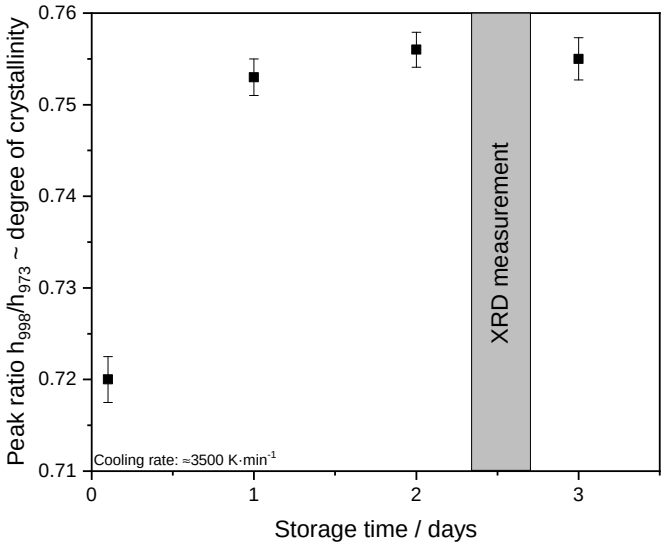

Figure 4.10: Peak ratio determined using FTIR measurements of a sample which was rapidly cooled in an salt-ice-water mixture under stirring.

was used for the determination of the degree of crystallinity, an overestimation of the degree of crystallinity may have occurred yielding slightly different results.

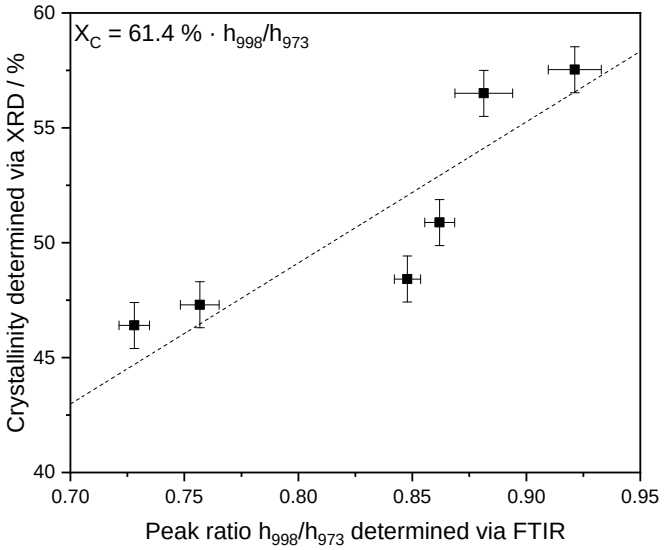

Figure 4.11: Calibration line for determining the degree of crystallinity of polypropylene using FTIR measurements.

The experimental data from this chapter were partially taken from Wenzke's master thesis (supervised by F. J. Lanyi) and analyzed independently within this thesis.

4.2.4 Thermogravimetric analysis (TGA)

Thermogravimetric analysis was used to determine the thermal degradation behavior of matrix polymers and additives. The experiments were performed on a TGA Q5000 (TA Instruments). The samples were heated from room temperature to 600 °C at a heating rate of 10 K· min^{-1} under a constant nitrogen or oxygen flow of 20 mL· min^{-1} unless otherwise specified. The relative weight as a function of temperature is derived from the quotient of the current weight of the sample and the initial weight.

4.2.5 Differential scanning calorimetry (DSC)

Differential scanning calorimetry measurements were performed on a DSC Q 2000 (TA Instruments). For each sample, two heating runs and one cooling run were conducted at a rate of 10 K · min^{-1} under constant nitrogen flow of 20 mL min^{-1}, unless otherwise specified. Pure polypropylene and polypropylene-additive blends were measured from -40 °C to 200 °C. Pure additives were measured from -60 °C to 80 °C. Between heating and cooling, the samples were kept at isothermal conditions for 180 seconds. The second heating run was used to determine material properties such as the melting temperature. The data evaluation was performed using the program TA Universal Analysis 2000 (Build 4.5.0.0.5). The melting temperature is defined as the minimum of the most pronounced melting peak. The procedure (measurement and evaluation) is a standard procedure according to DIN EN ISO 11357.

4.2.6 Gel permeation chromatography (GPC)

A gel permeation chromatography (PL-GPC 220 by Agilent) equipped with high temperature low shear GPC columns (1 x UT807, 3 x UT806 by Shodex) and coupled with a multi-angle light scattering detector (Dawn Eos by Wywatt Technology) was used for molecular characterization of the raw materials. By using a light scattering detector, the absolute weight average molar mass can be determined without being dependent on a polymer standard. Due to the poor solubility of polyolefins, both the solution preparation and the measurement itself had to take place under elevated temperature. The polypropylene was dissolved for 2 hours at 160 °C in 1,2,4-tricholobenzene in order to obtain

a solution with a concentration of 3 g L^{-1}. To compensate the thermal degradation of polypropylene, 1 g L^{-1} of Igranox 1035 (stabilizer) was added. The solution was injected into the GPC at a temperature of 140 °C, at a flow rate of 0.5 mL min^{-1} and an injection volume of 200 µL. To ensure the reproducibility of the results, 5 measurements were conducted for each polymer sample. The mean value and the standard deviation of the 5 measurements are reported. Since the light scattering detection is limited in ranges of small molar masses, a universal calibration by means of calibration polystyrenes in the range of 560 - $11 \cdot 10^6$ g mol^{-1} was used for the determination of the number-average molar mass. As a measure for the width of the molecular weight distribution, the polydispersity PD is used, which is calculated from the quotient of the weight-average and number-average molar mass:

$$PD = \frac{M_{\text{w, Light scattering}}}{M_{\text{n, PS calibration standards}}} \tag{4.13}$$

4.2.7 Microscopy

To evaluate the (crystal) morphology of the polypropylene using light microscopy, the samples were prepared using an etching procedure to remove amorphous regions and expose the crystallites according to a method by Aboulfaraj et al. [141].

The polypropylene samples were etched with a potassium permanganate-based acid solution prepared from 10 mL concentrated orthophosphoric acid (VWR Chemicals), 18.4 mL sulfuric acid (Carl Roth GmbH) and 0.67 g potassium permanganate (VWR Lifescience). The samples were etched for 18 hours, then cleaned in distilled water and acetone and finally dried. The microscopic images were taken on a VH-1000 microscope (Keyence), which was equipped with a VH-Z250R objective.

5 Materials

5.1 Polypropylene

In this work the linear, isotactic polypropylene HP561R supplied by LyondellBasell is used as a reference material for nearly all experiments. This polypropylene grade is a standard spingrade and one of the most widely used polypropylene grades for the production of nonwovens throughout Europe. In order to demonstrate the influence of the matrix polymer molar moss on the migration of additives, Exxon Mobil 3155 was selected as a low molar mass polypropylene grade (usually applied for the production of spunbond nonwovens) and Sabic 510 A as a high molar mass grade (usually applied for the production of coarse staple fibers).

In order to exclude any influence of the molar mass on the calibration of the methods using FTIR for quantification, polypropylene grades Borealis HL712 and Sabic PP 505p were selected, which exhibit even greater deviations of the molar mass from the reference polypropylene. For more detailed information on the polypropylenes used in this work, see table 5.1.

Table 5.1: Overview of the polypropylenes used in this work.

Producer	Trade name	MFI (230 °C / 2.16 kg) / g 10 min^{-1}	Industrial application	Utilization in this work
Borealis	HL712B	1200	Meltblown PP	Calibration standards FTIR
Exxon Mobil	3155	36	Spunbond PP	Low MW spin grade
Lyondell Basell	Moplen HP561R	25	Spunbond PP	Reference PP
Sabic	PP 510A	10.5	Coarse staple fibers & yarns	High MW spin grade
Sabic	PP 505p	2	Sheet & thermoforming	Calibration standards FTIR
Borealis	WB135	2.4	High melt strength PP	Add long-chain branches to PP

5.2 Potential melt additives

From a practical point of view, the properties of a hydrophilic melt additive should fulfill several boundary conditions, e.g.:

- *a melting point above room temperature*
  to ensure that the additive can achieve sufficient durability and can not be rubbed off the substrate
- *a high degradation temperature (> 290 °C)*
  to endure the process of fiber spinning which is usually performed at temperatures above 250 - 270 °C

- *sufficient immiscibility with the matrix polymer*
  to allow migration from a thermodynamic perspective
- *a rather low molar mass (< 5000 g mol^{-1})*
  to ensure the additive can still migrate inside the polyolefin matrix from a kinetic perspective
- *commercial availability in larger quantities*

In addition to these practical implications, the additives should be harmless to health. On the basis of these considerations, three main types of surfactants which are available within a broad range of molecular architectures were chosen to be tested for the use as a melt additive.

- Ethoxylated alcohols
- Polyoxyethylene-polyoxypropylene-block-copolymers
- Sorbitan monoesters

For further characterization of the additives, the hydrophilic-lipophilic balance (HLB value) is utilized, which indicates the ratio of hydrophilic and lipophilic components of the surfactant molecule:

$$\mathrm{HLB} = 20 \cdot \left(1 - \frac{M_{W,\mathrm{lipophilic}}}{M_{W,\mathrm{total}}}\right) \tag{5.1}$$

Ethoxylated alcohols

Ethoxylated alcohols are currently the only additives which are used in a commercial context as a hydrophilic melt additive for polypropylene. Techmer PM filed a patent [19] in 1998 where structures with the formula R-$C_6H_4(OCH_2CH_2)_nOH$, wherein R is an alkyl group having 8 to 22 atoms and n is in a range of 1 to about 10, are claimed as melt additives which are able to render polyolefin fibers hydrophilic. Datla investigated the use of ethoxylated alcohols with different chain lengths as melt additives, mainly for polypropylene films. Ethoxylated alcohols with 2 ethylene oxide units increase hydrophilicity of both polypropylene films and nonwovens [12, 14]. Datla's studies lack a basic understanding of the influence of molecular structure on the additive's ability to provide wettability to a polyolefin surface. Due to the reported ability to hydrophilize a polypropylene surface, a broad portfolio of ethoxylated alcohols was used for this study to evaluate their hydrophilization effect as a function of chemical structure. An overview of all ethoxylated alcohols used in this study can be found in table 5.2.

Polyoxyethylene (PEO) - Polyoxypropylene (PPO) - Block - Copolymers

PEO-PPO-PEO block copolymers are commonly used for emulsification and dispersion applications. Due to their high molar mass of 4500 - 15000 g mol^{-1} they allow the investigation of the migration behavior of comparatively large molecules. All molecules have a high number of hydrophilic PEO groups (high HLB value), making all additives highly soluble in water. Therefore good wetting of the surface in case of surface migration is assumed. Furthermore the additives are solid at room temperature and have a well-defined and comparatively low melting point between 50 and 60 °C. All PEO-PPO-PEO block copolymers used in this thesis are listed in table 5.3.

Sorbitan monoesters

Sorbitan monoesters are also used as wetting agents as well as emulsifiers and dispersants. They have a similar structure to ethoxylated alcohols, but their hydrophilic head group contains more -OH groups. With tail groups and molar masses comparable to those of ethoxylated alcohols, it is therefore possible to compare different head group architectures. An overview of all sorbitan monoesters used in this study can be found in table 5.4.

Table 5.2: Properties of ethoxylated alcohols with the structure CH_3-$(CH_2)_m$-CH_2-$(OCH_2CH_2)_n$OH. Values marked with * are calculated from data sheet information. All Brij types were kindly provided by Croda.

Additive trade name	m	n	terminology in thesis	M_W / g mol^{-1}	HLB	Physical state at T = 25 °C
Brij L4	10 - lauryl	4	$C_{12}PEO_4$	390	5.9*	liquid
Brij L23	10 - lauryl	23	$C_{12}PEO_{23}$	1150	15.6*	solid
Brij C2	14 - cetyl	2	$C_{16}PEO_2$	358	5.9*	liquid
Brij C20	14 - cetyl	20	$C_{16}PEO_{20}$	1150	15.6*	solid
Brij CS17	14/16	17	$C_{15}PEO_{17}$	1032	14.8*	solid
Brij CS20	14/16	20	$C_{15}PEO_{20}$	1164	15.4*	solid
Brij S2	16 - stearate	2	$C_{18}PEO_2$	386	4.9*	solid
Brij S10	16 - stearate	10	$C_{18}PEO_{10}$	738	12.4*	solid
Brij S10	16 - stearate	20	$C_{18}PEO_{20}$	1178	15.3*	solid
Brij S100	16 - stearate	100	$C_{18}PEO_{100}$	4698	18.8*	solid
Brij O2	16 - oleate	2	$C_{18,double}PEO_2$	386	5.4*	liquid
Brij O3	16 - oleate	3	$C_{18,double}PEO_3$	430	6.9*	liquid
Brij O5	16 - oleate	5	$C_{18,double}PEO_5$	518	9.2*	liquid
Brij O10	16 - oleate	10	$C_{18,double}PEO_{10}$	738	12.4*	liquid
Brij O20	16 - oleate	20	$C_{18,double}PEO_{20}$	1178	15.2*	solid
Unithox 450	24*	12*	$C_{26}PEO_{12}$	920	7.7*	solid
Unithox 720	36*	7*	$C_{38}PEO_7$	875	12.1*	solid
Unithox 750	37*	18*	$C_{39}PEO_{18}$	1400	12.0*	solid

Table 5.3: Properties of PEO-PPO-block-copolymers with the structure $(OCH_2CH_2)_x$-$(OCH_3CH_2)_y$-$(OCH_2CH_2)_z$. All additives were kindly provided by Croda.

Additive trade name	$M_{W,\ PPO}$ / g mol^{-1}	PEO proportion / %	$M_{W,\ total}$ / g mol^{-1}	HLB	Physical state at T = 25 °C
Synperonic 38	900	80	≈ 4500		solid
Synperonic 87	2400	70	≈ 8000		solid
Synperonic 88	2400	80	≈ 12000		solid
Synperonic 127	3600	70	≈ 12000	22	solid
Synperonic 908	2700	80	≈ 13500	>20	solid
Synperonic 108	3000	80	≈ 15000	24	solid

Table 5.4: Properties of sorbitan mono- and triesters with the structure CH_3-$(CH_2)_m$-CH_2-$C_7H_{11}O_6$. All additives were kindly provided by Croda.

Additive trade name	m	M_W / g mol^{-1}	HLB	Physical state at T = 25 °C
Span 20 (sorbitan monolaureate)	9 - laureate	340	8.6	liquid
Span 40 (sorbitan monopalmitate)	13 - palmitate	402	6.7	solid
Span 60 (sorbitan monostearate)	15 - stearate	430	5	solid
Span 65 (sorbitan tristearate)	15 - tristearate	960	2.1	solid

6 Results and discussion

6.1 Raw material characterization

This chapter covers the fundamental characterization of the polypropylenes and additives used in this thesis and serves mainly to list the basic properties of the materials.

6.1.1 Matrix polymers

Molar mass distribution

Table 6.1 lists the number average M_n, the weight average M_w and the polydispersity of the polypropylenes used in this thesis. The corresponding molar mass distribution functions can be found in figure A.4 in the appendix.

Table 6.1: Number and weight average molar masses and polydispersity of the polyproylenes used in this thesis.

Producer	Trade name	MFI (230 °C) / g 10 min^{-1}	M_n / kg mol^{-1}	M_w / kg mol^{-1}	Polydispersity
Borealis	HL712B	1200	18 ± 2.2	125.7 ± 1.7	7.1 ± 0.8
Exxon Mobil	3155	36	36.9 ± 3.9	176.4 ± 4.8	18 ± 0.3
Lyondell Basell	Moplen HP561R	25	43.4 ± 0.8	185.9 ± 2.1	4.3 ± 0.1
Sabic	PP 510A	10.5	31.4 ± 0.8	274.2 ± 1.4	8.7 ± 0.3
Sabic	PP 505p	2	77.2 ± 7.7	425.6 ± 9.2	5.6 ± 0.4
Borealis	WB135	2.4	64.0 ± 2.0	494.0 ± 12.0	7.7 ± 0.2

Thermal analysis

Table 6.2 shows the melting points T_m, the melting enthalpies ΔH_m and the glass temperatures T_g of all polypropylenes used in this work. There are only minor differences between the individual polypropylenes, as all polypropylenes besides the long chain branched WB-135 grade are linear isotactic polypropylenes. Especially the grades used for the spinning trials (HP561R, 3155 and PP 510A) are highly comparable when it comes to their thermal properties. The corresponding DSC curves can be found in the appendix in figure A.5.

Table 6.2: Thermal properties of the polypropylenes used in this thesis.

Producer	Trade name	T_g / °C	T_m / °C	ΔH_m / J g^{-1}
Borealis	HL712B	-2	156.5	79
Exxon Mobil	3155	ca. 5	160.2	92
Lyondell Basell	Moplen HP561R	-5	161.2	93.5
Sabic	PP 510A	4.6	163.1	100.9
Sabic	PP 505p	-1.9	162.2	97
Borealis	WB135		163	

6.1.2 Additives

Molar mass distribution

Since a broad spectrum of additives was selected as potential melt additives and the determination of the molecular weight distribution is comparatively complex, only the additives investigated in detail were analyzed by gel permeation chromatography (GPC). The results are presented in table 6.3 and show that the additives are narrowly distributed, i.e. very pure. The deviations from the calculated molar mass result from the circumstance that in the GPC experiment the molar masses are related to a polystyrene standard. This means that the molar mass determined for the additive molecule corresponds to that of a polystyrene molecule with the same hydrodynamic radius. For this reason, the calculated molar mass is always used for further calculations, since the uncertainty caused by the polystyrene standard can thus be neglected.

Thermal properties and additive melting point

Melting an additive greatly increases the mobility of the molecule. This in turn can lead to the additive migrating to the surface faster or not being durable or permanent due to a higher mobility on the surface. For this reason, DSC experiments were performed to determine the melting point of the additives. The results are shown in figure 6.1. The melting point increases with increasing CH_2 and PEO chain length, and thus with the molar mass. The length of the hydrophobic part of the surfactant is most decisive for the melting point. If there is a double bond in the hydrophobic part of the chain, the mobility of the molecule is restricted and the crystallization of the additive is strongly inhibited, which leads to a decrease of the melting point. For this reason, the

Table 6.3: Molecular properties determined via GPC measurements of the most frequently used additives in this work. The corresponding molecular weight distributions can be found in the appendix (figure A.8).

Additive	$M_{w,\,calculated}$ / g mol^{-1}	$M_{n,\,GPC}$ / g mol^{-1}	$M_{w,\,GPC}$ / g mol^{-1}	Polydispersity
$C_{18}PEO_2$	386	488	571	1.17
$C_{18}PEO_{10}$	738	995	1149	1.15
$C_{18}PEO_{20}$	1178	1614	1846	1.14
$C_{18}PEO_{100}$	4698	5446	5822	1.06

melting point of $C_{18,double}PEO_n$ additives is greatly reduced. However, the results shown are only to be seen as a rough estimate, since some additives (especially from the Unithox series) tend to have very broad melting peaks (see also figure A.7 in the appendix). These broad melting peaks are probably due to impure crystallization and a broad molar mass distribution of the additive. DSC curves of the most frequently used additives can also be found in appendix A.3.2. A complete characterization of the melting temperatures and peaks are presented in table A.1 of the appendix. The characterization of sorbitan monoesters and PEO-PPO-PEO block copolymers can also be found in the appendix (figure A.9).

a)

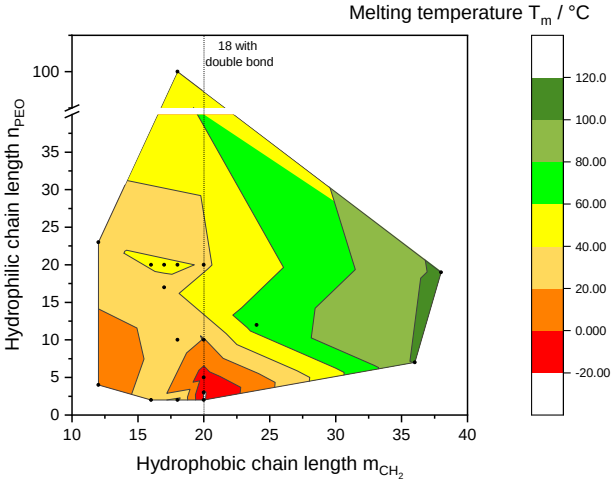

b)

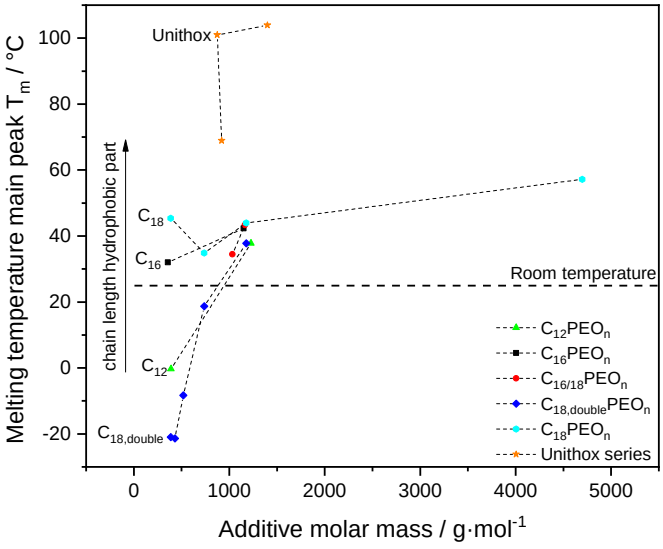

Figure 6.1: Melting temperature as a function of the molecular structure (a) and the molar mass (b) of the additives used in this thesis.

6.2 Degradation of matrix polymer and additives

Polypropylene is usually processed in the melt spinning process at temperatures between 250 °C and 290 °C. This is about 100 °C above the melting point of the polymer and approximately 200 °C above the melting point of the additives, which leads to the assumption that both the matrix polymer and the additive could significantly degrade during production. The following chapter will show whether the extrusion step can influence the matrix polymer or the additive. Furthermore, it is investigated whether polymer chains can be mechanically degraded as a result of the stretching during the process.

6.2.1 Degradation of matrix polymer

First, it was estimated to what extent the process conditions affect the degradation of the matrix polymer. The influence of the process temperature, the residence time and the stretching speed of the fibers was investigated. The process temperature and residence time increase or extend the thermal load in the process and can thus favor a thermal degradation of the polypropylene. At high stretching speeds, the polymer chains could be mechanically degraded or torn apart. Figure 6.2 shows a summary of the results.

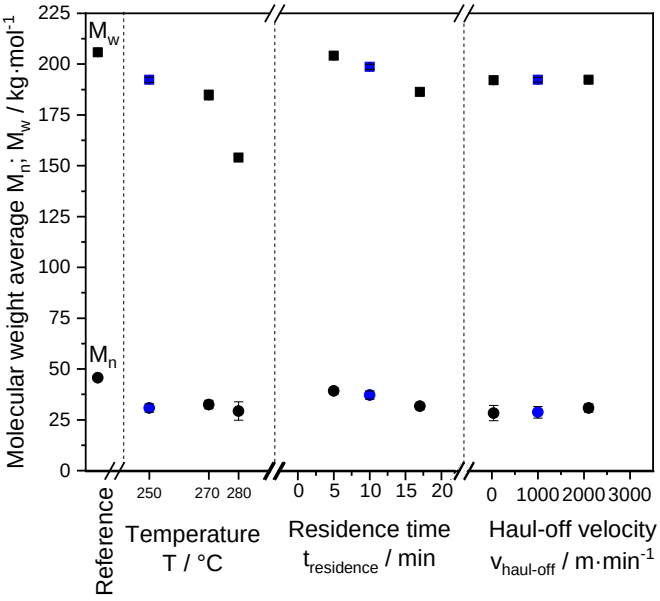

Figure 6.2: Influence of process temperature, residence time and haul-off velocity on the number and weight average molar mass of the matrix polypropylene. The process conditions were changed while maintaining the standard process parameters. The reference sample is virgin polypropylene which was not processed. Standard process settings highlighted in blue.

The experiment demonstrates that only the process temperature and the residence time have an influence on the thermal degradation of the polypropylene and that degradation is most pronounced at process temperatures of 280 °C and above. Commercial polypropylenes are provided with a stabilizer compound to compensate the thermal degradation in the process. At a temperature of 280 °C and above, the stabilizer is no longer able to compensate for the entire thermal degradation and the polymer is permanently thermally damaged. The same applies to a residence time that is significantly higher than the standard residence time of 10 - 12 minutes. An influence of the stretching conditions on the degradation of the polypropylene could not be demonstrated. The resulting forces are therefore only relevant for structure formation and too low to degrade the polymer mechanically.

In summary, it is concluded that under standard processing conditions no significant change of the polypropylene molar mass is to be expected. Detailed molecular weight distributions and polydispersities of the experiments can be found in the appendix in figure A.11, A.12 and A.13.

6.2.2 Degradation of additives during the process

In order to investigate the degradation of the additives and the influence of molecular architecture on degradation, TGA measurements of the pure materials were performed. All TGA measurements were carried out under nitrogen atmosphere. Since the material is melted and degassed in the extruder, a nitrogen atmosphere reflects the real process conditions better than an ambient air or oxygen atmosphere.

The additives $C_{18}PEO_2$, $C_{18}PEO_{10}$, $C_{18}PEO_{20}$ and $C_{18}PEO_{100}$ were investigated as they are most commonly studied in this thesis. These additives differ only in the number of PEO units in the hydrophilic part and thus in molar mass. Figure 6.3 shows the TGA measurements of these materials as well as polypropylene as a reference. With increasing PEO chain length the degradation temperature of the additive increases and runs into a plateau at about 400 °C. To obtain a comparable value for the degradation temperature, the maximum degradation rate was used, which is corresponding to the inflection point of the TGA curve. The degradation temperature of $C_{18}PEO_{100}$ (400 °C), corresponds approximately to the degradation temperature of pure PEO with a molar mass of 6000 g mol^{-1}[142] while 200 °C, the degradation temperature of $C_{18}PEO_2$ corresponds to the degradation temperature of pure octadecane [143]. In addition, as the PEO chain length increases, the degradation peaks become more narrow and the degradation more controllable and predictable.

The experiment illustrates that at a process temperature of 250 °C the additives with a higher PEO chain length (≥ 10 PEO units) do not experience any significant degradation phenomena. However, the degradation of $C_{18}PEO_2$ starts well before the process temperature. The first degradation phenomena already occur at approximately 200 °C and the maximum degradation rate of about 220 °C is 30 °C below the process temperature.

To investigate the degradation of $C_{18}PEO_2$ under more process-relevant conditions, isothermal TGA experiments were performed (figure 6.4). The experiments were not carried out with the pure additive but with the masterbatch, which contains 20 wt% $C_{18}PEO_2$ and 1 wt% Irgafos 168 as an antioxidant. Figure 6.4 shows that even under a nitrogen atmosphere considerable amounts of the additive seem to degrade thermally until the process temperature is reached. Assuming that the polypropylene is completely stable under these conditions, this means that about 85 % of the additive mass are lost during the process. The degradation under ambient air is even more pronounced, which also leads to permanent damage of the polypropylene.

In order to estimate the real degradation during the process using process-relevant additive amounts, fibers with an active additive concentration of approximately 1.8 wt% were spun using different residence times by alternating the melt pump speed. Melt films were produced from the fibers and measured using FTIR to detect the total additive amount in the fibers. The results are shown in figure 6.5. The experiments suggest that degradation is far less severe than it was initially assumed from the TGA experiments. A certain degradation in the process can be demonstrated, which is particularly evident at longer residence times. However, at a residence time of about 10 minutes, the degradation of the additive is relatively low at only about 10 - 15 % of the initial concentration. Since no degradation problems occurred during the regular processing of $C_{18}PEO_2$ in the melt spinning process, it is assumed that the TGA experiments show no degradation but evaporation effects. For this reason, TGA measurements can only be used to a limited extent to evaluate the stability of the additives. Since even the lowest molar mass additives did not show any significant degradation in the process, the additives used in this thesis are considered to be stable under standard process conditions.

a)

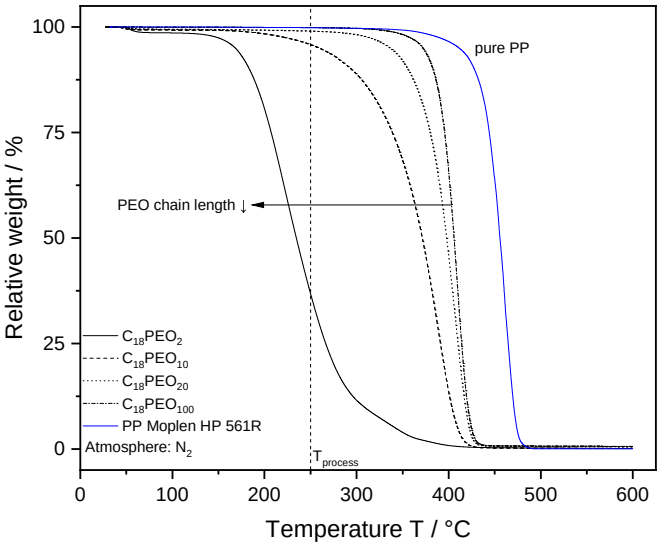

b)

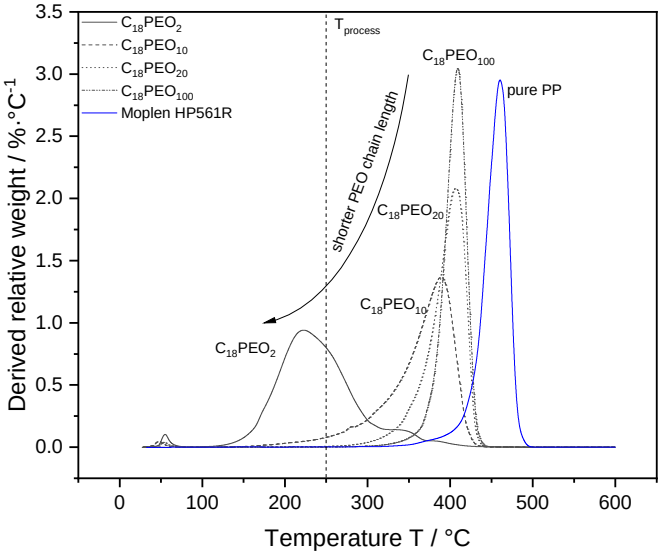

Figure 6.3: Standard (a) and derived (b) TGA curves of additives, which differ in the number of PEO units of the hydrophilic part of the surfactant. The observed weight loss is attributed to evaporation phenomena and not to degradation of the additive.

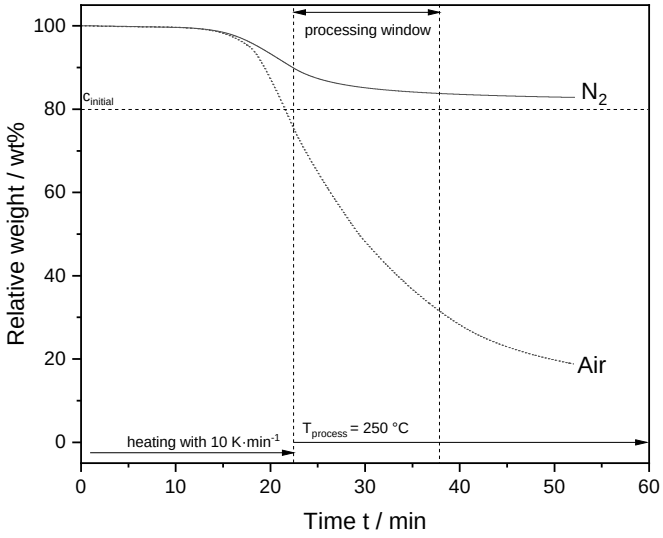

Figure 6.4: TGA measurement of the master batch which consists of polypropylene Moplen HP561R, 20 wt% $C_{18}PEO_2$ and 1wt% Irgafos 168 as stabilizing agent. The measurement was performed isothermally at 250 °C under nitrogen and ambient air atmosphere. The first 23 minutes were needed to heat up to a temperature of 250 °C with a heating rate of 10 K min^{-1}.

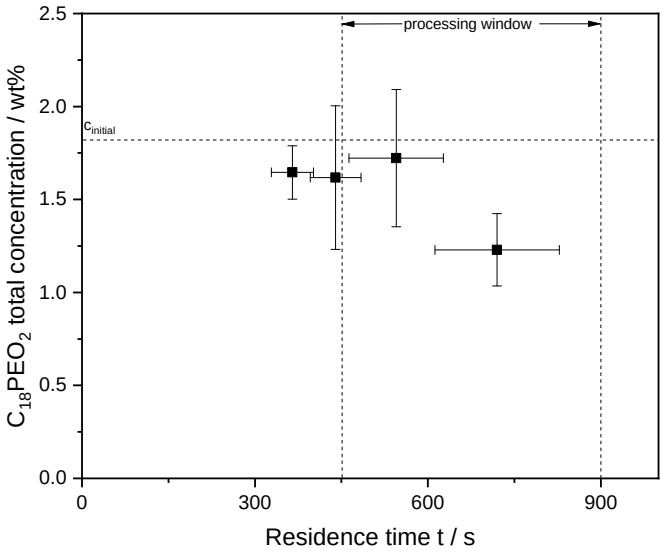

Figure 6.5: Total concentration of $C_{18}PEO_2$ in fibers produced in the melt spinning process with different residence times. Total concentration was determined via FTIR.

6.3 Miscibility of additives in the polypropylene matrix

In the following chapter a basic understanding of the miscibility between additive and polymer matrix shall be generated. As shown in chapter 2.3.2, the miscibility of additive and matrix polymer can have a significant influence on the migration behavior. In a study by Greenhalgh et al. [144] it was shown that the difference in Hansen solubility parameters $\Delta\delta$ is a tool for describing the interaction between two different substances. Compounds with a $\Delta\delta > 7.0\ \mathrm{MPa}^{0.5}$ have a tendency to be likely miscibile. The Hansen solubility parameters (HSP) of polypropylene and the most commonly used additives in this study are shown in table 6.4. Due to the low difference of the HSPs, it is assumed that at least partial miscibility may be present in the system. Based on the Flory-Huggins solution theory [145] it can be furthermore assumed that additives with a low molar mass dissolve better in the polypropylene than additives with a high molar mass. For this reason, the additives $C_{18}PEO_2$ and $C_{18}PEO_{20}$ were selected for the following experiments because they have a similar molecular structure and differ mainly in the molar mass.

Table 6.4: Hansen solubility parameters of polypropylene and the most commonly used additives in this study in $(MJ/m^3)^{0.5}$. Hansen solubility parameters of the additives were determined using a group contribution method according to van Krevelen [78].

	δ	δ_d	δ_p	δ_H
PP (source [146])	18.0	18.0	0.0	0.0
$C_{18}PEO_2$	18.9	2.1	16.7	8.5
$C_{18}PEO_{10}$	20.0	2.6	17.3	9.8
$C_{18}PEO_{20}$	20.7	2.6	17.6	10.6
$C_{18}PEO_{100}$	21.8	1.7	18.3	11.8

One method to determine the miscibility of polymers is the determination of melting point depression. By adding a miscible diluent to a polymer, the chemical potential of the polymer is reduced. If the polymer crystallizes, the reduction of the chemical potential results in a reduction of the equilibrium melting point. This in turn means that the melting point of a miscible system decreases as a function of the diluent content while it does not change in non-miscible or poorly miscible systems [147].

Figure 6.6 shows the melting point of polypropylene and the additives $C_{18}PEO_2$ and $C_{18}PEO_{20}$ as a function of the volume fraction ϕ. The melting point of

the additive and matrix decreases considerably when $C_{18}PEO_2$ is used as an additive. Therefore, significant interactions and at least partial miscibility are assumed. For additive $C_{18}PEO_{20}$, the changes of the melting points of the additive and the polypropylene are within the range of the experimental scattering, which is why no or only low miscibility is expected. An effect of the matrix molar mass could not be demonstrated. The experiments were performed with cooling rates between 5 and 50 K min^{-1}, but the melting points of the additive and the matrix did not change depending on the investigated cooling rates, which is why the samples produced with a cooling rate of 10 K min^{-1} are shown as an example.

A description of the melting point depression using an approach described in a study by Nishi [148] or Simek [149] which is commonly used to describe the melting point depression as a function of the χ-parameter in miscible systems [150–152] led to inconsistent results and can be found in appendix A.5. The results shown here therefore do not represent a complete discussion of the solubility of the additive / polymer system and serve as an example for the miscibility of low molar mass ethoxylated alcohols which decreases with increasing molar mass.

a)

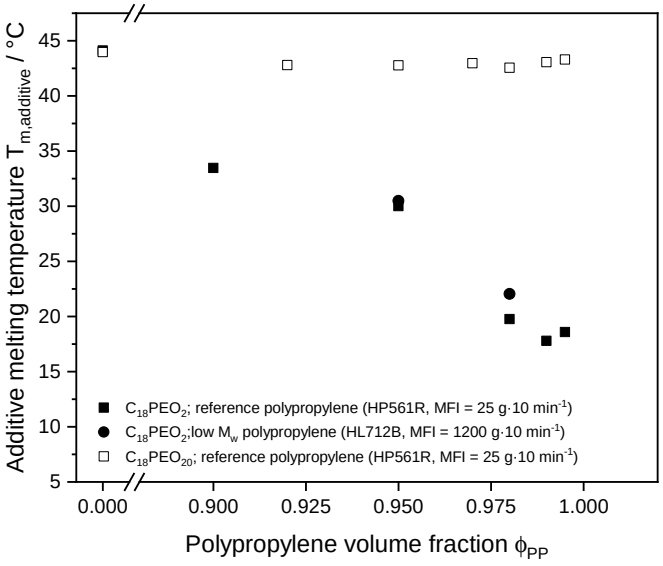

b)

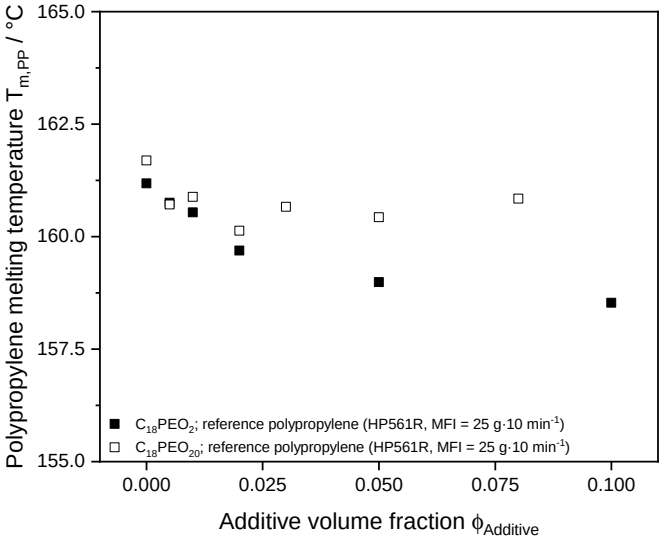

Figure 6.6: Melting point depression of mixtures of polypropylene with different molar mass and the additives $C_{18}PEO_2$ and $C_{18}PEO_{20}$ as a function of the volume fraction of the PP (a) and the additive (b).

6.4 Morphology development of fibers in the spinning process and its influence on additive migration

Since additive migration is very sensitive to subtle changes in fiber structure, in particular to changes in crystallinity and morphology in the broadest sense, small changes in processing conditions can lead to large changes in additive surface migration. In order to understand the influence of the morphology and the crystallinity of the matrix material on the migration behavior of an additive, the influence of the main production parameters on the (surface) crystallinity of fibers and nonwovens was studied.

6.4.1 Structure formation during the stretching process

Figure 6.7 shows the influence of the stretching speed on the surface and bulk crystallinity of the fibers. With increasing stretching speed, both the surface and the total crystallinity increase. In the fiber spinning process, the fiber is cooled from well above the melting temperature to room temperature, which means that the drawing process takes place both in the molten state and on the already solidified polymer. These non-isothermal stretching conditions lead to two interconnected phenomena of structure formation:

1. Stretching of the melt leads to strain-induced crystallization
2. Stretching of the solidified polymer leads to mechanical induced post-crystallization and orientation formation

These phenomena are the more distinct the more the fiber is stretched in the process.

The observations are largely in accordance with the literature. It is well-known that the crystallinity and orientation of fibers increases with increasing haul-off speed [153–155] which is commonly detected via birefringence measurements. This increase in crystallinity is usually attributed to strain-induced crystallization of the filaments. While most studies assume a uniform crystallization across the profile, figure 6.7 indicates different degrees of crystallinity depending on the penetration depth d_p of the IR radiation used.

A hypothesis was developed to explain the observed results. The fiber is extruded well above the melting temperature in the molten state. Due to the shear rate profile in the the nozzle, a pre-orientation of the polymer chains occurs during extrusion, which is most pronounced in the surface layer and decreases towards the core of the fiber. Due to low temperatures in the quench

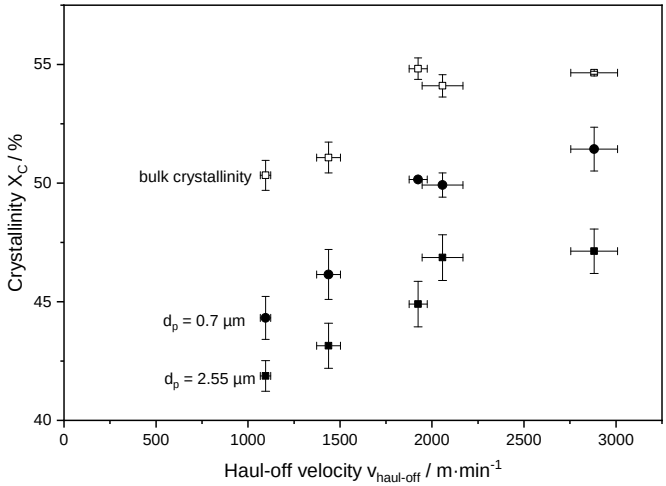

Figure 6.7: Influence of the haul-off velocity on the surfaces and bulk crystallinity of single fibers produced in the spunbonding process.

chamber and thinning of the fiber during stretching, the fiber cools down at the surface much faster than in the fiber core. Strain-induced crystallization of the still hot center results in a highly crystalline core, while quenching and freezing of the surface results in a highly oriented amorphous surface layer. The pre-oriented amorphous surface layer is then further oriented due to the high stretching forces, which leads to mechanically induced post-crystallization as a result of the forced alignment of the polymer chains. The superposition of the two phenomena that lead to the formation of morphology results in two maxima of the degree of crystallinity accross the profile:

1. In the core (strain-induced crystallization)
2. On the surface (orientation-induced crystallization)

Figure 6.8 shows a schematic sketch illustrating the structure formation during the spinning process. Two studies by Fung et al. [28, 156] confirm the morphology formation. They determined the birefringence of slices from relatively thick (70 - 120 µm) melt-spun PP and PE fibers which were cut using a microtome. Two maxima of birefringence are found at the surface and in the core of the fiber. The structural effects are much more pronounced with PE fibers than with PP fibers.

Figure 6.9 shows the ratio of surface to total crystallinity as a function of the haul-off speed to illustrate the post-crystallization of the surface as a result of the drawing process. While the strain-induced crystallinity of the core does

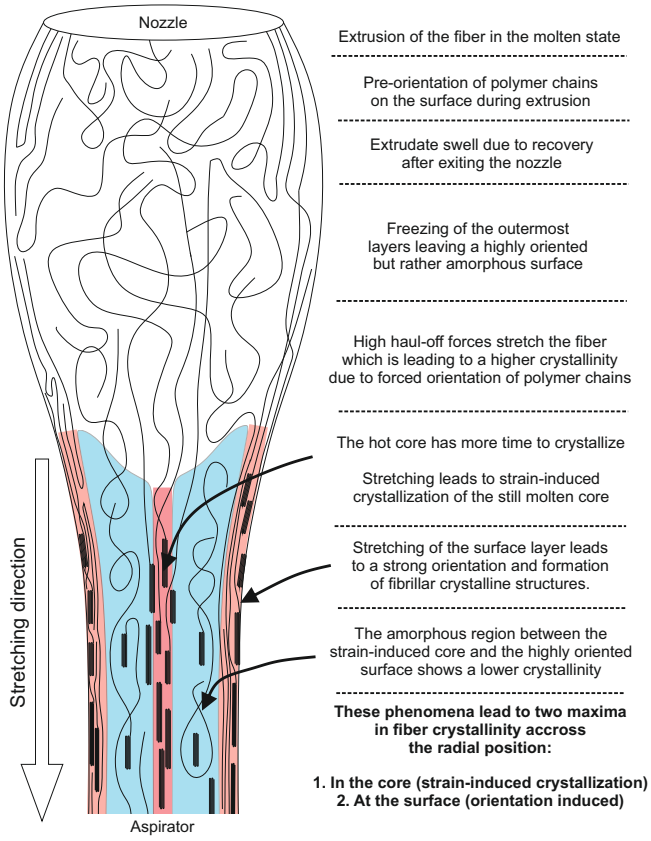

Figure 6.8: Sketch to illustrate the phenomena involved in morphology development during the stretching process.

not change above a certain haul-off speed (see also figure 6.7), the quenched surface can be further oriented with increasing stretching ratios. This leads to an increase of the ratio of surface to total crystallinity with increasing haul-off velocity. A study by Hautojärvi et al. [157] investigated the surface morphology of polypropylene fibers with varying degrees of stretching. It was found that the morphology of surface crystallites transforms from spherulitic structures to microfibrils to nanofibrils with increasing degree of stretching. The fibrillar structures consist of a crystalline thread (shish) on which epitaxial plates (kebab) grow. A similar shish-kebab surface structure formation is also assumed in the case of the fibers investigated in this thesis. Hautojärvi also found that haul-off forces, which are beyond the forces fibers experience during the aerodynamical stretching in the spunbond process, orient the lamellar plates to even finer nanofibrils with a diameter of about 10 nm. In

the core of the fibers a shish-kebab structure is assumed as well due to the strain-induced crystallization. As a result of the elongation and alignment of the melt, ribbon-like polypropylene crystals are formed on which epitaxially lamellar crystallites can then grow. This structure formation has already been shown in various studies which focused on the crystallization of polypropylene under shear [158–160].

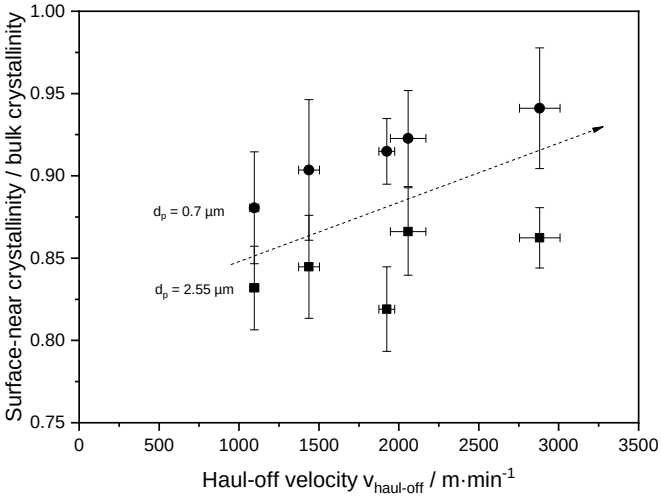

Figure 6.9: Ratio of surface crystallinity to total crystallinity of fibers produced at different haul-off velocities and measured with different penetration depths of IR radiation.

In order to support the hypothesis of forced post-crystallization by stretching the fibers in the solid state, fibers that were produced using low and high haul-off velocities were mechanically stretched in a tensile testing machine after production. The crystallinity of the fibers was determined before and after the tensile test.

Figure 6.10 illustrates that the surface crystallinity of the fibers increases as a result of the stretching process during the tensile test, while the total crystallinity of the fibers remains almost constant. The process of mechanically induced post-crystallization is much more pronounced in the case of fibers that were produced at low haul-off velocities and therefore oriented to a lower extent than in the case of fibers that were produced under high haul-off velocities. This indicates that the fibers are also stretched in the solid state during the spinning process and that not only the melt is stretched. While the core of the fiber is already in a terminal state due to the strain-induced crystallization, the surface layer morphology is unstable due to the super

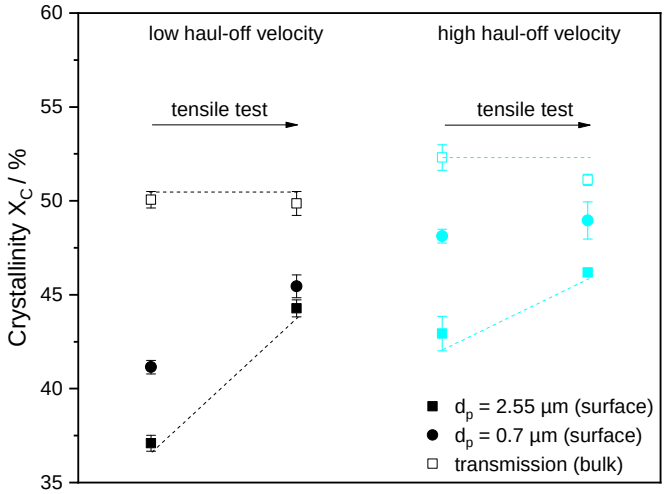

Figure 6.10: Surface and bulk crystallinity of fibers produced at different haul-off velocities. The measurements show the degree of crystallinity measured before and after a tensile test.

cooling in the quench chamber. Therefore the surface layer can be oriented by stretching and post-crystallized by mechanically induced crystallization.

Figure 6.11 shows an XRD diffractogram of stretched and gravity spun fibers. The gravity spun fibers show a mesomorphic structure, as they cool down fast and non-isothermally due to the high surface area, extrusion speed and cooling inside the quench chamber. The stretched fibers show an α-crystalline morphology as the stretching of the fibers in the process causes a phase transformation as a result of strain-induced crystallization. Furthermore, it is evident that the reflections of lattice planes with Miller's indices (131) and (111), which are normally seen in diffractograms of α-crystalline polypropylene, are missing. This implies that the crystals are strongly oriented towards the stretching direction and that crystals in the plane (001) are stretched and oriented towards the planes (100) and (010). The transformation of mesomorphic to α-crystalline structures was also found by Kang et al. [26]. They investigated the subsequent stretching of moderately stretched, mesomorphic fibers using in-situ XRD. It was found that the oriented mesophase of the moderately stretched fibers transforms into an oriented α-phase upon stretching.

The results discussed so far indicate that the fibers produced using high haul-off velocities are already strongly mechanically deformed during the process. Since the fibers produced at low stretching speeds are stretched considerably less during the spinning process, they can be elongated more in the subsequent

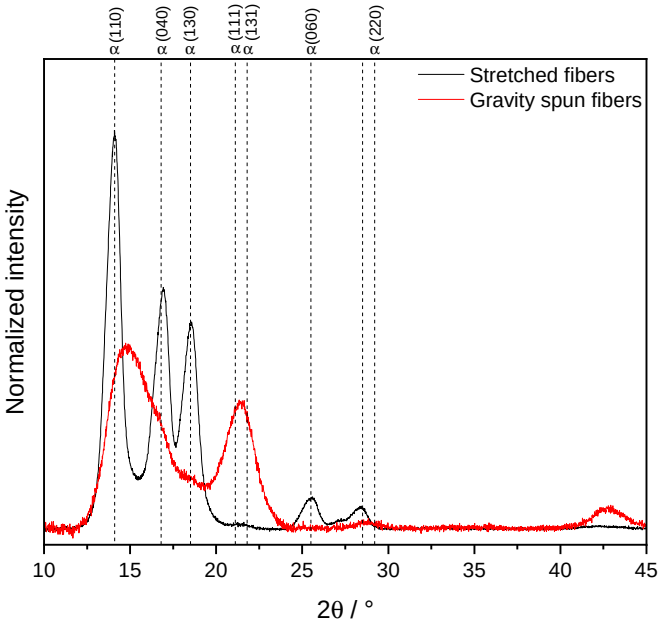

Figure 6.11: XRD diffractogram of stretched and gravity spun fibers as well as diffraction reflexes of the α-crystalline structure.

tensile test. This leads to an increasing elongation at break of less stretched fibers (Figure 6.12 (a)). Similar results have been found by Nadelle et al. [161, 162] and Gupta et al. [155].

In order to better compare the mechanical properties of the fibers, the true stress σ_{true} is plotted over the current fiber diameter d_{current} in figure 6.12 (b). These values are calculated using the initial diameter d_{initial} as well as the force F and elongation ϵ determined in a single fiber tensile test:

$$d_{\text{current}} = \frac{d_{\text{initial}}}{\sqrt{1 + \frac{\epsilon[\%]}{100\%}}} \tag{6.1}$$

$$\sigma_{\text{true}} = \frac{F}{\pi\left(\frac{d_{\text{current}}}{2}\right)^2} \tag{6.2}$$

a)

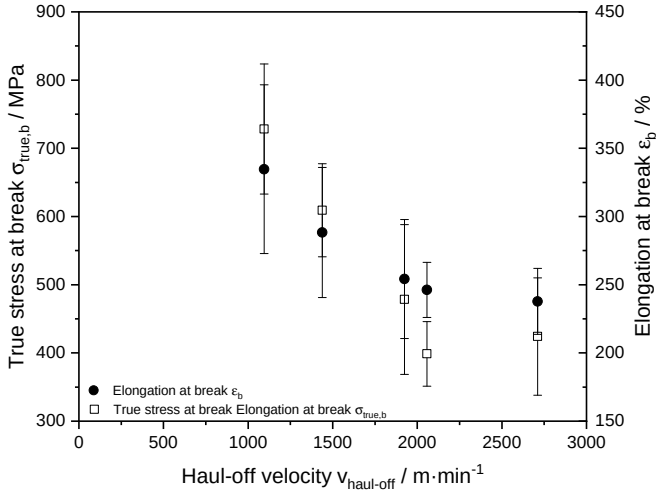

b)

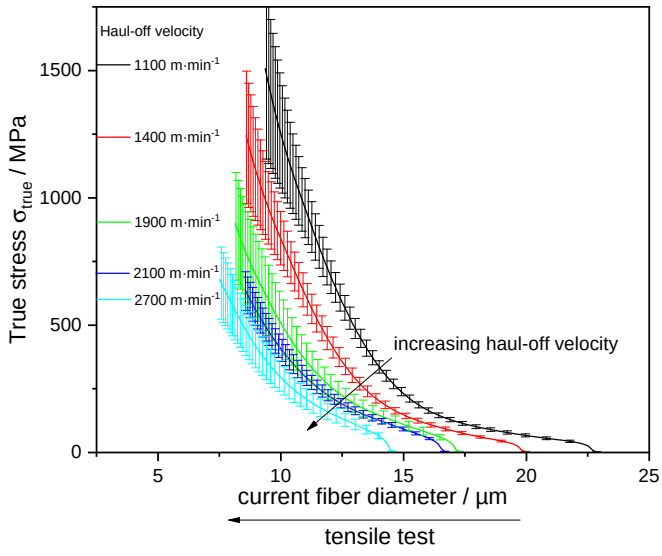

Figure 6.12: Mechanical properties and fracture behavior of fibers produced at different haul-off speeds.

From figure 6.12 two effects become obvious. On the one hand, the fibers all tear at a comparable final diameter of about 7-9 µm, regardless of the haul-off speed they were produced at. The slight increase in the diameter at break of the specimens produced at high draw-off speeds can be explained by the assumption that the fibers are stretched slightly more in the molten state at high stretching speeds. The stretching of the melt pre-aligns the polymer chains and leads to strain-induced crystallization. From the point at which the fiber surface solidifies, the fibers can only be stretched to a certain degree without mechanical failure. These results also explain that fibers can probably not be produced considerably thinner than 8 µm in the spunbonding process without significant changes in the stretching mechanism of the melt (as for example in the melt blowing process).

On the other hand, the fibers produced under lower haul-off velocities can withstand a higher load at the same current diameter. Since the fibers are stretched much more slowly (10 mm min^{-1}) in the tensile test than in the spinning process, the polymer chains have more time to align towards the stretching direction. This effect in turn leads to more force being transmitted at the same diameter and an increase of the stress at break.

The orientation of the polymer chains by stretching the fibers is also illustrated in figure 6.13. In this graph, the elastic modulus is plotted as a function of the haul-off velocity and as a function of the total crystallinity. The increase of the modulus is not exclusively due to the increase of the degree of crystallinity because the increase is too pronounced to be explained by a simple mixing rule of amorphous and crystalline regions. In addition, the dependence of Young's modulus on the degree of crystallinity of the fibers is not very pronounced and is rather divided into two areas of high and low haul-off speeds. Therefore, the increase of the modulus of elasticity as a function of the stretching speed is attributed to the increased orientation. This result has also been found by Gupta et al. [163] for HDPE fibers which were cold-drawn to varying degrees. In this study the orientation distribution in crystallites and in the amorphous regions of the fibers was quantitatively determined. It was found that the Young's modulus correlates primarily with the mean orientation in the amorphous regions. Nadella et al. [161, 162] were also able to correlate birefringence (e.g. the orientation) and the elastic modulus of as-spun as well as cold and hot drawn polypropylene fibers. On the basis of these results it can be concluded that the stretching of the fibers in the solid state primarily orients the amorphous regions to the point at which they cannot be further oriented and the fiber breaks. This hypothesis also supports the results from figure 6.12 that fibers can only be stretched to a certain diameter.

a)

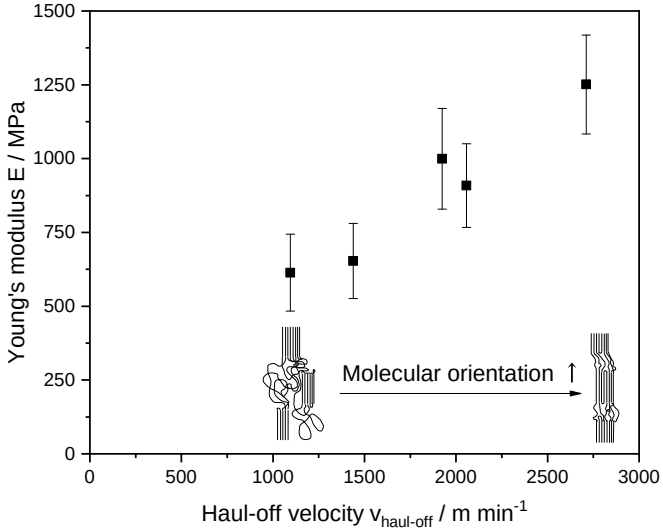

b)

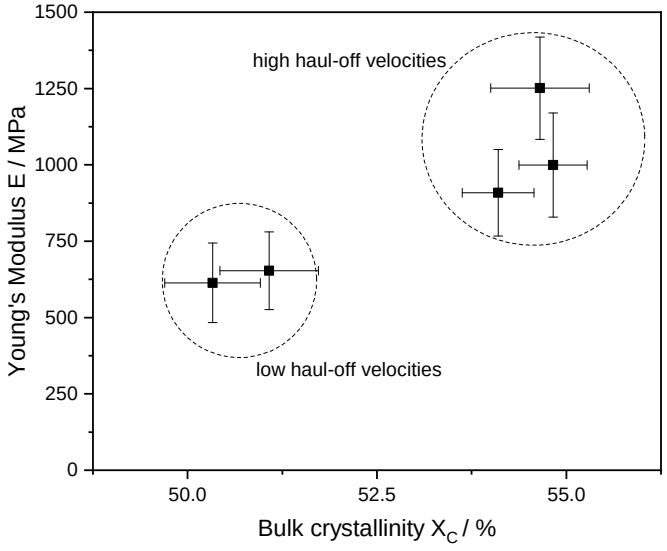

Figure 6.13: Young's modulus as a function of haul-off velocity (a) and bulk crystallinity (b) of fibers produced at different haul-off velocities.

6.4.2 Calendering

The calendering process bonds the fibers after they have been laid down by applying heat and pressure at specific points of the web. In the following section it will be investigated to what extent this introduction of heat has an influence on the resulting polymer morphology.

Figure 6.14 shows the dependence of the crystallinity on the calender temperature. The samples for this experiment were produced using a calender press (detailed description in chapter 4.1.2). Closing this press to build up the necessary pressure takes longer than with a real rolling calender. The residence time was estimated to be 0.56 s using a video camera. The residence time in the roll calender, which is integrated in the pilot plant, is approximately 0.19 s. At high line speeds, the residence time in the industrial process can drop to about 0.01 s and less due to line speeds up to 300 m min^{-1} [164]. This means that the contact with the calender rolls is shorter than the contact with the calender press plates and the post-crystallization due to the heat input is slightly overestimated in the experiment shown here. In addition, a much coarser press pattern was used to detect differences between calender point and non-calendered fibers using the FTIR measurement method. A smaller pattern would not allow to measure fibers and bonding points separately with an ATR crystal. The used pattern was a version of the standard pattern scaled up by a factor of 10, resulting in calender points with the biggest diameter of 8.8 mm and the smallest diameter of 5.4 mm.

Figure 6.14 demonstrates that a more pronounced post-crystallization takes place with increasing calender temperature which can be explained by the introduction of heat into the process. This post-crystallization is most pronounced at the bonding points, but can also be detected in the non-bonded areas, since heat is also radiated from the calender plates where no bonding points are in direct contact with the fibers. The graph further demonstrates that recrystallization already begins at a calender temperature of approximately 100 °C and becomes more pronounced as the temperature increases. It is assumed that the post-crystallization is most prominent at the fiber and bonding point surface and not in the core. This is due to the finding that there are stretched and oriented mesomorphic regions on the surface (see chapter 6.4.1), which are highly metastable and already subject to a transformation from the mesomorphic to the α-crystalline structure at temperatures of approximately 70 - 80 °C. In order to illustrate this recrystallization process, figure 6.15 shows DSC measurements of very fast and slowly cooled polypropylene samples (from the calibration set used in chapter 4.2.3.4 for the calibration of the FTIR method to detect crystallinity). Even if the crystalline structure

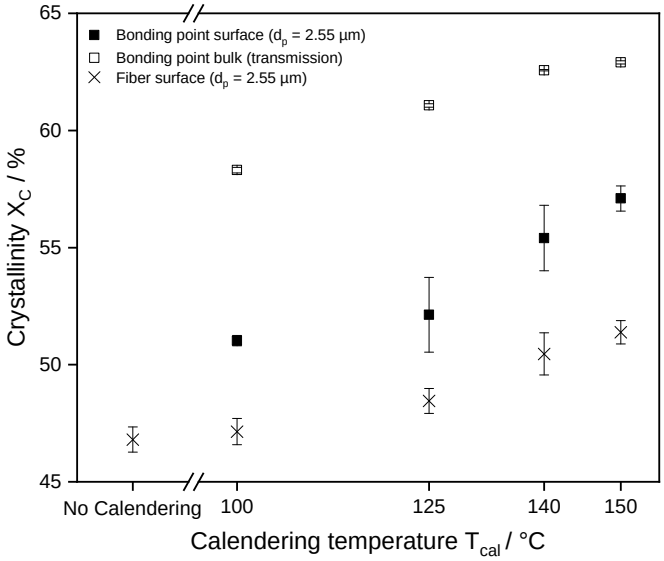

Figure 6.14: Influence of calendering temperature on the surface and bulk crystallinity of fibers spun under standard conditions. The used calender pattern was much coarser than the standard pattern to resolve effects of heat on the calendering points and fibers separately. The corresponding calendering line pressure of approximately 5 N mm^{-2} was estimated using equation A.12 (appendix A.2.1).

in the fibers is not completely comparable to that of the samples from the calibration set, the experiment clearly shows that a transformation from the mesormorphic to the α-crystalline phase occurs at comparatively low temperatures. Therefore, a transformation as a result of the heat input during calendering is highly realistic.

Furthermore, it was investigated whether the introduction of heat can lead to a relaxation of the strongly oriented crystallites in the fibers. To verify this, XRD measurements of stretched fibers and calendered nonwovens were performed. Figure 6.16 demonstrates that the crystalline structure before and after the calendering of the fibers does not differ significantly and that the reflections present in non-oriented α-crystalline PP at about 21.5° (crystal planes (131) and (111)) are also not present after the calendering step (see also chapter 6.4.1). It can therefore be concluded that the heat input leads to a certain post-crystallization of the metastable crystal regions especially on the surface of the fiber, but a reorientation and relaxation of the chains could not be demonstrated.

In order to exclude the possibility that the applied pressure during calendering may have an influence on the morphology due to the calendering process,

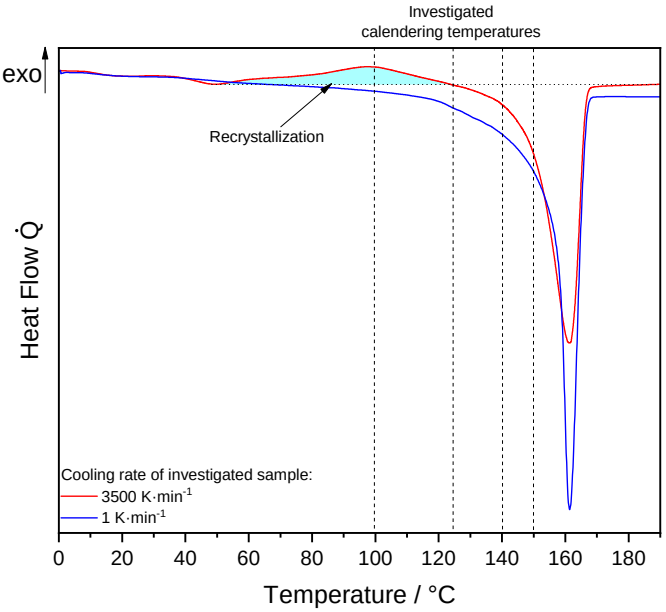

Figure 6.15: DSC heating curves of the samples from the calibration set (chapter 4.2.3.4) to illustrate recrystallization effects which may occur in fibers during the calendering process. Vertical lines correspond to the investigated calendering temperatures.

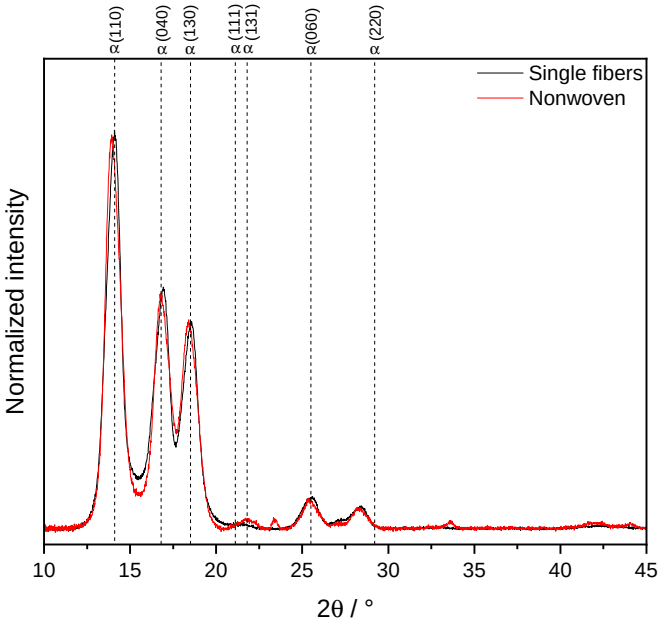

Figure 6.16: XRD study of fibers and nonwovens produced under the same production conditions. Nonwovens were calendered at a temperature of 145 °C.

samples were also produced using different calendering pressures. Figure 6.17 shows that the pressure has no influence on the post-crystallization and on the formation of different degrees of crystallization, neither on the surface nor the bulk material. A high pressure during calendering is nevertheless necessary to allow sufficient bonding of the fiber to the bonding points and thus to guarantee sufficient mechanical properties [164]. No higher pressures could be applied using the laboratory calender with the existing plates, which is why the pressures used in this study are significantly lower than the line pressures used in the industrial process. However, nonwovens produced using an industrial calender show a very comparable crystallinity at line pressures of 110 - 150 N mm^{-1}. Further information on the influence of the calender on polypropylene morphology can be found in Leucker's dissertation [165].

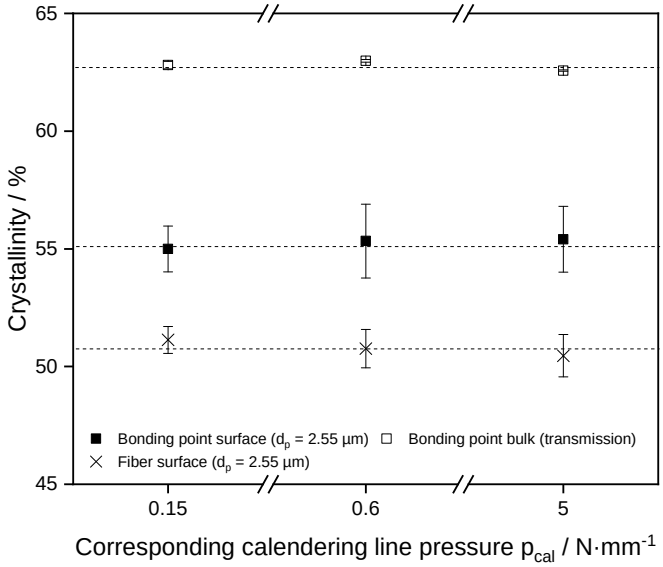

Figure 6.17: Influence of the calendering pressure on the degree of crystallinity of fibers and bonding points of nonwovens.

6.5 Morphology development in cast films

In order to create a better understanding of the influence of the stretching process on the morphology of the matrix polymer, cast films were produced and subsequently stretched using various processes. The samples were examined by FTIR spectroscopy for surface crystallinity and by XRD for crystal structure. Particular attention was paid to ensuring that the drawing conditions

are as close as possible to those in the fiber spinning process to transfer the knowledge generated from these experiments to the spinning process.

First, the influence of the chill roll temperature was examined. Figure 6.18 shows XRD diffractograms of films cast onto a hot (80 °C) and a cold (20 °C) chill roll. The crystal structure of the two samples differs considerably. The film which was produced using the hot chill roll shows an α-crystalline structure, while the film cast on the cold chill roll shows a mesomorphic structure. This phenomenon is due to significantly higher cooling rates to which the film is exposed on the cooled chill roll. The formation of the mesomorphic structure has been demonstrated for polypropylene which was crystallized isothermally between 0 and 30 °C [56], cooled with very high rates from the melt [58–60] or cast onto chill rolls which were cooled to 15 °C [24].

Since the films cast on the cold chill roll reflect the morphology of the unstretched fibers much better (see chapter 6.4, figure 6.11), only the films cast on a cooled chill roll were used for the following experiments.

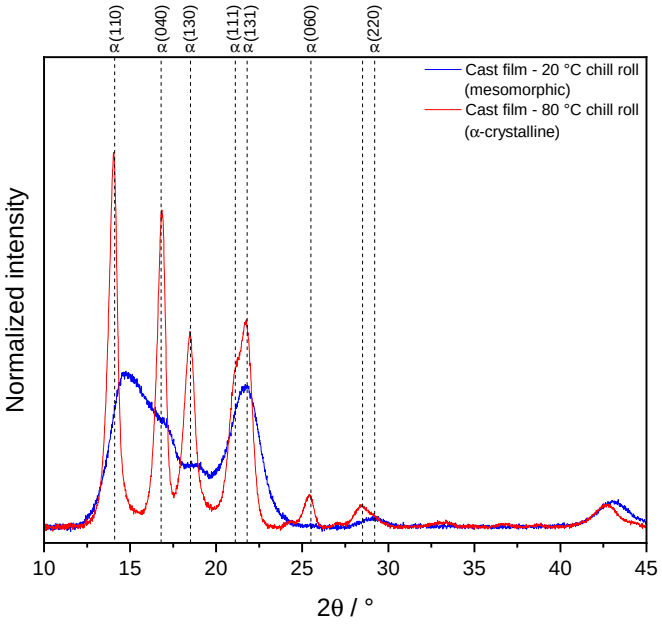

Figure 6.18: Comparison of XRD diffractograms of films cast on a water-cooled (20 °C) and a hot (80 °C) chill roll.

In order to demonstrate the influence of the subsequent stretching on the films, the films were heated to 140 °C for 45 seconds using a biaxial streching device and then uniaxially stretched by 800 %. To separate the influence of

stretching and heating, samples were compared immediately after heating with and without stretching using XRD. The results are shown in figure 6.19. Even the brief introduction of heat during the heating of the film leads to the transformation from the metastable mesophase to an α-crystalline structure. This transformation is due to the introduction of heat and can also be demonstrated by the DSC curves already discussed (figure 6.15, chapter 6.4.2). In the previous experiments a phase transformation and recrystallization of the mesomorphic crystal structure between approximately 60 °C and 140 °C was observed. Similar results were also obtained by Zhao et al. [66]. In Zhao's study, quenched mesomorphic isotactic polypropylene was reheated while WAXD diffractograms were recorded simultaneously. The results revealed that there is a phase transition from the α-crystalline to the mesomorphic structure from 85 °C onwards. They reported that an increase in the α-crystalline phase was mainly at the expense of the mesomorphic phase, while the amorphous phase fraction remained unchanged. From about 130 °C, the entire mesomorphic phase has transformed into the α-crystalline phase. Comparable results have also been published by Nitta and Odaka [64]. They reported that quenched iPP from about 60 °C transforms from a mesomorphic to an α-crystalline structure while the amorphous phase fraction decreased only slightly.

When stretching the α-crystalline phase, similar phenomena can be observed as already discussed for the case of fibers (chapter 6.4). As a result of the stretching process, the crystalline regions are also stretched and oriented along the stretching direction. As a result, reflections of the lattice planes with Miller's indices (131) and (111) disappear and reflections in the lattice plane (110) become more pronounced.

The experiments discussed so far have shown that the metastable mesomorphic crystal structure already transforms to the α-crystalline crystal structure due to a small heat input. In order to investigate the morphology of an isolated stretching process without any heat input, the films were cold stretched at a speed of 20 mm min^{-1} using a tensile testing machine. This was necessary because the forces needed to cold stretch a film can no longer be applied with the biaxial stretching device. In addition, comparatively low stretching speeds were selected to allow realignment of the polymer chains and prevent premature film tearing. The diffractograms of unstretched and 800% uniaxially stretched films are shown in figure 6.20. The stretching process does not result in a phase transformation, but rather in an orientation of the mesophase in the direction of the lattice plane (110), similar to the stretching of the α-crystalline phases. This orientation is accompanied by the disappearance of

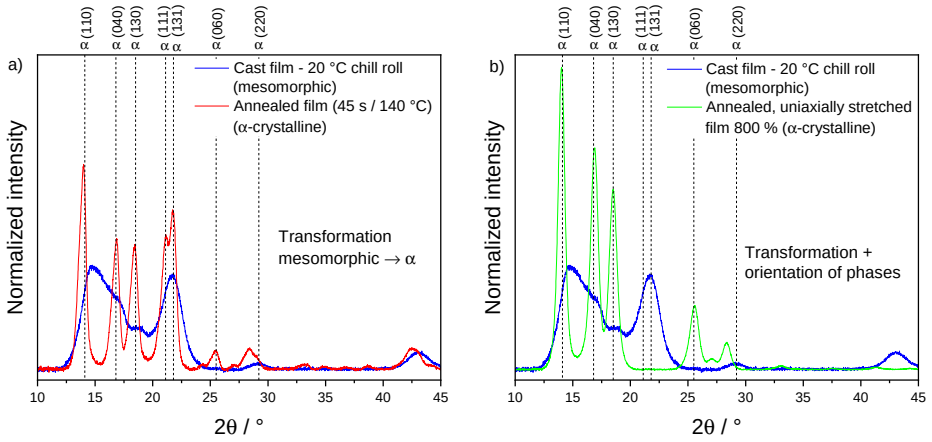

Figure 6.19: XRD spectra of mesomorphic PP films heated for 45 s to 140 °C without (a) and with (b) a subsequent stretching step showing morphological changes.

reflexes in plane (001) and an enlargement and intensification of the reflexes in lattice plane (110) and (010). Similar observations were made by Qiu et al. [166]. In Qui's study, structure and morphology changes of quenched iPP films after tensile tests at room temperature were investigated by synchrotron SAXS/WAXD techniques. It was found that the mesomorphic phase is not subject to any phase transformation due to deformation and that the crystal structures are strongly oriented.

This experiment further supports the hypothesis that shear-induced crystallization leads to the formation of an α-crystalline morphology in the stretched fibers. Although the gravity spun fibers show a mesomorphic structure due to the high cooling rate and the low drawing forces, the drawn fibers show an α-crystalline structure even at low haul-off speeds of about 1000 m min^{-1}. The experiment shown here proves that the mesomorphic phase is only oriented by cold stretching and not transformed into an α-crystalline phase due to the lack of heat input.

The investigation of the surface crystallinity by FTIR showed comparable changes of the crystallinity, as already found for fibers. The input of heat leads to a significant post-crystallization of the surface (figure 6.21 (a)), comparable to the post-crystallization as a result of the input of heat during calendering (see also chapter 6.4.2). A slight post-crystallization of the surface is also observed during cold stretching (figure 6.21 (b)), even though it is not as pronounced as for fibers (chapter 6.4). Nevertheless, similar mechanisms of structural development are assumed for films. Due to the strong post-stretching of the films, it is assumed that surface structures are stretched

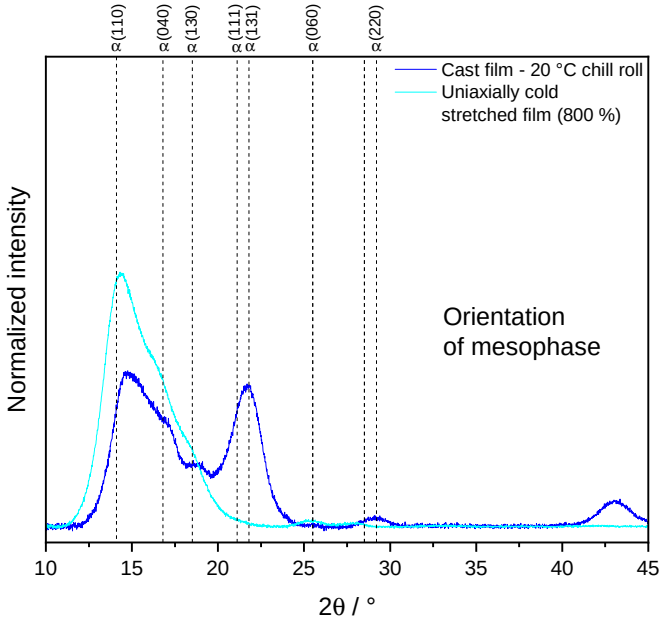

Figure 6.20: XRD diffractograms of as-cast films and films that have been uniaxially cold stretched by 800 % in a tensile testing device.

to highly compressed nanofibrillar crystallites already from an elongation of 200 %. The development of such nanofibrillar crystalline structures was reported by Hautojärvi et al. for fibers which have been extensively stretched after the spinning process [157, 167]. The nanofibrillar structures are packed very densely to such an extent that they should constitute a migration barrier. The slight drop in the degree of crystallinity in a penetration depth of 2.55 µm from unstretched to stretched films could not be explained within the scope of the investigations and may be a result of experimental scattering.

a)

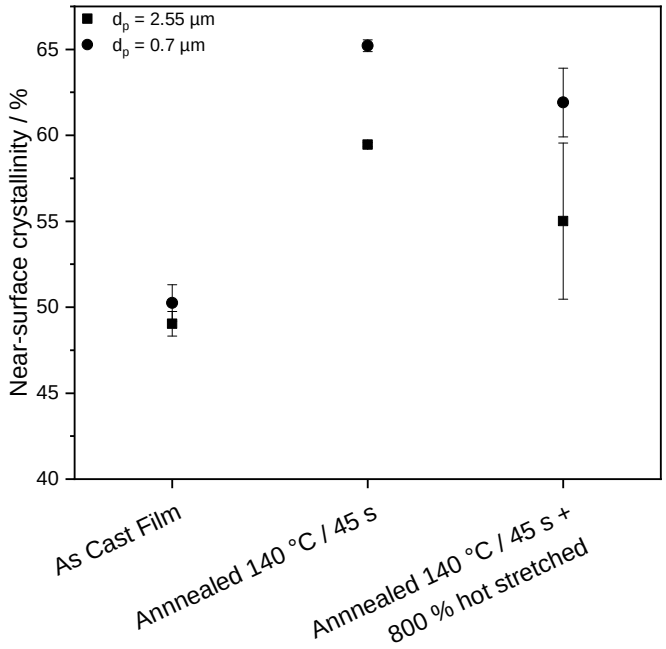

b)

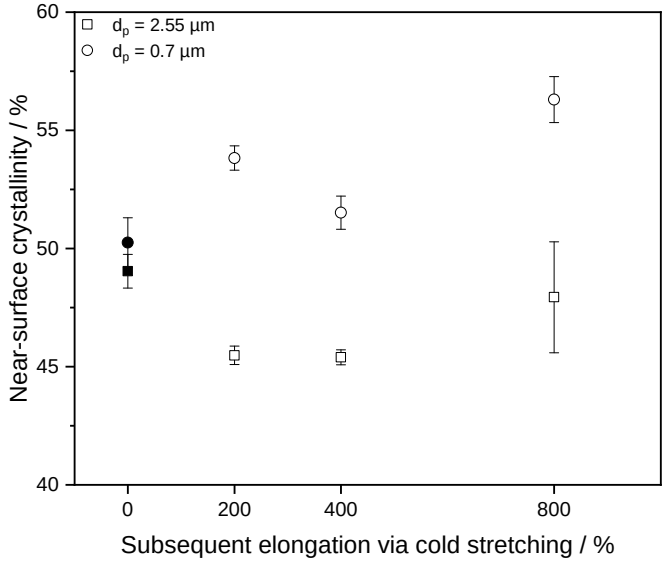

Figure 6.21: Near surface crystallinity of hot (a) and cold (b) stretched polypropylene films.

6.6 Morphology development in injection molded plates

In order to investigate the influence of cooling conditions on morphology formation in injection molded parts, the cooling conditions in the mold during the production of plates were varied and the crystalline morphology was determined by XRD, FTIR and microscopy.

Figure 6.22 shows XRD measurements of plates which were cooled quickly at low mold temperature (15 seconds at 40 °C) and slowly at high mold temperature (60 seconds at 80 °C). Although the cooling conditions differ significantly, both plates show a very similar α-crystalline structure. Comparable cooling conditions to those of the rapidly cooled plates caused a mesomorphic structure in the cast films (see chapter 6.5). However, since the injection molded plates are considerably thicker (2 mm) than the cast films (approximately 100 µm), heat is dissipated less effectively from the sample and the cooling rates in the core are not high enough to cause a mesomorphic structure formation over the whole sample even though it is assumed that the surface layer exhibits a mesomorphic structure due to the high cooling rates [64].

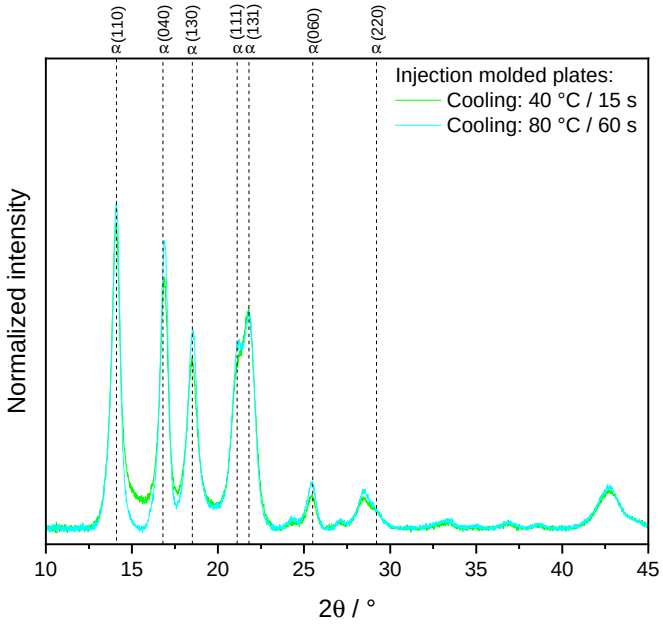

Figure 6.22: XRD diffractograms of injection molded plates produced with a cooled and a heated mold, both exhibiting an α-crystalline structure.

Figure 6.36 shows the surface crystallinity as a function of the mold temperature. The experiment illustrates that the surface crystallinity increases with increasing mold temperature. As the heat is poorly dissipated in the warm mold, the polymer chains in the surface layer can crystallize and arrange for a longer time, resulting in a higher overall crystallinity, which rises with increasing mold temperature.

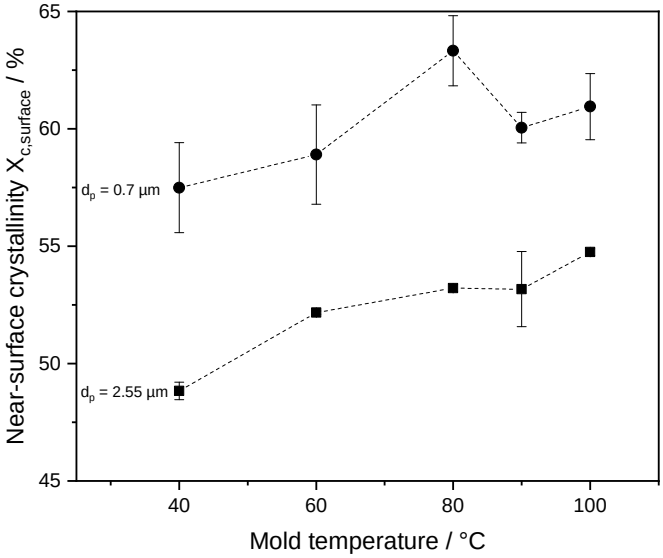

Figure 6.23: Near-surface crystallinity of injection-molded plates produced with different mold temperatures.

The mold temperatures also influences the resulting crystallite morphology. Figure 6.24 shows etched cross sections of the plates. In the samples which were produced with a mold which was cooled to 40 °C, hardly any spherulites can be seen in near-surface regions, while crystallites are already clearly visible from a mold temperature of 60 °C. It is assumed that the rapidly cooled samples show a mesomorphic and less ordered surface structure, while the samples produced at high mold temperature show a higher crystallinity and larger, ordered α-crystalline spherulites. In regions far from the surface, crystallites are also visible in samples produced using a 40 °C cold mold, which explains the α-crystalline structure determined by XRD. As the mold temperature rises, the crystallites that form become larger. In comparison to the crystallites with a diameter of 30 ± 5 µm, which form in a mold tempered to 60 °C, crystallites with a diameter of about 45 ± 5 µm appear in a mold which is tempered to 80 °C. It is assumed that the crystalline structures resulting from

the rising mold temperatures are increasingly difficult for additive molecules to penetrate.

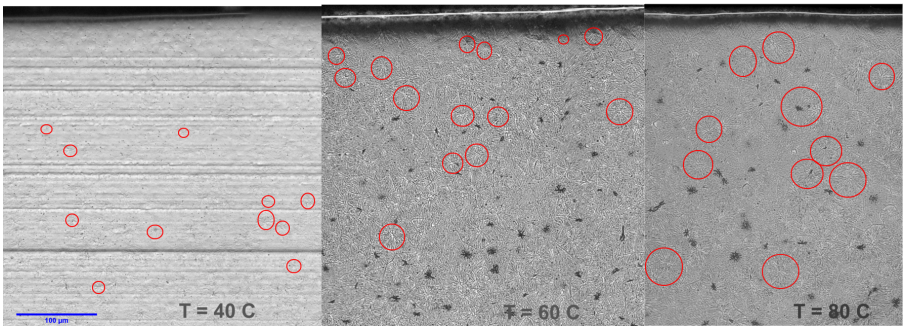

Figure 6.24: Microscopy images of etched cross-sections of injection molded polypropylene plates. Due to the poor visibility of the crystallites in the printed image, typical crystallite structures were framed in red to exemplary illustrate the crystallite size. In the injection molded plates cooled at 40 °C, no crystallite structures are visible near the surface.

6.7 Wetting behavior of additives applied as a coating

6.7.1 Wetting behavior of spincoated substrates

Influence of additive structure

Because nonwovens are poor substrates for reproducible wetting tests due to their complex and comparatively non-uniform pore structure, injection molded plates were initially used as substrates to characterize fundamental relationships between surfactant structure and its interaction with the polymer surface. The results will then be transferred to the findings from coated nonwovens. The plates have the following advantages over nonwovens:

- They offer a highly reproducible surface structure and can easily be produced in large numbers.
- The matrix polymer can be exchanged without changing the substrate geometry.
- They are not porous. This means that liquids do not penetrate the substrate in the event of wetting and therefore very low contact angles can also be measured.

In order to deposit the additive on the substrate in a reproducible manner, they were spincoated onto injection molded plates resulting in coatings with a uniform thickness of approximately 30 - 50 nm. Figure 6.25 shows the influence of the molecular architecture of the ethoxylated alcohols applied to PP plates on the water contact angle of the coated plates. The experiment illustrates that the chain length of the hydrophilic part of the surfactant has the greatest influence, while the hydrophobic part only plays a minor role. This finding is rather non-intuitive, as with increasing chain length of the hydrophilic part of the molecule, i.e. the more hydrophilic the molecule as such is, the more hydrophobic the coated substrate becomes. These dependencies are reflected in a sweet spot located at low PEO chain lengths and medium CH_2 chain lengths. According to the findings, a hypothesis is proposed which explains the influence of the attachment of molecules to a surface on the wetting of the surface with regard to the structure of the molecule.

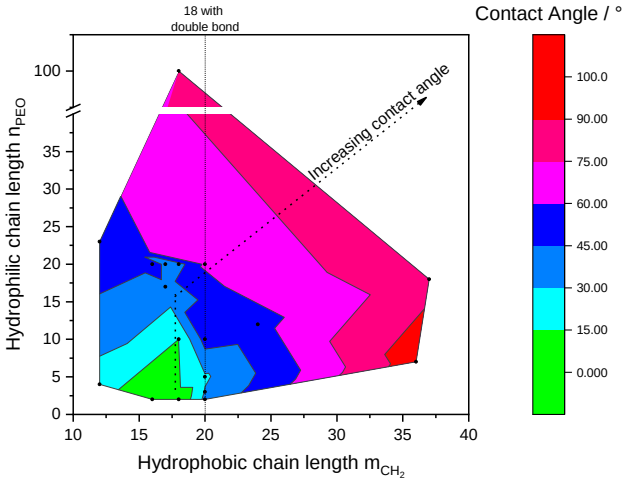

Figure 6.25: Contour plot demonstrating the influence of CH_2 and PEO chain length on the resulting water contact angle when the additive is applied as a coating onto an injection molded plate. The dotted line in the figure is drawn to guide the eye.

Figure 6.25 illustrates that longer PEO chains result in higher contact angles while there is no substantial dependence of the contact angle on the length of the CH_2 chain if it has less than 20 repeating units. A chain length of the hydrophobic part of the molecule of more than 20 repeating units also leads to increased contact angles. Since the PEO repeating unit has a significantly higher molar mass than the CH_2 repeating unit (44 g mol^{-1} compared to 14 g mol^{-1}), the strong influence of the PEO chain length observed in our experiments might reflect the influence of the molar mass of the additive. Comparable studies are discussed below. Rosen et al. [168] reported an

optimum of 12 - 14 CH_2 repeating units for an ideal wettability of cotton with an ethoxylated alcohol solution. Ivanova et al. studied the spreading of aqueous solutions of alkyl polyoxyethylene surfactants with a CH_2 chain length of 10 and a PEO chain length of 3 - 8 on parafilm, polytetrafluoroethylene (PTFE) and polypropylene substrates [31]. They also found an increase in the contact angle with an increasing number of PEO repeating units of the surfactant and explained this finding using two hypotheses. With increasing molar mass of the surfactant the area which has to be available for the adsorption of the molecule increases [169]. Since the -OH group at the end of the PEO part in the molecule is probably most responsible for the wetting behavior of the molecule due to the very pronounced polarity and the highest partial charge, the -OH groups per surface area ratio can be a decisive factor for the wetting behavior. Furthermore, repulsive forces between the individual PEO molecules might be responsible for the increasing contact angle.

Beck [170] also reported that the water contact angle of polypropylene substrates which were coated with CH_mPEO_n increases with an increasing number of PEO repeating units. He also showed that too long CH_2 chains lead to an increasing water contact angle. This result supports the hypothesis that if the molecule is lying on the surface, the contact angle is a function of the -OH groups per surface area and decreases with increasing PEO as well as with increasing CH chain length, i.e. with the molar mass of the surfactant in general. However, a detailed discussion of the observed phenomena did not take place in Beck's study.

The influence of the additive molar mass can also be explained by the following hypothesis. The surfactant molecule should align with the hydrophobic part towards the air interface in order to minimize the surface energy (see also chapter 2.3.1.1). When the surface is wetted, the interface changes from air to water, causing the thermodynamic boundary conditions to change and the molecule to turn around or flip. The preferred orientation of the hydrophilic part of the surfactant towards the water then allows the surface to be wetted. Molecules with a low molar mass are more mobile and therefore able to change their alignment more easily in order to enable the wetting of the surface. Larger molecules are less mobile, so they cannot flip and align easily towards the altered interface and therefore do not reduce the contact angle as much.

In the following, different publications on morphologies of adsorbed surfactants on different substrates will be discussed to gain an understanding of possible molecular arrangements that may explain the results of the previously discussed experiments. Corkill et al. conducted a study in which n-alkyl polyoxytheylene ethers were adsorbed from an aqueous solution onto

graphone [171]. It was observed that the surface coverage of the adsorbate corresponds approximately to that of a monolayer in which both the hydrophilic and hydrophobic parts of the adsorbate lie flat and are in contact with the surface. Ottewill et al. [172] studied the absorption of an aqueous n-dodecylhexaoxyethylene monoether ($C_{12}E_6$) solution on a monodisperse polystyrene latex dispersion. The adsorbed layer thickness was determined by sedimentation measurements. They found that the adsorbed layer of a solution near the critical micelle concentration has a thickness of 50 Å $\pm$ 5 Å. This layer thickness is consistent with the conclusions of the adsorption isotherms measured in this study and suggests that the molecules form a vertically oriented monolayer in the saturation region. If the concentration of the $C_{12}E_6$ solution is further increased, the sedimentation coefficient decreases. This indicates that there is a rearrangement from a vertical to a horizontal arrangement of the molecules on the surface. Similar rearrangements also occur in the adsorption of alkyl sulphinyl ethanol onto graphone [173].

Figure 6.26 shows the influence of a double bond in the hydrophobic part of the additive on the water contact angle of the coated PP plate. It can be seen that the contact angles of the molecules with double bonds are always above those of the molecules with a saturated hydrophobic chain, with otherwise the same molecular structure. The double bond primarily results in the molecule being restricted in its mobility. Assuming that the molecules mainly adsorb flat on the substrate, the double bond can lead to a non-uniform arrangement of the molecules on the substrate, resulting in a lower -OH density on the substrate's surface area and thus to poorer wettability.

Under the assumption of completely lying molecules, the reciprocal of the Van der Waals volume of the additive molecules can be used as a measure for the number of molecules which adsorb per surface area. Figure 6.27 indicates that the contact angle decreases with increasing surface coverage of the additive. This also supports the hypothesis that the additive molecules adsorb horizontally and that the wetting behavior correlates primarily with the number of -OH groups per surface area. The plot also illustrates that in the case of additives with double bonds in the hydrophobic part of the surfactant, the adhesion to the substrate is probably worse and therefore the contact angle is higher compared to additives with the same molecular architecture except the double bond.

In summary, both, the experiments shown in this study and the discussed literature suggest that the molecules are arranged more parallel to the substrate, than perpendicular. This behavior is due to the attractive forces (i.e. Van der Waals forces) between the methyl and methylene groups which are found

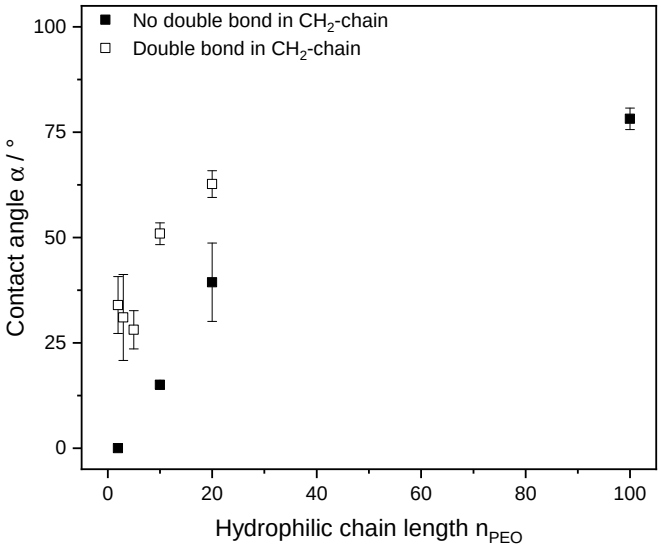

Figure 6.26: Influence of a double bond in the hydrophobic part of a surfactant with otherwise identical molecular structure on the wetting behavior of PP plates which are coated with the surfactant.

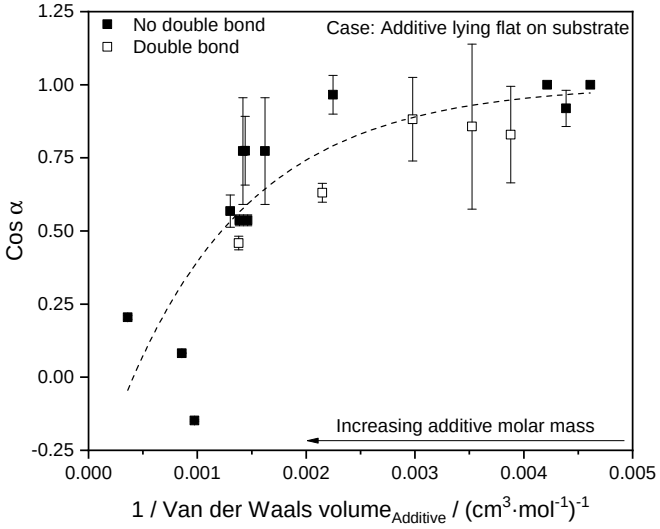

Figure 6.27: Cosine of the contact angle as a function of the reciprocal Van der Waals volume per additive molecule to illustrate the dependence of the contact angle on the number of OH groups per surface area. The model is based on the assumption that the additive molecules adsorb completely to the surface and lie flat. Van der Waals volumes of the molecules were estimated by increments according to van Krevelen [78]. The dashed line in the figure is drawn to guide the eye.

both in the polypropylene substrate and in the hydrophilic and hydrophobic part of the surfactant. In the case of a completely lying surfactant molecule, higher molar masses lead to significantly lower hydroxy group occupancy per unit surface area, which in turn results in deteriorated wetting with increasing PEO chain length in the surfactant. In the case of sorbitan monoesters a dependence of the wetting behavior on the chain length of the hydrophobic part of the surfactant was observed. Since no additives were available for the investigations in which the hydrophilic head of the surfactant was changed, no predictions can be made about the influence of the hydrophobic part of the molecule. The strong influence of the hydrophobic tail group suggests a different adsorption behavior compared to the ethoxylated alcohols. Due to the lower chemical similarity of the hydrophilic head group of sorbitan monoesters to the PP, a different adsorption mechanism might occur. Furthermore, it was shown that only the additive Span 20 caused a considerable reduction of the contact angle with water. All other additives showed no changes or a deterioration compared to the PP plate which was not coated. The results of sorbitan esters can be found in appendix A.6 in figure A.15. The PPO-PEO-PPO block copolymers were not investigated as a coating for the injection molded plates.

Influence of substrate

Based on the hypothesis that an additive strongly adsorbs on a chemically similar substrate and thus aligns parallel to the surface, the contact angle dependence of the -PEO chain length should be less pronounced with chemically less similar substrates. Figure 6.28 shows the influence of different substrates on the resulting contact angle with water after it has been coated with the corresponding surfactants. The experiment demonstrates that the trend of a longer PEO chain length leading to higher contact angles continues. However, this effect is more pronounced at lower substrate surface energies and higher chemical similarity between substrate and surfactant (PP and PE) and decreases with decreasing contact angle and lower chemical similarity (PA).

Comparable results were also reported by Beck [170]. In Beck's study, different n-alkyl polyoxyethylene ethers were applied to polypropylene and glass substrates as a coating. It was shown that the hydrophilization of the coated substrate decreases with increasing EO chain length and that the reduction of the contact angle by the surfactant is much more pronounced on the PP surface than on the glass surface. Furthermore, glass surfaces were treated with various inorganic media to achieve substrate contact angles of 30°, 50° and 70°.

It was found that the more non-polar the surface is, the more it can be hydrophilized by the surfactants and the more the maximum hydrophilic effect is shifted towards low EO chain lengths. Grant et al. [174] conducted a study in which thiohexadecanol was deposited on a gold substrate by chemisorption in order to gradually adjust the hydrophobicity of the substrate, which was subsequently coated with an alkyl polyoxyethylene surfactant solution. The results of the study indicate that the morphology of the adsorbed additive layer changes with increasing hydrophobicity of the substrate. On hydrophilic substrates, diffuse to densely packed micelles were formed due to weak adsorption by hydrophobic interactions and Van der Waals forces. On hydrophobic substrates, relatively homogeneous bi- and monolayers of the additive formed due to the larger interactions between substrate and solution. Ivanova et al. [31] demonstrated that the contact angle of an aqueous solution from C_mPEO_n which is formed on PTFE, parafilm and PP depends on the nature of the substrate. The more hydrophobic the substrate, the lower the resulting contact angle.

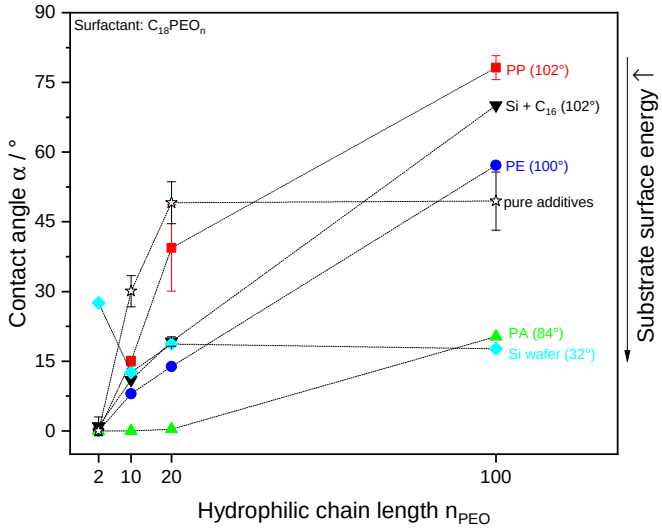

Figure 6.28: Influence of substrate material on the resulting contact angle with water. Water contact angle of the pure substrate in brackets. C16 coating on silicon wafers was performed according to a method by Bauer et al. [175].

These findings support the hypothesis that surfactants are more strongly adsorbed by the substrate if their chemical structure differs only slightly from that of the substrate. This in turn causes the surfactant molecules to deposit parallel to non-polar substrates such as PE or PP, which leads to a strong influence of the chain length on the resulting contact angle. On more polar

substrates, the molecular groups are not as strongly adsorbed and arrange more randomly on the substrate, which leads to a less pronounced molar mass dependence.

In summary, the phenomena leading to the results shown here cannot be fully explained by the methods and literature available and may be the focus of ongoing research. The results shown above and the discussed literature indicate that it is likely that the wetting behavior is a function of -OH groups per surface area. It is assumed that the surfactant molecules primarily adsorb parallel to the polypropylene substrate. The more similar the surfactant molecule and the substrate are chemically, the more the molecule is adsorbed onto the substrate and the greater the molar mass dependence. Therefore the wetting behavior is a combination of the adsorption behavior of the additive and its mobility. A sketch illustrating this hypothesis can be found in figure 6.29. Surfactants with a molar mass of up to 1000 g mol^{-1}, linear hydrophobic tail groups with 15 - 20 repeating units and short hydrophilic head groups are recommended for best wetting of the surface.

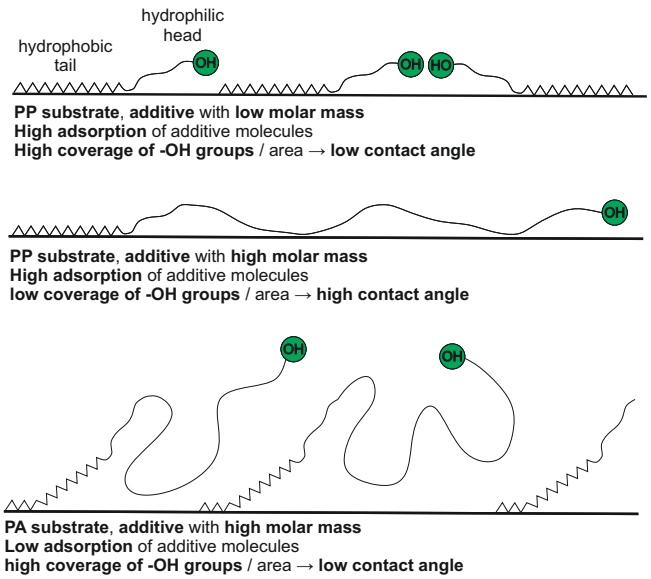

Figure 6.29: Sketch illustrating the adsorption behavior of low and high molar mass additives on different substrates and the associated influence on the resulting contact angle.

The experimental data from this chapter were partially taken from Rockmann's bachelor thesis (supervised by F. J. Lanyi) [176] and analyzed independently within this work.

6.7.2 Wetting behavior of coated nonwovens

Ethoxylated alcohols

Based on the results from chapter 6.7.1, this chapter discusses the transferability of the general findings on the wettability of spincoated plates to nonwovens. Figure 6.30 shows the wetting behavior of polypropylene nonwovens which were coated with the various surfactants. Since a contact angle measurement on nonwovens is not trivial, the much more practice-oriented strike-through time was used as a measure for wettability. The experiment shows that, as with the coated plates, the hydrophilic part of the surfactant has a much greater influence on the wetting behaviour of nonwovens than the hydrophobic part. Furthermore, fine differences in the wetting behavior of the additives which show only minor changes compared to the uncoated substrate cannot be resolved using a strike-through test. This is attributed to the circumstance that above a certain contact angle no liquid permeation of the nonwoven is observed, since the water can no longer spread on the substrate and thus penetrate it.

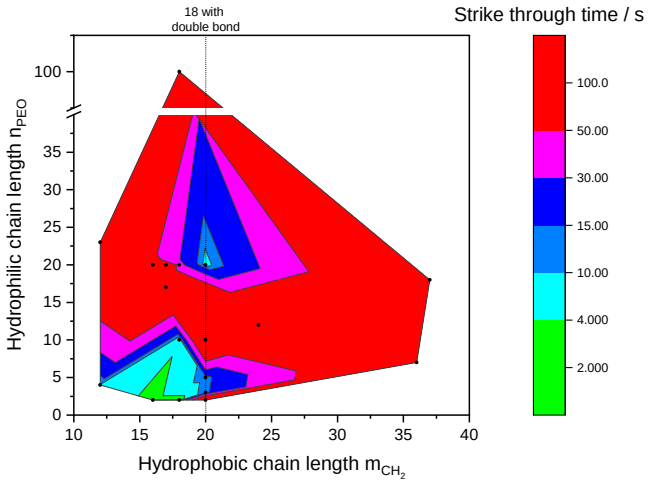

Figure 6.30: Strike-through time of polypropylene nonwovens with a base weight of 28 g/m² which were coated with approximately 0.5 wt% of surfactant.

The transferability of the preliminary tests with the plates to the wetting behavior of nonwovens is presented in figure 6.31. Areas with good wettability of nonwovens and plates overlap and a contact angle of approx. 30° - 45° on one plate is necessary to allow wetting of the nonwoven if both substrates are coated with the same additive. If the contact angle which forms on a coated injection molded plate is higher than 45°, the water will not strike through

the nonwoven. Beck [170] also found that the contact angle of a coated plated can be transferred to the wetting behavior of textiles. Beck's experiments indicated that particularly good wetting on a coated plate can be correlated with rapid wetting of textiles which are coated with the same additive. Rosen et al. [168] reported that in order to wet cotton with a surfactant solution in a short time, high diffusion rates of the additive, low molar masses of the additive and large surface areas per adsorbed molecule at the interface are necessary. These findings agree with the observations shown in this chapter and with the wetting behavior of the coated injection molded plates (see chapter 6.7.1) and explain that low molar mass surfactants with rather long hydrophobic parts and short hydrophilic parts are achieving the best wetting results.

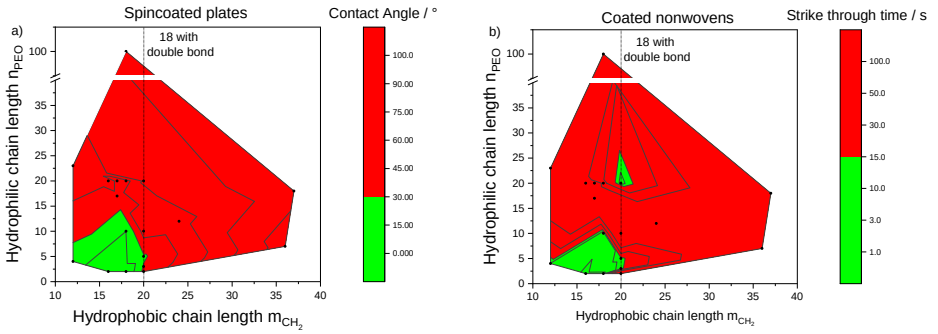

Figure 6.31: Water contact angle of the spin coated plates (a) and corresponding strike-through times of the coated nonwovens (b).

Figure 6.32 shows the strike-through time of nonwovens which are coated with an additive as a function of the contact angle which forms on a plate which is coated with the same additive. Since a determination of the strike-through time was only possible with nonwovens that were actually wettable, only the results from experiments where the strike-through of the nonwoven occured are plotted. The strike-through time as a function of the contact angle on a plate can be described by the function:

$$t_{\text{strike-through}}(\alpha) = t_0 \cdot \left(\frac{\alpha_c}{(\alpha_c - \alpha)} \right)^n \tag{6.3}$$

where t_o is the strike-through time without a nonwoven which acts as a barrier layer, α_c is the contact angle at which the liquid can no longer penetrate the nonwoven, and n is a factor for a better adjustment of the fit function. Strike-through tests without a nonwoven as a barrier layer resulted in t_o = 2 seconds.

Equation 6.3 reveals a value of 50° for the critical contact angle α_c. In the experiments performed in this work, no strike-through time below 150 seconds was observed for additives that had a contact angle of more than 45° on a plate. Within the range of the experimental error, it is assumed that the critical contact angle α_c is in the range of 45° - 60°. Higher contact angles result in the nonwoven no longer being permeable. This indicates that in principle it is possible to correlate the wetting behavior of nonwovens and plates and to use the wettability of plates as a simple test for the selection of potential coating additives.

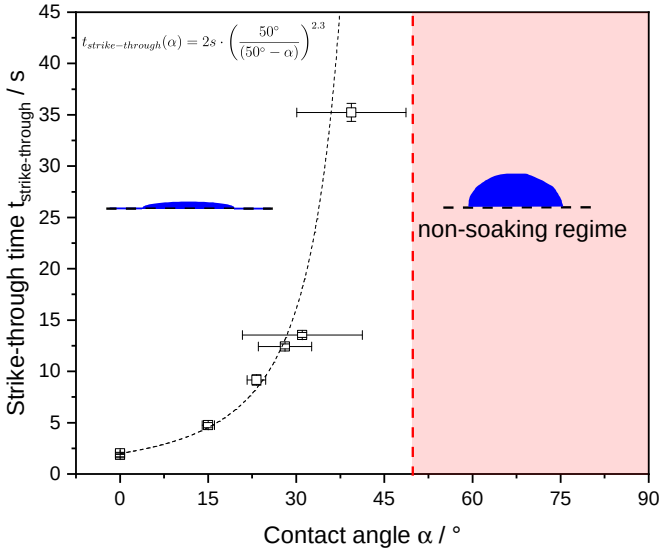

Figure 6.32: Correlation of strike-through time of a nonwoven which is coated with a specific additive and corresponding contact angle which forms on a plate which is coated with the same additive.

In this chapter, it was shown that spin-coated plates are a suitable benchmarking tool for coating additives. Findings from tests with coated plates can be transferred to the wetting behavior of nonwovens. By using plates as a substrate, disadvantages of nonwovens such as the uneven pore structure as well as disadvantages of the strike-through experiment such as poor resolution and reproducibility at high strike-through times can be avoided.

PEO-PPO block copolymers and sorbitan monoesters

None of the PEO-PPO block copolymers used improves the wetting of the nonwovens with water to such an extent that water was penetrating the nonwoven in the strike-through experiment. In the case of sorbitan monoesters,

only Span 20 resulted in a significant improvement in wetting behavior and showed good efficacy, at least in the coating context. Due to the reduction of the strike-through time to 2 seconds, Span 20 is considered to be an effective hydrophilic coating agent. The results can be found in the appendix A.6 (figure A.16).

6.8 Preliminary study on the wetting behavior of nonwovens and single fibers with melt additive

The aim of this thesis is to find melt additives for the production of hydrophilic polypropylene fibers and nonwovens and to investigate the influence of processing conditions on their migration to the surface. Since the portfolio of available potential additives (see chapter 5.2) is very large, the additive selection shall be severely restricted in preliminary experiments to investigate the influence of the production parameters and the structure formation of the polymer matrix on migration in more detail.

First, single fibers and nonwovens were produced under standard conditions and investigated with regard to wetting and migration behavior. The aim of this study is to systematically identify additive groups which can migrate to the surface under standard storage conditions (i.e. a storage temperature of 20 °C - 40 °C) and at the same time cause hydrophilization of the surface.

In order to evaluate the two phenomena hydrophilization and migration to the surface, auxiliary variables are introduced. Due to difficulties in characterizing the wetting behavior of single fibers and nonwovens resulting from the uneven surface structure of the substrates, a qualitative approach is chosen to assess the wetting behavior. The method is based on evaluating the wetting behavior in categories from 1 (very good) to 6 (no change compared to pure polypropylene) and described in chapter 4.2.1.3. Furthermore, a coefficient for the extent of surface saturation is introduced to evaluate the migration behavior. The coefficient is calculated from the quotient of the peak ratio, which is determined via ATR-FTIR (germanium, penetration depth 0.7 µm) and via transmission FTIR and reflects the additive enrichment in the near surface volume compared to the overall concentration of the additive inside the fibers:

$$\text{Coefficient of surface saturation} = \frac{\text{Peak ratio}_{d_p=0.7\mu m}}{\text{Peak ratio}_{\text{bulk measurement}}} \propto \frac{\text{Additive surface concentration}}{\text{Total additive concentration}} \quad (6.4)$$

The higher the coefficient of surface saturation, the more additive migrated to the surface. If this coefficient is less than 1, it indicates that the surface is desaturated. With the help of the coefficient of surface saturation it is possible to compare the migration behavior of different additives by normalizing the near-surface additive concentration to the total concentration. In addition, conclusions about the migration behavior of additives can be made without the use of complex calibration procedures.

Spinnability

The spinning experiments revealed that all additives mentioned in chapter 5.2, which were solid at room temperature, can be spun under standard conditions at a concentration of 2 wt% and after stabilization with Irgafos 168. Only the sorbitan esters exhibited rare spinning instabilities. This effect is attributed to the degradation of the additive, which also caused slight smoke formation during the experiments.

6.8.1 Wetting and migration behavior of single fibers

Ethoxylated alcohols

Based on the assumption that both, the migration of the additive to the surface and the hydrophilic effect of the additive as such, are necessary for hydrophilizing a surface, both phenomena are examined in figure 6.33. Figure 6.33 (a) illustrates the migration behavior of the additive in the single fibers and figure 6.33 (b) shows the hydrophilization effect of the additive as a coating on an injection molded plate (see also chapter 6.7.1). The migration behavior was determined after a storage period of at least 20 days. Some of the additives which are in the liquid state at room temperature were not used for these experiments due to difficulties in the production of a masterbatch from liquid additives with the extrusion lines available at the institute. In addition, due to the low molar mass of the liquid additives, it is assumed that they possess a relatively low decomposition point. Therefore large amounts of the additive may be degraded and thus will get lost in the production process of fibers (see also chapter 6.2). Due to the higher mobility in the liquid state, it is

also expected that liquid additives will cause problems with permanence and durability.

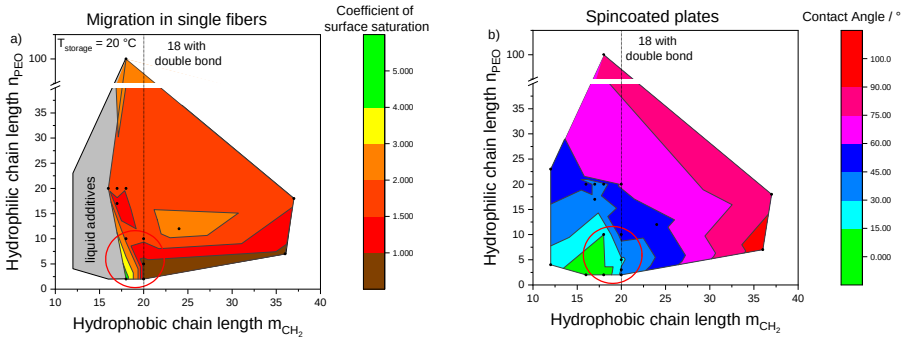

Figure 6.33: Migration behavior (a) of single fibers produced with the ethoxylated alcohols and contact angles of injection molded plates (b) coated with the additives. Red circles illustrate sweet spots of excellent migration behavior and high wettability of the additive.

The experiments show that the additives migrate relatively poorly at room temperature and that only in the case of $C_{18}PEO_2$ the coefficient of surface saturation is significantly higher than 2. However, the coefficient of surface saturation is above 1 in almost all cases. This indicates that all additives migrate to the surface, even if there are only small amounts of the additive present on the surface. Since at least a small enrichment of the additive is detected in near-surface regions of all samples and since, as described in chapter 6.7.1, almost all additives cause a reduction of the water contact angle, the improvement of the wetting behavior of almost all samples is expected.

Figure 6.34 shows the wetting behavior of fibers stored at room temperature (20 °C) and slightly elevated temperature (40 °C) for at least 20 days. After the production, the wetting behavior was determined at intervals of 1 - 3 days. Usually, the wetting behavior did not change after a storage time of about 7 - 10 days. This result is in line with the migration behavior discussed in more detial in chapter 6.11. Figure 6.34 demonstrates that the additives which cause a good performance as a hydrophilic melt additive lie in the intersection of the sweet spots of good wetability and good migration behavior in figure 6.33. It is therefore concluded that for the hydrophilization of the surface it is necessary that the external boundary conditions (e.g. degradation of the additive, molar mass and crystalline structure of the matrix polymer or miscibility of matrix and additive) allow migration to the surface and the additive hase to cause a strong hydrophilization of the surface (i.e. a reduction of the water contact angle significantly below 45 °, see chapter 6.7.2). The additive can only function as a hydrophilic melt additive if these two boundary

conditions are completely and optimally met. Furthermore, it is observed that some samples show a worsening of the wetting behavior at a storage temperature of 40 °C due to a reduction of the additive concentration on the surface as a result of the elevated storage temperatures. This effect is investigated in more detail in chapter 6.11.3.

a)

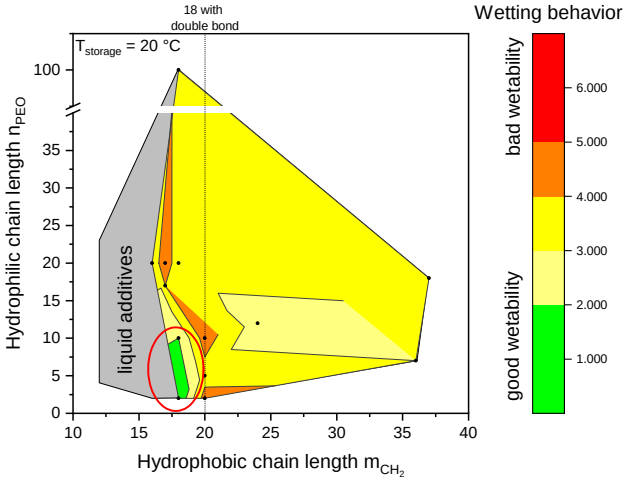

b)

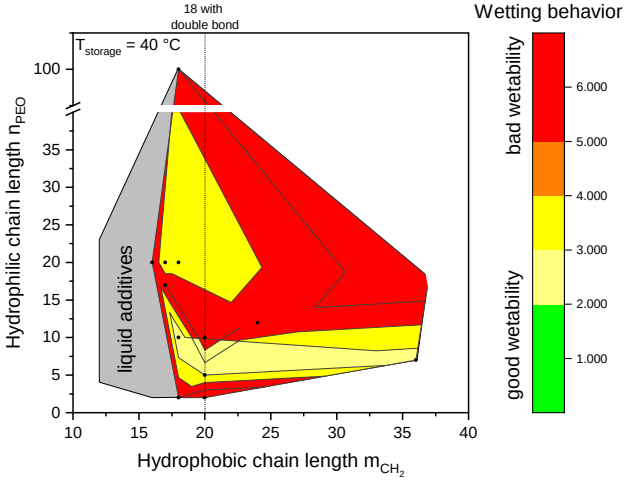

Figure 6.34: Wettability of single fibers stored for at least 20 days at a storage temperature of 20 °C (a) and 40 °C (b) . The red circle represents the regions where excellent wettability and migration are met, resulting in good wettability of the single fibers. Wetting behavior was qualitatively evaluated as described in chapter 4.2.1.3.

Sorbitan monoesters and PEO-PPO block copolymers

None of the PEO-PPO-PEO block copolymers was able to promote surface hydrophilization under standard process conditions. At a storage temperature of 20 °C and a storage time of one month, sporadic wetting of the fibers under high capillary forces was detected. However, no spontaneous wetting was found in any experiment. This behavior is due to the generally poor wetting behavior of PEO-PPO block copolymers and led to similar results when used as coating (see also chapter 6.7.2).

The sorbitan monoester showed comparable results to the PEO-PPO block copolymers. Only Span 40 was able to cause spontaneous wetting of the single fibers when stored at a temperature of 40 °C for one month. This result is probably due to the already described degradation of the additives in the spinning process, resulting in significantly less additive which is available for migration to the surface and the comparably poor wettability.

6.8.2 Wetting and migration behavior of nonwovens

Ethoxylated alcohols

Preliminary experiments which covered the wetting behavior in single fibers revealed that the hydrophilization of fibers is a superposition of the hydrophilization effect of an additive on the surface and the migration behavior. Accordingly, figure 6.35 shows the migration behavior of nonwovens stored for 6 months at 20 °C or 40 °C and the associated wetting behavior. Also in the case of nonwovens the hydrophilization of the surface depends on the migration to the surface as well as the hydrophilization effect of the additive as such. The experiments indicate that migration at room temperature in nonwovens is more effective for almost all the additives compared to the single fibers. This effect may be due to the heat input during calendering and is discussed in more detail in chapter 6.11.1.4. However, at a storage temperature of 40 °C considerably less additive is available at the surface, which in turn results in poorer wetting of the nonwovens. Furthermore, the saturation towards the surface decreases significantly (see appendix A.7, figure A.17). This phenomenon is illustrated by the surface concentration decreasing with decreasing FTIR penetration depth, indicating a desaturation of the surface. The mechanisms leading to the desaturation of the surface are explained in detail in chapter 6.9.2 and 6.11.3.

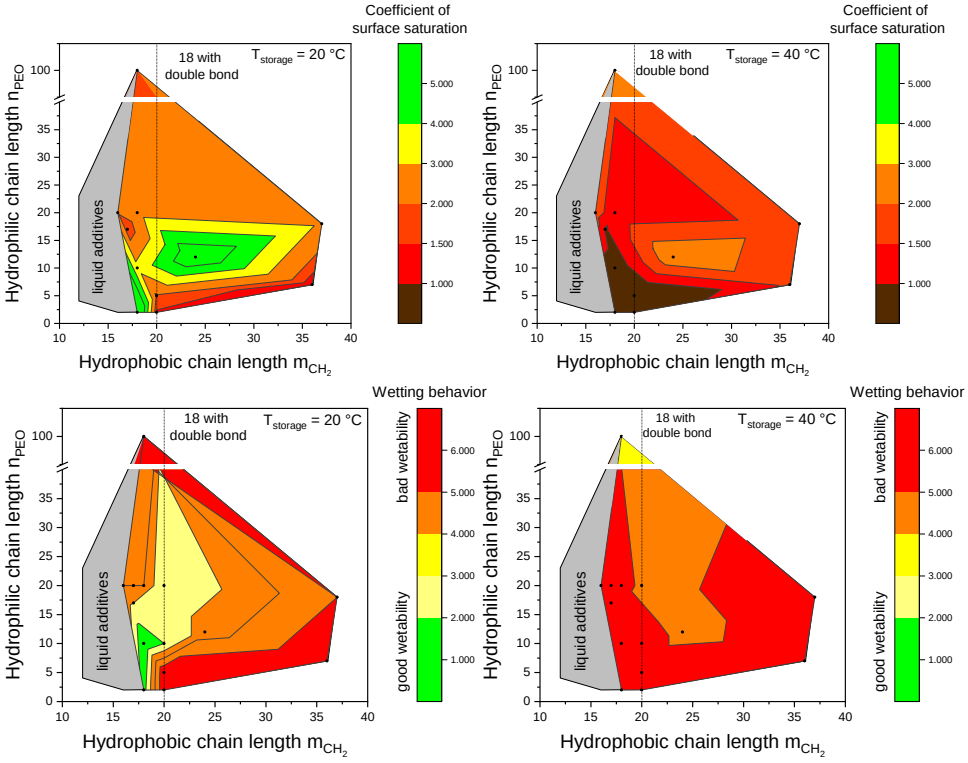

Figure 6.35: Migration behavior (upper row) and wetting behavior (lower row) of nonwoven samples which were stored at 20 °C (left column) and 40 °C (right column) for 6 months. Wetting behavior was qualitatively evaluated as described in chapter 4.2.1.3.

Sorbitan monoesters and PEO-PPO block copolymers

None of the PEO-PPO block copolymers or sorbitan monoesters used in this work cause a change in wetting behavior of nonwovens compared to pure polypropylene when used as a melt additive. Also longer storage times of up to 3 months or storage at an elevated temperature of 40 °C caused a change in the wetting behavior. In the case of PEO-PPO block copolymers, this is due to the poor wetting efficiency of the additives in general. Even applied as a coating, the additives were not able to promote wetting of nonwovens (see chapter 6.7). In the case of sorbitan monoesters, the poor efficacy is probably due to degradation in the process. In comparison to other additives, the low molar mass sorbitan monoesters showed increased smoke formation during production. Due to the bad performance of PEO-PPO-block-copolymers and sorbitan monoesters, the following experiments were conducted on ethoxylated alcohols only.

Summary

This chapter revealed that the successful use of a chemical as a hydrophilic melt additive depends on the migration of the additive to the surface and the ability of the additive to greatly reduce the water contact angle. Based on the observations from this and previous chapters, the selection of additives for the evaluation of the influence of production parameters and matrix structure on the migration was severely restricted. Since $C_{18}PEO_2$ and $C_{18}PEO_{10}$ showed the best performance in preliminary tests for the use as melt additives in single fibers and nonwovens, the $C_{18}PEO_x$ series was used as a starting point. $C_{18}PEO_x$ additives offer the advantage that without changing the hydrophobic part of the molecule, they cover a wide range of common molar masses of melt additives and are present in the solid state at room temperature. Furthermore, the same additives are available with a double bond in the hydrophobic chain (Brij O series), which allow to further study the influence of different molecular architectures.

6.9 Surface migration of additives in injection molded plates

As shown in the previous chapters, fibers and nonwovens represent a rather poorly reproducible structure for wetting tests and migration studies due to the rough and porous surface which is hard to reproduce. To solve this problem, injection molded plates were utilized to determine basic correlations of the migration behavior. The plates have the advantage that they can be produced in a fast way, have a high reproducibility in terms of surface quality and additive distribution and possess a pore-free surface with low roughness. In addition, the low surface crystallinity and the small spherulite sizes enable a much better migration of additives in the plates than with cast films or fibers if the plates were manufactured with appropriate production parameters. The aim of this chapter is to describe the migration of additives with different molecular architectures as a function of storage temperature and time and thus to establish fundamental relationships to migration behavior.

6.9.1 Influence of surface crystallinity and morphology

Figure 6.36 shows the time-dependent migration of $C_{18}PEO_2$ in plates produced at different mold temperatures. The experiment demonstrates good migration in plates which were produced with a mold temperature of 40 °C and 60 °C. Above a critical mold temperature between 60 °C and 80 °C the migration behavior deteriorates significantly.

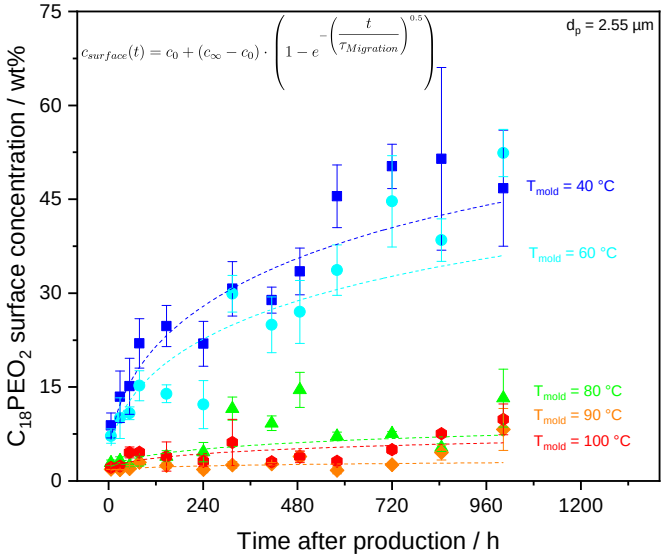

Figure 6.36: Migration behavior of $C_{18}PEO_2$ in injection molded plates produced at different mold temperatures. Fit with equation 2.9 using a constant τ for all samples.

As discussed in chapter 6.6, at a mold temperature of 40 °C there are no crystallite structures in the outer 500 µm of the plate which can be detected using a light microscope. Therefore, it is assumed that the outer layer consists primarily of mesomorphic structures or very small crystallites, which do not represent a major obstacle to the migration of additives. From a mold temperature of 60 °C, crystallites are visible in near-surface regions. The size of the crystallites grows with increasing mold temperature. From a temperature of 80 °C the migration to the surface decreases significantly which is reflected in a decreasing plateau concentration (figure 6.37). The blocking effect is attributed to the growth of the crystallites and the poorer permeability of the α-crystalline structures as well as the increasing surface crystallinity (see also figure 6.23, chapter 6.6). Furthermore the entrapment of additives as a result of co-crystallization may play a role [177]. Figure 6.38 shows an illustration of this hypothesis.

Alin et al. [80] studied the migration behavior of antioxidants from various packaging polymers during microwave heating. It was found that the migration to the surface decreases with increasing degree of crystallinity of the matrix. Maghsoud et al. [79] correlated the total crystallinity of a HDPE matrix with the migration behavior of Irganox 1010. They observed that the total amount of Irganox 1010 which migrates to the surface decreases with increasing degree of crystallinity. Maghsoud et al. assumed that the migration

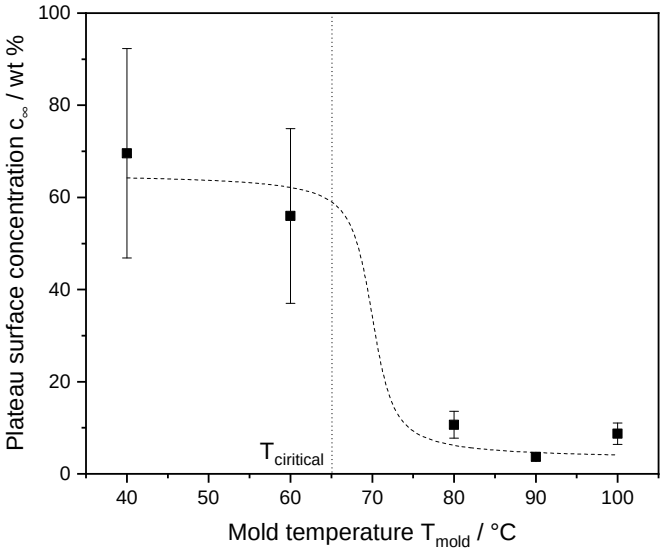

Figure 6.37: Plateau surface concentration as a function of the mold temperature of the samples shown in figure 6.36. The dashed line in the figure is drawn to guide the eye.

to the surface is a function of total crystallinity while the crystallite size and distribution only influence the migration kinetics. In both studies, however, no deeper considerations were made about the surface with regard to its morphology or crystallinity.

In summary, it is concluded that the cooling conditions have a significant influence on morphology formation and crystallization in the injection molding process. These in turn have a substantial influence on the migration behavior, since crystalline structures are not permeable for the additive molecules and thus block the migration. The plates produced at a mold temperature of 40 °C showed the best migration behavior. Therefore, samples for the following experiments were all produced with a mold temperature of 40 °C in order to resolve differences in migration behavior as a result of different molecular architectures as best as possible.

The experimental data from this chapter were taken from Sharma's master thesis (supervised by F. J. Lanyi) [178] and analyzed independently within this thesis.

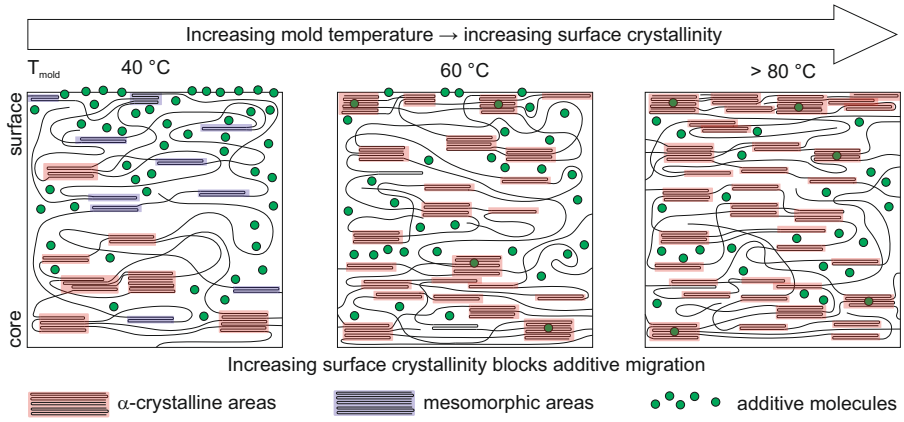

Figure 6.38: Graphical representation of how a higher surface crystallinity due to an increased mold temperature in injection molding results in inhibition of additive migration.

6.9.2 Influence of storage temperature and time

This chapter reveals the influence of the storage temperature and time on the migration of additives with different molar masses. For the experiments the additives $C_{18}PEO_2$ and $C_{18}PEO_{10}$ were selected as they showed the best results with regard to the hydrophilization of the surface in preliminary studies (chapter 6.8). In addition, the additive $C_{18}PEO_{20}$ was selected in order to study an additive with a higher molar mass while the additive structure is not significantly different from the other two investigated molecules as the hydrophobic part of the molecule is kept constant.

The following graphs show the surface concentration as a function of the storage time for different storage temperatures. All near-surface concentrations were determined using ATR-FTIR at a penetration depth of 2.55 µm as these experiments were more reproducible compared to experiments conducted at a penetration depth of 0.7 µm. The corresponding curves measured at a penetration depth of 0.7 µm can be found in the appendix (figure A.18).

All experiments indicate an additive enrichment towards the surface due to an increasing additive concentration with decreasing penetration depth. This behavior is discussed in detail in chapter 6.12. Furthermore, most experiments reveal a time-independent surface concentration (plateau concentration) after a sufficiently long storage time. This plateau value is usually highly dynamic due to external boundary conditions and experimental scattering (e.g. air humidity, slight temperature fluctuations, punctual segregation of

the additive, etc.). However, the plateau is only quasi-stationary within the experimentally observed range. Due to the low surface-area-to-volume ratio of the plates, an almost unlimited additive reservoir is available, allowing even more additive molecules to reach the surface after significantly longer storage times than observed in this study. These experiments would have gone beyond the experimental framework. A migration experiment which was conducted over the storage period of almost one year can be found in appendix A.10, figure A.26.

The measurement data is fit with equation 2.10 (chapter 2.3.3) to describe the kinetics and thermodynamics of the migration. The fit parameters are discussed in chapter 6.9.3 with regard to the molecular architecture of the additive molecules. Although the description of the experimental data is not completely accurate in cases where migration and degradation strongly overlap, the fit data was sufficient to draw conclusions about kinetics and thermodynamics of the investigated systems.

$$c_{\text{surface}}(t) = c_0 + (c_\infty - c_0)\cdot \underbrace{\left(1 - e^{-\left(\frac{t}{\tau_{\text{Migration}}}\right)^{0.5}}\right)}_{\text{Migration term}} \cdot \underbrace{\left(e^{-\left(\frac{t}{\tau_{\text{Degradation}}}\right)^{c}}\right)}_{\text{Degradation term}} \quad (2.10)$$

Figure 6.39 shows the migration behavior of $C_{18}PEO_2$ at different storage temperatures. The additive does not migrate at a storage temperature of - 12 °C, 40 °C and 50 °C, while it migrates to the surface at a temperature of 4 °C, 20 °C and 30 °C. The absence of migration at -12 °C can be explained by the glass temperature of the matrix polymer. As demonstrated in chapter 6.1, the investigated polypropylenes have a glass temperature of about -5 °C to +5 °C. Below the glass temperature, the amorphous regions of the polymer are not mobile and the molecules are hindered by the matrix to migrate to the surface. If the storage temperature is increased, the amorphous regions in the polymer become flexible and the additive can migrate towards the surface because it is no longer kinetically hindered. At a temperature of 4 °C, the additive migrates very slowly to the surface. Since a temperature of 4 °C is only slightly above the glass temperature, the polymer chains in the amorphous regions are still very rigid and the additive molecules are only moderately mobile. This in turn leads

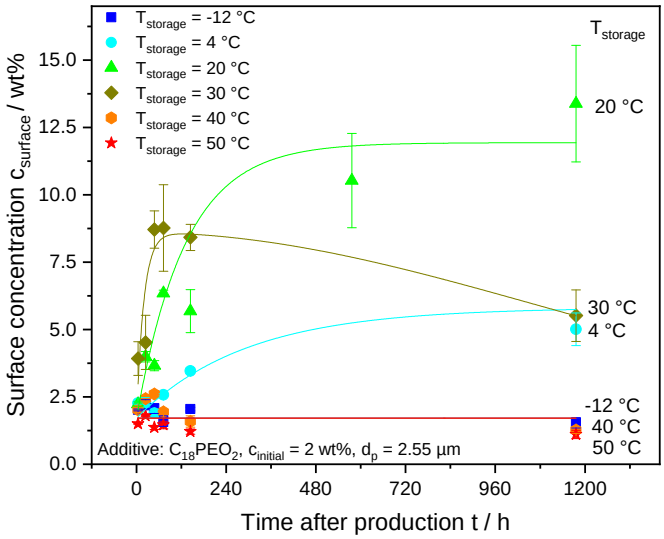

Figure 6.39: Migration curves of injection molded plates with 2 wt% of $C_{18}PEO_2$ stored at different temperatures. Fits with equation 2.10 (chapter 2.3.3)

to the result that the additive may migrate, but the migration takes place very slowly and the diffusion constant is comparatively low. At a temperature of 20 °C, migration is considerably faster. After a storage period of about 40 days, there is significantly more of the additive on the surface than at lower storage temperatures. From a temperature of 30 °C the migration is superimposed by effects which lead to a desaturation of the surface. Although the migration rate increases, the maximum achievable surface concentration is lower than at a storage temperature of 20 °C. From a temperature of 40 °C and above, migration to the surface can no longer be detected. The concentration remains at the level of the initial concentration even after more than 1000 hours. For samples stored at 50 °C, surface concentration even decreases to 1.1 wt%, i.e. slightly below the initial concentration. This effect might be attributed to a migration back to the core, which has been suggested by Shuler et al. for similar effects found for the migration of erucamide in polypropylene [22]. Another potential factor that might influence the reduction of the additive on the surface is the evaporation of the additive due to the elevated temperature. Horike et al. [179] reported that $C_{12}PEO_4$ begins to evaporate at a temperature of about 50 °C under vacuum. Despite the higher molar mass of the additives used in our study, evaporation processes at elevated storage temperatures of 50 °C and above might contribute to a reduction in surface concentration.

Földes and Szigeti-Erdei consider the solubility and the diffusion coefficient as the two main factors for the migration rate of small molecules [85]. In order to achieve high migration rates, the additive must exhibit very low solubility and a high diffusion coefficient. Another study conducted by Földes shows that a high solubility of an antioxidant in the polymer matrix can significantly reduce the migration of the additive [177]. The inhibition of migration is preferred for antioxidants, where leaching of the antioxidant due to high migration rates has to be prevented. This observation can also be transferred to the additive $C_{18}PEO_2$, since there is evidence that the additive is well miscible with the matrix polypropylene due to its high chemical similarity and low molar mass (see also chapter 6.3). The recrystallization of the polymer during annealing is another factor for the deteriorated migration at elevated temperatures, which is considered in Földes' study. It is assumed that small amounts of the additive co-crystallize with the polymer chains and thus become immobile. Even though no evidence was found that the molecules used in our study were hindered by co-crystallization at elevated temperatures, it is a realistic scenario as recrystallization effects already occur in quenched polypropylene samples at 50 - 60 °C (see chapter 6.4.2 figure 6.15). Wakabayashi et al. [72] expect that erucamide in polypropylene films migrates considerably worse to the surface at temperatures close to the melting temperature of the additive ($T_{m,\ Erucamide}$ = 78 °C) and attribute this behavior to the solubility of the additive in polypropylene. From a temperature of 40 °C and above, the solubility of erucamide in polypropylene increases considerably, leading to less additive being available for migration to the surface. They assume that the amount of additive available for migration is the difference between the initial amount of additive and the saturation solubility of the additive in the matrix. Wakabayashi et al. used the poorly soluble behenamide in addition to the highly soluble erucamide and demonstrate that behenamide migrates better with increasing storage temperatures. However, they do not show experiments where the worsened migration of erucamide at elevated temperatures is demonstrated. Dulal et al. [112] studied the migration behavior of erucamide as a slip agent for polypropylene bottle caps. They report that there is no migration of erucamide at a temperature of 4 °C and 23 °C, while the migration starts slowly at a storage temperature of 38 °C and is most pronounced at a temperature of 50 °C. Due to the high solubility of erucamide, migration is expected to decrease considerably from a temperature of 50 °C onwards.

Figure 6.40 shows the migration as a function of time for the additive $C_{18}PEO_{10}$. Compared to $C_{18}PEO_2$ the migration at a temperature of 20 °C is slower and the plateau concentration is lower. With increasing storage temperature

the migration proceeds faster and the plateau concentration increases. This phenomenon is attributed to a higher diffusion coefficient due to increased mobility of the additive and the polymer matrix. From a storage temperature of 60 °C and above, the surface concentration initially increases rapidly, passes through a maximum and then drops off. The speed at which the surface concentration decreases, i.e. the speed at which the surface is desaturated, depends on the storage temperature. The plates stored at 80 °C and 115 °C show a strong discoloration and embrittlement after storage for 350 hours (see appendix figure A.10), which is why the desaturation of the surface is attributed to a degradation of the additive. Due to that circumstance, storage experiments at 80 °C and 115 °C were terminated after approximately 350 hours. Since the degradation effects superimpose the migration (the surface concentration goes through a maximum in the experiments carried out at elevated temperatures), it is assumed that the matrix solubility of $C_{18}PEO_{10}$ plays only a minor role for the desaturation effect. In the case of $C_{18}PEO_2$ it is considered that due to the increased matrix solubility the migration at elevated storage temperatures was completely suppressed and therefore did not pass a maximum. The solubility of the low molar mass additives in polypropylene was demonstrated in chapter 6.3.

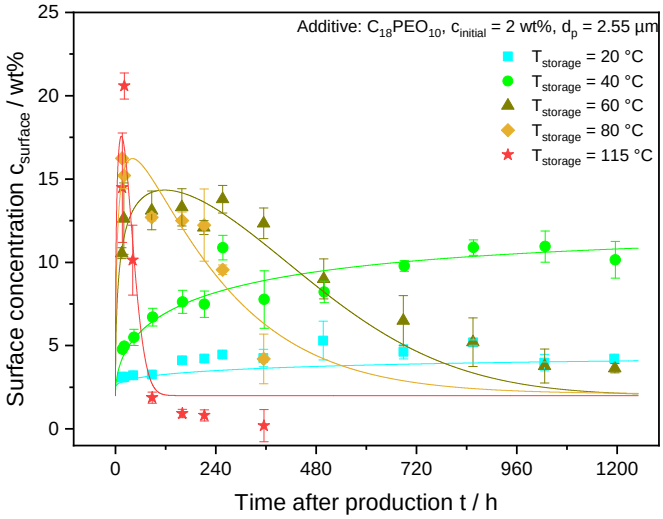

Figure 6.40: Near surface concentration as a function of storage time of injection molded plates with 2 wt% of $C_{18}PEO_{10}$ stored at different temperatures. Fits with equation 2.10 (chapter 2.3.3)

As the degradation of samples stored at temperatures above 80 °C was accompanied by a strong increase in the diffusion coefficient, short-term measurements were conducted in which the storage time was limited to 1 - 4 hours.

The samples were stored in a hot air oven in order to enable the migration before degradation can set in. The results are shown in figure 6.41. The plot illustrates that degradation phenomena can be almost eliminated at storage times of only a few minutes to hours and that migration to the surface takes place within very short periods of time. In the experiments, the solubility of the additive in the matrix polymer becomes apparent. Although the enrichment of the surface occurs very quickly at a temperature of 150 °C and 130 °C, the enrichment is lower than at a temperature of 115 °C. Therefore, the loss of additive amounts that are available for migration is attributed to the solubility of the additive in the matrix.

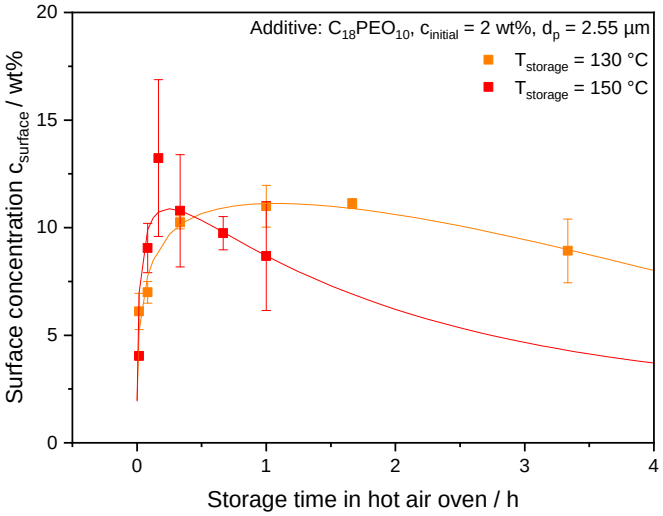

Figure 6.41: Migration curves of injection molded plates with 2 wt% of $C_{18}PEO_2$ stored at different temperatures for short storage times. Fits with equation 2.10 (chapter 2.3.3)

Figure 6.42 shows the migration curves of $C_{18}PEO_{20}$, which are very similar to those of $C_{18}PEO_{10}$ with the difference that the phenomena discussed above are shifted to even higher temperature ranges. This means that the migration to the surface is also faster with increasing temperature and these phenomena are superimposed by a degradation of the additive at higher temperatures, which is why the surface desaturates again. The superposition of migration and degradation results in a maximum surface concentration, which is reached after a few minutes to hours depending on the storage temperature.

The experimental data from this chapter were partially taken from Kleebauer's bachelor thesis (supervised by F. J. Lanyi) [180] and analyzed independently within this thesis.

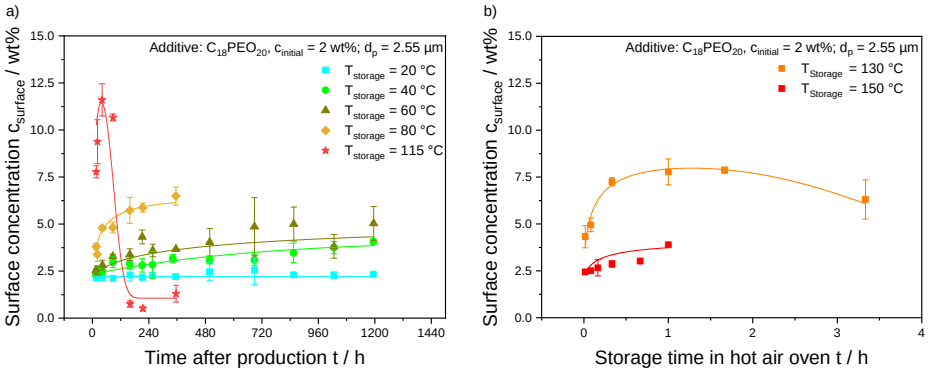

Figure 6.42: Near surface concentration of injection molded plates with 2 wt% of $C_{18}PEO_{20}$ stored at different temperatures for short (a) and long (b) storage times. Fits with equation 2.10 (chapter 2.3.3)

6.9.3 Influence of additive molecular structure

In order to demonstrate the influence of the molecular structure on the migration behavior, all migration curves shown in the previous chapter were fitted with equation 2.10 (chapter 2.3.3). Figure 6.43 shows the migration coefficient $\tau_{\text{Migration}}$ (a) and the degradation coefficient $\tau_{Degradation}$ (b) as a function of the storage temperature for the investigated additives. Both graphs illustrate that the influence of temperature on all three additives used is comparable due to similar mechanisms leading to degradation or migration of the additive. The resulting curve shape is similar and shifted to higher or lower temperatures depending on the molar mass of the additive.

The slower migration of larger molecules compared to smaller molecules in the same polymer matrix is already well studied. Földes [177] demonstrated that the diffusion coefficient of antioxidants in polypropylene decreases with increasing ratio of additive volume to the specific overall free-volume of the system. Another study by Földes [85] has shown a linear relationship between the relative chain length and the additive amount of esters which migrates from an ethylene-vinyl acetate (EVA) layer to a PE layer at 25 °C and 50 °C. Möller and Gevert determined the diffusion coefficient of hindered phenols with different molecular sizes in LLDPE at different temperatures [181]. They revealed that the diffusion coefficient decreases with increasing number of methylene groups of the molecule. This relationship can be described by an exponential function. Similar findings have been made by Asfour et al. [84] as well as Moisan et al. [182] for n-alkanes in LDPE or by Dubini et al. [183] for esters and hydroxybenzophenones in isotactic polypropylene. The slower

a)

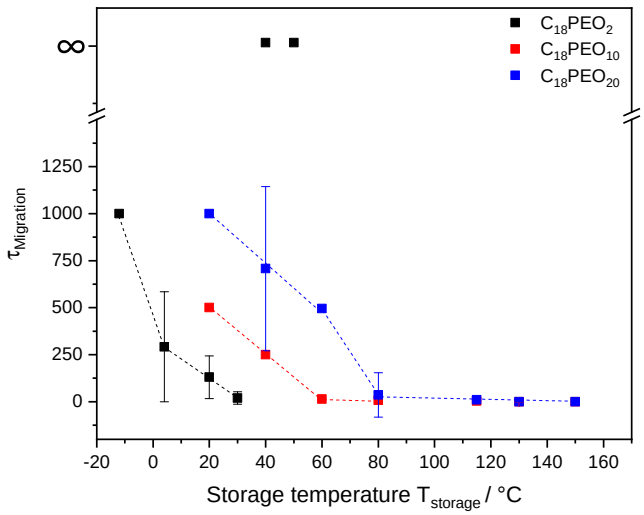

b)

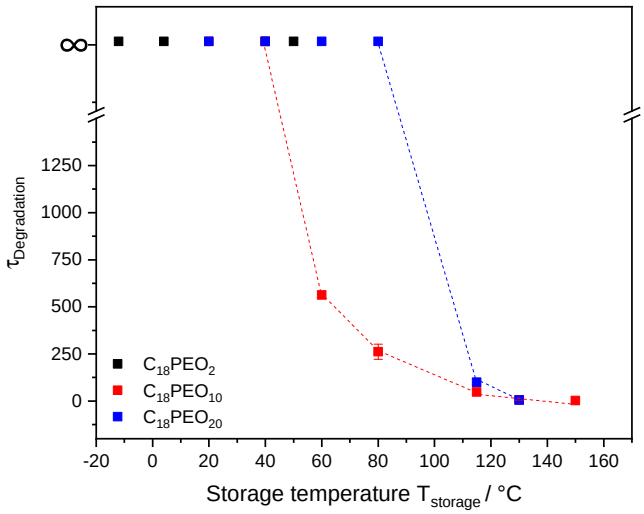

Figure 6.43: Temperature dependence of the coefficients of migration $\tau_{\text{Migration}}$ (a) and degradation $\tau_{Degradation}$ (b) of three additives which differ in the molar mass of the hydrophilic part of the surfactant. The dotted lines are drawn to guide the eye.

degradation of additives with increased molar mass has been discussed in chapter 6.2.

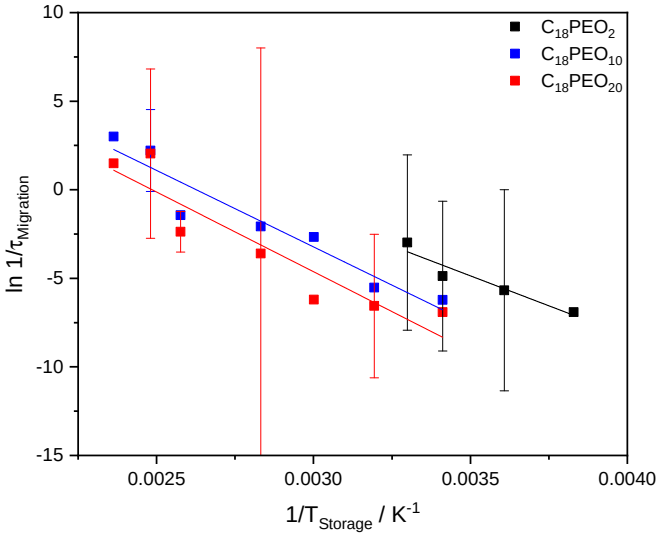

Figure 6.44: Temperature dependence of the reciprocal of the coefficient of migration $\tau_{Migration}{}^{-}1$ of three additives which differ in the molar mass of the hydrophilic part of the surfactant.

Figure 6.44 shows that the reciprocal of the migration coefficients $\tau_{Migration}{}^{-1}$ of the investigated additives follow an Arrhenius function. Since the reciprocal of the migration coefficient $\tau_{Migration}{}^{-1}$ shows a proportionality to the diffusion coefficient, equation 6.5 can be used to determine an activation energy E_A for the diffusion.

$$D \propto \frac{1}{\tau_{Migration}} = A \cdot e^{\frac{-E_A}{R \cdot T}} \tag{6.5}$$

Due to the experimental scattering of the measurement data, the standard deviations of the prefactor A and the activation energy E_A are relatively large (table 6.5). Both, the prefactor and the activation energy increase with increasing molar mass of the hydrophilic part of the surfactant, but are almost equal within the experimental scattering.

Koszinowski [184] investigated the diffusion behavior of n-alkenes with different molar masses in different polyolefins. It was demonstrated that the prefactor and the activation energy increase with increasing molar mass of the n-alkenes and that the diffusion coefficient at the same temperature is lower

Table 6.5: Fit parameters of the data from figure 6.44 using equation 6.5

Additive	Activation Energy E_A / kJ mol^{-1}	Prefactor ln A
$C_{18}PEO_2$	56.2 ± 25.1	18.8 ± 10.7
$C_{18}PEO_{10}$	71.8 ± 10.7	22.7 ± 3.7
$C_{18}PEO_{20}$	74.4 ± 10.7	22.4 ± 3.7

for molecules with a higher molar mass. In Hiemer's master thesis [185] the diffusion behavior of additives $C_{18}PEO_2$ and $C_{18}PEO_{10}$ in a polypropylene matrix was simulated. It was found that the diffusion coefficients of the additives behave according to an Arrhenius function. Within the statistical scattering the additives $C_{18}PEO_2$ and $C_{18}PEO_{10}$ have the same activation energy of 34.7 ± 4.2 kJ mol^{-1} and the prefactor increases with increasing molar mass of the additive. Wakabayashi et al. [72] report an activation energy of 104 kJ mol^{-1} for erucamide and 122 kJ mol^{-1} for behenamide in polypropylene. They also found an increase of E_A as a function of the molecular size of the additive. Möller et al. [181] found an activation energy of 87 kJ mol^{-1} to 104 kJ mol^{-1} for the diffusion of hindered phenols with a molar mass of 292 g mol^{-1} to 530 g mol^{-1} in LDPE. In comparison with the studies discussed, the activation energies determined in this thesis are in a realistic range. Based on the available literature it is assumed that the activation energy increases with increasing molar mass of the additive. However, since the relative errors are very large, no definitive statement can be made. Within the scope of the error it is also possible that, as shown in Hiemer's study, the activation energy of the investigated additives is the same and that they differ only in the prefactor.

A plot of the plateau concentration c_∞ as a function of the storage temperature (Figure 6.45) illustrates that the plateau surface concentration of the investigated additives passes through a maximum and is shifted to higher storage temperatures with increasing additive molar mass. As already discussed for the case of $C_{18}PEO_2$, this maximum is most likely due to the increased solubility of the molecule starting from or slightly below the melting point of the additive. The higher solubility significantly reduces the additive amount which is available for migration to the surface. Therefore, the plateau concentration decreases from a critical temperature (30 °C in the case of $C_{18}PEO_2$) to the initial concentration. Due to the low molar mass of $C_{18}PEO_2$, the matrix solubility is considerably increased compared to the other two additives, which is why even at low storage temperatures less additive is available which can migrate to the surface. For this reason, the maximum plateau concentration is

lower than in the case of $C_{18}PEO_{10}$. The curve shape of the additives $C_{18}PEO_{10}$ and $C_{18}PEO_{20}$ is comparable. The maximum of both curves is found at a storage temperature of 115 °C. The reduced maximum surface concentration at a temperature of 130 °C and above may be due to an entrapment of the molecules in recrystallized areas of the polypropylene [177], due to a recrystallization of the matrix surface which blocks the additive (see chapter 6.9.1), degradation of the additive (see also chapter 6.2) or due to increased solubility of the additive in the matrix polymer [72]. The lower maximum of $C_{18}PEO_{20}$ compared to $C_{18}PEO_{10}$ can be explained by the lower diffusion coefficient of the larger molecule and the thermodynamic boundary conditions which causes the maximum plateau concentration to shift to ranges of higher storage temperatures. However, from a temperature of 130 °C the maximum is superimposed by effects such as recrystallization, solubility of the additive in the matrix or melting of the polymer matrix.

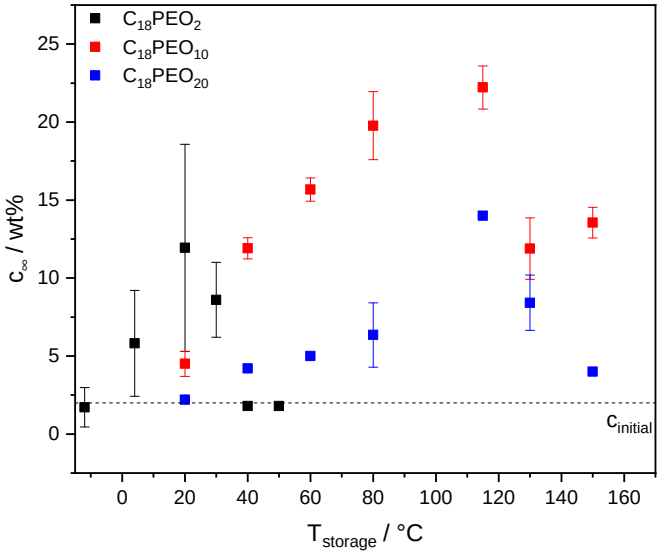

Figure 6.45: Temperature dependence of the surface concentration after infinitely long storage times c_∞ when no degradation is taken into account. The three investigated additives differ only in the molar mass of the hydrophilic part of the surfactant.

In summary, it is concluded that the influence of the storage temperature on the migration of the additive to the surface cannot be explained trivially. Usually a sweet spot is found depending on the storage temperature and molecular architecture. At high storage temperatures migration is limited due to solubility of the additive in the matrix, blocking phenomena due to recrystallization of the matrix or thermal degradation of the additive. Low

storage temperatures lead to slow migration due to low diffusion coefficients within the limits of process relevant storage times.

6.9.4 Influence of matrix molar mass and nucleating agents

In this chapter the influence of the molar mass of the polymer matrix on the migration behavior of the additive is investigated. It is examined whether an increase in molar mass without a change in polydispersity causes a change in migration behavior and if the addition of a long-chain branched polypropylene to the matrix polymer influences the migration behavior. This assumption is based on the fact that long-chain branches increase the free volume in the polymer due to the increased number of free chain ends, allowing additives to diffuse more rapidly, resulting in an increased migration rate.

For the experiments the reference PP with a weight average molar mass of 186 kg mol^{-1} (PP_{LowMw}), a high molar mass PP with a weight average molar mass of 425 kg mol^{-1} (PP_{HighMw}) and the reference PP to which 10 wt% of a long-chain branched PP was added (PP_{LCB}) were used as matrix polymer (see also chapter 6.1). According to Kunzelmann [32], the weight-average molar mass of the low molar mass polypropylene and the long-chain branched polypropylene should be subject to a linear mixing rule, resulting in a weight average molar mass of 211 kg mol^{-1} for PP_{LCB}.

Figure 6.46 (a) shows the migration behavior of $C_{18}PEO_2$ in the polypropylene matrices with different molar masses. The graph illustrates that migration in PP_{HighMw} and PP_{LCB} is significantly less pronounced compared to PP_{LowMw} resulting in a lower surface concentration after a storage time of approximately 1200 hours. While the migration is comparable for all investigated samples in the beginning, the additive in PP_{HighMw} and PP_{LCB} migrates much worse after about 500 hours. Although the molar mass of PP_{LowMw} and PP_{LCB} differs only slightly, the added long-chain branches hinder migration quite considerably. This suggests that the molar mass alone is not responsible for the deteriorated migration behavior.

Studies on the influence of the matrix molar mass on the diffusion of additives are quite rare. There are only studies on the diffusion of polystyrene in a matrix of polystyrene with different molar masses [106, 107, 186, 187]. In these studies it is concluded that the diffusion coefficient is independent of the molar mass of the matrix if the molar mass of the matrix is significantly higher than that of the diffusing polystyrene. However, the studies are only comparable to a limited extent, since diffusion coefficients were always determined in the melt and the matrix polymer is amorphous.

Based on the assumption that the matrix molar mass is not directly influencing the migration kinetics of the additive, the resulting matrix morphology or crystallinity might be a reason for the poor migration behavior. Therefore, it was investigated whether the molar mass has an influence on the surface crystallinity to explain the deteriorated migration.

Figure 6.46 (b) shows the near-surface crystallinity of the samples from figure 6.46 (a). The graph indicates that the high molar mass PP has the lowest surface crystallinity right after production. It is assumed that longer polymer chains as well as long-chain branches hinder the arrangement of polymer chains in crystallites, resulting in a low degree of crystallinity directly after production. Since crystallization is kinetically inhibited, there is no state of equilibrium of crystallization, which is why (PP_{HighMw}) and (PP_{LCB}) tend to post-crystallize. During post-crystallization additive molecules might be entrapped due to co-crystallization which prevents further migration to the surface [177]. This hypothesis would explain the comparable migration behavior after short storage times and the larger differences after longer storage times. However, the difference in the near-surface crystallinity of the individual samples is not large enough to fully explain the differences in migration behavior.

Since the methods used for morphology analysis only determine an average crystallinity in the surface volume up to a penetration depth of 2.55 µm and provide no information on crystallite size and orientation, it can not be explained completely why the increased matrix molar mass hinders migration. More experiments would be necessary to decouple morphology effects from the effects of matrix molar mass as such, which might be a motivation for further studies. In summary, it is concluded that the molar mass of the matrix has a significant influence on the migration of additives. There are indications that the worsened migration is an effect of the morphology resulting from an increased molar mass or added long-chain branches.

The addition of nucleating agents results in more crystallization sites in the polymer, which leads to the formation of more crystallites that hinder each other's growth and are therefore smaller. Milliken NX 10 is a nucleating agent that works on this principle and is therefore used to reduce haze of injection molded products. Since the additives cannot penetrate crystallites during migration to the surface, it is assumed that smaller crystallites shorten migration paths and thus accelerate migration to the surface. However, no evidence of improvement or deterioration of migration behavior in the injection molded plates was found (figure 6.47). This is probably due to the fact that the crystallite structures of a plate produced with a cooled mold (T_{mold} = 40 °C) are

a)

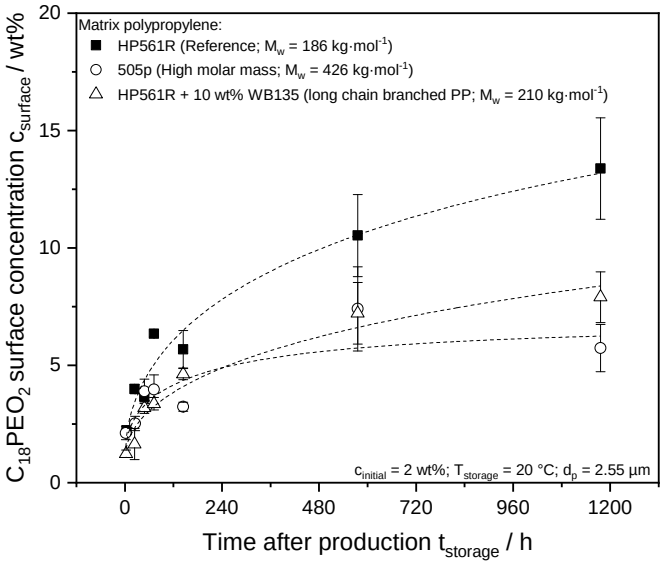

b)

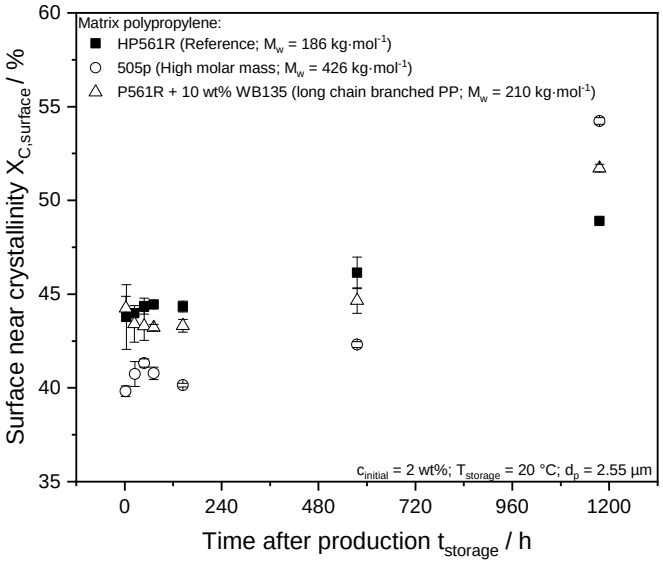

Figure 6.46: Influence of molar mass and long chain branches of the matrix polymer on the migration behavior of $C_{18}PEO_2$ (a) and the surface crystallinity of the matrix (b). Dotted lines are fits with equation 2.9 to guide the eye.

already very well permeable for the additives. For this reason no improvement results from the use of nucleating agents (see also chapter 6.9.1).

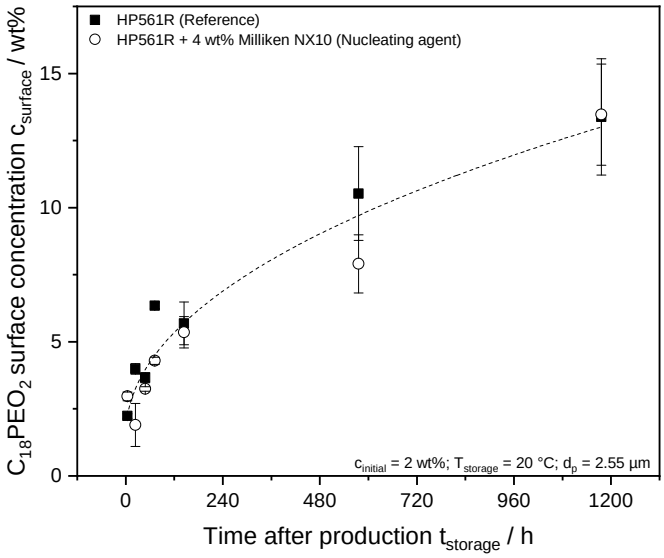

Figure 6.47: Influence of the addition of nucleating agents to the matrix polypropylene on the migration of $C_{18}PEO_2$ to the surface. Dotted line is a fit with equation 2.9 to guide the eye.

6.10 Surface migration of additives in cast and stretched films

Chapter 6.9 investigated the fundamental influence of storage time and temperature as well as the molecular structure of additive and matrix on the migration of additives in injection molded plates. In this chapter cast films are used to investigate the influence of matrix morphology on migration behaviour. Cast films have the advantage that their production and processing is comparable to that of fibers and nonwovens and establish a logical connection between the morphology of injection molded parts and fibers. In both processes, the additive is blended with the matrix polymer using a twin-screw extruder, extruded through a die and cooled rapidly. The cooled fiber or film is subsequently stretched to varying degrees. In contrast to fibers, in which the stretching is performed both in the melt and in the solid state right after extrusion, the films are post-stretched after cooling. In cast films the stretching process is carried out independently of the extrusion step, allowing the process parameters of the stretching step to be easily controlled. Furthermore, the cooling of the extruded film can be adjusted precisely via the temperature

control of the chill roll. Due to the comparatively good transferability of the process conditions in the cast film process to those of fiber spinning, the influence of process-related structure development of the matrix polymer on the migration of the additive is investigated in the following chapter.

In the industrial production of biaxially stretched films, the stretching of the films is performed in two directions either step-wise or at the same time directly after extrusion. For the stretching step the film is preheated in an oven. The stretching process is conducted on a laboratory scale in a similar way. The film is first heated to 140 °C by hot air for 45 seconds and subsequently stretched by a predefined ratio.

In order to separate the effects of thermally induced post-crystallization from the morphological changes induced by stretching, one sample was heated without a subsequent stretching process, since post-crystallization of the sample surface can already take place during the preheating step. Figure 6.48 shows the migration behavior and the associated surface crystallinity for films that have been hot-stretched and heated without subsequent stretching. The reference sample is the cast film, which was extruded onto a cooled chill roll ($T_{chil\ roll}$ = 20 °C) and not post-treated.

The experiment reveals that even brief heating leads to a significant increase in surface crystallinity. Furthermore, heating converts the mesomorphic phase into an α-crystalline phase (see also chapter 6.5, figure 6.21). The crystallites (especially on the surface) act as a migration barrier and hinder the migration of additives to the surface even after long storage times. However, due to the strongly pronounced effect of post-crystallization as a result of the heat introduction, the morphology-changing effect of stretching is superimposed.

For this reason, after extrusion, the films were cold drawn at room temperature by 200 %, 400 % and 800 % using a tensile testing machine. The migration curves and the associated surface crystallinities are presented in figure 6.49.

It is assumed that the total crystallinity changes only insignificantly since there is no heat input during cold stretching. Therefore the driving force to effect a heat-induced post-crystallization is not high enough. However, the morphology of the film changes considerably as it is stretched. On the one hand, the mesomorphic crystal phase is strongly oriented (see also chapter 6.5, figure 6.20), on the other hand, a crystallization gradient develops towards the surface. The morphology development is comparable to that of a fiber when it is stretched by an aspirator after extrusion (see chapter 6.4), although fibers and films differ slightly in the resulting structure.

a)

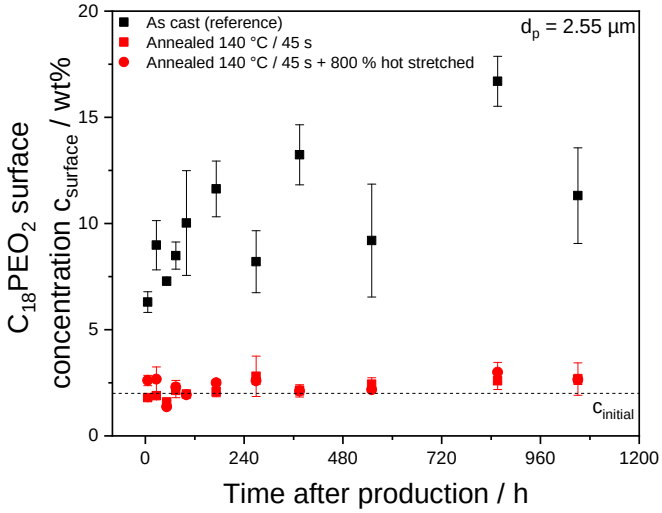

b)

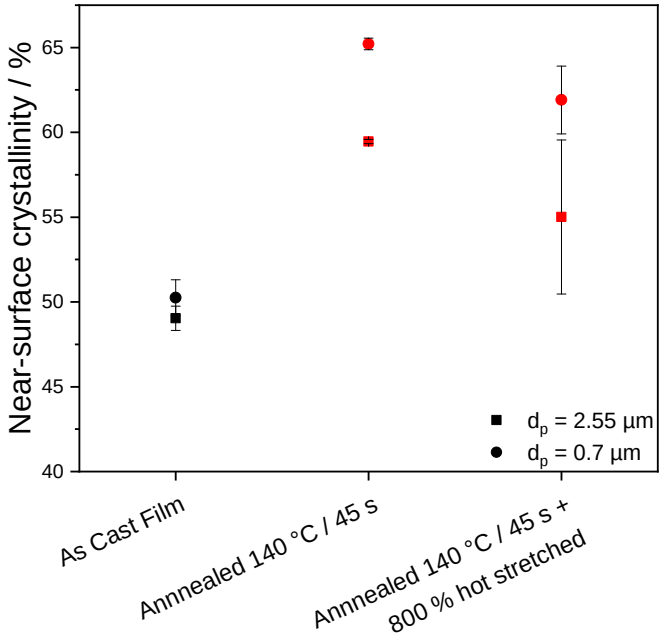

Figure 6.48: Migration behavior (a) and surface crystallinity (b) of cast films, which were heated to 140 °C for 45 seconds before stretching compared to the untreated film.

a)

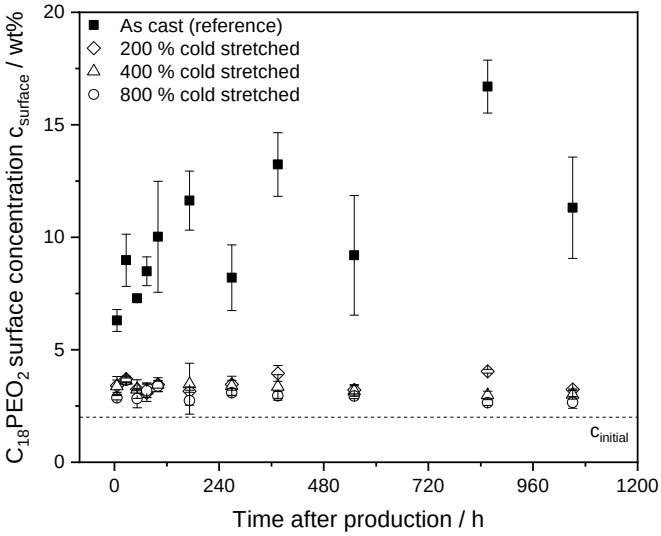

b)

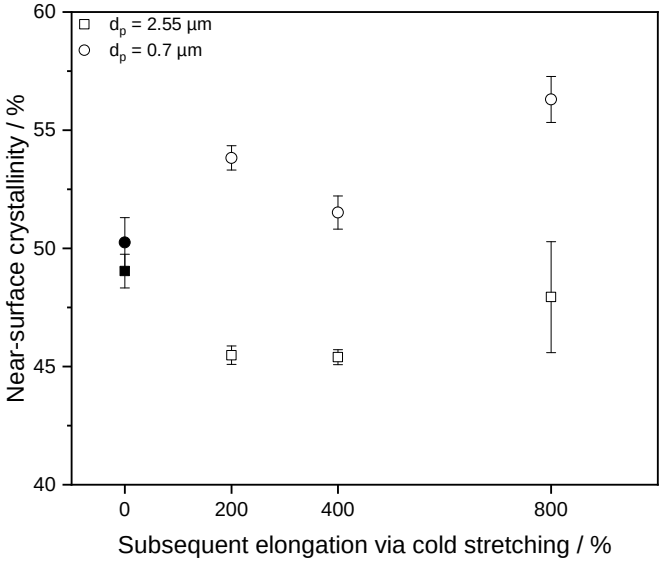

Figure 6.49: Migration behavior (a) and surface crystallinity (b) of cast films which were cold stretched without a previous heating step compared to the unstretched reference film.

Due to the stretching of fibers in the melt and in the solid state, a stretched α-crystalline structure is developed as a result of the strain-induced crystallization. However, since the cast films show a mesomorphic structure after extrusion and are subsequently cold-stretched, an oriented mesomorphic structure is observed (chapter 6.5. Qiu et al. [166] reported that mesomorphic PP films exhibit a highly oriented mesophase as soon as they exceed the yield strength. This is also assumed in the study conducted here, since the films stretched by 200 % already exceeded the yield point. The corresponding tensile curves of the films can be found in the appendix (figure A.24). In contrast to the aerodynamically stretched fibers, it is further assumed that the films were subjected to even greater post-stretching. This results in nanofibrillar crystallites being formed instead of shish-kebab structures. This effect has already been demonstrated by Hautojärvi et al. [157] for mechanically post-stretched polypropylene fibers. The highly oriented amorphous regions and the nanofibrillar crystallites in the cold-stretched films may act as an effective migration barrier without the need for thermally induced post-crystallization.

When comparing the migration behavior of cold- and hot-stretched / annealed films (figure 6.50 (a)) the surface concentration of the additive in the cold-stretched films is always higher than in the annealed films. Due to the recrystallization of the surface of the hot-stretched samples (figure 6.48 (b)) the migration barrier is even more pronounced leading to a worsened migration to the surface. As with the injection molded plates (see also chapter 6.9.2), this effect may be attributed to solubility effects of the additive at elevated temperatures, which result in less additive being available for migration, or to co-crystallization of additive and polymer after heat treatment. The contact angle measurements reflect the migration phenomena (figure 6.50 (b)) quite well. Only in the case of the untreated cast film a sufficient amount of additive migrates to the surface to reduce the water contact angle significantly. Although the surface concentration of the cold-stretched films is slightly higher than that of the annealed / hot-stretched films, a complete blocking effect of additive migration due to stretching or post-crystallization as a result of heating is assumed for all stretched or post-heated samples. An illustration of the hypotheses discussed in this chapter is shown in figure 6.51.

The experimental data from this chapter were taken from Sharma's master thesis (supervised by F. J. Lanyi) [178] and analyzed independently within this thesis.

a)

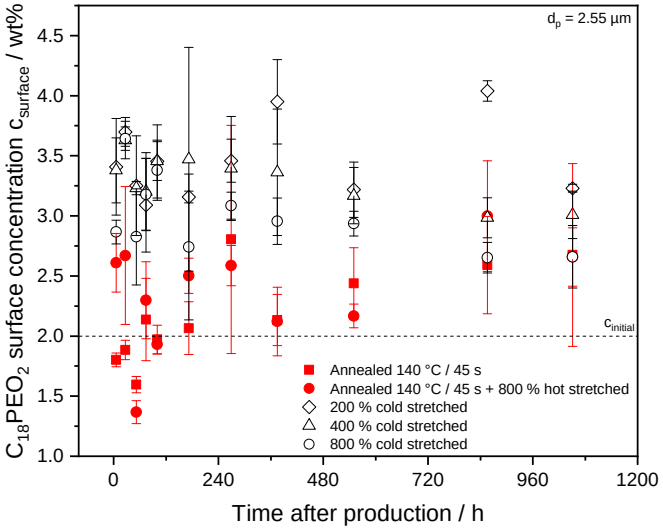

b)

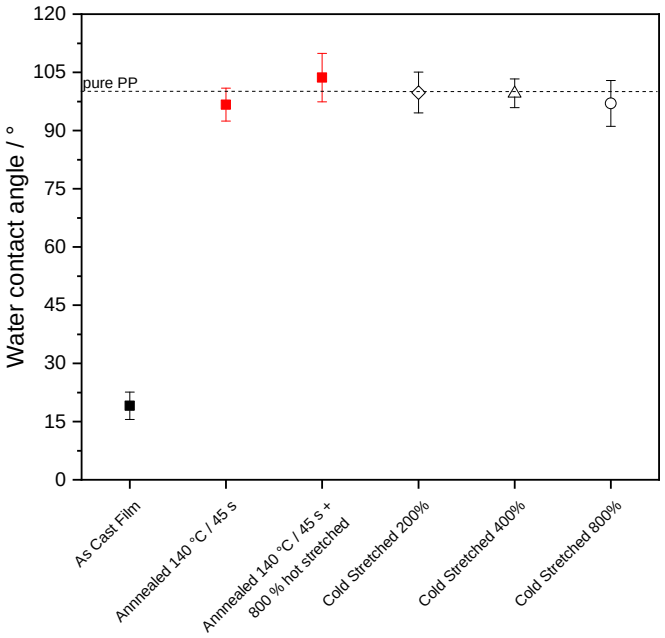

Figure 6.50: Comparison of the migration behavior of cold and hot stretched films (b) as well as water contact angles of the samples investigated in this chapter.

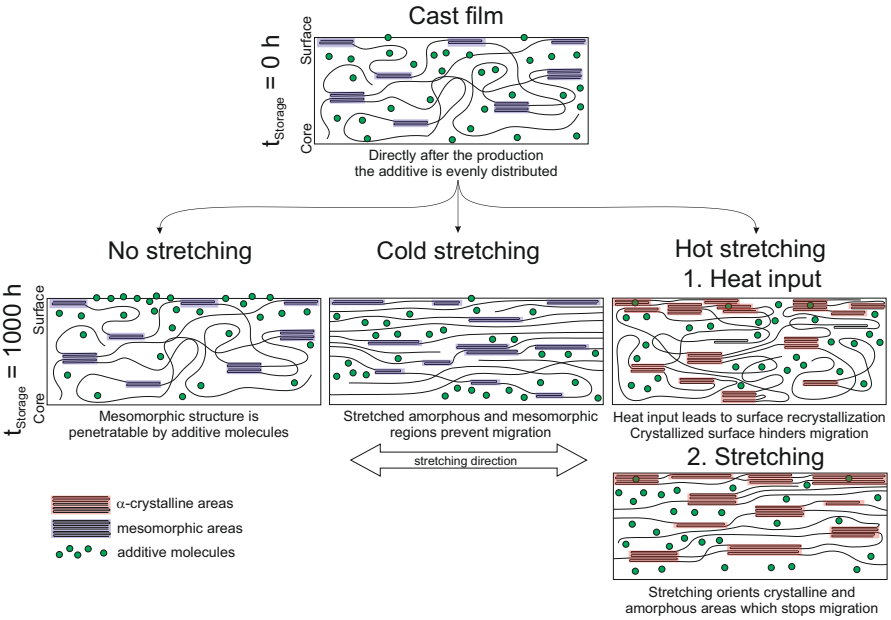

Figure 6.51: Illustration of the phenomena that lead to blocked migration in cold- and hot-stretched films.

6.11 Surface migration of additives in fibers and nonwovens

This chapter explains the migration behavior of fibers and nonwovens based on the findings of injection molded plates (chapter 6.9) and cast films (chapter 6.10) depending on the production parameters in the process and the molecular architecture of additive and matrix polymer. Since there are only few publications on migration behavior in fibers and nonwovens, most hypotheses are based on the findings from previous experiments. A distinction is usually made between single fibers which are not bonded and calendered nonwovens, since the bonding step causes a significant change in morphology.

6.11.1 Influence of production parameters in the spinning process

6.11.1.1 Initial additive concentration

First, the influence of the initial concentration of the additive on the migration kinetics and on the plateau concentration after long storage times is investigated. Furthermore, the minimum amount of additive necessary to allow migration and hydrophilization of the surface is determined.

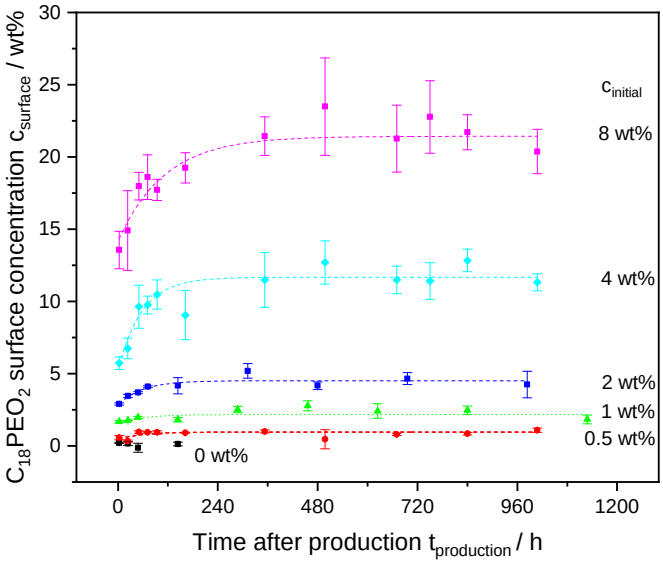

Figure 6.52: Migration behavior of single fibers with different initial additive contents which were produced and stored under identical conditions.

Figure 6.52 shows the migration behavior in fibers produced under standard conditions, containing different initial concentrations of $C_{18}PEO_2$. The graph indicates that the plateau surface concentration increases with increasing initial concentration. All curves show a similar shape and the plateau concentration is reached after a comparably long time. In order to describee the kinetics and thermodynamics of surface enrichment, the curves were fitted with equation 2.9 (chapter 2.3.3):

$$c_{\text{surface}}(t) = c_0 + (c_\infty - c_0) \cdot \left(1 - e^{-\left(\frac{t}{\tau_{\text{Migration}}} \right)^{0.5}} \right) \qquad (2.9)$$

It was possible to fit all curves with a constant coefficient of migration $\tau_{Migration}$ of 49.5 ± 20 hours. Accordingly, the fit function only differs with regard to the initial concentration c_0 and the final concentration c_∞. The same value for $\tau_{Migration}$ suggests that the kinetics describing the time-dependent enrichment of the surface are independent of the initial concentration. Under the assumption that the initial concentration of the additive does not change the morphology formation in the spinning process, it is therefore obvious that the diffusion rate towards the surface should not change as a function of the initial concentration.

If the plateau concentration is plotted over the initial concentration, a linear correlation is found (figure 6.53). This correlation indicates that about three times the initial concentration migrates to the surface. Furthermore, the positive point of intersection with the x-axis suggests that a minimum initial concentration of approximately 0.2 wt% $C_{18}PEO_2$ is necessary in order to effect an enrichment of the surface. This behavior may be due to the marginal solubility of the additive in the matrix polymer and has already been discussed in chapter 6.3 and chapter 6.9.2 for injection molded plates. Fibers with an initial concentration of 0.5 wt% or 1 wt% only show a slight saturation of the surface which was not high enough to hydrophilize the fibers. At least 2 wt% of $C_{18}PEO_2$ were needed in order to hydrophilize the fiber surface. A more detailed approach to describe the enrichment of additives in films, fibers and injection molded plates as well as investigations of the developing additive concentration profile can be found in chapter 6.12.

A linear correlation between initial concentration and the amount of additive which migrates to the surface was also found by Földes for oleamides in various polyethylenes. Földes showed that the total additive amount which was added to the samples migrates to the surface and that the plateau concentration does not depend on the storage conditions or the matrix polymer used [85]. Rawls et al. [118] also discovered a proportionality between initial and final surface concentration for erucamide in LLDPE films. Similar results were also reported by Chen et. al. [132] for a blend of Polystyrene and Poly(dimethylsiloxane)-co-polystyrene.

The experimental data from this chapter were partially taken from Kattinger's master thesis (supervised by F. J. Lanyi) [188] and analyzed independently within this thesis.

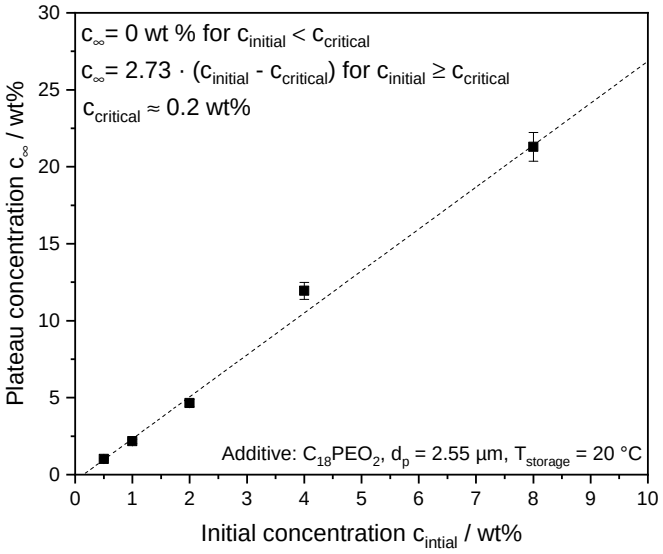

Figure 6.53: Plateau concentration of single fibers as a function of the initial concentration.

6.11.1.2 Haul-off pressure

In chapter 6.4.1 it has been demonstrated that the haul-off speed has a strong influence on the morphology of fibers and in particular on their surface. Furthermore, it has been shown that (cold-)stretching of cast films can completely suppress the migration of additives to the surface in chapter 6.10. Accordingly, the stretching conditions of the fibers might allow to control the migration behavior of the additive. On the basis of previous observations, unstretched fibers should exhibit the best migration behavior since they have the lowest orientation, the lowest near-surface crystallinity and additionally a mesomorphic crystal structure. Cast films with comparable morphological properties showed a very good migration behavior (see also chapter 6.10, figure 6.49). Due to the decreasing fiber diameter caused by stretching, gravity spun fibers also have the smallest surface to volume ratio. In order to achieve the same surface concentration compared to very thin fibers, less additive has to migrate from the inner volume to the surface. Overall, it is expected that gravity spun fibers show the best migration behavior and that migration to the surface deteriorates with a higher degree of stretching up to the complete blocking of migration.

Figure 6.54 shows the migration behavior of $C_{18}PEO_2$ in single fibers that were produced using different haul-off pressures and therefore stretched to various extents. Due to the pronounced experimental scattering, the measurement

data do not allow a clear interpretation of the results because of the strong overlapping of the individual curves.

In chapter 6.11.1.1 it was shown that the time required to reach the plateau concentration in fibers is usually less than 100 hours. Therefore, it is assumed that fibers which have been stored for 250 hours have reached a terminal surface concentration. In order to keep the influence of experimental scattering as low as possible, all measured values from 250 hours onwards were averaged and plotted as a function of the resulting fiber diameter (figure 6.54 (b)). It can be seen that the resulting surface concentration depends on the fiber diameter. This result is discussed and modeled in more detail in chapter 6.12. No critical haul-off pressure was found from which the migration of the additive is completely blocked. This result is contradictory to the previous results. For further considerations it is assumed that the lower plateau concentration of the thinner fibers is only an effect of the increased surface-to-volume ratio and that there is no significant effect of the degree of stretching on the migration behavior.

The results could be explained by the formation of intercrystalline migration paths due to an increase in the distance between crystallite structures as a result of stretching. Hautojärvi et al. [167] showed by means of AFM measurements that the stretching process during fiber production leads to a transformation from a spherulitic to a fibrillar crystal morphology. It was found that the orientation of the molecular chains during stretching increases the distance between the epitaxially crystallized shish-kebab structures. In another study by Hautojärvi et al. [157] it was shown that the surface of highly stretched fibers consists of microfibrils which are connected by lamellar platelets. The existence of these platelets indicates that the fibrils on the surface are not yet fully oriented and may therefore be permeable for smaller additive molecules. If the fibers are produced by tow drawing (subsequent stretching of the fibers after the spinning process), significantly higher forces are exerted on the fibers. As a result, the fibers are stretched even more and nanofibrillar lamellar structures are formed. Fibers produced via tow drawing showed lamellar crystallites which cannot be further stretched and amorphous regions that are oriented to the maximum. It is assumed that such a pronounced stretching does not occur during the aeordynamic stretching of fibers.

It is considered that the comparatively low forces during aerodynamic stretching of the fibers lead to the formation of a shish-kebab structure on the surface of the fibers. As the haul-off velocity increases, the distance between the epitaxial crystallites increases and the crystallites become permeable. In cold-stretched films, the high forces during post-stretching result in complete

a)

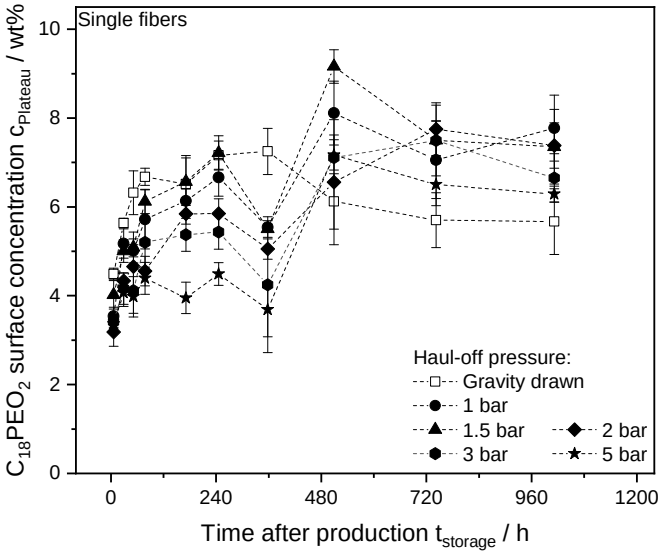

b)

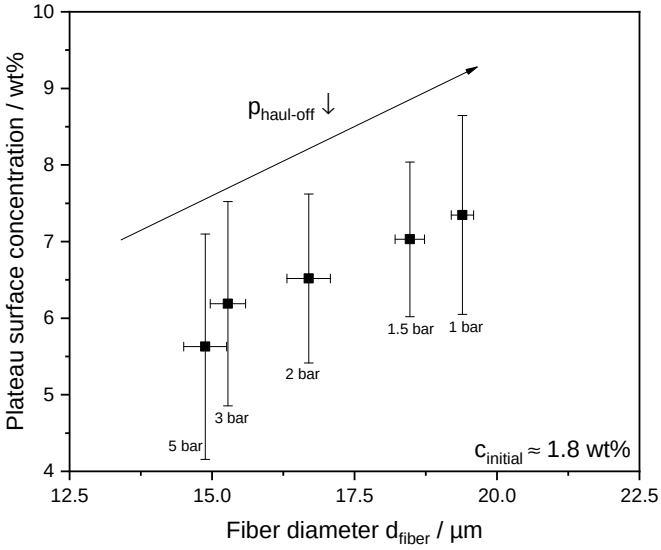

Figure 6.54: Migration behavior of $C_{18}PEO_2$ in single fibers produced at different haul-off pressures as a function of storage time (a) and plateau concentration of these fibers as a function of resulting fiber diameter (b). The correct initial concentration $c_{initial}$ was determined by producing melt films from the single fibers and measuring them via FTIR in transmission.

alignment of the crystallites, which leads to nanofibrillation of the surface, thus preventing migration. Figure 6.55 shows a schematic representation of this hypothesis.

In summary, it is suggested that the orientation of the amorphous regions and the increasing crystallinity due to stretching prevent migration. However, the increase of the distance between the crystallites leads to the formation of migration paths. Both phenomena have an opposite effect on the migration and might explain why there is no clear influence of the stretching process on the migration behavior. However, the assumptions on morphology formation are only a hypothesis based on findings from the literature and could be the focus of further investigations.

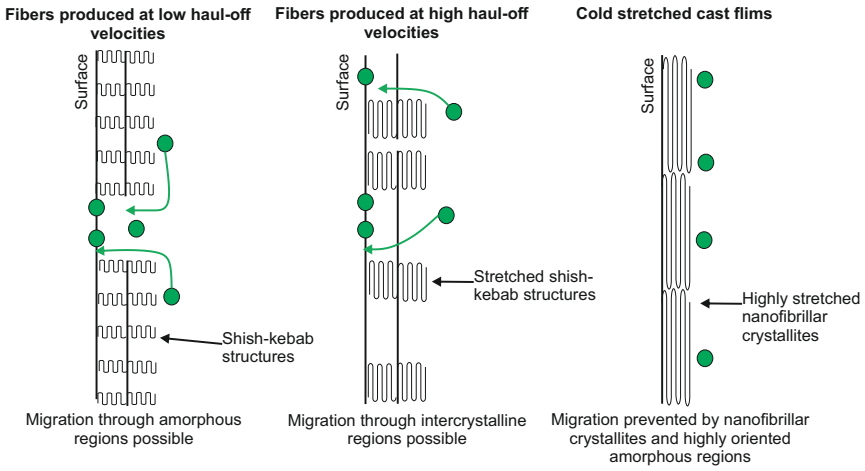

Figure 6.55: Sketch illustrating the influence of (crystalline) morphology on migration behavior in fibers and cold-stretched cast films.

The experimental data from this chapter were partially taken from Kattinger's master thesis (supervised by F. J. Lanyi) [188] and analyzed independently within this thesis.

6.11.1.3 Cooling temperature and profile

In the following chapter, the influence of the conditioning of the quench chamber during fiber spinning (i.e. air velocity profile, air temperature and air velocity) on the additive migration in single fibers is investigated.

It was found that the air velocity profile can only be changed slightly within the limits of the pilot plant's adjustment possibilities. Consequently, a change in migration behavior due to a change in the cooling profile could not be

demonstrated in this work. However, the influence of the air velocity profile cannot be completely excluded. A more extensive modification of the cooling profile could lead to a morphological change of the fibers that influences the migration behavior. The air velocity profiles of the quench chamber and the associated migration experiments can be found in appendix A.9.1.

Figure 6.56 shows the migration behavior of additives in single fibers which were spun using different quench chamber temperatures and quench air velocities. In the experiment an air temperature of 20 °C and 40 °C was used since it was not possible to use the standard setting of an air temperature of 12 °C. The temperature in the quench chamber depends on the air velocity and a temperature of 12 °C was not achievable for high air velocities. Figure 6.56 (a) indicates that the temperature of the quench chamber has a small influence on the migration of the additive to the surface. It is assumed that the slower cooling of the fiber at 40 °C provides more time for the additive to accumulate in near-surface areas and finally migrate to the surface. An influence of the blow air temperature on the surface crystallinity could not be proven. Overall, it was found that the tempering of the quench chamber has only a minor influence on the migration behavior.

The influence of the cooling air velocity on additive migration could not be demonstrated (Figure 6.56). (b)). There are probably two main reasons for this. On the one hand, relatively low blow air velocities were used in the experiments since higher blow air velocities caused instabilities in the spinning process and led to fiber breakage. On the other hand, the thermal diffusivity of air is very low. Therefore, even at higher flow velocities, air dissipates heat too slowly from the fiber to cause significant changes in morphology and thus migration. The influence of air velocity on the migration behavior was also investigated for polypropylene matrices with different molar masses. The results were comparable and are presented in figure A.21 in the appendix A.9.1.

In summary, it is concluded that the influence of the air velocity and the air velocity profile in the quench chamber on the migration behaviour is not existent. This is mainly due to the adjustment possibilities of the pilot plant. However, there is evidence that the tempering of the blow air has a minor influence on the migration.

The experimental data from this chapter were taken from Kattinger's master thesis (supervised by F. J. Lanyi) [188] and analyzed independently within this thesis.

a)

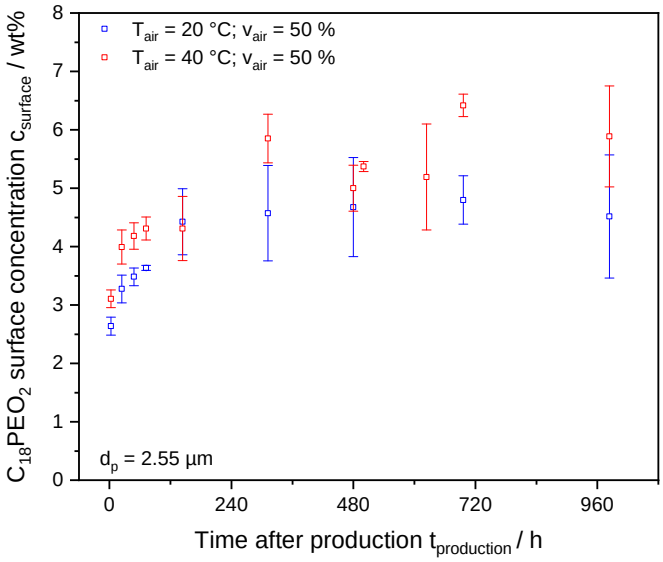

b)

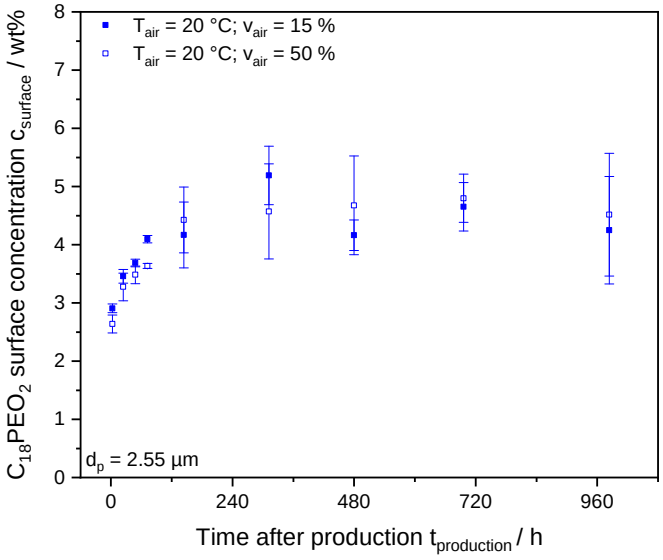

Figure 6.56: Influence of air temperature (a) and air velocity (b) in the quench chamber on the migration behavior of 2 wt% $C_{18}PEO_2$ in single fibers.

6.11.1.4 Heat calendering

The following chapter discusses the influence of the calendering process on the morphology of the fibers and how this change in morphology affects the migration behavior of additives.

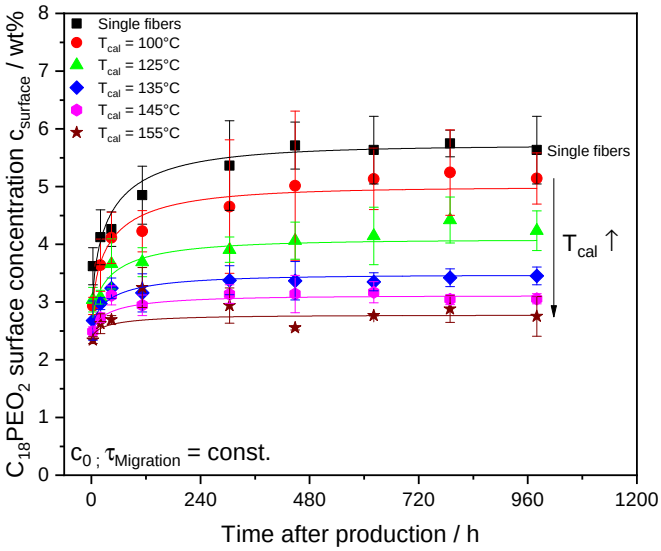

Figure 6.57: Influence of calendering temperature on migration behavior of fibers spun under standard conditions with an additive content of 2 wt% and $C_{18}PEO_2$ used as additive. Samples were produced with the calender press with a corresponding line pressure of 5 N mm^{-1}.

Figure 6.57 shows the surface enrichment of $C_{18}PEO_2$ in polypropylene fibers which were calendered at different temperatures. It is evident that the surface enrichment decreases significantly with increasing calendering temperature T_{cal}. A fit with equation 2.9 reveals that the difference between the migration curves is mainly in the plateau value as the curves were fitted with a constant coefficient of migration $\tau_{Migration}$. This indicates that the migration follows similar kinetics for all samples independently of the calendering temperature. Based on these findings, the surface crystallinity of the samples is investigated.

Figure 6.58 illustrates that the surface crystallinity increases with increasing calendering temperature. Apart from a small increase in the first 3 - 5 days due to to relaxation phenomena, there is no significant time dependence and the surface crystallinity is regarded as constant over time. Since it is excluded that the input of thermal energy by the calendering process leads to degradation of the additive (see chapter 6.2), the difference in the migration behavior is attributed to morphological changes in the polymer. Figure 6.59 shows the plateau value of the migration curves as a function of the calender

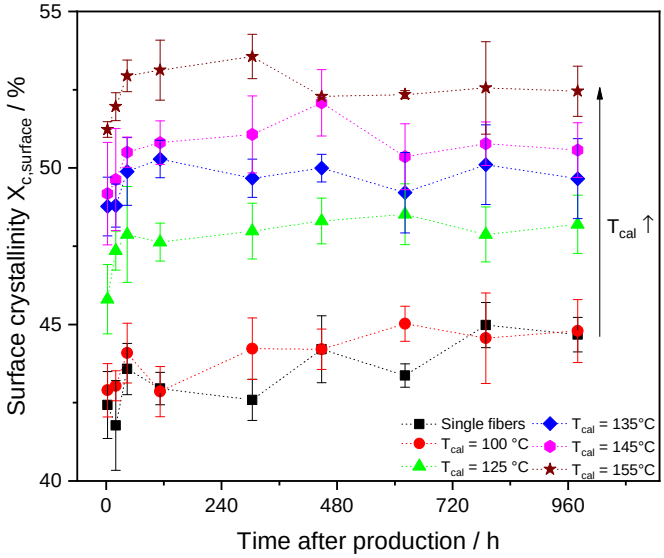

Figure 6.58: Influence of the calender temperature on the surface crystallinity of the nonwoven samples shown in figure 6.57. Samples were produced with the calender press with a corresponding line pressure of 5 N mm^{-1}.

temperature (a) and the surface crystallinity of the nonwovens (b). The plot reveals that the plateau surface concentration decreases linearly with both the calender temperature and the surface crystallinity. The plateau surface concentration decreases by 0.04 wt% per °C calendering temperature and by 0.3 wt% per % surface crystallinity.

Due to the post-crystallization, less free matrix volume is available on the surface in which the additive may be present. Furthermore, the post-crystallized regions on the surface may act as a migration barrier. The heat input may cause a certain amount of the additive to dissolve in or co-crystallize with the polypropylene, which is why less additive is available to migrate to the surface. However, the results indicate that the enrichment process of the surface in general is similar for all samples, which is why no change in the migration kinetics could be demonstrated. The correlation of the migration of additives to the surface and the total crystallinity of the matrix was also reported by Maghsoud et al. using antioxidants in a HDPE matrix. It was concluded that migration kinetics depend primarily on the crystal morphology (i.e. size and shape) while the total amount of additive migrating to the surface is a function of the degree of crystallinity [79].

a)

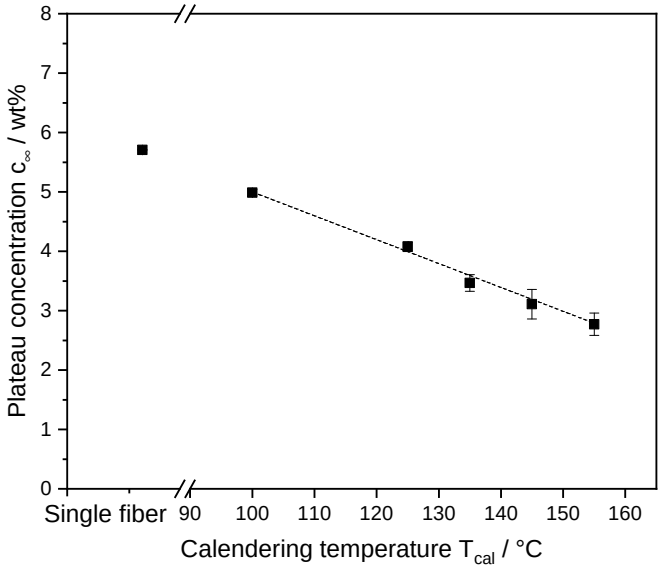

b)

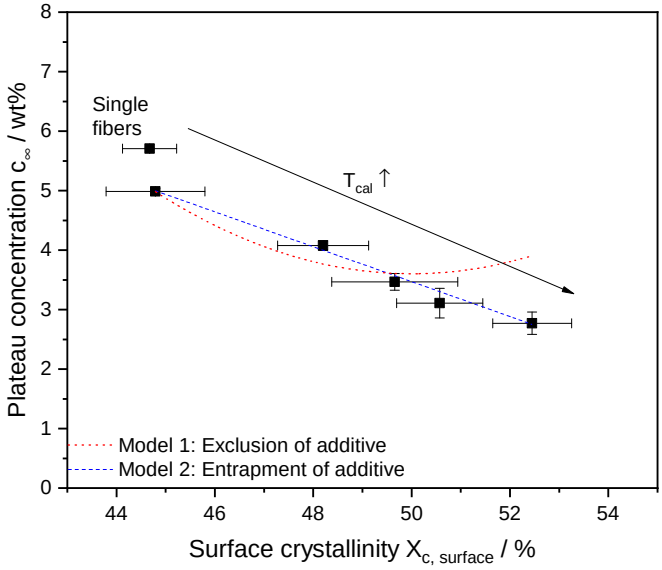

Figure 6.59: Plateau surface concentration as a function of the calender temperature (a) and the surface crystallinity of the nonwovens (b). The surface concentration decreases by 0.04 wt% per °C calender temperature and by 0.3 wt% per % surface crystallinity.

A simple model can be created to explain the phenomena. It is expected that post-crystallization leads to one of these phenomena:

1. The additive is excluded from the crystallites during post-crystallization. This increases the additive concentration in the amorphous regions.
2. The additive volume available for migration is reduced due to entrapment in the crystalline regions during post-crystallization or due to miscibility with the polymer. The concentration of the additive in the amorphous regions thus remains constant.

If the first assumption is correct, the surface enrichment should depend on the amorphous phase fraction and the additive concentration in the amorphous phase. The additive concentration in turn is linearly dependent on the crystalline phase fraction.

From this results the following equation:

$$c_{\text{total}} = c_0 + (1 - \phi_{\text{crystalline}}) \cdot c_{\text{constant}} \cdot \phi_{\text{crystalline}} \tag{6.6}$$

If the second assumption is correct, the additive concentration in the amorphous phase should be constant and thus independent of the crystalline phase fraction. This results in the following equation:

$$c_{\text{surface}} = c_0 + (1 - \phi_{\text{crystalline}}) \cdot c_{\text{constant}} \tag{6.7}$$

As shown in figure 6.59, only equation 6.7 describes the data sufficiently, which is why a reduction of the migratable additive volume caused by entrapment, miscibility or co-crystallization during post-crystallization is assumed [177].

In summary, it is concluded that the surface concentration decreases with increasing calender temperature. This effect is caused by the post-crystallization of the fibers as a result of the heat input during calendering. It is assumed that the additive volume which is available for migration is significantly reduced as additive molecules are entrapped by the crystallites (entrapment or co-crystallization) or dissolved in the matrix polypropylene as a result of the heat input. Furthermore, the newly formed crystallites may constitute a migration barrier.

The experimental data from this chapter were partially taken from Kattinger's master thesis (supervised by F. J. Lanyi) [188] and analyzed independently within this thesis.

6.11.2 Influence of the molecular architecture of the additive

After the migration behavior of all additives in single fibers and nonwovens was examined rudimentarily in chapter 6.8, this chapter investigates how an increase in the molar mass and a change in the chemical architecture of the additive affects the migration of the additive to the surface.

Single fibers

Figure 6.60 shows the migration behavior of additives with a different molecular architecture in single fibers which were produced under standard conditions. The graph demonstrates that $C_{18}PEO_2$ molecules show by far the best migration behavior. Both an increase of the molar mass by extension of the hydrophilic part of the surfactant or the introduction of a double bond in the hydrophobic part of the additive molecule lead to an inhibition of migration due to the higher molecule size. With an increase in molar mass as well as the introduction of a double bond, the spatial dimensions of the molecule increase and the migration of the additive is restricted.

This effect has already been discussed in chapter 6.9.3 for injection molded plates and is a result of the steric hindrance of the molecule. The double bond increases the molecular dimensions of the additive, which in turn leads to a worsened diffusion to the surface.

Nonwovens

Figure 6.61 shows the migration behavior of additives in calendered nonwovens. The graph reveals that $C_{18}PEO_{10}$ migrates best and that the migration of the other investigated additives is almost completely blocked.

The deteriorated migration of smaller molecules is attributed to a reduction of the additive volume which is available for migration as a result of the heat input and post-crystallization during calendering (see also chapter 6.11.1.4) on the basis of experiments and examples from the literature. However, the heat input can also significantly improve the migration of larger immiscible molecules due to the increased diffusion coefficient at higher temperatures. This effect was demonstrated in chapter 6.9.2 for $C_{18}PEO_{10}$ and $C_{18}PEO_{20}$ in injection molded plates. In comparison to lower storage temperatures, the additives enriched the surface much faster at a storage temperature of 130 °C. For larger molecules, the effect of an increase of the diffusion coefficient is greater than the effect of dissolution in the matrix and the blocking effect by post-crystallization of the matrix. Therefore larger molecules migrate better in nonwovens than smaller molecules. Accordingly, the nonwovens containing

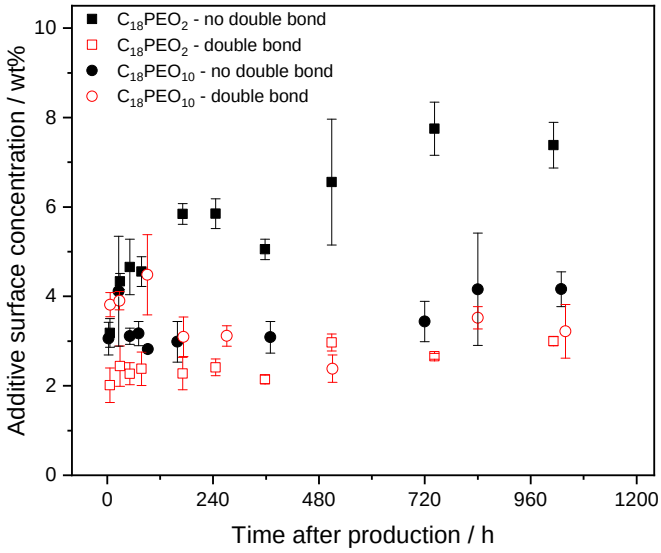

Figure 6.60: Migration curves of single fibers containing 2 wt% of ethoxylated alcohols of different chemical architecture. Black symbols represent additives with different lengths of hydrophilic parts of the surfactant. Red transparent symbols represent the same additive having a double bond in the hydrophobic part of the surfactant.

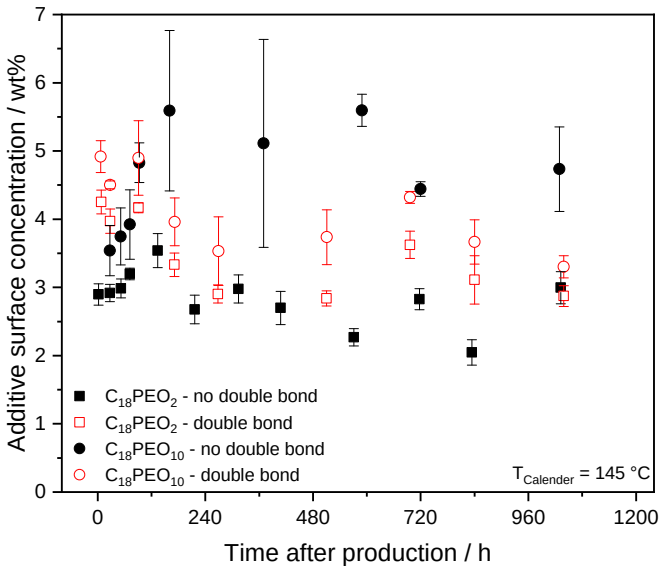

Figure 6.61: Migration behavior of additives with different molecular architecture in nonwovens.

$C_{18}PEO_{10}$ were hydrophilized immediately after calendering, while the single fibers were only slightly better wettable with water after the production.

In the case of small additive molecules, which have good miscibility with the matrix, the calendering step leads to a deterioration of the migration behavior. In the case of larger, poorly miscible molecules, however, the calendering process provides sufficient heat input to push the additive to the surface or at least into areas close to the surface, thus improving migration (figure 6.62). If the additive has a double bond in the hydrophobic part of the chain, migration deteriorates and less additive can migrate to the surface due to steric hindrance of the molecule. The phenomena that lead to a worsening of the migration and wetting behavior are the same as for single fibers.

The experimental data from this chapter were partially taken from Sharma's master thesis (supervised by F. J. Lanyi) [178] and analyzed independently within this thesis.

6.11.3 Influence of storage temparature

The storage temperature has a decisive influence on the migration kinetics and the plateau surface concentration in injection molded plates (chapter 6.9.2). This chapter focuses on the influence of the storage temperature on the migration in fibers and nonwovens. Figure 6.63 (a) shows the time-dependent migration to the surface of single fibers with 1.4 wt% $C_{18}PEO_2$ stored at a temperature of -12 °C to 50 °C. Due to the high surface-to-volume ratio of fibers, surface saturation is less pronounced compared to films or injection molded plates. In order to resolve minor influences of the storage temperature, the individual measurements are plotted over the storage temperature (figure 6.63 (b)). The results largely correspond to the learnings made for injection molded plates (chapter 6.9.2), but are significantly less pronounced. Below or near the glass temperature of the polypropylene the migration is inhibited due to the low matrix mobility. From the melting temperature of the additive (approximately 40 °C) the migration efficiency decreases considerably. This behavior has also been observed with injection molded plates and is discussed in more detail in chapter 6.9.2. The effect that the surface even desaturates slightly at elevated storage temperatures, i.e. that the surface concentration falls below the initial concentration, was also found for injection molded plates. The reduction was attributed to a migration back to the core [22] or to evaporation of the additive during long storage times at elevated temperature [179].

a)

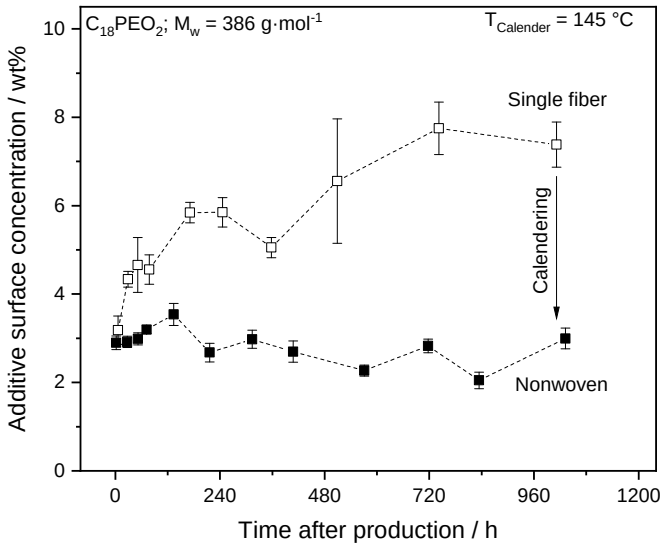

b)

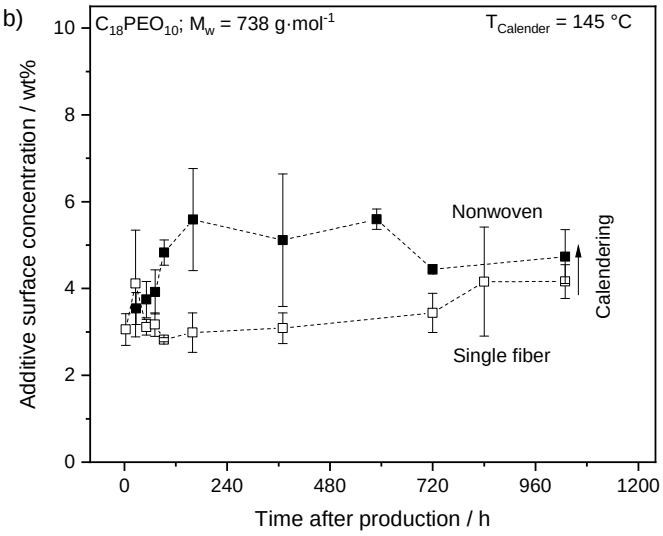

Figure 6.62: Comparison of the migration behavior of $C_{18}PEO_2$ (a) and $C_{18}PEO_{10}$ (b) in single fibers and nonwovens.

The inhibited migration at temperatures below 4 °C and the decreasing surface concentration from a storage temperature of about 35 - 40 °C leads to an optimal storage temperature of fibers at about 20 °C - 30 °C. At this temperature single fibers with 2 wt% $C_{18}PEO_2$ are wettable with water after approximately 7 - 10 days. A temperature of 20 °C to 30 °C is comparable to the optimum storage temperature for injection molded plates (see also chapter 6.9.2).

Figure 6.64 shows the migration of $C_{18}PEO_2$ in single fibers at room temperature after they have been stored for 9 days at -12 °C or 50 °C. The experiment illustrates that the surface concentration does not change for single fibers stored below the glass temperature of the polypropylene. If the fibers are subsequently stored at room temperature, the surface concentration increases, comparable to fibers which were stored immediately after production at room temperature. Fibers which were previously stored at 50 °C show a considerably deteriorated migration behavior at room temperature. This experiment also supports the hypothesis that the migratable additive volume is lost through miscibility or entrapment when the samples are stored at high temperatures.

Figure 6.65 shows the migration behavior of $C_{18}PEO_2$ in nonwovens at different storage temperatures. The effects are similar to those found for single fibers, but the temperature for maximum surface migration is shifted to even lower temperatures of -12 °C and 4 °C.

For the additives $C_{18}PEO_{10}$ and $C_{18}PEO_{20}$, the influence of calendering superimposes the effects of different storage temperatures (see appendix A.9.2). Due to the blocking effect of calendering (chapter 6.11.1.4), migration to the surface was suppressed to such an extent that no significant differences in migration behavior up to a storage temperature of 60 °C are detectable.

In summary, it was found that the learnings from the injection molded plates can in principle be transferred to fibers and nonwovens. Due to the high surface-to-volume-ratio of fibers, the blocking effect as a result of calendering and the low initial concentration used in the experiments, the influence of the storage temperature was only slightly pronounced. Therefore results are not as distinctive as with injection molded plates or cast films.

6.11.4 Influence of the molar mass of the matrix polymer

This chapter investigates the influence of the molar mass of the matrix polymer on the migration behavior of additives in single fibers and nonwovens.

a)

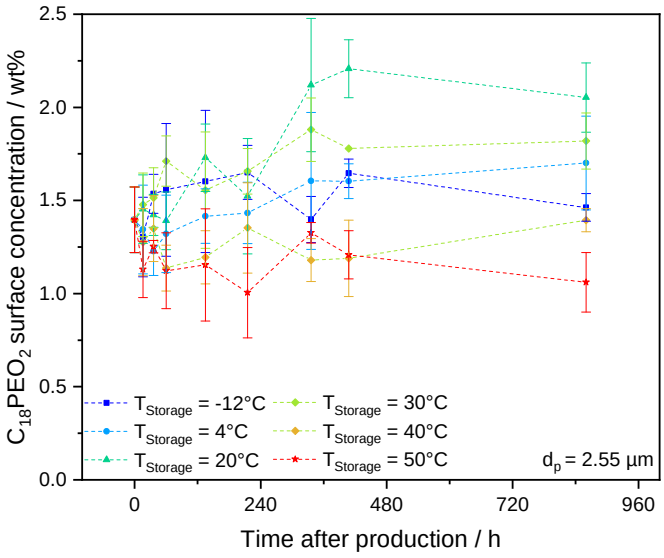

b)

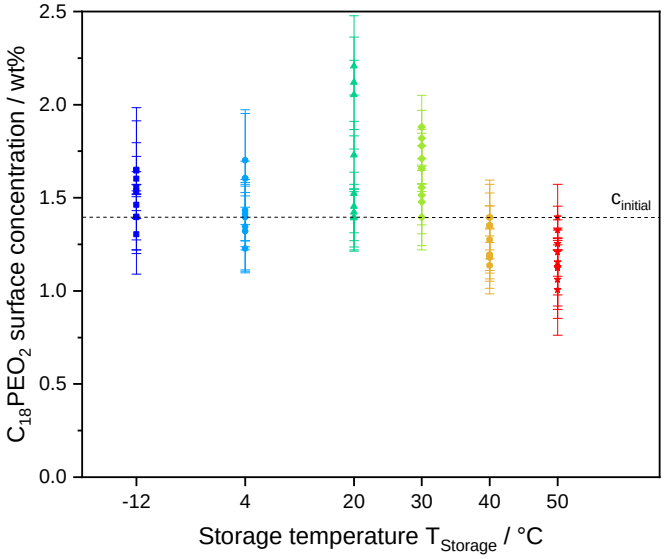

Figure 6.63: Influence of the storage temperature on the migration behavior of single fibers with 1.4 wt% $C_{18}PEO_2$. In order to resolve differences in the migration behavior better, the individual measurements are plotted time-independently over the storage temperature in graph (b).

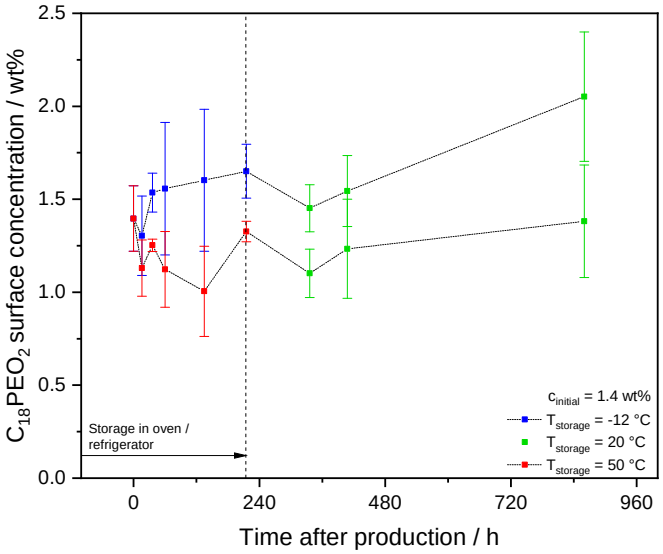

Figure 6.64: Migration behavior of $C_{18}PEO_2$ in single fibers which were initially stored for 9 days at -12 °C or 50 °C and subsequently at room temperature.

Single fibers

Figure 6.66 (a) shows the additive surface concentration as a function of the storage time for single fibers made of polypropylene with different molar masses. The experiment indicates that the low molar mass polypropylene and the reference polypropylene have similar migration kinetics. The additive migrates more slowly in the high molar mass polypropylene and also the additive plateau surface concentration is considerably lower compared to the other two polypropylene grades.

In chapter 6.9.4, injection molded plates were used to demonstrate that the molar mass of the matrix polymer plays a subordinate role for migration behavior. Due to the higher molar mass the crystallization kinetics change, which in turn influences the migration. The high molar mass polypropylene exhibits a higher surface crystallinity (figure 6.66 (b)) than the other polypropylenes. During extrusion the polymer chains are highly pre-oriented, especially in the near-surface regions of the fiber (see also chapter 6.4). During cooling, the pre-oriented polymer chains can crystallize more easily. This effect is more pronounced with the high molar mass grade compared to the polypropylenes with a low molar mass, resulting in a higher surface crystallinity in the high molar mass grade. The surface crystallites can subsequently act as a migration barrier and thus prevent the molecules from migrating to the surface. These

a)

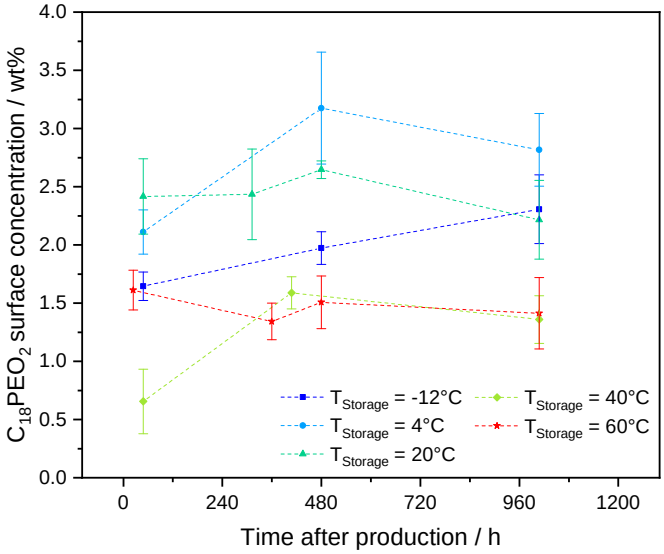

b)

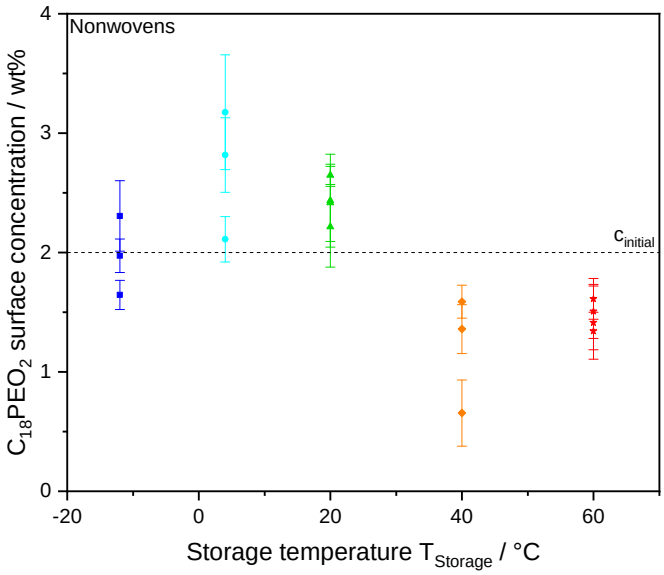

Figure 6.65: Influence of the storage temperature on the migration behavior of nonwovens with 1.7 wt% $C_{18}PEO_2$. In order to resolve differences in the migration behavior better, the individual measurements were plotted time-independently over the storage temperature in graph (b).

findings are highly comparable to other studies. Nogales et al. reported that during crystallization under shear, long polypropylene chains are aligned and oriented in the direction of flow, which increases nucleation and causes lamella growth perpendicular to the direction of flow [189]. Duplay demonstrated in a similar study that the growth rate of crystals under shear of a polypropylene melt increases with the molar mass of the polymer [190] .

Nonwovens

In contrast to single fibers, no significant differences in the migration behavior of additives in the matrix polypropylenes with different molar masses are observed for nonwovens (figure 6.67). The experiment shows that the calendering process deteriorates the migration behavior of the two low molar polypropylenes more than that of the high molar mass polypropylene. A comparison of the surface crystallinity of single fibers and nonwovens of the reference polypropylene (figure 6.68 (a)) and the high molar mass polypropylene (figure 6.68 (b)) reveals that the post-crystallization as a result of the calendering process is less pronounced in the high molar mass polypropylene.

The longer polymer chains of the high molar mass polypropylene are less mobile and cannot post-crystallize rapidly as a result of a short heat input such as calendering. Furthermore, the single fibers made from high molar mass polypropylene already exhibit a higher surface layer crystallinity, which leads to a less pronounced post-crystallization. Accordingly, after calendering, all three polypropylene grades possess a similar near-surface crystallinity, which represents a comparable barrier to surface migration for additives in all investigated matrices.

The observations from this chapter are also confirmed by plotting the plateau surface concentration c_∞ as a function of the weight average molar mass M_W (figure 6.69). The graph illustrates that calendering hardly influences the migration in the polypropylene with the higher molar mass. In the low molar mass polypropylenes the calendering process leads to a significant reduction of the additive surface concentration. Despite a clearly different melt flow index, the difference in the molar mass of the two low molar mass grades is too low to influence the migration behavior.

In summary, no direct influence of the matrix molar mass on the migration behavior of additives could be found. However, since the molar mass of the polymer changes the crystallization kinetics, differences in the migration behavior are observed in different polypropylene matrices.

a)

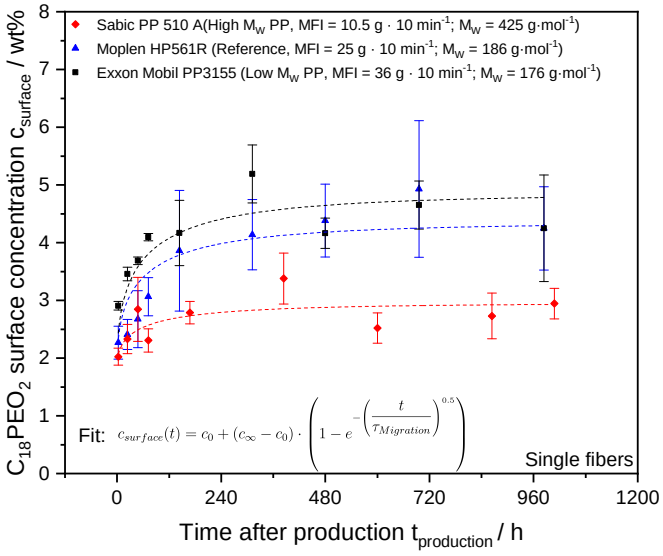

b)

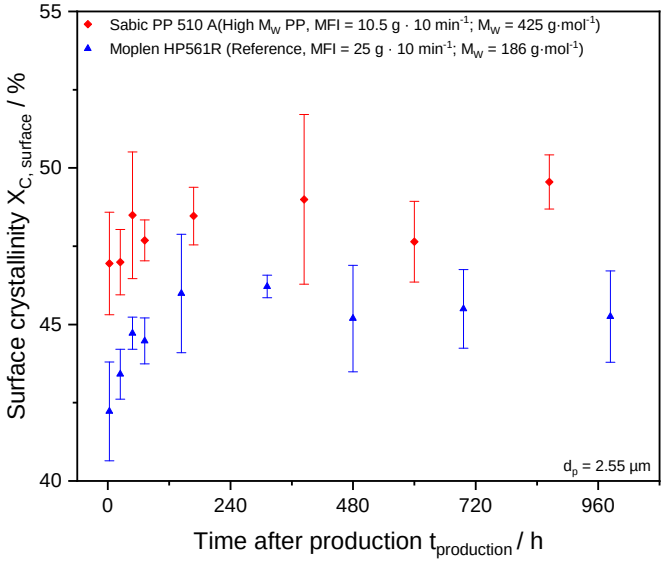

Figure 6.66: Influence of the matrix molar mass on the migration behavior (a) and the surface crystallinity (b) of single fibers with 2 wt% $C_{18}PEO_2$.

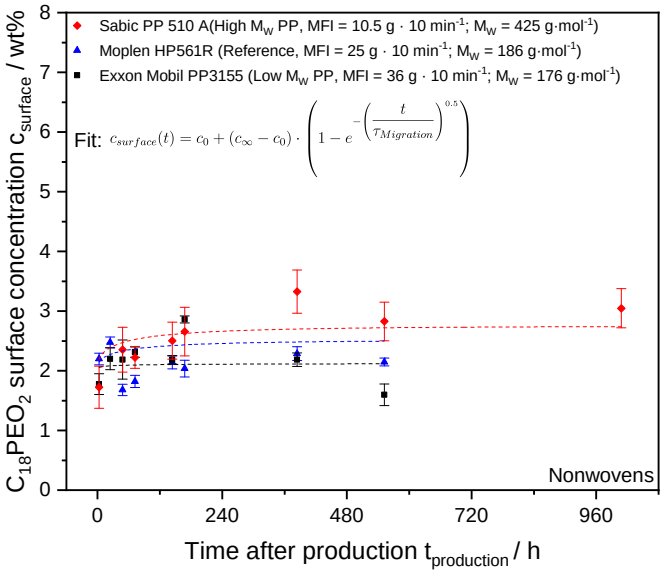

Figure 6.67: Influence of the molar mass of the matrix polypropylene on the migration behavior of nonwovens with 2 wt% $C_{18}PEO_2$.

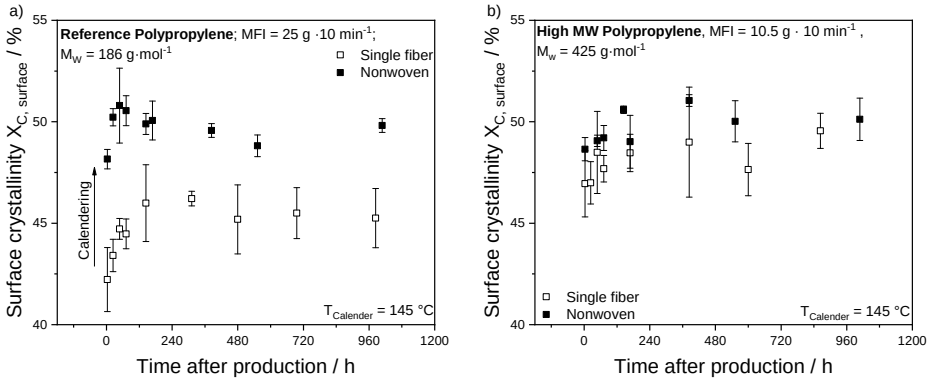

Figure 6.68: Influence of the calendering step on the post-crystallization of fibers of a low molar mass polypropylene grade (a) and a high molar mass polypropylene grade (b).

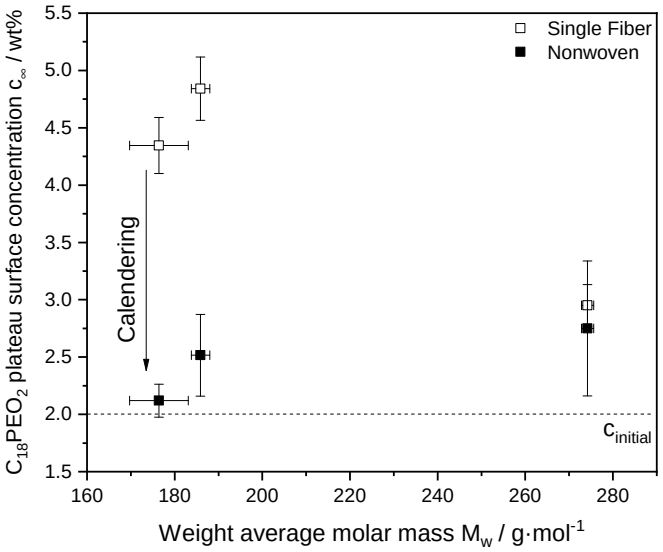

Figure 6.69: Influence of the weight average molar mass on the plateau surface concentration c_∞ in single fibers and nonwovens with 2 wt% $C_{18}PEO_2$.

6.11.5 Influence of nucleating agents

Single fibers

Under the premise that larger crystallite structures or highly oriented regions are not permeable for additive molecules, it is investigated whether the addition of a nucleating agent improves the migration of additives to the surface. It is assumed that the nucleating agent produces more, but smaller crystallites, which are easier for the additive molecule to circumvent than large crystallite structures allowing the additive to reach the surface better. Single fibers were produced with an addition of 4 wt% of a nucleating agent (Milliken Millad NX 10). According to the data sheet [191], an amount of 4 wt% is recommended for a very strong nucleation effect. Figure 6.70 (a) shows the time-dependent migration of the additive in single fibers which were produced using different haul-off pressures, with and without a nucleating agent. The graph illustrates that the addition of a nucleating agent has a negative effect on the migration behavior. The additive surface concentration of all samples produced with the nucleating agent is on average lower than those produced without the nucleating agent. Figure 6.70 (b) shows the associated surface crystallinity for an FTIR penetration depth of 0.7 µm and 2.55 µm. Although the crystallites which are formed in presence of a nucleating agent are probably smaller, the total (surface layer) crystallinity of the fibers is significantly higher. Regardless

of the haul-off pressure, the surface crystallinity of the nucleated fibers is always higher than that of the non-nucleated fibers. As with other sample geometries, the crystallites in turn act as a migration barrier for the additive, which is why fewer additive molecules can reach the surface even after long storage times. Furthermore, it is assumed that the crystallites are oriented as a result of the stretching process, which is why the effect of shorter migration paths is superimposed by the orientation effect (see also chapter 6.11.1.2). The increase of the surface crystallinity by the nucleating agents thus influences the migration in fibers more strongly than the presumed shortening of migration paths.

Nonwovens

Considering the migration behavior of nonwovens produced with nucleating agents, different results are obtained compared to single fibers (figure 6.71). The nucleated nonwovens show a slightly better migration behavior of additives than the non-nucleated nonwovens. The nucleated samples are wettable with water after a storage period of 40 days while the non-nucleated nonwovens do not show a hydrophilic surface. The differences in migration behavior are very small, but on average the additive surface concentration of the nucleated samples is slightly above the samples which were produced without a nucleating agent. The calendering process and the associated partial melting of the fibers leads to a post-crystallization of the fibers (see also chapter 6.4.2) and a partial reorganization of the morphology which was induced by the stretching process. It is assumed that the newly generated crystallites in the nucleated samples are smaller and thus the shortening of migration paths becomes more important. This effect is considered to slightly improve the migration of the additive to the surface. The nucleating agent may therefore restrict the negative effect of post-crystallization through the calendering step and thus enable hydrophilization of the nonwoven surface.

The experimental data from this chapter were partially taken from Sharma's master thesis (supervised by F. J. Lanyi) [178] and analyzed independently within this thesis.

a)

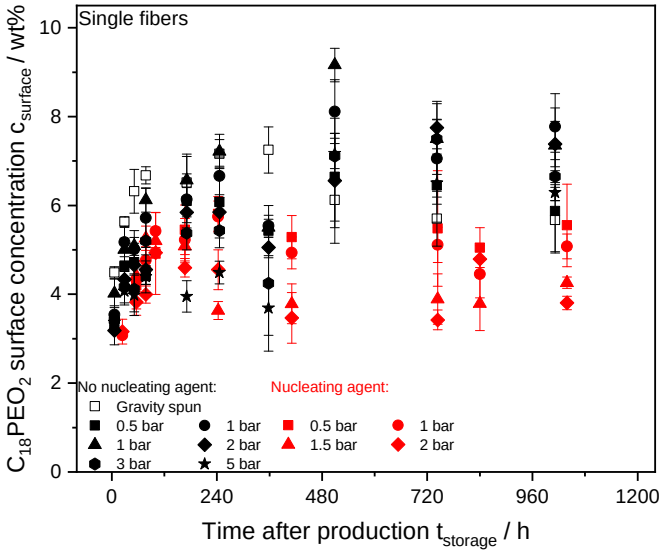

b)

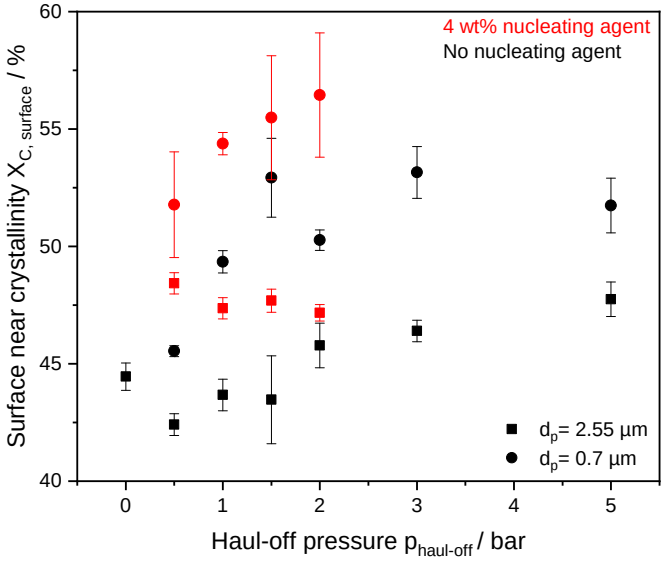

Figure 6.70: Migration behavior (a) and surface crystallinity (b) of single fibers with 2 wt% $C_{18}PEO_2$, which were produced without (black symbols) and with (red symbols) a nucleating agent.

a)

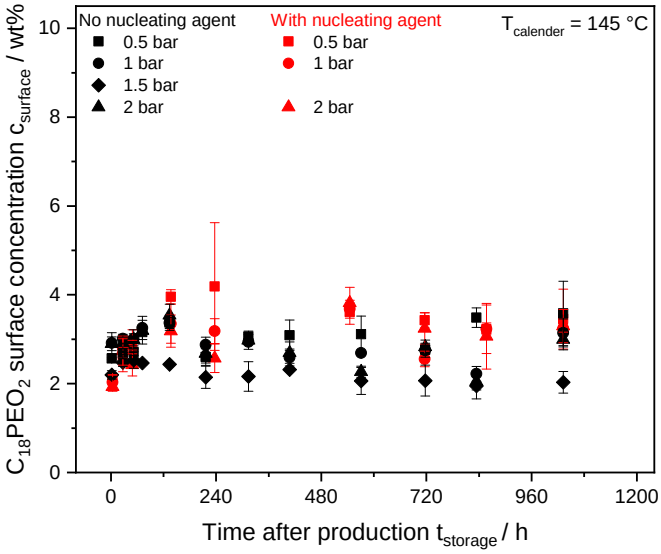

b)

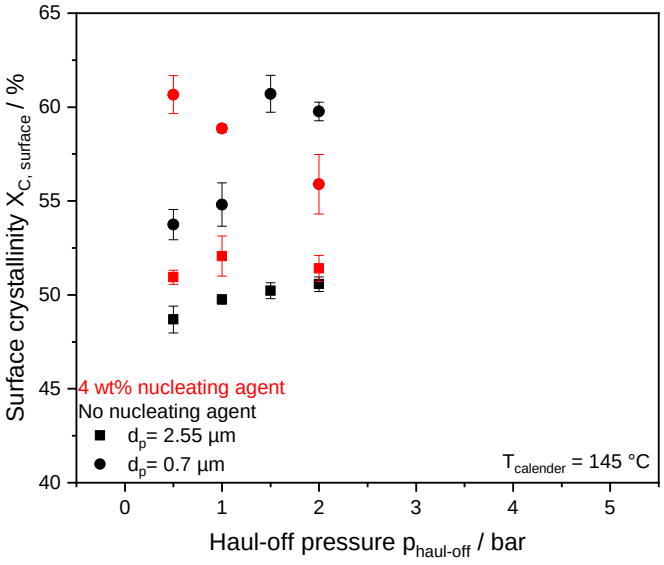

Figure 6.71: Migration behavior (a) and surface crystallinity (b) of nonwovens with 2 wt% $C_{18}PEO_2$, which were produced without (black symbols) and with (red symbols) a nucleating agent.

6.12 Additive concentration profile and enrichment towards the surface

In this chapter the concentration profile which develops as a result of the migration of additives to the surface is discussed. Figure 6.72 (a) shows time-dependent concentration measurements at two different penetration depths of FTIR radiation from injection molded plates with the additive $C_{18}PEO_{10}$ which was stored at a temperature of 40 °C. This sample has been chosen as a representative example, but other additives and storage conditions used in this thesis show comparable results (see also appendix, figure A.25). The experiment illustrates that the additive enriches towards the surface, since the concentration always increases with decreasing IR penetration depth, independently of the storage time. Furthermore, the extent of surface saturation is increased with the storage time, which is associated with an additive desaturation of the core of the injection molded plate (see figure 6.72 (b)).

In order to study the additive desaturation of the matrix core in more detail, an injection molded plate which was stored for about 10 months was cut starting from the surface using a microtome to yield thin film samples with a thickness of approximately 30 µm. By using thin film specimen it was possible to determine the additive concentration in 30 µm steps by measuring each slice via FTIR in transmission mode. The results are presented in figure 6.73. The graph reveals that, despite a very high additive surface saturation of almost 100 wt%, an additive concentration at the same level as the initial concentration is found at a distance of about 30 µm from the surface. Furthermore, the additive is distributed very evenly up to the center of the plate (plate diameter d = 2000 µm). This indicates that the matrix core is not completely desaturating even after long storage times, but the enrichment of the surface only takes place at a distance of less than 30 µm from the surface. This result suggests a maximum distance that an additive molecule can migrate over a finite time.

a)

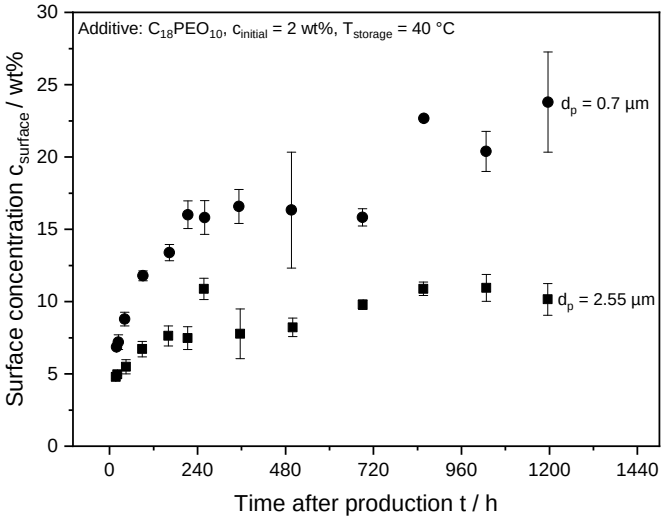

b)

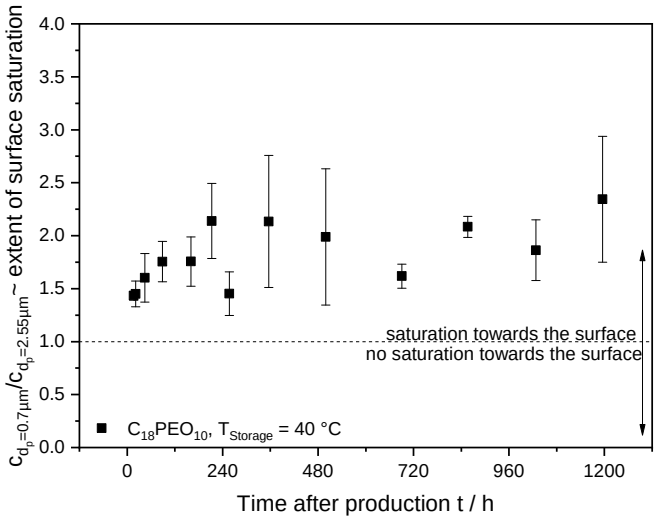

Figure 6.72: $C_{18}PEO_{10}$ surface enrichment in injection molded plates as a function of storage time (a) and extent of surface concentration represented by quotient of surface concentration at two penetration depths (b). Both graphs illustrate the concentration gradient towards the surface increases with increasing storage time.

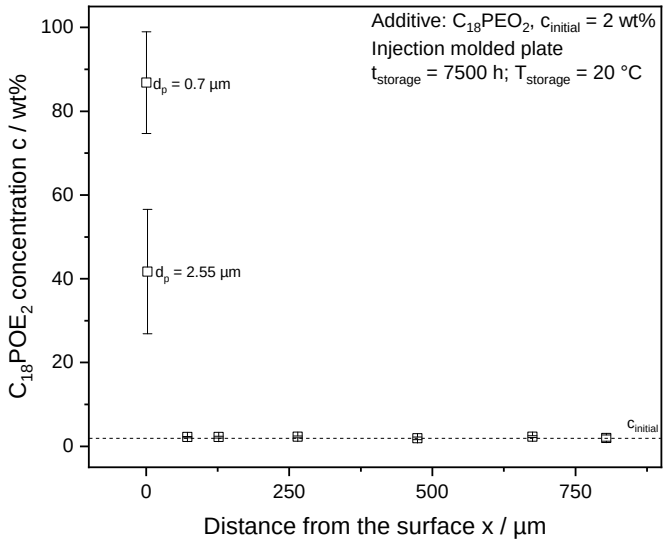

Figure 6.73: Stationary concentration profile in an injection molded plate with 2 wt% $C_{18}PEO_{10}$. The concentration up to a penetration depth of 0.7 µm and 2.55 µm was measured using ATR-FTIR. All other measurements were determined using microtome slices which were measured using FTIR in transmission.

In order to relate these results to other studies and to draw further conclusions on the development of the concentration profile, a literature search was carried out. Most concentration profiles that describe additive concentration c in a depth of x published in other studies follow a shape comparable to an exponential function:

$$c(x) = c_0 + (c_{\text{surface}} - c_0) \cdot e^{-\left(\frac{x}{l}\right)}$$

$$\text{where } \int_0^{\frac{d}{2}} c(x)dx = constant \text{ for all } t \quad (6.8)$$

where l is the decay length of the concentration profile, c_0 is the concentration in the core of the matrix and $c_{surface}$ is the enrichment of additive on the surface. Accordingly, $c_{surface}$ is a measure for the extent of the increase of additive concentration towards the surface. Since the concentration profiles were usually not fit in the available publications, but the decay length l represents a comparable parameter for all published profiles, it was estimated from the

graphs. The initial and final state of a typical concentration profile can be found in appendix A.1.1 (figure A.1).

Chen et al. investigated the migration behavior of poly(ethylene glycol) (PEG) with different molar masses in polypropylene using ATR-FTIR [124]. They used an FTIR-ATR crystal with an adjustable penetration in a way that profiles with a penetration depth of 0.7 - 4.0 µm were detectable. They found that the saturation of the additive towards the surface increases and that the initial concentration is already reached at a penetration depth of about 4 µm, i.e. that a decay length of about 1 - 3 µm exists for the investigated system. The saturation of the additive towards the surface becomes more pronounced with a lower additive molar mass. Another study by Chen et al. investigated the migration behavior of polypropylene-graft-poly(methyl methacrylate) in polypropylene [75]. In this study decay lengths between 1.5 and 3 µm were found as well.
By coupling FTIR and photoacoustic spectroscopy, penetration depths of up to 25 µm can be detected. Sankhe et al. used this method to study the migration behavior of erucamide in LLDPE [117]. They report an enrichment of the additive to the surface. Furthermore, they observed that the initial concentration is reached at a penetration depth of about 10 µm, i.e. decay lengths in the range of 5 µm exist. Another study utilizing FTIR-ATR with a variable penetration depth to demonstrate the surface enrichment of polyethylene-poly(ethylene glycol) block cooligomers in HDPE was conducted by Bergbreiter and Srinivas revealing decay lengths of 1 - 2 µm [73].
Lee and Archer used microtome slices which were cut from samples made of polystyrene-b-poly(dimethyl siloxane) and polystyrene to study the surface segregation of this blend [74]. Similar to the findings from this thesis, they report that the initial concentration is already reached in the first slice (thickness of about 40 µm), i.e. the decay length is significantly below 40 µm.

Another method to measure additive concentration profiles is X-ray photoelectron spectroscopy (XPS). The use of XPS allows the detection of profiles up to a penetration depth of approximately 2 - 100 nm. Bhatia et al. showed concentration profiles of blends of polystyrene and poly(vinyl methyl ether) utilizing XPS [88]. They report decay lengths of about 50 - 100 nm. However, the study is only comparable to this thesis to a limited extent, since considerably higher blend ratios of 80:20 and 50:50 were used and the investigated materials exhibit comparatively high molar masses. Similar results and decay lengths to those from Bhatia's study were obtained for the surface segregation of PS-PDMS / PS blends by Cowie et al.[192]. Decay lengths of about 10 nm were measured by Kano et al. using XPS. In Kano's study a blend

of poly(ethyl acrylate) and poly(vinylidene fluoride-co-hexafluoroacetone) was investigated. All these studies suggest that profiles measured using XPS differ significantly from profiles measured via FTIR. However, the enrichments shown in this thesis are best comparable to those of studies that have also utilized FTIR for profile measurements. Furthermore, it should be noted that there are hardly any studies that consider profiles of low molar mass additives in a low concentration using XPS. In the literature discussed above blends with a ratio of 20:80 to 50:50 and high molar mass polymers were investigated. The comparability of the studies is therefore not completely given as separation and diffusion phenomena differ considerably for polymer blends and low molar mass additives. Other studies suggest profiles which are not at all in comparison to results from this thesis. This might be related to completely different blend systems and mixing ratios of additive and polymer which result in different migration mechanisms. A frequently discussed profile suggests the enrichment of the surface as a result of desaturation of near-surface areas, leading to a concentration minimum in the range of a few nanometres away from the surface (critically damped sine wave) [192, 193].

When examining the migration behavior of the fibers discussed in chapter 6.11.1.1, it is found that the fibers reach a plateau surface concentration considerably faster compared to injection molded plates (figure 6.39 (chapter 6.9.2) and figure A.26 (appendix)) and the plateau concentration is proportional to the initial concentration (figure 6.53 (chapter 6.11.1.1)).

Since the fibers have a significantly higher surface-to-volume ratio than the injection molded plates, it is assumed that the maximum surface concentration in the case of the fibers is limited by the complete desaturation of the core. This means that the surface concentration reaches a terminal state as soon as no more additive can migrate from the core. Assuming that the fibers are evenly distributed on the FTIR crystal during the measurement and the entire additive migrates to the surface, a fit function can be derived which describes the maximum detectable surface enrichment depending on the fiber diameter and the initial concentration of the additive. The derivation of the fit as well as the fit function can be found in the appendix A.10.1.

Figure 6.74 reveals that it is a realistic scenario the entire additive migrates into regions which are detectable via ATR-FTIR. This finding in turn permits the assumption that the additive surface concentration in the stationary state is determined exclusively by the initial concentration and the diameter of the matrix, if the following two boundary conditions apply:

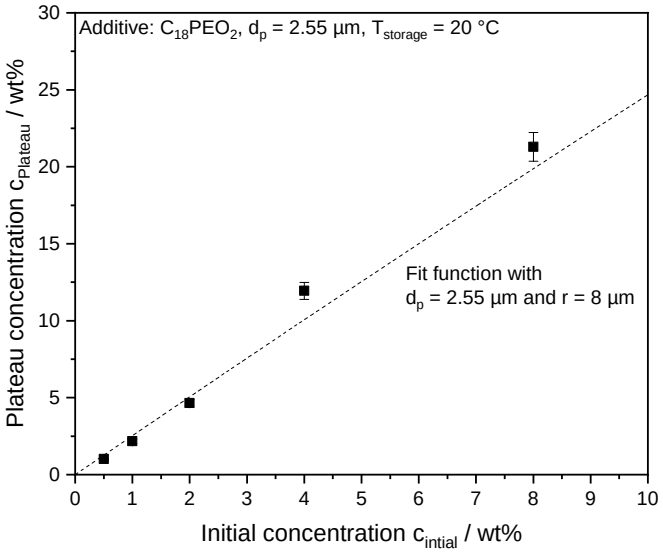

Figure 6.74: Plateau concentration of single fibers after a storage time of 1000 hours as a function of the initial concentration. Fit function according to the model described in appendix A.10.1.

- Morphological effects (e.g. introduced by strong stretching or calendering) do not influence or prevent migration
- The radius of the matrix structure lies within the range of the decay length of the migration profile

To confirm the hypothesis, the model was also applied for the results of single fibers produced using different haul-off speeds (chapter 6.11.1.2). Figure 6.75 illustrates that the model describes the results well. The best fit is achieved for an initial concentration of 1.3 wt%. The difference between the real initial concentration of 1.8 wt% and the best fit for a concentration of 1.3 wt% can be explained by the marginal solubility of $C_{18}PEO_2$ already described in chapter 6.3, which slightly reduces the additive volume available for migration.

In summary, it is concluded that the matrix core desaturates with increasing storage time and the additive enriches towards the surface. The decay length of the concentration profile lies between a minimum of 3 µm and a maximum of 20 µm. Comparisons with results from the literature suggest values between 1 µm and 5 µm. As discussed in previous chapters, surface enrichment is always a function of the morphology present in the near surface regions (crystallite sizes, orientation, crystal morphology, etc.) and the available amorphous matrix polymer volume. If the decay length of the concentration profile is in the order of the matrix radius (e.g. with fibers or very thin films), it is realistic

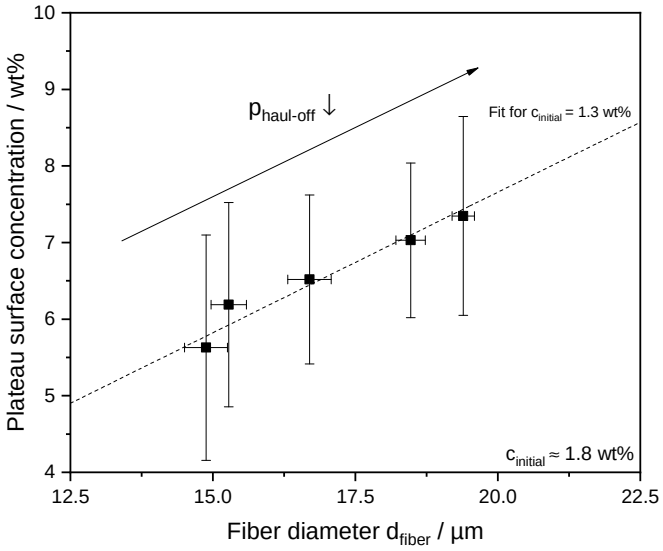

Figure 6.75: Plateau concentration as a function of the fiber diameter of single fibers produced using different haul-off pressures. The function used to model the results is explained in appendix A.10.1.

that the core completely desaturates and the initial additive concentration thus determines the maximum surface concentration. For further investigation, it would be helpful to determine the concentration in more penetration depths (e.g. using multiple ATR crystals or an adjustable ATR crystal or other methods such as XPS) in order to estimate the concentration profile more reliably.

6.13 Advantages of additives applied as a melt additive

The following chapter discusses the advantages of hydrophilic melt additives over conventional surface hydrophilization methods. The focus of the investigations is primarily on the subsequent activation of hydrophilic and hydrophobic areas as well as on the evaluation of permanence and durability.

General advantages of melt additives not discussed in detail

Since all investigated additives have a comparatively low molar mass, they usually also act as plasticizers. As a result, fibers with the melt additive feel much softer than fibers made of pure polypropylene. This is probably due to a reduction of the modulus of elasticity and a reduction of the coefficients of friction after the additive migrated to the surface. However, the softness

benefit was not experimentally investigated in this thesis and could be the focus of further research.

Furthermore, all substrates show a very uniform surface distribution and an even hydrophilization of the surface, if the additive migrates to the surface and can also hydrophilize it in general (e.g. in the case of $C_{18}PEO_2$). A comparison of the distribution quality of additives used as melt additives and as a coating can be found in appendix A.11 (figure A.28). The quality of the surface distribution is slightly better with regard to uniform wetting in the case of melt additives. Coated samples occasionally show non-wettable spots. In addition, compared to the coating, the melt additive shows a lower standard deviation of the surface concentration. However, since the coating process applied in this thesis is not fully comparable to that used in an industrial process, this finding is not definitive.

The ethoxylated alcohols are processable without further steps or changes in the process parameters. Thus, the additives shown here can be integrated into the process without any processing problems and do not require further process steps, expensive equipment or an adjustment of the running process.

6.13.1 Subsequent activation methods

One advantage of additives which are used as melt additives is their subsequent activatability. Additives which do not migrate to the surface during the process can obtain the energy necessary to sufficiently increase the diffusion coefficient by a targeted heat input. Accordingly, the additive can migrate to the surface and hydrophilize it.

Especially the location sensitive activation of the additives is of great economical importance. By selectively activating nonwovens using suitable methods, it would be possible to make them permeable to water at specific sports while leaving others hydrophobic. In the case of hygiene articles, this would offer significant advantages in fluid management, i.e. the selective routing of liquids in the final product.

In the following chapter, two methods for the subsequent activation of additives are presented. On the one hand, the activation is conducted with a hot air gun, i.e. by means of hot air applied in a targeted manner. On the other hand, hot water steam is used for the activation. The hot steam changes the interfacial energy while at the same time introducing heat into the material.

In order to activate the nonwovens, a hot air gun or hand held steamer was attached at a distance of about 20 cm from the nonwoven. The nonwoven was

then activated for about 30 seconds with either 130 °C hot air or 100 °C hot steam. After cooling and drying, the wetting behavior was determined.

Figure 6.76 shows contour plots of the samples from chapter 6.8 (figure 6.35) and their changes in wetting behavior as a result of heat activation. To calculate these graphs, the value for wetting performance of the activated nonwoven was subtracted from the initial value for wetting performance. Accordingly, a numerical value for the improvement or deterioration of the wetting behavior is received for each of the activation processes. For further experiments, samples which exhibit the greatest possible change, even if it was a worsening, are used. By a deterioration of the wetting behavior it would be possible to systematically hydrophobize defined areas instead of hydrophilizing and thus also to achieve selective wetting of the nonwoven.

The experiment demonstrates that only a few nonwovens show a significant change in wetting behavior upon heat input.

This is due to the circumstance that most samples show a rather deteriorated wetting behavior due to the heat input (see also chapter 6.11.3). If the wetting behavior was already poor before the heat input, it will change hardly or not at all as a result of the heat input.

The samples with the additives $C_{18}PEO_2$, $C_{18}PEO_{10}$ and $C_{18}PEO_{20}$ were selected for further activation studies, as these are were already well wettable before the heat activation, fully characterized within the scope of this work and also show the most significant change of the wetting behavior as a result of heat input or steaming.

6.13.1.1 Hot air heat activation

Figure 6.77 shows the influence of the duration of the hot air treatment on the migration behavior of the additive $C_{18}PEO_{10}$. The experiment illustrates that the additive migration to the surface is not very pronounced, even with an activation time of 60 seconds. However, all samples became hydrophobic as a result of the heat input. This behavior has already been described in chapter 6.9.2 and 6.11.3, where storage at high temperatures was often accompanied by a reduction in the (near-)surface concentration. The wetting behavior depends on the arrangement of the molecules in a few Å from the surface. It is assumed that in the case of short-term activation with heat, the phenomena leading to a reduced surface concentration only occur directly on the surface and cannot be detected and distinguished by ATR-FTIR due to the rather high penetration depth of IR radiation. The phenomena causing hydrophilization can be a rearrangement of the molecules, which considerably changes the

a)

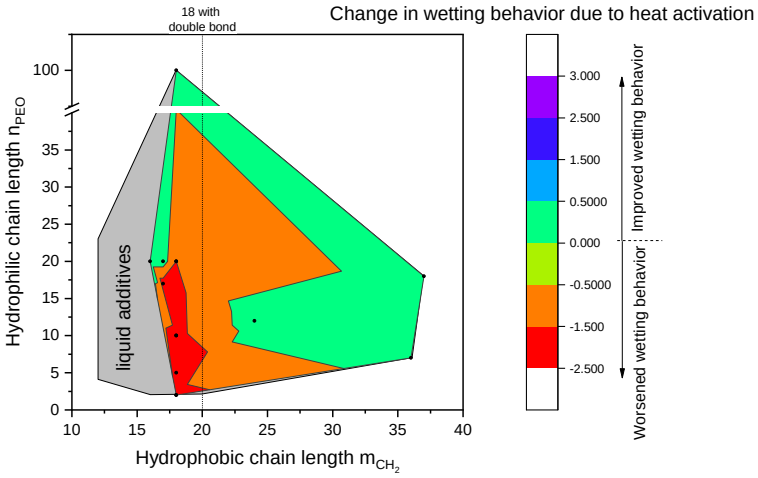

b)

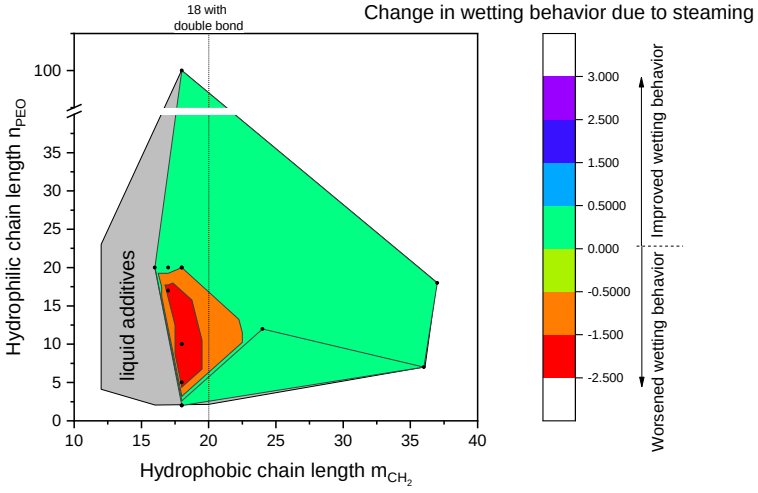

Figure 6.76: Change in the wetting behavior of nonwovens which have been treated with hot air (a) or hot steam (b). All nonwovens were produced with an initial additive concentration of 2 wt%.

wetting behavior, or a desaturation of the surface due to heat input. The available methods do not allow final conclusions to be drawn as to why these phenomena could be the focus of further research. The experiments were also conducted using the additives $C_{18}PEO_2$ and $C_{18}PEO_{20}$. The results are comparable and can be found in appendix A.11 (figure A.29).

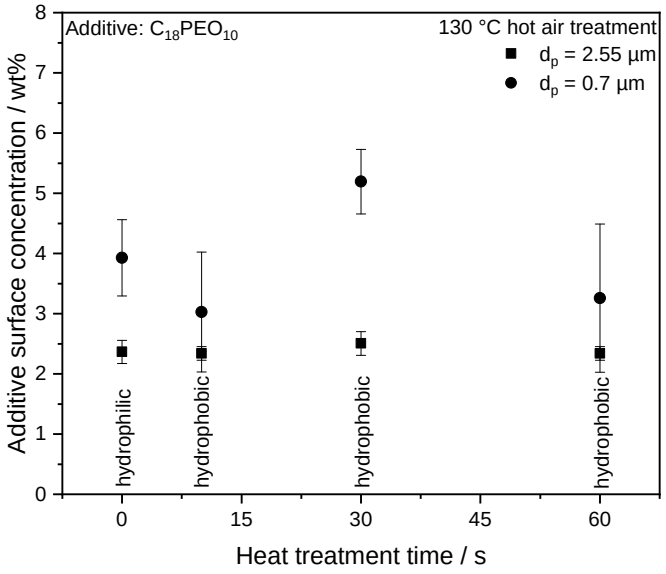

Figure 6.77: Influence of heat treatment time on the migration behavior of 2 wt% $C_{18}PEO_{10}$ in nonwovens.

Selective activation

Figure 6.78 shows the wetting behavior and the corresponding additive surface concentration of a nonwoven with $C_{18}PEO_{10}$ which was selectively activated. The activated areas are highlighted in blue using image editing software for better differentiation. The selective activation was realized by using a steel template, which was only permeable for the hot air in specific places. Therefore, only defined areas of the sample were heated while the rest of the nonwoven remained cold. The activation time was about 10 - 15 seconds. In the sample the non-uniform additive surface distribution overlays the effect of the heat input. Even though the additive concentration in the near surface regions of the heat-activated areas, is always a little higher than in the adjacent non-activated zone, the heat activation leads to hydrophobization (figure 6.78 (b)) of the selectively activated areas. As described above, it is assumed that the changes in the arrangement of the additives take place in areas not detectable by ATR-FTIR. Therefore, they are not discussed here. However, it

was demonstrated that it is possible to selectively hydrophilize nonwovens by hydrophobizing specific areas as a result of a targeted treatment with hot air.

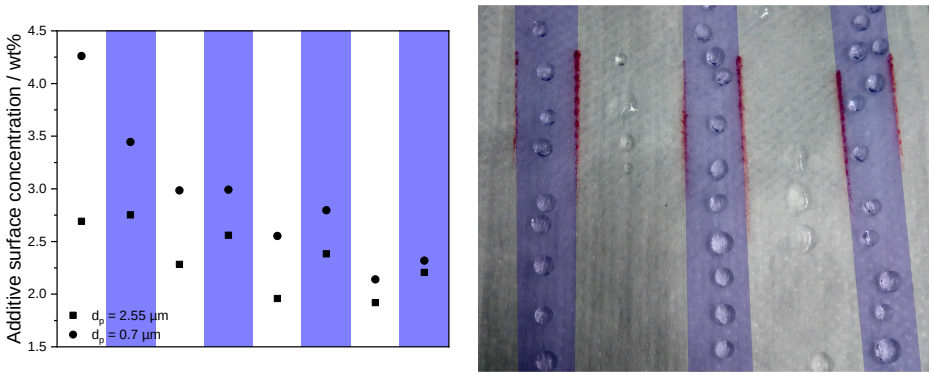

Figure 6.78: Selective heat activation of the nonwoven by using hot air. Associated migration data (a) as well as an image of the wetting behavior of the (de-)activated nonwoven. Treated areas were successfully hydrophobized while untreated areas stayed hydrophilic. Blue areas in the image (b) were subsequently inserted using image editing and serve to illustrate the areas which were hydrophobized using hot air.

6.13.1.2 Water vapor steaming

Figure 6.79 shows the additive surface concentration of nonwovens treated with hot steam for 10 seconds. In the case of additive $C_{18}PEO_2$ the previously hydrophobic nonwovens were hydrophilized after the steam treatment. Furthermore, all nonwovens exhibit an enrichment of the additive at the surface. On the one hand, energy in the form of heat is very effectively introduced into the nonwoven by the steam, which increases the diffusion coefficient and allows the additive to migrate towards the surface. On the other hand, the water steam changes the interface from polymer-air to polymer-water. As in the case of activation by hot air, the change in wetting behavior is probably caused by changes in regions which cannot be detected by ATR-FTIR. For this reason, only assumptions can be made about the phenomena that occur.

Based on the findings from chapter 6.7, it is assumed that the surfactant molecules lie flat on the surface and thus wettability with water may be restricted. Due to the interface change and the increased additive mobility due to the heat input, it is plausible that the additives will align with the hydrophilic part of the surfactant towards the water and thus become wettable for water. Furthermore, the interface change can lead to an improvement of the migration to the surface, especially in the outermost surface layers. These effects are assumed to be the reason for hydrophilization of nonwovens with $C_{18}PEO_2$.

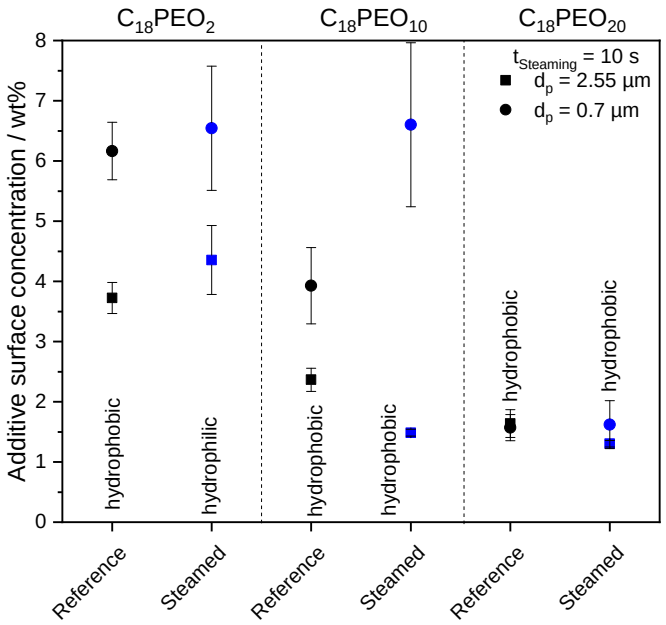

Figure 6.79: Influence of a steam treatment on the migration behavior of different additives in nonwovens. $C_{18}PEO_2$ showed a hydrophilization of a previously hydrophobic nonwoven due to the treatment.

Selective activation

As in the selective heat activation study with hot air, a steel template was used to selectively activate the nonwovens with $C_{18}PEO_2$ by using hot water steam. The steel template held off the steam in order to only treat the nonwoven in the permeable strips. Figure 6.80 shows the wettability with water and the migration data of the additive after the steaming procedure. The activated areas are highlighted in blue using image editing software. It is demonstrated that it is possible to activate areas very precisely with water vapor and thus selectively hydrophilize specific areas of a nonwoven.

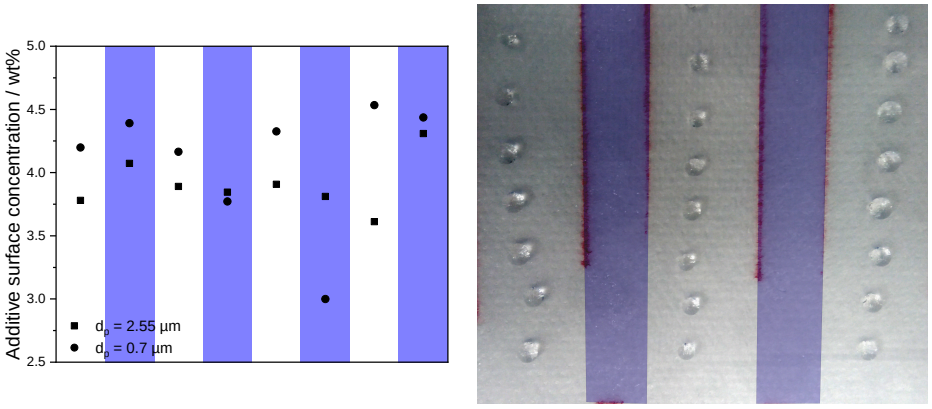

Figure 6.80: Proof of concept of the selective hydrophilization of nonwovens with $C_{18}PEO_2$ by water vapor. Associated migration data (a) and an image of the wetting behavior (b) of the treated areas. Activated regions are highlighted in blue. Regions which were treated with hot vapor were hydrophilized while untreated areas remained hydrophobic. Blue areas in the image (b) were subsequently inserted using image editing and serve to illustrate the areas which were hydrophilized using hot water steam.

6.13.2 Permanence and durability

Permanence is defined as the non-existent transfer of the additive present on the surface to or into adjacent polymer layers over time and at elevated temperatures. Durability is defined as the non-existent transfer in water upon contact with it. Both properties are particularly important for the properties of the final products, as it is essential for reproducible product quality that the additives remain in place during use and storage. Under the hypothesis that melt additives at least partially anchor themselves to the surface with the hydrophobic part of the surfactant during the migration, it is assumed that they have a better permanence and durability compared to additives applied conventionally as a surface coating. In order to prove or disprove this hypothesis, the additives $C_{18}PEO_2$ and $C_{18}PEO_{10}$ were tested both as melt additives and as coatings, as these two additives had the best wetting properties in the application context. Further additives were not tested as the experimental effort for testing the criteria is very high.

6.13.2.1 Permanence

Figure 6.81 shows the transfer from nonwovens with an additive to the surface of pure polypropylene nonwovens. It can be seen that all samples show a certain transfer, which is within the detection limit of the FTIR method. Only with additive $C_{18}PEO_2$, which was stored at a temperature of 60 °C, a certain

transfer to the surface of adjacent polymer layers was detected. Furthermore, the larger $C_{18}PEO_{10}$ molecules show a lower surface transfer than the smaller $C_{18}PEO_2$ molecules. This may be due to a lower mobility of the larger molecules in the matrix polymer and on the surface especially at elevated temperatures. To increase the permanence, the molar mass of the additive may be used as a design criteria. In order to determine whether an application-relevant transfer to the pure polyproyplene nonwovens took place, they were wetted with water droplets and strike-through tests were carried out. It was found that none of the tested samples let water strike-through and that the wetting behavior of the nonwovens does not change. Although small amounts of the additive might be transferred during storage, the amount is not sufficient to alter the performance of adjacent layers. An improvement of the permanence by the use as a melt additive in comparison to coatings could not be proven.

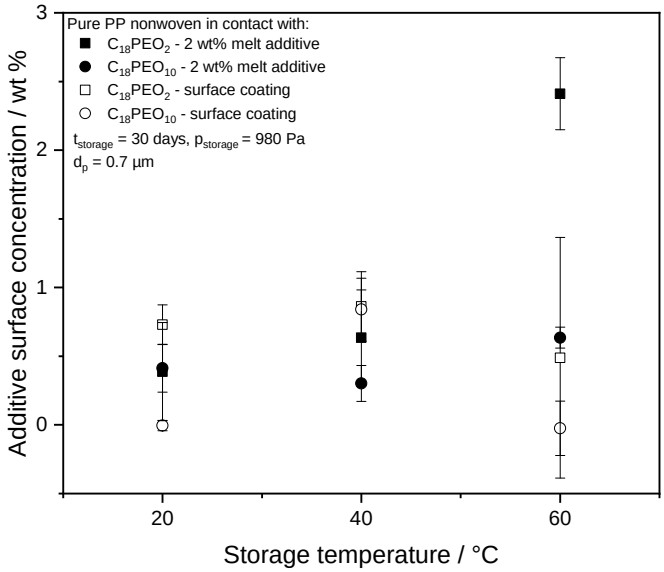

Figure 6.81: Additive surface concentration of pure polypropylene nonwovens which were in contact with nonwovens with an additive. None of the adjacent pure polypropylene nonwovens showed a hydrophilic surface after storage.

6.13.2.2 Durability

Figure 6.82 shows the decrease in surface concentration as a result of washing with water (a) and the associated change in strike-through time (b). For nonwovens with $C_{18}PEO_{10}$, a decrease of the surface concentration is accompanied by a hydrophobization of the surface. The nonwovens which were coated with $C_{18}PEO_{10}$ also show a considerable weight loss, which indicates a complete

washing off of the additive. In the case of $C_{18}PEO_{10}$, which is used as a melt additive, a sufficient amount of additive is washed off the surface to prevent re-hydrophilization of the surface even after subsequent 30 days of storage. Accordingly, $C_{18}PEO_{10}$ is considered to be non-durable. $C_{18}PEO_2$ showed no deterioration in wetting behavior after washing. In the case of nonwovens with melt additive there was even an improvement. As already described in chapter 6.13.1.2, this improvement can probably be attributed to a change in the orientation of the additive molecules on the surface or to a migration of additive molecules from near-surface layers to the surface by a change of the interface. A change of the surface concentration as a result of the washing process was detectable but not relevant for the application. In all nonwovens tested, the water used to wash the nonwovens did not pass through pure polypropylene nonwovens in the strike-through test. This means that no application-relevant transfer of the additive into water took place. The better durability of $C_{18}PEO_2$ compared to $C_{18}PEO_{10}$ can be due to a higher solubility of $C_{18}PEO_{10}$ in water. In ethoxylated alcohols the water solubility increases with increasing hydrophilic chain length and decreasing hydrophobic chain length [194]. Furthermore, it is assumed that due to the strong adsorption of the C_{18} chain on the polypropylene surface and the relatively short PEO_2 chain, larger parts of the molecule adsorb to the substrate (see also chapter 6.7). Accordingly, the water solubility and the ratio of hydrophobic and hydrophilic part (also known as the HLB value) could be used as design criteria for durable additives. However, further experiments would be necessary to fully confirm these hypothesises. In terms of durability, there was also no difference between melt additives and coatings. In summary, no difference in the permanence and durability of ethoxylated alcohols could be demonstrated by their use as melting additives compared to their use as a coating. For this reason, an anchoring mechanism of the hydrophobic part of the surfactant does not seem to be responsible for the fixation of the additive on the polymer surface. It is assumed that the adsorption of the molecules is the main reason for the permanent binding.

a)

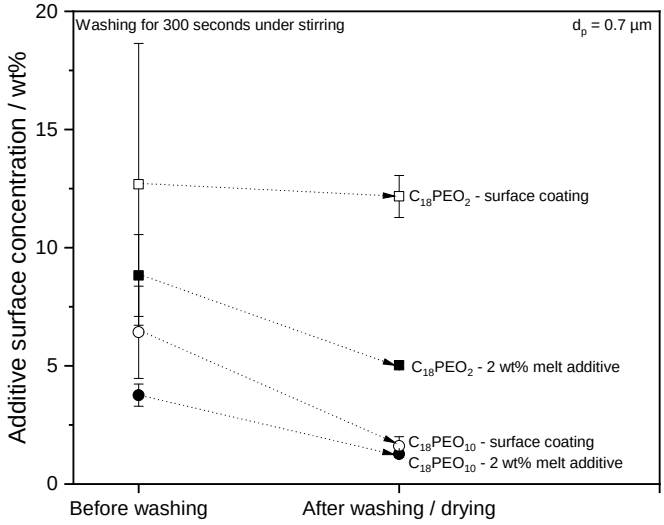

b)

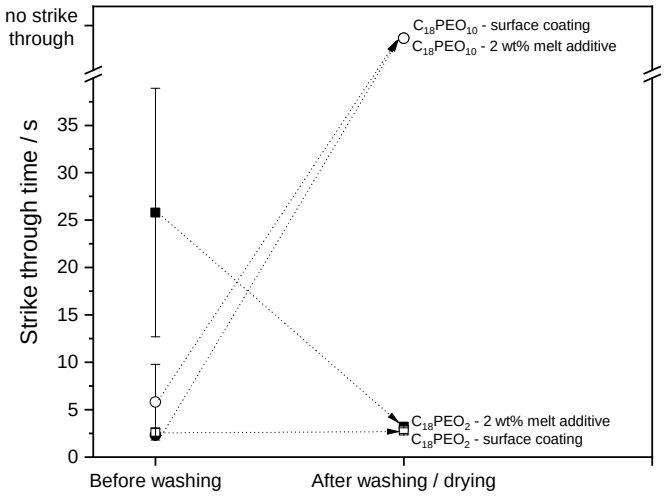

Figure 6.82: Additive surface concentration (a) and change in strike-through behavior (b) of nonwovens before and after washing in water for 300 seconds.

7 Summary and Outlook

The aim of this work was to find melt additives for the hydrophilization of the surface of polypropylene to open up new fields of application for polypropylene and avoid disadvantages of industrially established processes for hydrophilization. Various commercially available surfactants with different molecular architecture and functional groups were investigated with respect to their processability, hydrophilization potential and migration behavior. The focus of the work is on the correlation of morphology development during the production process and the migration behavior of the additives with regard to their molecular structure.

Nonionic surfactants (ethoxylated alcohols, sorbitan esters and PEO-PPO-PEO block copolymers) which differ in the length of their hydrophilic and hydrophobic molecular parts were selected as potential additives due to their current application in an industrial context and their good processing properties.

To tailor the surface properties by means of a melt additive, the following steps have to be performed:

1. The additive is mixed with the polymer in the melt. It is sufficiently compatible with the polymer and thermally stable at process-relevant temperatures. Otherwise process instabilities or the loss of additive occur.
2. During cooling, the additive segregates from the polymer as a result of matrix crystallization. Excessive miscibility with the matrix prevents migration to the surface.
3. The additive migrates to the surface. The migration behavior depends on the matrix morphology developed in the process and is a function of the storage time and temperature.
4. After the additive migrated to the surface, the molecule has to impart hydrophilicity to the surface. This ability is highly connected to the adsorption behavior.
5. The additive remains attached to the surface and is therefore permanent and durable.

Method development and preliminary tests

The use of Fourier-transform infrared spectroscopy (FTIR) allowed the development of methods to determine the degree of crystallinity of polypropylene as well as the additive concentration rapidly, location-sensitive and non-destructively at the surface and in the volume of polypropylene. This made it possible to track migration and morphology formation during the process and storage.

In preliminary tests, the additives were applied to nonwovens and injection molded polypropylene plates using a coating process. It was demonstrated that the contact angle which forms on a coated plate correlates with the strike-through time of coated nonwovens. Subsequent spinning trials revealed that all additives investigated in this thesis are spinnable and have a sufficient thermal stability for the fiber spinning process. Minor problems with spinnability only occurred with sorbitan esters, which exhibit rare extrusion instabilities. It was demonstrated that the hydrophilization of the surface by melt additives is a superposition of the migration to the surface and the ability of the additive to significantly reduce the water contact angle. The hydrophilic properties of the additives are strongly linked to their adsorption behavior. It is assumed that the additives adsorb flat to the substrate due to the high chemical similarity to polypropylene. The resulting water contact angle correlates with the amount of -OH groups per surface area.

Both in the coating experiments and in fiber spinning trials, ethoxylated alcohols with a low molar mass, a long hydrophobic part and a short hydrophilic part (low HLB value) showed the best hydrophilization behavior. Contrary to expectations, surfactants consisting mainly of hydrophilic molecule groups (high HLB value) do not show a good potential for hydrophilization of the surface. For the following experiments the additive selection was therefore reduced to ethoxylated alcohols with the structure $C_{18}PEO_x$, where x was between 2 and 20 and the hydrophobic part of the molecule may contain double bonds.

Morphology development and migration of additives

All investigated sample geometries, show an enrichment of the additive towards the surface which is accompanied by a desaturation of the core. The surface concentration increases with increasing storage time and reaches a

plateau value after 7 - 30 days. The time-dependent surface concentration can be described by the equation:

$$c_{\text{surface}}(t) = c_0 + (c_\infty - c_0) \cdot \left(1 - e^{-\left(\frac{t}{\tau_{\text{Migration}}} \right)^{0.5}} \right) \quad (7.1)$$

where $\tau_{\text{Migration}}$ is the characteristic time after approximately 63 % of the additive have migrated to the surface and c_0 and c_∞ are the surface concentration after no and infinitely long time have passed, respectively. The migration experiments suggest that the evolving concentration profile can be described by:

$$c(x) = c_{core} + (c_{\text{surface}} - c_{core}) \cdot e^{-\left(\frac{x}{l} \right)}$$

$$\text{where } \int_0^\infty c(x)dx = constant \text{ for all } t \quad (7.2)$$

where l is the decay length of the concentration profile, c_{core} is the concentration in the core of the matrix and c_{surface} is the concentration of the additive on the surface. The results from this thesis and an evaluation of the available literature, suggest that the decay length is in the range of 1 µm to 5 µm. The surface concentration of the additive determined by ATR-FTIR correlates with the contact angle which forms on injection molded plates as well as the wetting behavior of nonwovens.

In general, the amount of additive which migrates to the surface is a function of the non-miscible, migratable additive volume which can be reduced by miscibility or co-crystallization with the polymer matrix. Accordingly, the plateau surface concentration c_∞ which is reached after sufficiently long storage times is directly proportional to the initial additive concentration c_{initial}.

The migration behavior of the additive is strongly dependent on the storage temperature. High storage temperatures lead to an increase of the diffusion coefficient and thus to a faster migration. Simultaneously, the miscibility of additive and polymer increases, which reduces the additive volume available for migration. Accordingly there is a trade-off between the increasing miscibility of the additive with the polymer and the increase of the diffusion

coefficient. These effects result in an optimum storage temperature, which depends on the molecular structure of the additive. The increase of the molecular dimensions or the steric hindrance by double bonds in the additive deteriorate the migration.

A direct influence of the polymer matrix molar mass on the migration behavior could not be demonstrated. However, the increase of the molar mass or the addition of long chain branches to the PP leads to a change of the crystallization behavior which influences the migration. Usually, an increase in the matrix molar mass leads to an indirect deterioration in migration behavior.

In order to correlate polymer morphology and migration, the crystallinity of samples produced via fiber spinning, film casting and injection molding is determined as a function of the most relevant process parameters. The combination of X-ray diffraction (XRD), (ATR-)FTIR and light microscopy, allowed the development of novel model assumptions for the morphology formation during the process. The migration behavior depends on the packing density of the polymer chains, since strongly oriented amorphous regions or crystallites are not permeable for additive molecules. The more densely the surface is packed, the less additive can migrate to the surface.

Injection molded plates

Injection molded samples possess a mesomorphic surface layer if produced with a cooled mold. With an increase in mold temperature, samples become more crystalline and show larger crystallites in near surface regions. Due to the low surface crystallinity, rapidly cooled injection molded samples exhibit a very good migration behavior. Mold temperatures above 60 °C result in almost complete blockage of migration due to the high crystallinity of the sample surface.

Cast films

Cast films show a mesomorphic structure if they are quenched on a chill roll which is cooled to 20 °C. If mesmomorphic films are stretched at room temperature, a highly oriented mesophase develops. If the films are heated to 145 °C before stretching, as it is usual in the industrial process, recrystallization occurs. As a result, thermally treated films exhibit an α-crystalline structure, which can be stretched and oriented like mesomorphic structures.

Due to the low crystallinity and the mesomorphic structure, good migration is observed for unstretched cast films, comparable to that of injection molded plates. The good migration behavior is due to the good permeability of the low oriented mesomorphic structure. The heating of films prior to stretching

suppresses the migration due to the post-crystallization of the surface or co-crystallization of additive molecules with the polymer. Stretching at room temperature also completely prevents migration. Due to the orientation of the mesomorphic crystal phase and the amorphous regions, the polymer chains are packed highly dense and a diffusion barrier is generated which is not permeable for the additive molecules.

Fibers and nonwovens

Gravity spun fibers exhibit a mesomorphic structure, which is comparable to that of unstretched cast films. In contrast to films, fibers are stretched during quenching and solidification. This causes the strain-induced crystallization of the hot fiber core, while quenching and freezing of the surface results in a highly oriented amorphous surface layer. The pre-oriented amorphous surface layer is further oriented during stretching, leading to mechanically induced post-crystallization. Accordingly, a maximum of the degree of crystallinity is found in the core (strain-induced) and on the surface (orientation-induced) of the fiber. The subsequent thermal bonding step for the production of nonwovens from single fibers (calendering) leads to post-crystallization causing a crystalline and strongly oriented surface in nonwovens.

Fibers exhibit the lowest additive surface concentration of all investigated sample geometries. This is probably due to the high surface-to-volume ratio of the fibers. Although the stretching conditions have a strong influence on the evolving morphology, no significant impact of the stretching conditions on the migration behavior was observed. It is assumed that during the stretching process, the surface is oriented and new migration paths are created by increasing the distance between surface crystallites. Both effects have an opposite influence on the migration and cancel each other out. The recrystallization of the fiber surface as a result of calendering, prevents the migration of low molar mass additives to the surface of nonwovens. In the case of larger molecules ($C_{18}PEO_{10}$), the heat input leads to an enrichment of the additive and thus to direct hydrophilization of the surface.

Practical application and recommendations

Based on the conducted experiments, it is possible to define requirements which should be met by molecules in order to utilize them as hydrophilic melt additives:

- **Nonionic surfactants with long hydrophobic tail and short hydrophilic head (low HLB value)**
  show good processability and high surface hydrophilization
- **Solid at room temperature (T_m > 40 °C)**
  to immobilize the additive when it has migrated to the surface to ensure permanence and durability
- **Functional group(s) with high polarity**
  to impart high hydrophilicity as -OH groups / surface area correlate with wetting behavior
- **Low molar mass in the range from 300 g mol^{-1} to a maximum of 1000 g mol^{-1}**
  as larger molecules are less mobile and do not migrate to the surface
- **Low miscibility with matrix polymer**
  as miscibility with matrix reduces additive volume which is available for migration
- **High thermal stability up to about 300 °C**
  to prevent degradation during fiber spinning

For practical applications, the additive $C_{18}PEO_2$ is recommended for the hydrophilization of fibers, cast films and injection molded parts. The additive $C_{18}PEO_{10}$ is recommended for the hydrophilization of nonwovens. An additive concentration of at least 2 wt% is required for uniform hydrophilization. Both additives can also be used as coatings and provide comparably good wetting properties.

Compared to the use of the additives as coatings, no significant difference in permanence and durability could be demonstrated by the sole use as melt additive. An anchoring mechanism of the additive inside the polypropylene as a result of the migration process is therefore not necessarily to be expected. The immobilization of the additive molecules on the surface is assumed to be caused by adhesion. This concerns both the use as a coating and the use as a melt additive. Nevertheless, it was possible to find permanent and durable melt additives for the hydrophilization of polypropylene. The subsequent

treatment of the nonwovens with hot air or water vapor allows to hydrophilize or hydrophobize specific areas of the nonwoven.

Outlook

Siloxane-based surfactants (e.g. marketed as SILWET series by Momentive) or sugar surfactants (e.g. Glucamides, Glucosides or Sucrose esters) could be potential substances for even more effective melt additives as they fulfil all the above defined requirements for the use as hydrophilic melt additives. Furthermore, mixtures of surfactants with different short- and medium-length hydrophilic molecule parts such as $C_{18}PEO_2$ and $C_{18}PEO_{10}$ could combine the advantages of various additives. The addition of $C_{18}PEO_2$ causes a significant increase in the softness of single fibers and can therefore be used to produce soft and hydrophilic polypropylene fibers. This specific increase of softness of the fibers might be the subject of further investigations.

The correlations found for additive migration and morphology development could be transferred to other additive classes and applications of melt additives. For example, the use of erucamide for the reduction of the friction coefficient also requires a strong migration to the surface, whereas migration should be prevented when molecules are utilized as stabilizer. The results and design criteria presented in this thesis may optimize the use of melt additives or even allow the development of novel additive types.

Most of the open questions in this thesis are related to the molecular arrangement of the additive molecules in the polymer and on the polymer surface. The investigation of the arrangement of additive molecules on the surface might explain, how the additives are adsorbed to the surface, how the immobilization of the additives on the surface works and how the additives rearrange as a result of heat input. Furthermore, it is not fully understood whether miscibility or co-crystallization with the polymer leads to a strongly deteriorated migration at elevated temperatures or if other mechanisms, such as micellization of surfactants, play a role.

In this thesis different profiles and novel models are proposed for the development of morphology as well as for additive distribution in different sample geometries. These models could be confirmed or disproved by Raman microscopy or ATR-FTIR with adjustable penetration depths.

Conclusion

Permanent and durable melt additives for the hydrophilization of polypropylene surfaces were found, which can be used in injection molding, film casting as well as fiber spinning and nonwoven making. The use of melt additives

is an easy to implement and cost-effective process for tailoring the surface properties of polypropylene. In addition, methods were found which allow local hydrophilization and hydrophobization of defined areas of nonwovens.

While previous studies [13, 14, 16, 95] mainly focus on the selection and the effect of different additives or investigate only partial aspects of the migration behavior of additives [71, 85, 120, 195], the present study provides a comprehensive understanding of the migration behavior of additives and the morphology development in polypropylene.

The combination of FTIR and XRD made it possible to develop innovative methods for the fast and non-destructive determination of the additive concentration and the degree of crystallinity at the surface and in the volume of polypropylene. This allowed to generate novel model assumptions for the development of morphology in important industrial processes with regard to the most relevant process parameters. Furthermore, the migration and hydrophilization behavior of low molar mass surfactants is described as a function of morphology, process parameters and the molecular architecture of the additive.

The present study allows processes to be designed more efficiently and thus more economically. The specific control of process steps may allow the use of melt additives that have not been applicable before, not only in the context of hydrophilization of polypropylene surfaces.

8 Zusammenfassung und Ausblick

Ziel dieser Arbeit war es, Schmelzadditive für die Hydrophilierung der Oberfläche von Polypropylen zu finden, um somit neue Anwendungsfelder für Polypropylen zu erschließen und die Nachteile von industriell etablierten Verfahren zur Hydrophilierung zu umgehen. Dazu wurden verschiedene Tenside mit unterschiedlicher molekularer Architektur und funktionellen Gruppen hinsichtlich ihrer Verarbeitbarkeit, ihres Hydrophilierungspotentials sowie ihres Migrationsverhaltens untersucht. Der Fokus der Arbeit lag dabei auf der Korrelation der Morphologieentwicklung während des Produktionsprozesses und dem Migrationsverhalten der Additive in Abhängigkeit ihres molekularen Aufbaus.

Als potentielle Additive wurden nichtionische Tenside (ethoxylierte Alkohole, Sorbitanester und PEO-PPO-PEO-Blockcopolymere) aufgrund ihrer gegenwärtigen Anwendung im industriellen Kontext und ihrer guten Prozessierung ausgewählt. Die Tenside unterscheiden sich jeweils hinsichtlich der Länge ihres hydrophilien und hydrophoben Molekülteils.

Um eine Oberfläche mittels eines Schmelzadditivs benetzbar zu machen, müssen folgende Schritte nacheinander ablaufen:

1. Das Additiv wird mit dem Polymer in der Schmelze vermischt. Das Additiv weist eine hinreichende Kompatibilität mit dem Polymer auf und ist bei prozessrelevanten Temperaturen thermisch stabil. Andernfalls kommt es zu Instabilitäten im Herstellungsprozess oder zum degradationsbedingten Verlust des Additivs.
2. Während des Abkühlens kristallisiert die Matrix wodurch die Löslichkeitsgrenze überschritten wird und das Additiv vom Matrixpolymer separiert. Zu starke Mischbarkeit mit der Matrix verhindert die Migration an die Oberfläche.
3. Das Additiv migriert an die Oberfläche. Dieser Schritt ist stark abhängig von der im Prozess ausgebildeten Matrixmorphologie und ist eine Funktion von Lagertemperatur und -Zeit.
4. Nachdem das Additiv an die Oberfläche migriert ist, muss das Molekül die Oberfläche benetzbar machen können. Diese Fähigkeit ist stark mit dem Adsorptionsverhalten verbunden.
5. Das Additiv bleibt an der Oberfläche fixiert und ist somit permanent und haltbar.

Methodenentwicklung und Vorversuche

Durch die Nutzung von Fourier-Transform-Infrarotspektroskopie (FTIR) konnten Methoden entwickelt werden, welche den Kristallinitätsgrad von Polypropylen sowie die Additivkonzentration schnell, ortsempfindlich und zerstörungsfrei an der Probenoberfläche und im Volumen bestimmen können. Dadurch war es möglich, die Migration und die Morphologieausbildung während des Prozesses und der Lagerung zu tracken.

In Vorversuchen, wurden die Additive auf Vliesstoffe sowie auf spritzgegossene Platten aus Polypropylen mittels eines Beschichtungsverfahrens aufgetragen. Es konnte gezeigt werden, dass der Kontaktwinkel, der sich auf einer beschichteten Platte ausbildet, mit der Strike-through Zeit von beschichteten Vliesstoffen korreliert. In darauf folgenden Spinnversuchen konnte gezeigt werden, dass alle in der Arbeit verwendeten Additive spinnbar sind und über eine für den Faserspinnprozess hinreichende thermische Stabilität verfügen. Leichte Probleme mit der Spinnbarkeit traten nur bei den Sorbitanfettsäureestern auf, welche seltene Extrusionsinstablitäten zeigten.

Die Hydrophilierung der Oberfläche durch Schmelzadditive ist eine Überlagerung der Migration zur Oberfläche und der Fähigkeit des Additivs, den Wasserkontaktwinkel signifikant zu reduzieren. Die hydrophilen Eigenschaften der Additive sind stark mit deren Adsorptionsverhalten verknüpft. Es wird angenommen, dass die Additive aufgrund der hohen chemischen Ähnlichkeit zum Polypropylen flach auf dem Substrat adsorbieren. Der sich ausbildende Wasserkontaktwinkel korreliert mit der Anzahl der -OH-Gruppen pro Oberfläche.

Sowohl in den Beschichtungsversuchen als auch beim Faserspinnen zeigten ethoxylierte Alkohole mit einer geringen Molmasse, einem langen hydrophoben Anteil und einem kurzen hydrophilen Anteil (niedriger HLB-Wert) das beste Hydrophilierungsverhalten. Entgegen der Erwartungen zeigen Tenside, welche vorwiegend aus hydrophilen Molekülgruppen (hoher HLB Wert) bestanden, kein Potential zur Benetzbarmachung der Oberfläche.

Für die folgenden Versuche wurde daher die Additivauswahl auf ethoxilierte Alkohole mit der Struktur $C_{18}PEO_x$ reduziert, wobei x zwischen 2 und 20 lag und der hydrophobe Teil des Moleküls Doppelbindungen enthalten konnte.

Morphologieausbildung

Alle untersuchten Probengeometrien zeigen eine Anreicherung des Additivs hin zur Oberfläche, die mit einer Entsättigung des Matrixkerns einher

geht. Die Oberflächenkonzentration nimmt mit steigender Lagerzeit zu und erreicht nach 7 - 30 Tagen einen Plateauwert. Die zeitabhängige Oberflächenkonzentration kann durch die Gleichung:

$$c_{\text{surface}}(t) = c_0 + (c_\infty - c_0) \cdot \left(1 - e^{-\left(\frac{t}{\tau_{\text{Migration}}} \right)^{0.5}} \right) \tag{8.1}$$

beschrieben werden, wobei $\tau_{\text{Migration}}$ die charakteristische Zeit ist, nachdem etwa 63 % des Additivs an die Oberfläche migriert sind und c_0 und c_∞ die Oberflächenkonzentration sind, nachdem keine beziehungsweise unendlich lange Zeit vergangen ist.

Die Migrationsexperimente deuten darauf hin, dass das sich entwickelnde Konzentrationsprofil durch die Gleichung

$$\begin{aligned} c(x) =& c_{\text{core}} + (c_{\text{surface}} - c_{\text{core}}) \cdot e^{-\left(\frac{x}{l} \right)} \\ & \text{wobei } \int_0^\infty c(x)dx = constant \text{ für alle } t \end{aligned} \tag{8.2}$$

beschrieben wird, wobei l die Abklinglänge des Konzentrationsprofils ist und c_{core} sowie c_{surface} die Additivkonzentration im Kern der Matrix beziehungsweise an der Oberfläche ist. Die Ergebnisse dieser Arbeit und eine Bewertung der verfügbaren Literatur deuten darauf hin, dass die Abklingzeit im Bereich von 1 µm bis 5 µm liegt. Die mittels ATR-FTIR bestimmte Oberflächenkonzentration des Additivs korreliert mit dem Benetzungsverhalten von Vliesstoffen sowie dem Kontaktwinkel, der sich auf spritzgegossenen Platten bildet.

Die Menge des Additivs, welches an die Oberfläche migrieren kann, ist eine Funktion des nicht mischbaren, migrierbaren Additivvolumens, das durch Mischbarkeit oder Co-Kristallisation mit der Polymermatrix reduziert wird. Dementsprechend ist die Plateauoberflächenkonzentration c_∞, die nach ausreichend langen Lagerzeiten erreicht wird, direkt proportional zur ursprünglich zugegeben Additivkonzentration c_{initial}.

Das Migrationsverhalten der Additive ist stark von der Lagertemperatur abhängig. Hohe Lagertemperaturen führen zu einer Erhöhung des Diffusionskoeffizienten und damit zu einer schnelleren Migration. Gleichzeitig steigt

die Mischbarkeit von Additiv und Polymer, was das für die Migration verfügbare Additivvolumen reduziert. Dementsprechend besteht ein gegenläufige Abhängigkeit zwischen der zunehmenden Mischbarkeit des Additivs mit dem Polymer und der Erhöhung des Diffusionskoeffizienten. Die Überlagerung beider Effekte führt zu einer optimalen Lagertemperatur, die von der Molekularstruktur des Additivs abhängt. Die Erhöhung der Molekülgröße oder Doppelbindungen im Additiv bewirken im Vergleich mit sonst identischen Molekülen eine Verschlechterung des Migrationsverhalten, da die Diffusion des Additivs sterisch gehindert wird.

Ein direkter Einfluss der Polymermolmasse auf das Migrationsverhalten konnte nicht nachgewiesen werden. Die Erhöhung der Molmasse oder die Zugabe von Langkettenverzweigungen führt jedoch zu einer Veränderung des Kristallisationsverhaltens, welches wiederum Migration beeinflusst. In der Regel führt daher ein Anstieg der Matrixmolmasse indirekt zu einer Verschlechterung des Migrationsverhaltens.

Um Polymermorphologie und Migration zu korrelieren, wurde die Kristallinität von spritzgegossenen Platten, Castfolien sowie Fasern und Nonwovens in Abhängigkeit der wichtigsten Prozessparameter bestimmt. Die Kombination von Röntgenbeugung (XRD), (ATR-) FTIR und Lichtmikroskopie ermöglichte die Entwicklung neuer Modellvorstellungen für die Morphologieausbildung während des Prozesses. Das Migrationsverhalten ist von der Packungsdichte der Polymerketten abhängig, da stark orientierte amorphe Bereiche oder Kristallite für die Additivmoleküle nicht durchdringbar sind. Je dichter die Oberfläche gepackt ist, desto weniger Moleküle können an die Oberfläche migrieren.

Spritzgegossene Platten

Spritzgegossene Platten bilden bei einer Werkzeugtemperatur unter 60 °C eine mesomorphe Randschicht aus, die mit steigender Werkzeugtemperatur kristalliner wird und größere Kristallite in oberflächennahen Bereichen zeigt. Die Migration von Additiven ist in stark abgekühlten Platten aufgrund der sich bildenden niedrigkristallinen, mesormophen Randschicht sehr gut. Ab einer Werkzeugtemperatur von 60 °C führt die stärke Kristallisation der Probenoberfläche zu einer fast vollständigen Hinderung der Migration.

Castfolien

Castfolien zeigen nach dem Abkühlen auf einer 20 °C kalten Kühlwalze eine mesomorphe Struktur. Werden die Folien anschließend bei Raumtemperatur verstreckt bildet sich eine hochorientierte Mesophase aus. Werden die Folien,

wie im industriellen Prozess üblich, vor dem Verstreckvorgang auf über 140 °C aufgeheizt, findet eine Rekristallisation der Oberfläche statt. In der Folge weisen die getemperten Folien eine α-kristalline Struktur auf, welche wie die mesomorphe Struktur verstreckt und orientiert werden kann.

Aufgrund der niedrigen Kristallinität und der mesomorphen Struktur wurde bei unverstreckten Castfolien eine gute Migration, vergleichbar mit der von spritzgegossenen Platten, beobachtet. Auch hier ist das gute Migrationsverhalten auf die leichte Durchdringbarkeit der wenig orientierten mesomorphen Phase zurückzuführen. Der Wärmeeintrag während des Heißverstreckens unterdrückt die Migration aufgrund der Nachkristallisation der Oberfläche oder der Co-Kristallisation von Additivmolekülen mit dem Polymer. Das Verstrecken bei Raumtemperatur unterdrückt die Migration ebenfalls vollständig. Durch die Orientierung der mesomorphen Kristallphase und der amorphen Bereiche werden die Polymerketten hochdicht gepackt und es entsteht eine Diffusionsbarriere, die von Additivmolekülen nicht durchdrungen werden kann.

Fasern und Vliesstoffe

Unverstreckte Fasern zeigen ebenfalls eine mesomorphe Struktur, welche mit der von unverstreckten Castfolien vergleichbar ist. Im Gegensatz zu Folien werden Fasern jedoch während des Erstarrens verstreckt. Dadurch wird im noch heißen Faserkern eine dehninduzierte Kristallisation hervorgerufen, während das Abschrecken und Erstarren der Oberfläche zu einer hochorientierten amorphen Randschicht führt. Die Oberfläche wird während des Verstreckprozesses weiter orientiert, was zu einer mechanisch induzierten Nachkristallisation führt. Entsprechend bildet sich ein Maximum des Kristallinitätsgrades im Kern (dehninduzierte Kristallisation) und an der Oberfläche (orientierungsinduzierte Kristallisation) der Faser. Der anschließende thermische Verfestigungsschritt zur Herstellung von Vliesstoffen aus Einzelfasern (Kalandrieren) führt zu einer Nachkristallisation der Faseroberfläche. Es entsteht eine kristalline, stark orientierte Randschicht in den Vliesstoffen.

Die Rekristallisation der Faseroberfläche infolge des Kalandrierens verhindert die Migration von niedrigmolekularen Additiven in Nonwovens fast vollständig. Im Falle von großen Molekülen ($C_{18}PEO_{10}$) führt jedoch der Wärmeeintrag zur Erhöhung des Diffusionskoeffizienten und damit zur Anreicherung des Additivs sowie der direkten Hydrophilierung der Oberfläche.

Praktische Anwendung und Empfehlungen

Basierend auf den durchgeführten Experimenten ist es möglich, Anforderungen für Moleküle zu definieren, um diese als hydrophile Schmelzadditive nutzen zu können:

- **Nichtionische Tenside mit möglichst langem hydrophoben und recht kurzem hydrophilen Molekülteil (niedriger HLB-Wert)**
  für gute Prozessierbarkeit und hohes Hydrophilierungspotential
- **Fester Aggregatzustand bei Raumtemperatur (T_m > 40 °C)**
  um das Additiv nach der Migration an der Oberfläche zu immobilisieren
- **Funktionelle Gruppen mit hoher Polarität**
  Für ein hohes Hydrophilierungspotential, da Benetzbarkeit der Oberfläche mit den -OH-Gruppen / Fläche korreliert
- **Niedrige Molekulargewichte im Bereich von 300 g mol^{-1} bis maximal 1000 g mol^{-1}**
  da größere Moleküle weniger mobil sind und schlechter zur Oberfläche migrieren
- **Niedrige Mischbarkeit mit dem Matrixpolymer**
  da Mischbarkeit mit dem Polymer das für die Migration zur Verfügung stehende Volumen reduziert
- **Hohe thermische Stabilität bis etwa 300 °C**
  Um die Degradation im Prozess zu verhindern

Für die praktische Anwendung empfiehlt sich das Additiv $C_{18}PEO_2$ für die Hydrophilierung von Fasern, Castfolien und Spritzgussbauteilen und das Additiv $C_{18}PEO_{10}$ für die Hydrophilierung von Vliesstoffen. Für die reproduzierbare und gleichmäßige Hydrophilierung ist eine Additivkonzentration von mindestens 2 wt% notwendig. Beide Additive können zudem als Beschichtung verwendet werden und führen dabei zu vergleichbar guten Benetzungseigenschaften.

Im Vergleich zur Verwendung der Additive als Beschichtung konnte kein signifikanter Unterschied der Permanenz und Haltbarkeit durch die alleinige Verwendung als Schmelzadditiv gezeigt werden. Von einer Verankerung des Additiv während des Migrationsvorganges ist daher nicht zwangsläufig auszugehen. Die Fixierung an der Oberfläche scheint vielmehr durch Adhesion bedingt. Dies betrifft sowohl die Verwendung als Beschichtung als auch die Nutzung als Schmelzadditiv. Dennoch ist es gelungen, permanente und haltbare Schmelzadditive zur Hydrophilierung von Polypropylen

zu entwickeln. Durch die Steuerung des Migrationsverhaltens ist es durch die anschließende Behandlung mittels Heißluft oder Wassderdampf möglich, definierte Bereiche des Nonwovens nachträglich zu hydrophilieren oder zu hydrophobisieren, sodass nur bestimmte Bereiche des Vliesstoffes benetzbar werden.

Ausblick

Siloxan-basierte Tenside (beispielsweise vertrieben unter dem Handelsnamen SILWET von Momentive) oder Zuckertenside (wie Glucamide, Glucoside oder Sucrose ester) könnten potentielle Substanzen für noch effektivere Schmelzadditive darstellen, da sie alle oben definierten Anforderungen für den Einsatz als hydrophile Schmelzadditive erfüllen. Darüber hinaus könnten Mischungen aus Tensiden mit verschiedenen kurz- und mittellangen hydrophilen Kettenteilen wie $C_{18}PEO_2$ und $C_{18}PEO_{10}$ die Vorteile von verschiedenen Additiven vereinen. Die Zugabe von $C_{18}PEO_2$ bewirkt eine signifikante Steigerung der Weichheit von Einzelfasern. Es kann daher zur Erzeugung von weichen und gleichzeitig hydrophilen Polypropylenfasern verwendet werden. Dieser gezielte Steigerung der Weichheit der Fasern könnte Gegenstand weiterer Studien sein.

Die gefundenen Korrelationen von Additivmigration und Morphologieentwicklung könnten auf andere Additivklassen und Anwendungsbereiche von Schmelzadditiven übertragen werden. Beispielsweise ist bei der Reduktion des Reibkoeffizienten durch den Einsatz von Erucamid als Schmelzadditiv ebenfalls eine starke Migration an die Oberfläche erwünscht, während die Migration bei Stabilisatoren möglichst vollständig unterdrückt werden soll. Die in dieser Arbeit gezeigten Ergebnisse könnten den Einsatz von Schmelzadditiven optimieren oder sogar die Nutzung von neuartigen Additivtypen zur Änderung der Oberflächeneigenschaften ermöglichen.

Die meisten der offenen Fragen in dieser Arbeit beziehen sich auf die molekulare Anordnung der Additivmoleküle im Polymer und an der Polymeroberfläche. Die Untersuchung der Anordnung der Additivmoleküle auf der Oberfläche könnte erklären, wie die Additivmoleküle an der Oberfläche adsorbieren, wie die Immobilisierung der Additive auf der Oberfläche funktioniert und wie sich die Additive nach einem Wärmeeintrag neu anordnen. Darüber hinaus ist nicht vollständig geklärt, ob die Mischbarkeit oder Co-Kristallisation mit dem Polymer zu der stark verschlechterten Migration bei erhöhten Lagertemperaturen führt oder ob andere Mechanismen, wie die Mizellenbildung von Tensiden, eine Rolle spielen.

In dieser Arbeit wurden verschiedene Profile für die Morphologieausbildung sowie der Additivverteilung in verschiedenen Probengeometrien vorgeschlagen. Diese könnten durch Ramanmikroskopie oder FTIR Spektroskopie mit variabler Eindringtiefe bestätigt oder widerlegt werden.

Zusammenfassung

Es konnten permanente und haltbare Schmelzadditive für die Hydrophilierung von Polypropylenoberflächen gefunden werden, welche für die Herstellung von Spritzgussteilen, Folien sowie Einzelfasern und Vliesstoffen eingesetzt werden können. Die Verwendung von Schmelzadditiven stellt somit ein einfach zu implementierendes und kostengünstiges Verfahren zur Änderung der Oberflächeneigenschaften dar. Darüber hinaus wurden Methoden gefunden, die eine lokale Hydrophilierung und Hydrophobisierung definierter Bereiche von Vliesstoffen ermöglichen.

Während sich vorangegangene Studien [13, 14, 16, 95] in erster Linie mit der Auswahl und Wirkung von verschiedenen Additiven beschäftigen oder nur Teilaspekte des Migrationsverhaltens von Additiven untersuchen [71, 85, 120, 195], bietet die vorliegende Studie ein umfassendes Verständnis des Migrationsverhaltens von Additiven und der prozessbedingten Morphologieentwicklung in Polypropylen. Die Kombination von FTIR und XRD ermöglichte die Entwicklung innovativer Verfahren zur schnellen und zerstörungsfreien Bestimmung der Additivkonzentration und des Kristallinitätsgrades an der Oberfläche und im Volumen von Polypropylen. Dadurch konnten neue Modellannahmen für die Morphologieausbildung in relevanten industriellen Prozessen in Hinblick auf die wichtigsten Prozessparameter entwickelt werden. Darüber hinaus wird das Migrations- und Hydrophilierungsverhalten von Tensiden mit niedriger Molmasse als Funktion der Morphologie, der Prozessparameter und der molekularen Architektur des Additivs beschrieben.

Die vorliegende Studie ermöglicht es daher, Prozesse effizienter und somit wirtschaftlicher zu gestalten. Die gezielte Steuerung von Prozessschritten kann den Einsatz von bisher nicht verwendbaren Schmelzadditiven, nicht nur im Rahmen der Hydrophilierung von Polypropylenoberflächen, ermöglichen.

A Supplementary information and graphics

A.1 Fundamentals

A.1.1 Diffusion

By substituting the solution of the Fickian concentration profile of a film in a sorption experiment [196] at any time t into the decay profile of an evanescent wave in the ATR-FTIR experiment, Fieldson et al. [108] obtain the equation:

$$\frac{A_t}{A_\infty} = 1 - \frac{8\frac{1}{d_p}}{\pi\left[1-\exp\left(-2\frac{L}{d_p}\right)\right]} \cdot \sum_{n=0}^{\infty}\left[\frac{\exp(g)\left(f\exp\left(-2\frac{L}{d_p}\right)+(-1)^n\left(2\frac{1}{d_p}\right)\right)}{(2n+1)\left(4\frac{1}{d_p}+f^2\right)}\right] \quad \text{(A.1)}$$

where

$$g = \frac{-D\pi^2 t}{4L^2} \quad \text{(A.2)}$$

and

$$f = \frac{(2n+1)\pi}{2L} \quad \text{(A.3)}$$

This equation can be simplified by eliminating all terms in the series after the first term as it yields highly comparable results for long storage times and if there is only limited data available for short storage times:

$$\frac{A_t}{A_\infty} = 1 - \frac{8\frac{1}{d_p}}{\pi\left[1 - \exp\left(-2\frac{L}{d_p}\right)\right]} \cdot \left[\frac{\exp\left(\frac{-D\pi^2 t}{4L^2}\right)\left(\frac{\pi}{2L}\exp\left(-2\frac{L}{d_p}\right) + \left(2\frac{1}{d_p}\right)\right)}{2\frac{1}{d_p}^2 + \frac{\pi^2}{4L^2}}\right] \quad \text{(A.4)}$$

This equation provides comparable results to equation A.1 and can be used when limited data are available for short storage periods.

If

$$4\left(\frac{1}{d_p}\right)^2 \gg \frac{\pi^2}{4L^2} \quad \text{(A.5)}$$

and

$$1 \gg e^{-2\frac{L}{d_p}} \quad \text{(A.6)}$$

equation A.4 can be further simplified to equation A.7. The requirements A.5 and A.6 are met for all sample geometries investigated in this thesis.

$$\frac{A_t}{A_\infty} = 1 - \frac{4}{\pi}\exp\left(\frac{-D\pi^2 t}{4L^2}\right) \quad \text{(A.7)}$$

Further considerations on migration kinetics

Figure A.1 shows the initial and final state of a typical concentration profile described by the equation (see also chapter 6.12):

$$c(x) = c_0 + (c_{\text{surface}} - c_0) \cdot e^{-\left(\frac{x}{l}\right)}$$

$$\text{where } \int_0^\infty c(x)dx = constant \text{ for all } t \quad \text{(A.8)}$$

where l is the decay length of the concentration profile, c_0 is the concentration in the core of the matrix and c_{surface} is the enrichment of additive on the surface. The distance $\sqrt{\langle \overrightarrow{L^2} \rangle}$ (root of the mean squared distance), a molecule migrates during a random walk with N steps, is within the decay length and can be approximated by:

$$l \approx \sqrt{\langle \overrightarrow{L^2} \rangle} \sim (D \cdot t)^{0.5} \quad \text{(A.9)}$$

where D is the diffusion constant and t is the time needed for diffusion. This relationship allows the transformation of a length unit to a time unit:

$$\sqrt{\langle \overrightarrow{L^2} \rangle} \sim \sqrt{t} \quad \text{(A.10)}$$

This results in an exponent of 0.5 in the migration equation:

$$c_{\text{surface}}(t) = c_0 + (c_\infty - c_0) \cdot \left(1 - e^{-\left(\frac{t}{\tau_{\text{Migration}}} \right)^{0.5}} \right) \quad \text{(A.11)}$$

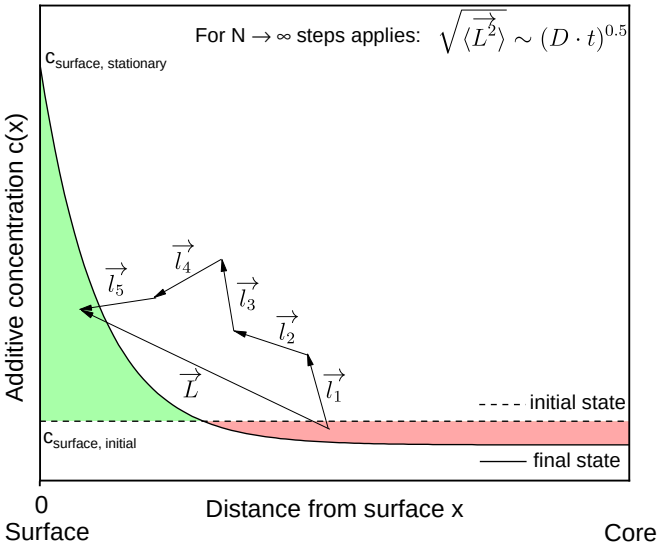

Figure A.1: Sketch of the initial and final state of a typical concentration profile occurring for migration. $\sqrt{\langle \vec{L^2} \rangle}$ describes the average distance of a molecule migrates during a random walk with N → ∞ steps.

A.2 Experimental

A.2.1 Fiber spinning

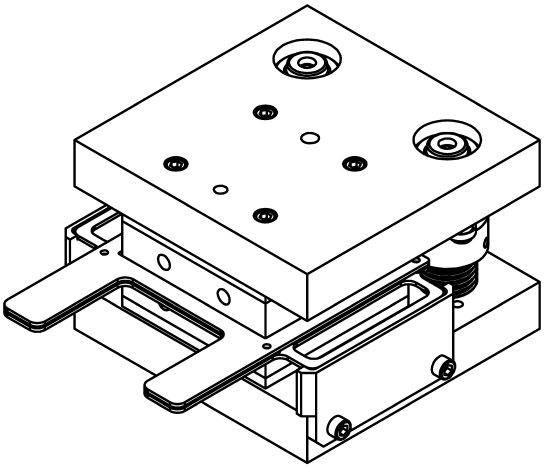

Figure A.2: Illustration of the laboratory calender press used in this work for the calendering of fibers.

The corresponding line pressure p_{line} of the laboratory calender press (figure A.2) which applies a pressure of p_{press} can be determined via an estimation of the Hertzian stress:

$$p_{line} = \frac{(p_{\text{press}})^2 \cdot \pi \cdot r \cdot (1 - \upsilon^2)}{E_{\text{steel}}} \tag{A.12}$$

using r = 300 mm as the radius of the corresponding calender rolls, E_{steel} = 210000 MPa as the Young's modulus of steel and υ = 0.3 as the Poisson number of steel. The applied pressure of the laboratory calender in the utilized hot press can be estimated using the following equation:

$$p_{press} = 5.02 \frac{N}{bar} \cdot \frac{p_{\text{hydraulic}}}{A} \tag{A.13}$$

For most of the experiments using the laboratory calender, calendering plates with an area A of 81 mm² were used at a hydraulic pressure $p_{hydraulic}$ of 400 bar.

A.2.2 Calibration procedure for the determination of the degree of crystallinity

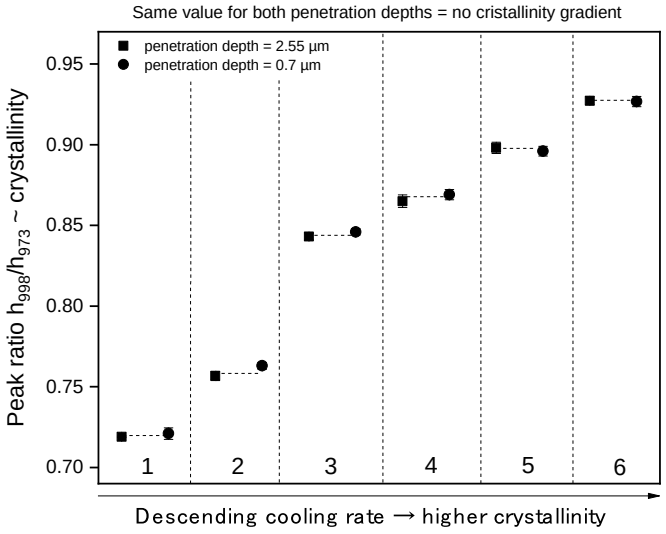

Figure A.3: Peak ratio determined for two different penetration depths of all samples used in the calibration set. Sample IDs according to table 4.3.

A.3 Raw material characterization

A.3.1 Polypropylene

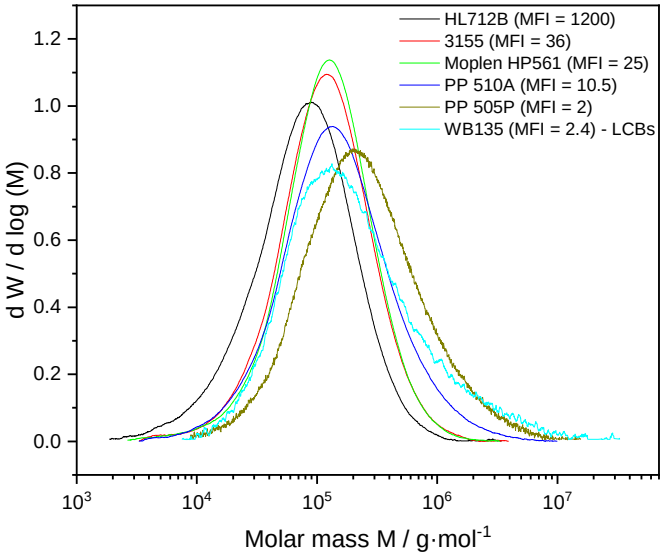

Figure A.4: Molecular weight distributions of all polypropylenes used in this thesis.

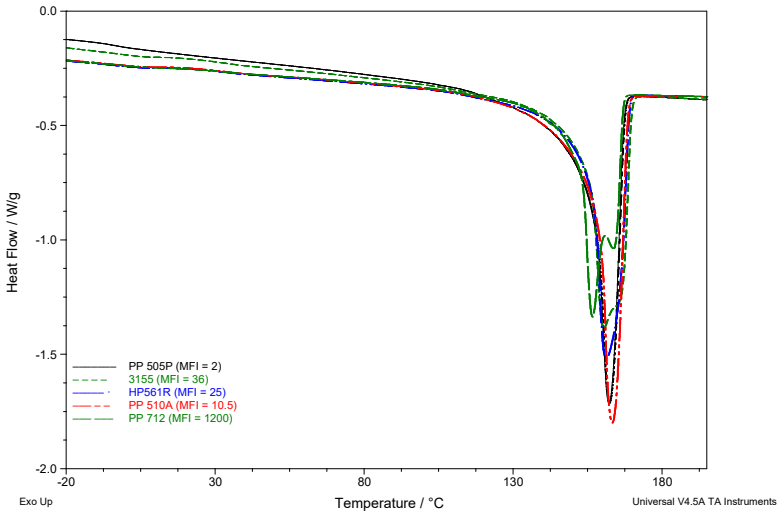

Figure A.5: DSC curves of the polypropylenes used in this thesis.

A.3.2 Additives

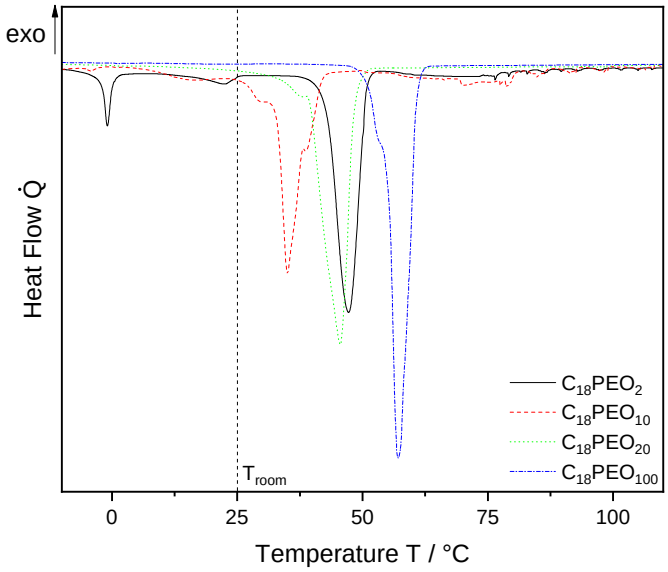

Figure A.6: DSC curves to illustrate the melting behavior of the additives most frequently used in this thesis.

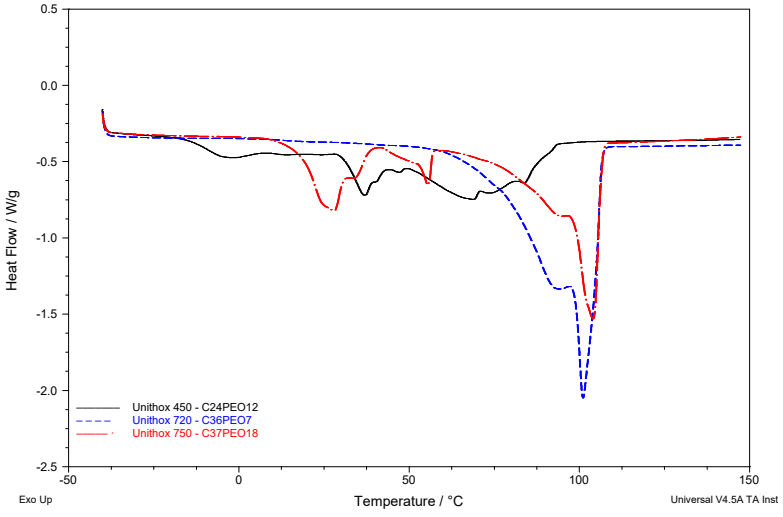

Figure A.7: DSC curves to illustrate the melting behavior of additives from the Unithox series.

Table A.1: Thermal properties of all ethoxylated alcohols used in this thesis. The peak width is defined as the maximum width of the melt peak. If several melting point maxima were detectable in the peak, they were listed as $T_{m,1}$ to $T_{m,4}$. The main melting peak is defined as the most pronounced melting peak.

Material	Molar mass	Main melting peak T_m	Main melting peak onset $T_{m,onset}$	Melting Peak width	$T_{m,1}$	$T_{m,2}$	$T_{m,3}$	$T_{m,4}$	Δ H
	g mol^{-1}	°C	°C	°C	°C	°C	°C	°C	J g^{-1}
$C_{16}PEO_2$	358	32.0	27.4	40	-17.8	35.7			124
$C_{16}PEO_{20}$	1150	42.3	36.6	26	43.6				127.5
$C_{15}PEO_{17}$	1032	34.5	39.6	30	37.5	41.8			122.6
$C_{15}PEO_{20}$	1164	43.3	38.0	20	45.5				23.78
$C_{12}PEO_4$	390	-0.3	-6.1	18	-0.3				40.15
$C_{12}PEO_{23}$	1226	37.8	29.5	53	33.0	42.1	48.2		122.6
$C_{18,double}PEO_{10}$	738	18.7	-13.1	70	-21.7	-4.8	15.3		65.18
$C_{18,double}PEO_2$	386	-20.9	-33.8	87	-36.3	-28.4	-20.8	16.2	78.24
$C_{18,double}PEO_{20}$	1178	37.7	31.8	41.5	33.9	41.3			107.8
$C_{18,double}PEO_3$	430	-21.3	-28.8	82	-31.7	-21.5	1.0		66.75
$C_{18,double}PEO_5$	518	-8.3	-35.6	66	-20.1	-5.7			66.64
$C_{18}PEO_{100}$	4698	57.1	54.9	18	57.1				170.1
$C_{18}PEO_2$	386	45.4	39.2	20	-1.8	45.1			126.2
$C_{18}PEO_{20}$	1178	43.9	38.6	31	45.5				160.3
$C_{18}PEO_{10}$	738	34.8	32.1	46	-19.4	34.7			102.7
$C_{26}PEO_{12}$	920	68.9	28.5	128	-12.1	31.8	43.4	80.2	151.9
$C_{38}PEO_7$	875	101.0	96.4	56	100.6				171.6
$C_{39}PEO_{18}$	1400	103.9	96.0	104	20.7	50.3	104.7		161.3

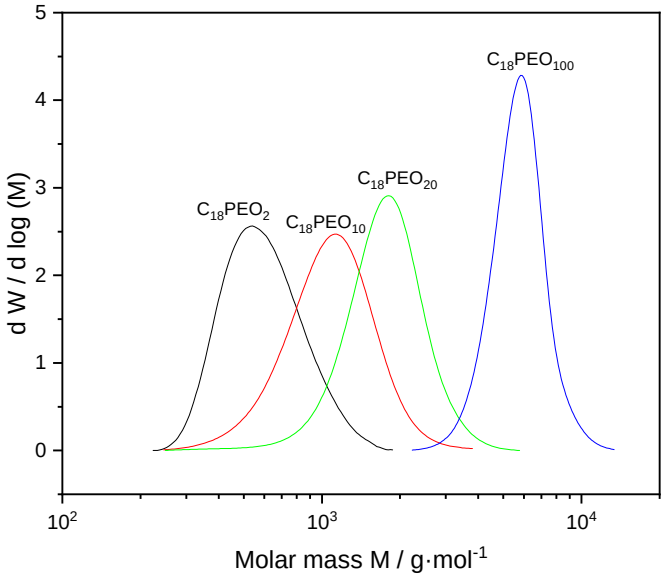

Figure A.8: Molecular weight distributions of the additives which were most frequently used in this thesis.

a)

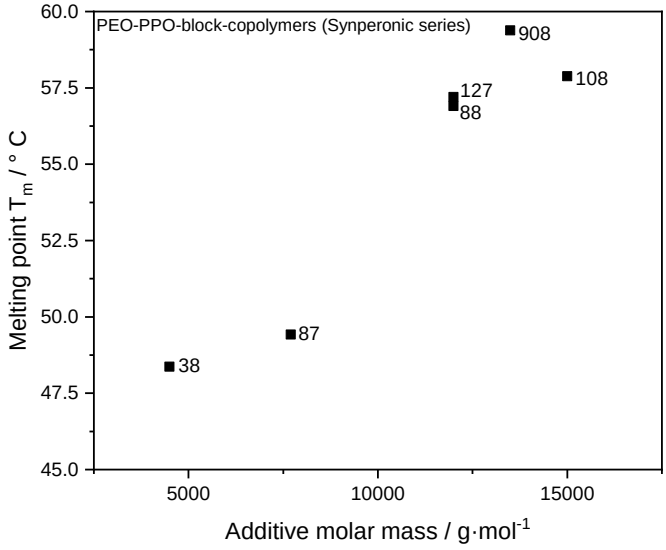

b)

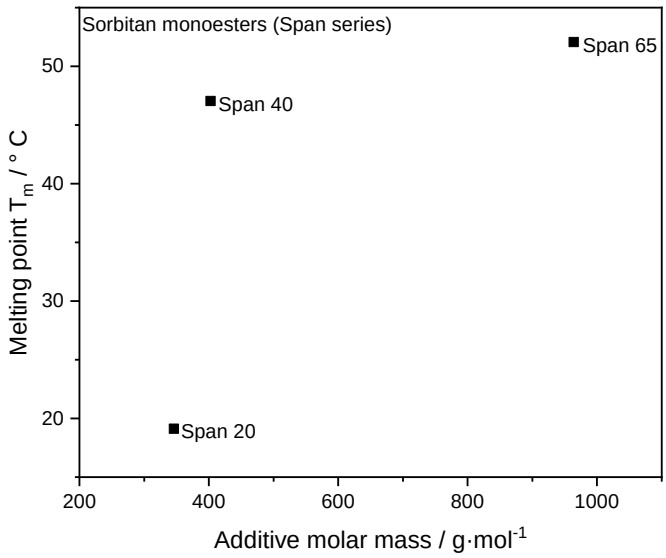

Figure A.9: Melting temperature as a function of the of molar mass the PEO-PPO-block-copolymers (Synperonic series) (a) and the sorbitan monoesters (Span series) (b).

A.4 Degradation of matrix polymer and additives

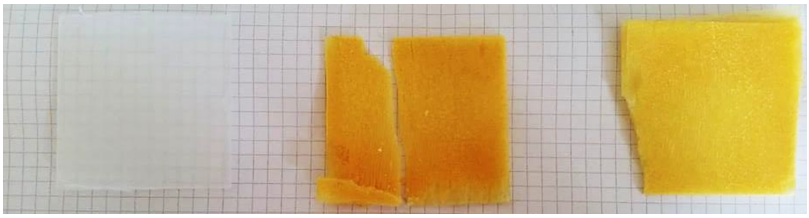

Figure A.10: Polypropylene plates without an additive (left), with 2 wt% $C_{18}PEO_{10}$ (center) and with 2 wt% $C_{18}PEO_{20}$ (right) stored for approximateley 350 hours at 80 °C. Discolorization of the samples indicates significant degradation phenomena.

Influence of process temperature

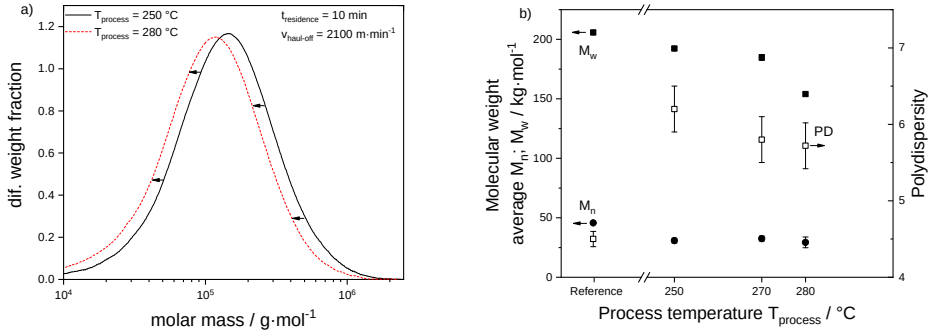

Figure A.11: Influence of the process temperature on the degradation of polypropylene fibers.

Influence of residence time

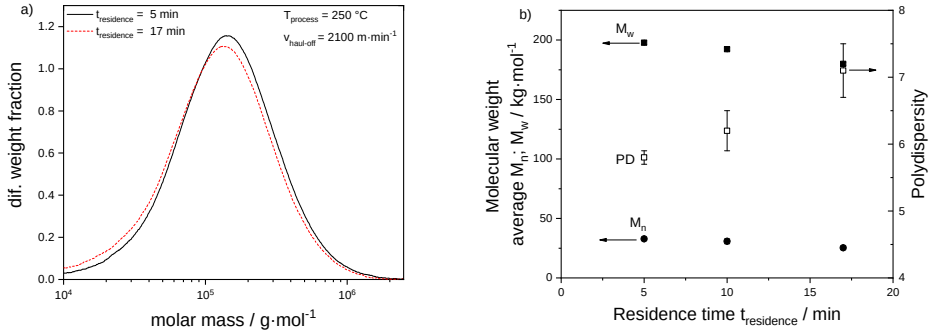

Figure A.12: Influence of the residence time in the process on the degradation of polypropylene fibers.

Influence of haul-off speed

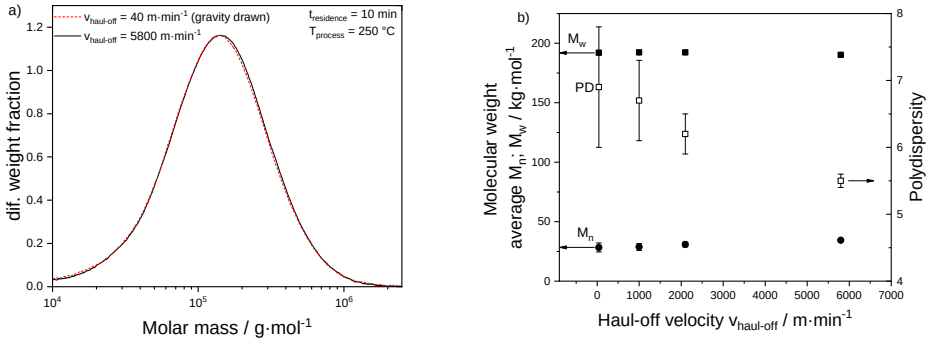

Figure A.13: Influence of the haul-off speed on the degradation of polypropylene fibers.

A.5 Miscibility of additives in the polypropylene matrix

According to Nishi et al. [148] based on an approach by Flory [197], the melting point depression ΔT of a crystalline polymer which is diluted by a polymer or additive can be described by the following equation:

$$\Delta T = \frac{1}{T_m} - \frac{1}{T_m^0} = \frac{R}{\Delta H_{\text{polymer},u}} \frac{V_{\text{polymer},u}}{V_{\text{additive}}} \cdot \left(\frac{\ln \phi_{\text{polymer}}}{m_{\text{polymer}}} + \left(\frac{1}{m_{\text{polymer}}} - \frac{1}{m_{\text{additive}}} \right) \cdot \phi_{\text{additive}} - \chi \phi_{\text{additive}}^2 \right) \quad \text{(A.14)}$$

where T_m is the melting temperature of the polymer-dilutent mixture, T_m^0 is the melting point of the pure polymer, $\Delta H_{\text{polymer},u}$ and $V_{\text{polymer},u}$ are the heat of fusion and the molar volume per chain repeat unit, respectively, V_{additive} and ϕ_{additive} are the molar volume and the volume fraction of the additive and m_{polymer} and m_{additive} are the degrees of polymerization of the polymer and the additive, respectively. For low molar mass additives the equation is reduced to:

$$\Delta T = \frac{1}{T_m} - \frac{1}{T_m^0} = -\frac{R}{\Delta H_{\text{polymer},u}} \frac{V_{\text{polymer},u}}{V_{\text{additive}}} \left(\phi_{\text{additive}} - \chi \phi_{\text{additive}}^2 \right) \quad \text{(A.15)}$$

For a high-molecular-weight additive and a high-molecular-weight polymer, the equation is reduced even further:

$$\Delta T = \frac{1}{T_m} - \frac{1}{T_m^0} = -\frac{R}{\Delta H_{\text{polymer},u}} \frac{V_{\text{polymer},u}}{V_{\text{additive}}} \left(\chi \phi_{\text{additive}}^2\right) \tag{A.16}$$

Accordingly, a plot of $\Delta T_{\text{polymer}} / \phi_{\text{additive}}$ as a function of ϕ_{additive} should result in a straight line with a slope proportional to the χ-parameter (Figure A.14) going through the origin. According to this equation, a positive interaction parameter would lead to a melting point increase. In the real world, however, a positive interaction parameter will cause a phase separation due to the thermodynamic unfavorable state.

It can be seen that the measured data does not represent a straight line. On the one hand, this can be attributed to the methodology used to determine the melting point, which does not detect the exact equlibrium melting temperature and does not consider morphological effects and crystallite growth and perfection [147]. For the determination of the melting point the maximum of the melting peak was used. Frequently the point at which the last trackable trace of crystallinity disappears is used. This method showed comparable but less reproducible results. On the other hand, however, more complex mixing and interaction phenomena may also exist which were not considered in this study.

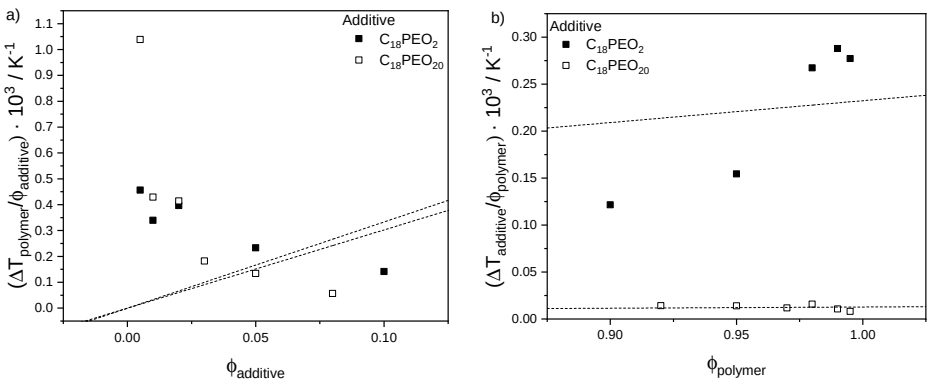

Figure A.14: Melting point depression as a function of the volume fraction of the polymer (a) and the additive (b). Fit with a straight line through the origin according to equation A.16.

A.6 Wetting behavior of additives applied as a coating

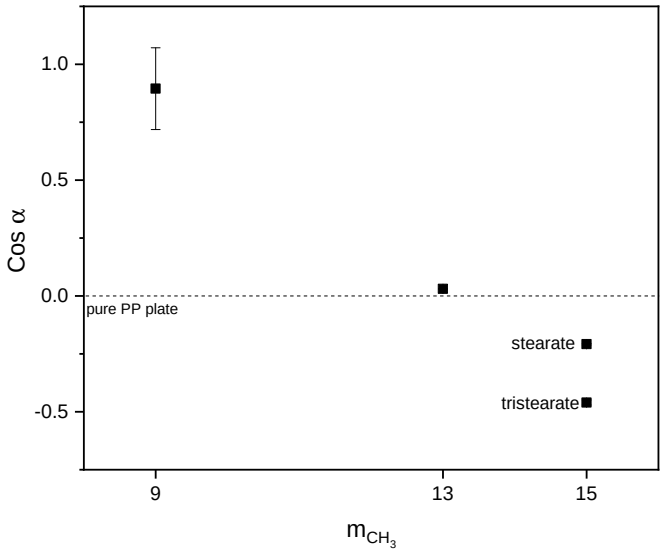

Figure A.15: Wetting behavior of sorbitan monoesters as a function of the chain length of the hydrophobic tail of the surfactant molecule.

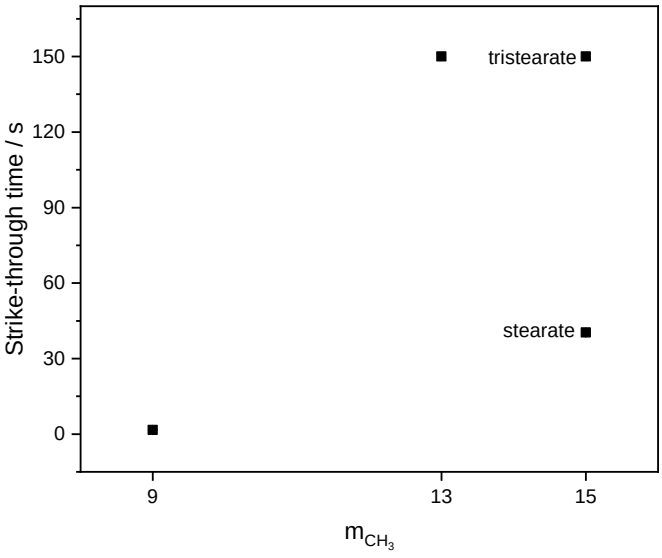

Figure A.16: Strike-through times of nonwovens coated with different Sorbitan monoesters.

A.7 Preliminary study on the wetting behavior of nonwovens

The following graphs demonstrate that the saturation towards the surface decreases significantly. To illustrate this behavior, the ratio of the surface concentration in two penetration depths is utilized. If the coefficient is less than 1, it is assumed that the surface desaturates considerably.

$$\frac{\text{Peak ratio}_{\text{penetration depth}=0.7\mu m}}{\text{Peak ratio}_{\text{penetration depth}=2.55\mu m}} \leq 1 \tag{A.17}$$

a)

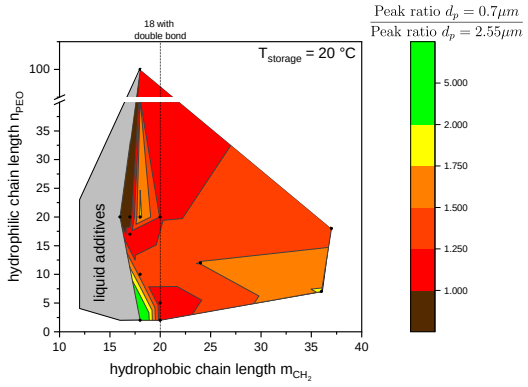

b)

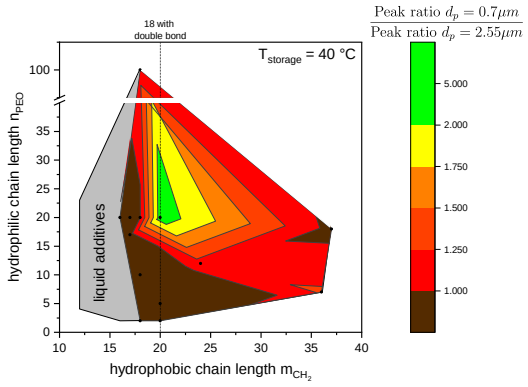

Figure A.17: Quotient of the peak ratio determined at low and high penetration depths to illustrate the extent to which the additive segregates towards the surface. High values of the quotient indicate a strong segregation behavior. The nonwovens were stored at (a) 20 °C and (b) 40 °C for 6 months.

A.8 Surface migration of additives in injection molded plates

a)

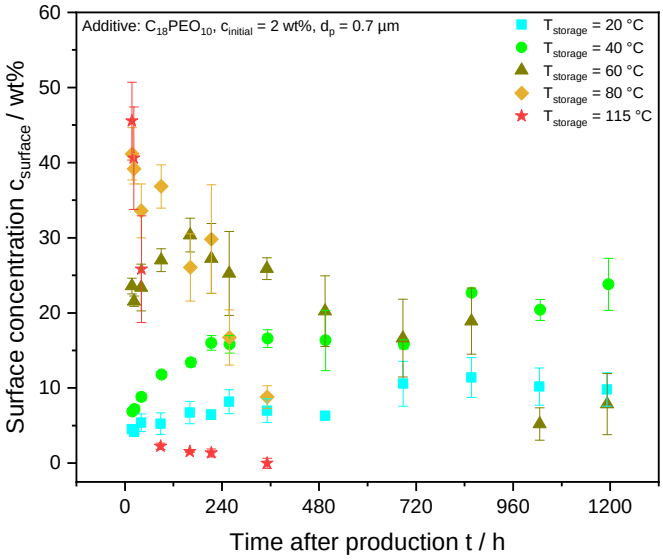

b)

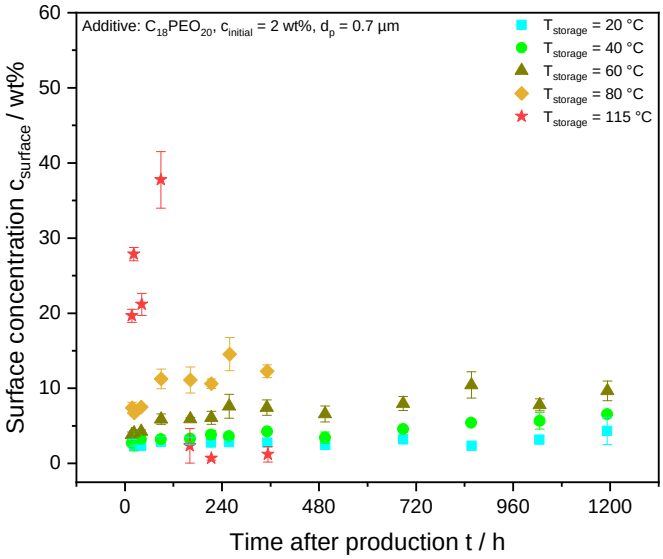

Figure A.18: Migration curves of injection molded plates with 2 wt% of $C_{18}PEO_{10}$ (a) $C_{18}PEO_{20}$ (b) stored at different temperatures. The samples were measured via ATR-FTIR at a penetration depth of 0.7 µm.

A.9 Surface migration of additives in fibers and nonwovens

A.9.1 Influence of cooling profile and temperature

Air velocity profile

The maximum possible change of the blowing air profile of the laboratory spin line is tested with respect to the resulting air velocity profile. Figure A.19 shows four different profiles which were examined in this thesis. Profiles C and D represent the extreme points of the adjustable cooling profile. The adjustment of the metal sheet which is used to vary the profile leads to irreversible deformation of the sheet or to the sheet jumping out of the holding device.

There are only slight changes in the blow-air profile with respect to the profile change. Since the adjusted profiles were very similar, the influence on the change of the air profile and thus on the morphology and migration behavior of the fibers is also very small. The influence of the profile change on the migraton behavior is shown in figure A.20, where the surface concentration of $C_{18}PEO_2$ is plotted over time for the investigated air profiles. The surface enrichment of the three samples does not differ significantly.

a)

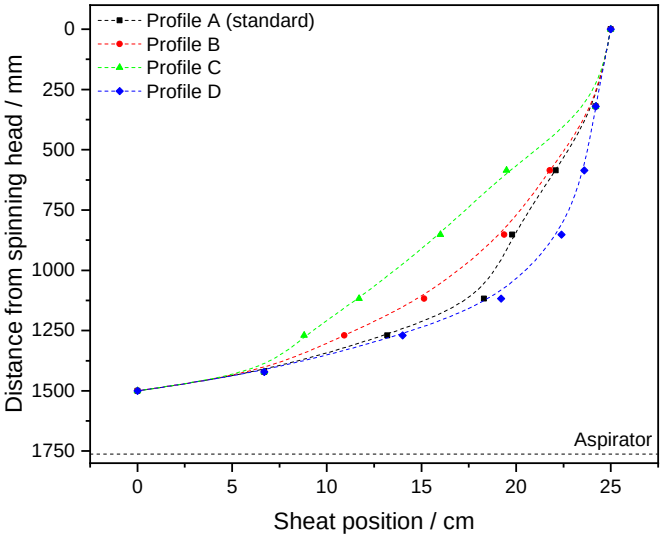

b)

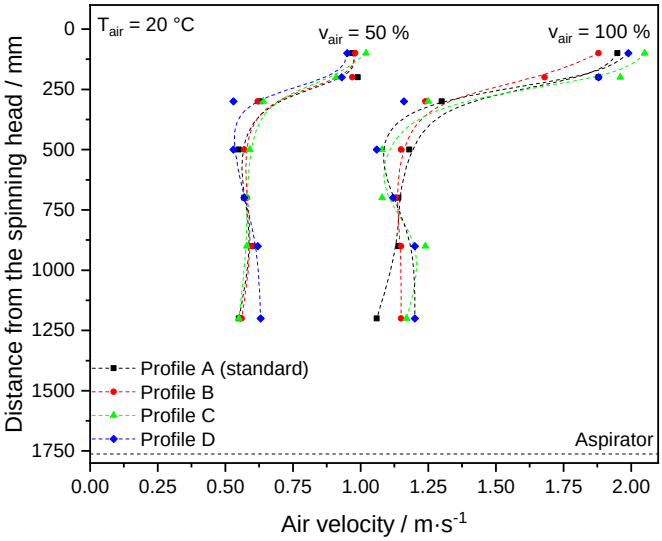

Figure A.19: Set sheet position and resulting air velocity profile in the quench chamber. The dotted line indicates the position of the aspirators in the fiber spinning line. A schematic sketch of the spinning line, which also describes the possibilities of adjusting the sheet position, can be found in chapter 4.1.2. Since the air velocity is only controlled by the speed of a mounted fan, the percentage of the maximum achievable fan speed is indicated here. The profile, which was used with the standard settings of v_{air} = 15%, could not be measured with the available measuring apparatus due to air velocities below 0.1 m min^{-1}. Points show the measured data points. The dotted lines indicate the curve shape by using a spline fit.

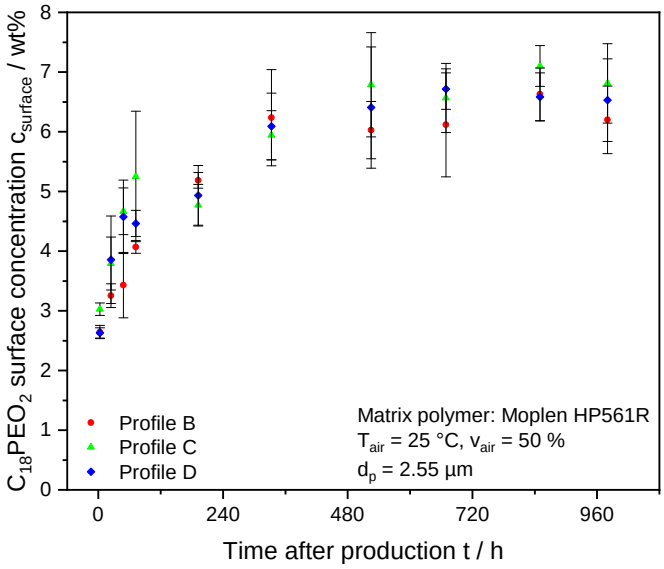

Figure A.20: Surface enrichment of $C_{18}PEO_2$ from samples produced under different cooling profiles in the quench chamber.

Cooling temperature

a)

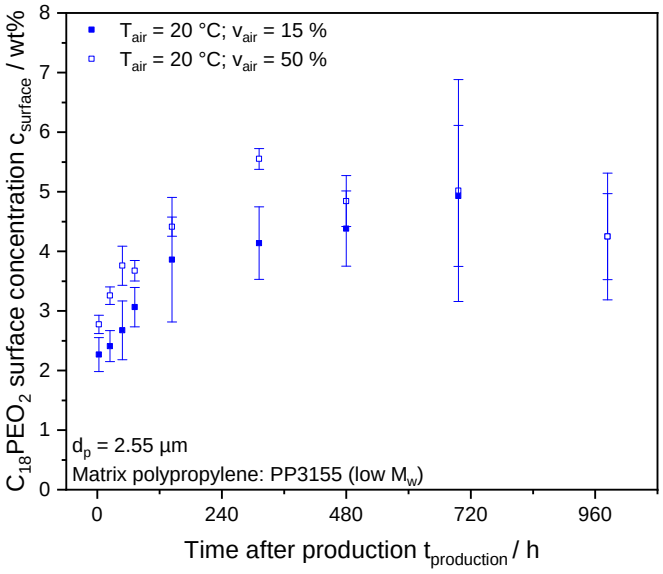

b)

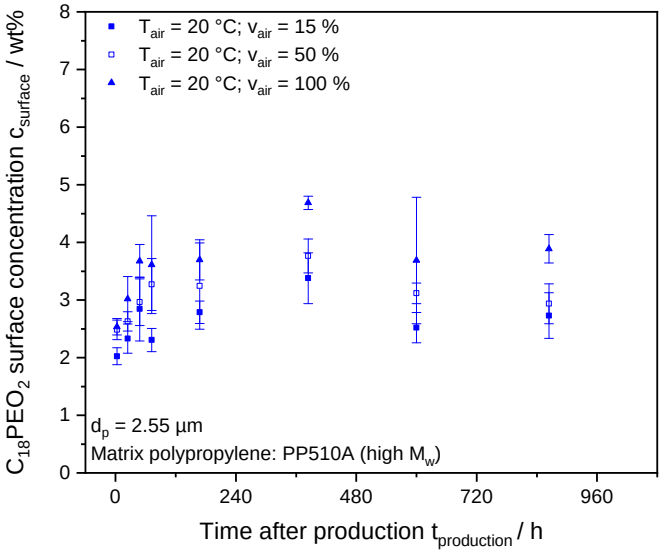

Figure A.21: Influence of the blowing air velocity on the migration behavior of $C_{18}PEO_2$ in low (a) and high molar mass (b) polypropylene matrices.

A.9.2 Influence of storage temperature

a)

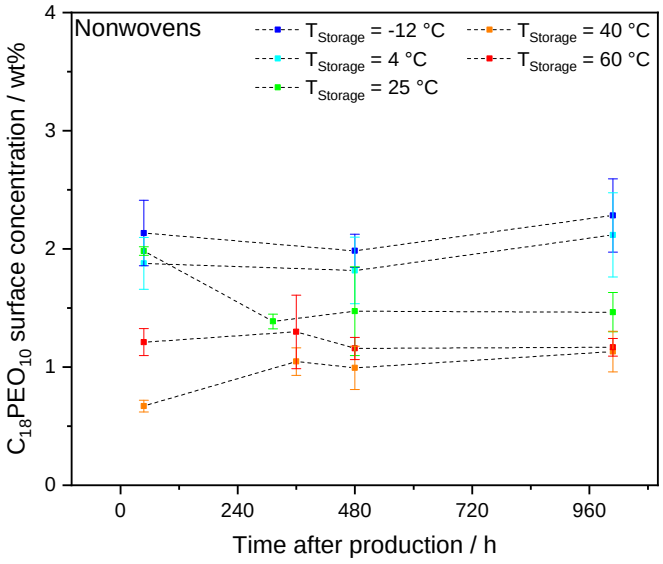

b)

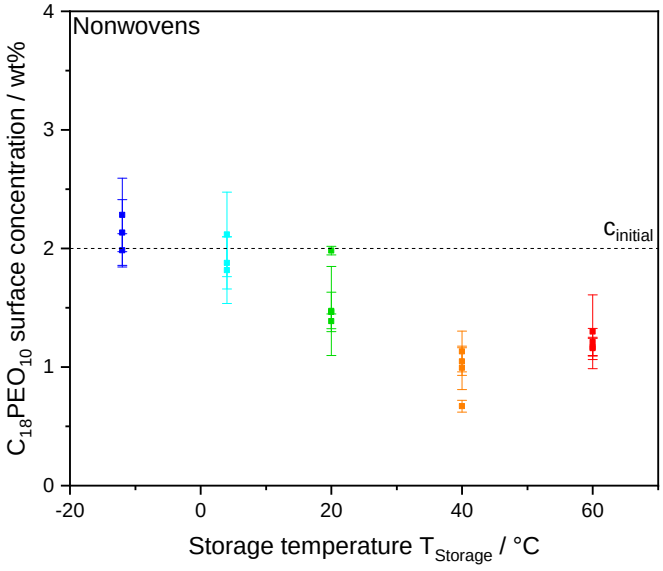

Figure A.22: Influence of storage temperature on migration behavior of nonwovens with 2 wt% $C_{18}PEO_{10}$. In order to resolve differences in migration behavior better, the individual measurements were plotted time-independently over the storage temperature in the graph (b).

a)

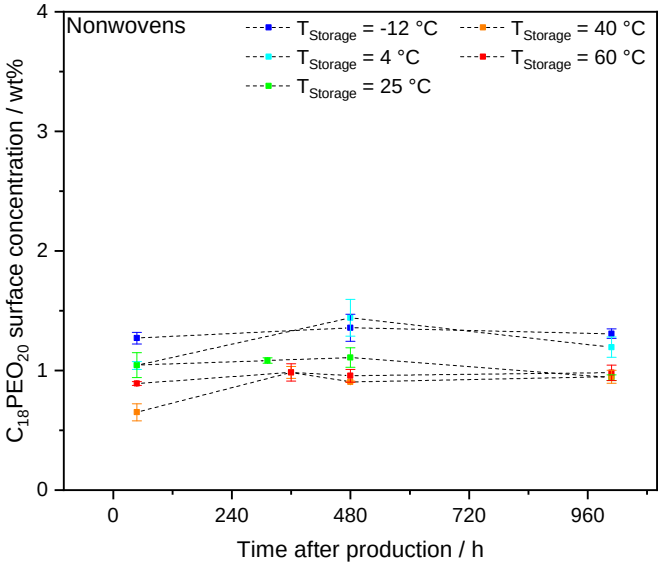

b)

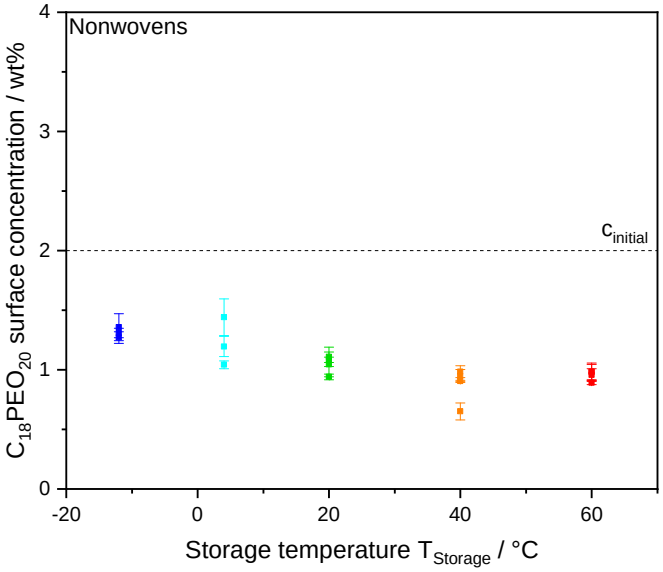

Figure A.23: Influence of storage temperature on migration behavior of nonwovens with 2 wt% $C_{18}PEO_{20}$. In order to resolve differences in migration behavior better, the individual measurements were plotted time-independently over the storage temperature in graph (b).

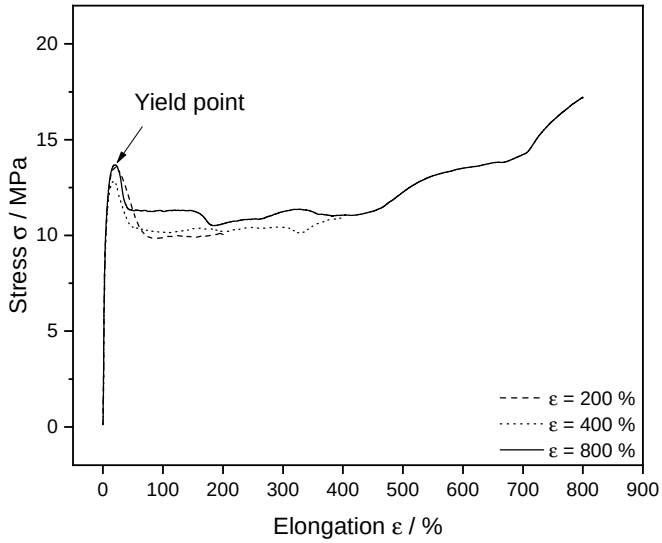

Figure A.24: Stress-strain diagram of cold-stretched films.

A.10 Additive concentration profiles and enrichment towards the surface

a)

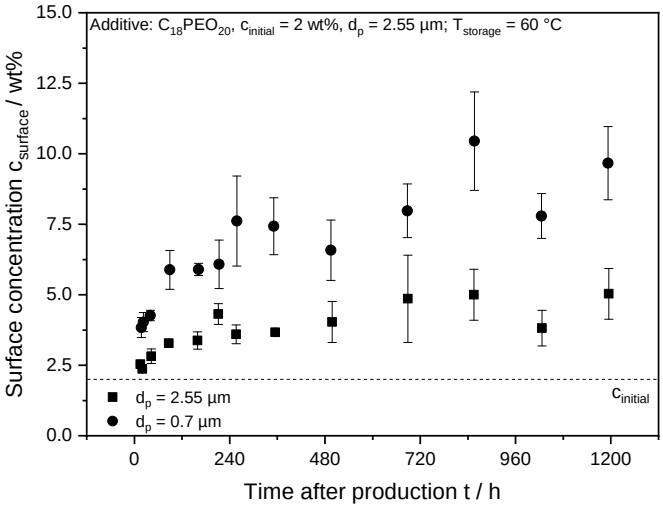

b)

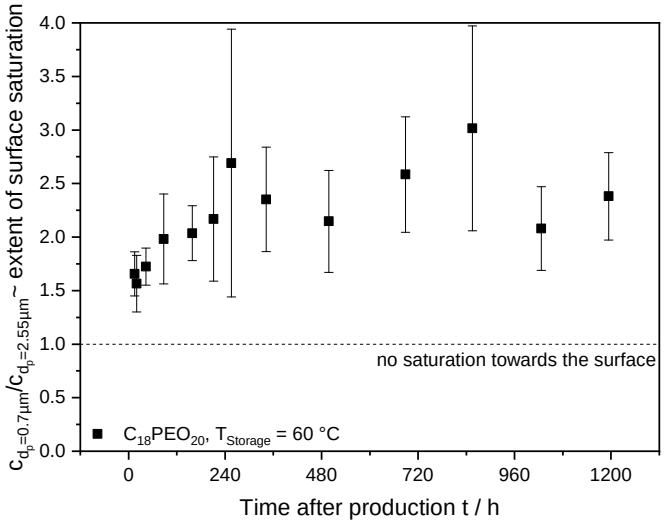

Figure A.25: Surface concentration of an injection molded plate with 2 wt% $C_{18}PEO_{20}$ as a function of storage time (a). The measurements were performed at two different penetration depths. Figure (b) shows the ratio of the two concentrations to illustrate the extent of surface segregation. High values of the quotient indicate a high surface segregation.

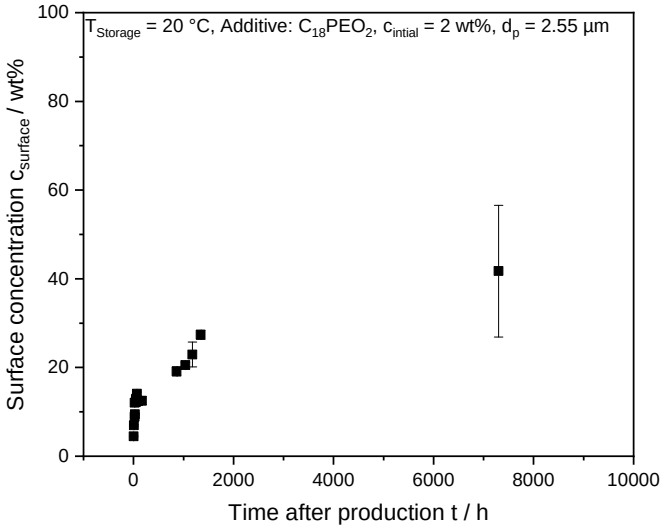

Figure A.26: Long term migration study of an injection molded plate. The graph shows that the surface concentration is not really running into a plateau, even after storage times of 10 months.

A.10.1 Model to describe surface concentration of fibers

Figure A.27 shows a simplified representation of the ATR-FTIR experiment when investigating fibers in which the entire additive migrates to the surface. Assuming that the fibers are evenly distributed over the ATR crystal and the entire additive present in the fiber migrates into the surface layer detectable by ATR-FTIR, the plateau concentration can be determined by the equation:

$$c_{\text{Plateau}} = \frac{A_{\text{total}} - A_{\text{PP}}}{A_{\text{total}}} \tag{A.18}$$

The two segments A_{total} and A_{additive} of the circle can be calculated using the equations:

$$A_{\text{total}} = r^2 \arccos\left(1 - \frac{d_p}{r}\right) - ((r - d_p) \cdot \left(\sqrt{2rd_p - d_p^2}\right) \tag{A.19}$$

and

$$A_{\text{additive}} = (r-l)^2 \arccos\left(1 - \frac{(d_p - l)}{(r-l)}\right) - (((r-l) - (d_p - l)) \cdot (\sqrt{2(r-l)(d_p - l) - (d_p - l)^2}) \quad \text{(A.20)}$$

The annulus length l can be determined using the equation:

$$l = r - \sqrt{(1 - \phi_{\text{additive}}) \cdot r^2} \quad \text{(A.21)}$$

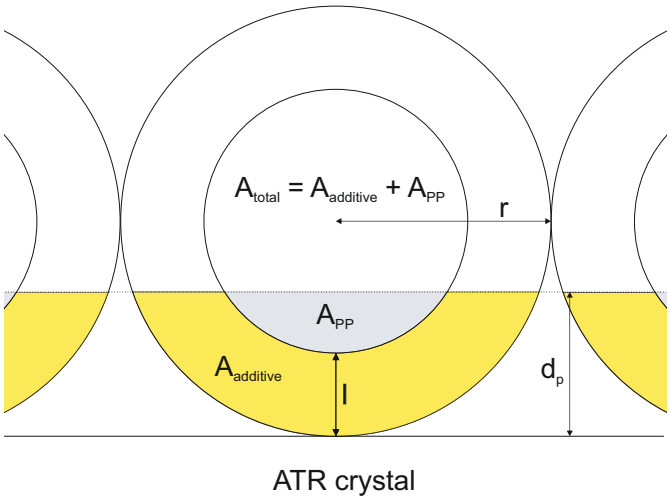

Figure A.27: Simplified representation of an ATR-FTIR experiment of single fibers in which the entire additive migrated to the surface.

Using these equations, the plateau concentration can be calculated as a function of the initial additive concentration if the fiber diameter is known. Furthermore, the plateau concentration can be calculated as a function of the fiber diameter if the initial concentration is known.

A.11 Advantages of additives applied as a melt additive

A.11.1 Additive surface distribution

a)

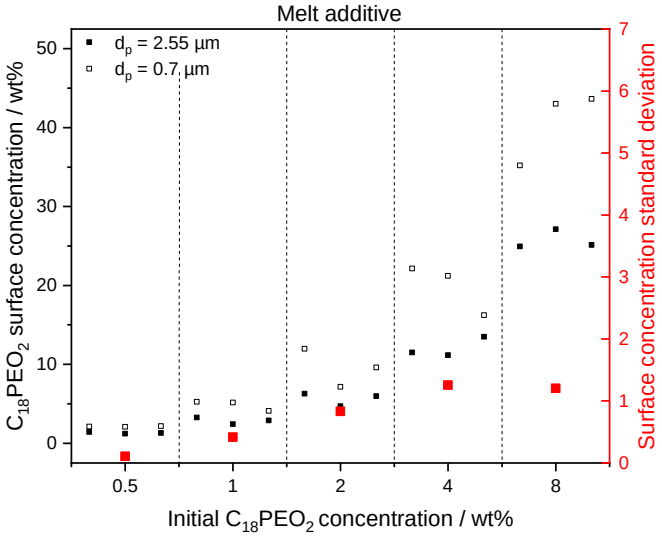

b)

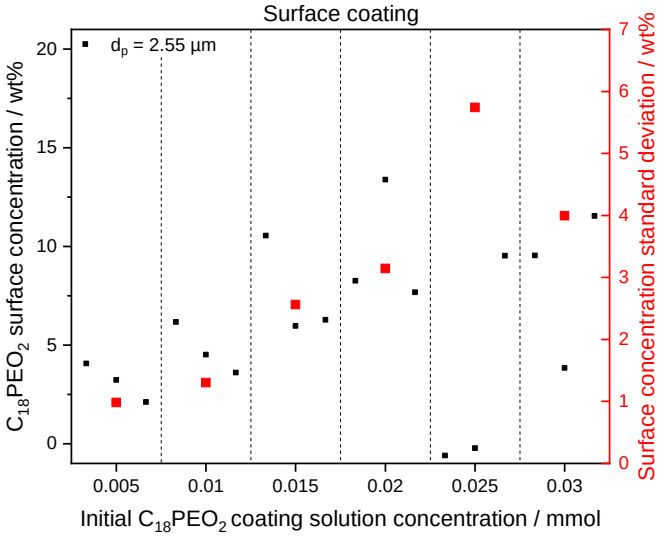

Figure A.28: Additive surface distribution of additives which migrated to the surface as melt additives (a) and were applied by coating (b) as a function of the initial concentration or the concentration of the coating solution. The graph shows the surface concentration of individual measurements determined by FTIR at 3 different spots on a sample.

A.11.2 Subsequent activation methods

a)

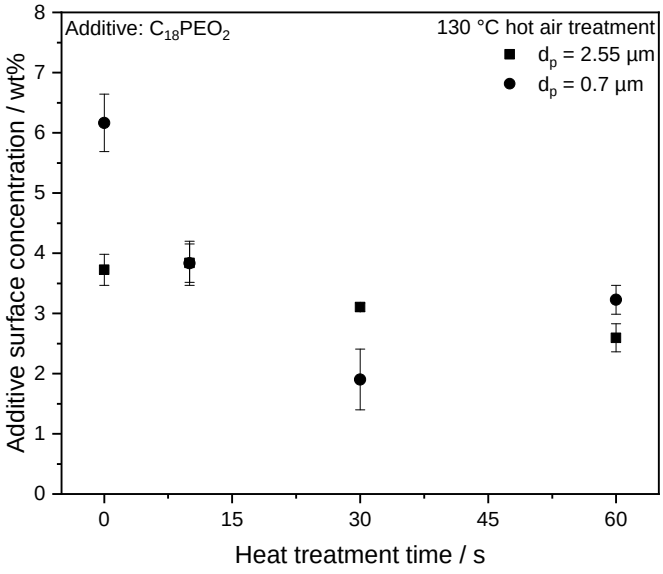

b)

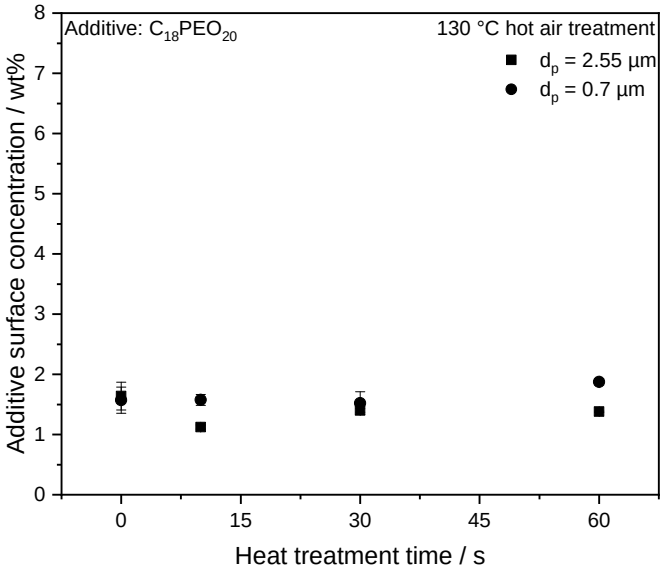

Figure A.29: Influence of heat treatment time on the migration behavior of $C_{18}PEO_2$ (a) and $C_{18}PEO_{20}$ (b) in nonwovens.

Bibliography

[1] Plastics Europe. *Plastics - the Facts 2019: An analysis of European plastics production, demand and waste data.* 2019.

[2] Reports and Data. *Polypropylene Market By Type, By Grade, By Molding Techniques, By Application, By End-Users (Automotive, Packaging, Construction, Electrical & Electronics, Consumer Goods, and Others), And Segment Forecasts, 2016-2026*. 2019.

[3] Grand View Research. *PP (Polypropylene) Nonwoven Fabric Market Analysis By Product (Spunbonded, Staples, Meltblown, Composite) And Segment Forecast To 2020*. San Francisco: Grand View Research, 2014.

[4] EDANA and INDA. *Worldwide Outlook for the Nonwovens Industry 2018 - 2023*. 2018.

[5] Sandra Husmann, Michaela Munzar, and Wolfgang Warncke. "Verwendung einer tensidzusammensetzung zur hydrophilen ausrüstung von textilfasern und daraus hergestellten textilerzeugnissen." EP3077590 (A1). 2016.

[6] Kraus Michael Dr and Wolfgang Warncke. "Zusammensetzung zur permanenten hydrophilierung von polyolefinfasern und deren verwendung." EP2917398 (A1). 2015.

[7] Christine Wild and Ulrich Issberner. "Polyolefinhaltige Wischtücher." EP1589145 (A1). 2005.

[8] Chi-Ming Chan. "Surface treatment of polypropylene by corona discharge and flame." *Polypropylene*. Ed. by J. Karger-Kocsis. Vol. 2. Polymer Science and Technology Series. Dordrecht: Springer Netherlands, 1999, pp. 800–805.

[9] Martina Lindner et al. "Surface energy of corona treated PP, PE and PET films, its alteration as function of storage time and the effect of various corona dosages on their bond strength after lamination." *Journal of Applied Polymer Science* 135.11 (2018), p. 45842.

[10] L'. Černáková et al. "Surface Modification of Polypropylene Non-Woven Fabrics by Atmospheric-Pressure Plasma Activation Followed by Acrylic Acid Grafting." *Plasma Chemistry and Plasma Processing* 25.4 (2005), pp. 427–437.

[11] Igor Novák et al. "Study of surface and adhesive properties of polypropylene grafted by maleic anhydride." *Polymer Engineering & Science* 47.8 (2007), pp. 1207–1212.

[12] Vasantha Madhuri Datla. "Surface Modification of Fibers and Nonwovens with Melt Additives" (2007).

[13] V. Datla, E. Shim, and B. Pourdeyhimi. "Surface modifications of polypropylene with nonylphenol ethoxylates melt additives." *Polymer Engineering & Science* 52.9 (2012), pp. 1920–1927.

[14] Vasantha M. Datla, Eunkyoung Shim, and Behnam Pourdeyhimi. "Polypropylene surface modification with stearyl alcohol ethoxylates to enhance wettability." *Journal of Applied Polymer Science* 121.3 (2011), pp. 1335–1347.

[15] Qiang Lu et al. "A directional entrapment modification on the polyethylene surface by the amphiphilic modifier of stearyl-alcohol poly(ethylene oxide) ether." *Applied Surface Science* 441 (2018), pp. 130–137.

[16] Siqiang Zhu and Douglas E. Hirt. "Hydrophilization of polypropylene films by using migratory additives." *Journal of Vinyl and Additive Technology* 13.2 (2007), pp. 57–64.

[17] Anunay Gupta et al. "Polyolefin film compositions with permanent antifog properties." US20042348o1 (A1). 2004.

[18] Steffen Bornemann, Volker Joerres, and Michael Voges. "Hydrophilic polyolefin materials and method for producing the same." EP1581590 (A1). 2005.

[19] Ebrahim Mor and Vasanthakumar Narayanan. "Wettable polymer fibers, compositions for preparaing same and articles made therefrom." US6146757. 2000.

[20] Tomohiro Kato, Yoshio Takasu, and Makoto Minafuji. "Fluid-permeable agent for non-woven sheets of polyolefin fibers and method of application thereof: N,N-di-hydroxyethyl amide and polyoxyalkylene-modified silicone." US4921622 (A). 1990.

[21] Prasad S. Potnis, Ashok M. Adur, and Wayne Chu. "Wettable polypropylene composition and related method of manufacture." WO0031181 (A1). 2000.

[22] Christopher A. Shuler, Amol V. Janorkar, and Douglas E. Hirt. "Fate of erucamide in polyolefin films at elevated temperature." *Polymer Engineering and Science* 44.12 (2004), pp. 2247–2253.

[23] Gaetano Lamberti and Valerio Brucato. "Real-time orientation and crystallinity measurements during the isotactic polypropylene film-casting process." *Journal of Polymer Science Part B: Polymer Physics* 41.9 (2003), pp. 998–1008.

[24] Daniela Mileva et al. "Crystal structure: A way to control properties in cast films of polypropylene." *Polymer Bulletin* B31.19 (2018), p. 501.

[25] M. R. Kantz, H. D. Newman, and F. H. Stigale. "The skin-core morphology and structure–property relationships in injection-molded polypropylene." *Journal of Applied Polymer Science* 16.5 (1972), pp. 1249–1260.

[26] Young-Ah Kang et al. "In-situ analysis of fiber structure development for isotactic polypropylene." *Polymer* 52.9 (2011), pp. 2044–2050.

[27] Huseyin Benli Ismail Karacan. "An X-ray Diffraction study for isotactic polypropylene fibers produced with take-up speeds of 2500-4250 m/min." *Tekstil ve Konfeksiyon* 3 (2011), pp. 201–209.

[28] P. Y.-F. Fung, E. Orlando, and S. H. Carr. "Development of stress-crystallized morphology during melt-spinning of polypropylene fibers." *Polymer Engineering and Science* 13.4 (1973), pp. 295–299.

[29] Gaetano Lamberti, Valerio Brucato, and Giuseppe Titomanlio. "Orientation and crystallinity in film casting of polypropylene." *Journal of Applied Polymer Science* 84.11 (2002), pp. 1981–1992.

[30] Yan Li et al. "Adsorption and association of a symmetric PEO-PPO-PEO triblock copolymer on polypropylene, polyethylene, and cellulose surfaces." *ACS applied materials & interfaces* 3.7 (2011), pp. 2349–2357.

[31] N. A. Ivanova, Zh.B. Zhantenova, and V. M. Starov. "Wetting dynamics of polyoxyethylene alkyl ethers and trisiloxanes in respect of polyoxyethylene chains and properties of substrates." *Colloids and Surfaces A: Physicochemical and Engineering Aspects* 413 (2012), pp. 307–313.

[32] Peter Kunzelmann. *Korrelation der rheologischen Eigenschaften von Mischungen aus Polypropylenen unterschiedlicher molekularer Struktur mit deren Verarbeitungsverhalten im Spinnprozess*. Werkstoffwissenschaften. München: Verlag Dr. Hut, 2017.

[33] V. B. Gupta and V. K. Kothari. *Manufactured Fibre Technology*. Dordrecht: Springer Netherlands, 2012.

[34] E. Masaeli, M. Morshed, and H. Tavanai. "Study of the wettability properties of polypropylene nonwoven mats by low-pressure oxygen plasma treatment." *Surface and Interface Analysis* 39.9 (2007), pp. 770–774.

[35] K. L. Mittal. *Polymer surface modification, vol. 3: Relevance to adhesion*. Leiden: VSP, 2004.

[36] Mark Strobel et al. "Surface modification of polypropylene with CF_4, CF_3H, CF_3Cl, and CF_3Br plasmas." *Journal of Polymer Science: Polymer Chemistry Edition* 23.4 (1985), pp. 1125–1135.

[37] Joanna Izdebska and Sabu Thomas. *Printing on polymers: Fundamentals and applications / Joanna Izdebska, Sabu Thomas*. Norwich: William Andrew, 2015.

[38] Sheng Shing Li et al. "Wettable polyolefin fibers and fabrics." US2002169429 (A1). 2002.

[39] Ronald S. Nohr and J. Gavin Macdonald. "Method of forming a nonwoven web from a surface-segregatable thermoplastic composition." US4857251 (A). 1989.

[40] Wayne K. Dunshee et al. "Hydrophilic polypropylene fibers having antimicrobial activity." CA2369088 (A1). 2000.

[41] Lawrence H. Sawyer and George W. Knight. "Wettable olefin polymer fibers." US4578414 (A). 1986.

[42] Torsten Lindner et al. "Thermoplastic Polymeric Materials With Heat Activatable Compositions." US2018256773 (A1). 2018.

[43] Frank Goene et al. "Synthetic nonwoven wiping fabric." US2006068673 (A1). 2006.

[44] Manabu Kaneda, Koji Tanaka, and Yoshiharu Usui. "Hydrophilic nonwoven fabric." JP2004100084 (A). 2004.

[45] Steven Lee Barnholtz et al. "Fibrous elements and fibrous structures employing same." WO2011053956 (A1). 2011.

[46] Prashant S. Kulkarni, Shagufta U. Patel, and George G. Chase. "Layered hydrophilic/hydrophobic fiber media for water-in-oil coalescence." *Separation and Purification Technology* 85 (2012), pp. 157–164.

[47] Larry L. Kinn, Clement J. Haley, and Gregory N. Henning. "Laminated battery separator material." WO02068746 (A2). 2002.

[48] Larry L. Kinn et al. "Durable hydrophilic nonwoven mat for rechargable alkaline batteries." WO0041254 (A1). 2000.

[49] Timothy Michael Kneale. "Improved Anfifog Composition for Polyolefin Packaging Films." CA2281662 (A1). 1998.

[50] J. Karger-Kocsis. *Polypropylene: Structure, blends and composites. Vol.1, Structure and morphology / edited by J. Karger-Kocsis*. London: Chapman & Hall, 1995.

[51] Robert L. Miller. "On the existence of near-range order in isotactic polypropylenes." *Polymer* 1 (1960), pp. 135–143.

[52] V. Caldas et al. "The structure of the mesomorphic phase of quenched isotactic polypropylene." *Polymer* 35.5 (1994), pp. 899–907.

[53] Takashi Konishi, Koji Nishida, and Toshiji Kanaya. "Crystallization of Isotactic Polypropylene from Prequenched Mesomorphic Phase." *Macromolecules* 39.23 (2006), pp. 8035–8040.

[54] G. Natta and P. Corradini. "Structure and properties of isotactic polypropylene." *Il Nuovo Cimento* 15.S1 (1960), pp. 40–51.

[55] P. Corradini et al. "On the structure of the quenched mesomorphic phase of isotactic polypropylene." *Macromolecules* 19.11 (1986), pp. 2699–2703.

[56] Felice de Santis et al. "Isothermal Nanocalorimetry of Isotactic Polypropylene." *Macromolecules* 40.25 (2007), pp. 9026–9031.

[57] Antonino Martorana, Stefano Piccarolo, and Francesco Scichilone. "The X-ray determination of the amounts of the phases in samples of isotactic poly(propylene) quenched from the melt at different cooling rates." *Macromolecular Chemistry and Physics* 198.2 (1997), pp. 597–604.

[58] Sara A. Arvidson, Saad A. Khan, and Russell E. Gorga. "Mesomorphic–α-Monoclinic Phase Transition in Isotactic Polypropylene: A Study of Processing Effects on Structure and Mechanical Properties." *Macromolecules* 43.6 (2010), pp. 2916–2924.

[59] Junchai Zhao et al. "In situ FT-IR spectroscopy study on the conformational changes of quenched isotactic polypropylene during stepwise heating." *Polymer Bulletin* 67.8 (2011), pp. 1649–1659.

[60] J. A. Gailey and R. H. Ralston. "The quenched state of polypropylene." *Polymer Engineering & Science* 4.1 (1964), pp. 29–33.

[61] Jan Broda. "Polymorphism in polypropylene fibers." *Journal of Applied Polymer Science* 89.12 (2003), pp. 3364–3370.

[62] F. L. Binsbergen and B.G.M. de Lange. "Morphology of polypropylene crystallized from the melt." *Polymer* 9 (1968), pp. 23–40.

[63] D. C. Bassett and R. H. Olley. "On the lamellar morphology of isotactic polypropylene spherulites." *Polymer* 25.7 (1984), pp. 935–943.

[64] Koh-hei Nitta and Kazunari Odaka. "Influence of structural organization on tensile properties in mesomorphic isotactic polypropylene." *Polymer* 50.16 (2009), pp. 4080–4088.

[65] Daniela Mileva et al. "Temperature of Melting of the Mesophase of Isotactic Polypropylene." *Macromolecules* 42.19 (2009), pp. 7275–7278.

[66] Junchai Zhao et al. "Phase transitions in prequenched mesomorphic isotactic polypropylene during heating and annealing processes as revealed by simultaneous synchrotron SAXS and WAXD technique." *The journal of physical chemistry. B* 116.1 (2012), pp. 147–153.

[67] Zhi-Gang Wang et al. "Phase transformation in quenched mesomorphic isotactic polypropylene." *Polymer* 42.18 (2001), pp. 7561–7566.

[68] Carla Marega, Valerio Causin, and Antonio Marigo. "A SAXS–WAXD study on the mesomorphic-α transition of isotactic polypropylene." *Journal of Applied Polymer Science* 109.1 (2008), pp. 32–37.

[69] Frank Welle. "Activation energies of diffusion of organic migrants in cyclo olefin polymer." *International journal of pharmaceutics* 473.1-2 (2014), pp. 510–517.

[70] S. J. Ebbens and J. P. S. Badyal. "Surface Enrichment of Fluorochemical-Doped Polypropylene Films." *Langmuir* 17.13 (2001), pp. 4050–4055.

[71] José A. Garde et al. "Characterizing the migration of antioxidants from polypropylene into fatty food simulants." *Food Additives and Contaminants* 18.8 (2001), pp. 750–762.

[72] Makoto Wakabayashi et al. "New bleeding model of additives in a polypropylene film under atmospheric pressure." *Journal of Applied Polymer Science* 104.6 (2007), pp. 3751–3757.

[73] David E. Bergbreiter and B. Srinivas. "Surface selectivity in blending polyethylene-poly(ethylene glycol) block cooligomers into high-density polyethylene." *Macromolecules* 25.2 (1992), pp. 636–643.

[74] Hojun Lee and Lynden A. Archer. "Functionalizing Polymer Surfaces by Field-Induced Migration of Copolymer Additives. 1. Role of Surface Energy Gradients." *Macromolecules* 34.13 (2001), pp. 4572–4579.

[75] Hanjia J. Chen et al. "Surface enrichment of polypropylene-graft-poly (methyl methacrylate) on polypropylene." *Journal of Polymer Research* 14.6 (2007), pp. 489–496.

[76] N. E. Schlotter and P. Y. Furlan. "A review of small molecule diffusion in polyolefins." *Polymer* 33.16 (1992), pp. 3323–3342.

[77] P. N. Lowell and N. G. McCrum. "Diffusion mechanisms in solid and molten polyethylene." *Journal of Polymer Science Part A-2: Polymer Physics* 9.11 (1971), pp. 1935–1954.

[78] D. W. van Krevelen and K. te Nijenhuis. *Properties of polymers: Their correlation with chemical structure ; their numerical estimation and prediction from additive group contributions / D.W. van Krevelen*. 4th, completely rev. ed. / rev. by K. te Nijenhuis. Amsterdam and Boston: Elsevier, 2009.

[79] Z. Maghsoud, M. Rafiei, and M.H.N. Famili. "Effect of processing method on migration of antioxidant from HDPE packaging into a fatty food simulant in terms of crystallinity." *Packaging Technology and Science* 31.3 (2018), pp. 141–149.

[80] Jonas Alin and Minna Hakkarainen. "Type of polypropylene material significantly influences the migration of antioxidants from polymer packaging to food simulants during microwave heating." *Journal of Applied Polymer Science* 211 (2010), pp. 1084–1093.

[81] R. K. Eby. "Diffusion in a Polymer With Lamellar Morphology, Polyethylene." *Journal of Applied Physics* 35.9 (1964), pp. 2720–2724.

[82] J. Y. Moisan. "Diffusion des additifs du polyethylene—III." *European Polymer Journal* 16.10 (1980), pp. 997–1002.

[83] M. Saleem et al. "Diffusion of organic penetrants through low density polyethylene (LDPE) films: Effect of size and shape of the penetrant molecules." *Journal of Applied Polymer Science* 37.3 (1989), pp. 617–625.

[84] Abdul-Fattah A. Asfour et al. "Diffusion of saturated hydrocarbons in low density polyethylene (LDPE) films." *Journal of Applied Polymer Science* 38.8 (1989), pp. 1503–1514.

[85] Enikö Földes and Andrea Szigeti-Erdei. "Migration of additives in polymers." *Journal of Vinyl and Additive Technology* 3.3 (1997), pp. 220–224.

[86] Cosme Llop et al. "Control of the migration behavior of slip agents in polyolefin-based films." *Polymer Engineering & Science* 51.9 (2011), pp. 1763–1769.

[87] Jones et al. "Surface enrichment in an isotopic polymer blend." *Physical review letters* 62.3 (1989), pp. 280–283.

[88] Qamardeep S. Bhatia, David H. Pan, and Jeffrey T. Koberstein. "Preferential surface adsorption in miscible blends of polystyrene and poly(vinyl methyl ether)." *Macromolecules* 21.7 (1988), pp. 2166–2175.

[89] D.H.-K. Pan and W. M. Prest. "Surfaces of polymer blends: X-ray photoelectron spectroscopy studies of polystyrene/poly(vinyl methyl ether) blends." *Journal of Applied Physics* 58.8 (1985), pp. 2861–2870.

[90] C. J. Jalbert et al. "Surface Depletion of End Groups in Amine-Terminated Poly (dimethylsiloxane)." *Macromolecules* 27.9 (1994), pp. 2409–2413.

[91] S. Affrossman et al. "Surface concentration of chain ends in polystyrene determined by static secondary ion mass spectroscopy." *Macromolecules* 26.23 (1993), pp. 6251–6254.

[92] Keiji Tanaka, Atsushi Takahara, and Tisato Kajiyama. "Surface Molecular Aggregation Structure and Surface Molecular Motions of High-Molecular-Weight Polystyrene / Low-Molecular-Weight Poly (methyl methacrylate) Blend Films." *Macromolecules* 31.3 (1998), pp. 863–869.

[93] Hojun Lee and Lynden A. Archer. "Functionalizing polymer surfaces by surface migration of copolymer additives: Role of additive molecular weight." *Polymer* 43.9 (2002), pp. 2721–2728.

[94] Richard M. Jendrejack et al. "Shear-induced migration in flowing polymer solutions: simulation of long-chain DNA in microchannels corrected." *The Journal of Chemical Physics* 120.5 (2004), pp. 2513–2529.

[95] Ahmad Rezaei Kolahchi, Abdellah Ajji, and Pierre J. Carreau. "Enhancing hydrophilicity of polyethylene terephthalate surface through melt blending." *Polymer Engineering & Science* 55.2 (2015), pp. 349–358.

[96] Jozef Bicerano. *Prediction of Polymer Properties*. Vol. 20024638. CRC Press, 2002.

[97] Yoshihisa Kano, Saburo Akiyama, and Tomoyuki Kasemura. "Surface segregation and miscibility in blends of poly(vinylidene fluoride-co-hexafluoro-acetone) with poly(butyl acrylate)." *Journal of Adhesion Science and Technology* 11.3 (1997), pp. 407–418.

[98] M. Wakabayashi et al. "Study on the Bleeding Mechanism of Slip Agents in a Polypropylene Film using Molecular Dynamics." *International Polymer Processing* 24.2 (2009), pp. 133–139.

[99] Michael B. Clark, Cindy A. Burkhardt, and Joseph A. Gardella. "Surface studies of polymer blends. 3. An ESCA, IR and DSC study of poly (epsilon-caprolactone) / poly(vinyl chloride) homopolymer blends." *Macromolecules* 22.12 (1989), pp. 4495–4501.

[100] Menno A. van Dijk and André Wakker. *Concepts of polymer thermodynamics*. Vol. v.2. Polymer thermodynamics library. Lancaster, Pa.: Technomic Pub. Co. Inc, 1997.

[101] Glenn H. Fredrickson, Andrea J. Liu, and Frank S. Bates. "Entropic Corrections to the Flory-Huggins Theory of Polymer Blends: Architectural and Conformational Effects." *Macromolecules* 27.9 (1994), pp. 2503–2511.

[102] Thomas Lindvig, Michael L. Michelsen, and Georgios M. Kontogeorgis. "A Flory–Huggins model based on the Hansen solubility parameters." *Fluid Phase Equilibria* 203.1-2 (2002), pp. 247–260.

[103] H. Ronald Thomas and James J. O'Malley. "Surface studies on multicomponent polymer systems by x-ray photoelectron spectroscopy: polystyrene/poly(ethylene oxide) homopolymer blends." *Macromolecules* 14.5 (1981), pp. 1316–1320.

[104] T. H. Begley et al. "Diffusion behaviour of additives in polypropylene in correlation with polymer properties." *Food additives & contaminants. Part A, Chemistry, analysis, control, exposure & risk assessment* 25.11 (2008), pp. 1409–1415.

[105] Giuseppe Ferrara et al. "Diffusion coefficient and activation energy of Irganox 1010 in poly(propylene-co-ethylene) copolymers." *Polymer Degradation and Stability* 73.3 (2001), pp. 411–416.

[106] Stanley F. Tead and Edward J. Kramer. "Polymer diffusion in melt blends of low and high molecular weight." *Macromolecules* 21.5 (1988), pp. 1513–1517.

[107] Markus Antonietti, Jochen Coutandin, and Hans Sillescu. "Diffusion of linear polystyrene molecules in matrixes of different molecular weights." *Macromolecules* 19.3 (1986), pp. 793–798.

[108] G. T. Fieldson and T. A. Barbari. "The use of FTi.r.-a.t.r. spectroscopy to characterize penetrant diffusion in polymers." *Polymer* 34.6 (1993), pp. 1146–1153.

[109] Wenji Guo et al. "In Situ Monitoring the Molecular Diffusion Process in Graphene Oxide Membranes by ATR-FTIR Spectroscopy." *The Journal of Physical Chemistry C* 120.13 (2016), pp. 7451–7456.

[110] F. A. Long and David Richman. "Concentration Gradients for Diffusion of Vapors in Glassy Polymers and their Relation to Time Dependent Diffusion Phenomena 1,2." *Journal of the American Chemical Society* 82.3 (1960), pp. 513–519.

[111] Nabeen Dulal et al. "Slip-additive migration, surface morphology, and performance on injection moulded high-density polyethylene closures." *Journal of colloid and interface science* 505 (2017), pp. 537–545.

[112] N. Dulal et al. "Migration and performance of erucamide slip additive in high-density polyethylene bottle caps." *Journal of Applied Polymer Science* 135.43 (2018), p. 46822.

[113] I. Quijada-Garrido et al. "Solubility of erucamide (13-cis docosenamide) in isotactic poly(propylene) and thermal behaviour of their blends." *Polymer* 38.20 (1997), pp. 5125–5135.

[114] I. Quijada-Garrido et al. "Desorption of Erucamide Vapor in Vacuum from Erucamide/Isotactic Polypropylene Films 1." *Macromolecules* 29.27 (1996), pp. 8791–8797.

[115] I. Quijada-Garrido, J. M. Barrales-Rienda, and G. Frutos. "Diffusion of Erucamide (13- cis -Docosenamide) in Isotactic Polypropylene." *Macromolecules* 29.22 (1996), pp. 7164–7176.

[116] Maria X. Ramirez, Keisha B. Walters, and Douglas E. Hirt. "Relationship between erucamide surface concentration and coefficient of friction of LLDPE film." *Journal of Vinyl and Additive Technology* 11.1 (2005), pp. 9–12.

[117] Shilpa Y. Sankhe, Amol V. Janorkar, and Douglas E. Hirt. "Characterization of Erucamide Profiles in LLDPE Films: Depth-Profiling Attempts Using FTIR Photoacoustic Spectroscopy and Raman Microspectroscopy." *Journal of Plastic Film & Sheeting* 19.1 (2003), pp. 16–29.

[118] Amy S. Rawls et al. "Evaluation of surface concentration of erucamide in LLDPE films." *Journal of Vinyl and Additive Technology* 8.2 (2002), pp. 130–138.

[119] Shilpa Y. Sankhe and Douglas E. Hirt. "Characterization of Erucamide Profiles in Multilayer Linear Low-Density Polyethylene and Propylene-Ethylene Copolymer Films Using Synchrotron-Based FT-IR Microspectroscopy." *Applied Spectroscopy* 56.2 (2002), pp. 205–211.

[120] Kanishka Bhunia et al. "Migration of Chemical Compounds from Packaging Polymers during Microwave, Conventional Heat Treatment, and Storage." *Comprehensive Reviews in Food Science and Food Safety* 12.5 (2013), pp. 523–545.

[121] Maria F. Poças et al. "A critical survey of predictive mathematical models for migration from packaging." *Critical reviews in food science and nutrition* 48.10 (2008), pp. 913–928.

[122] Anna Zheng et al. "Antistatic modification of polypropylene by incorporating Tween/modified Tween." *Applied Surface Science* 258.22 (2012), pp. 8861–8866.

[123] Torsten Lindner et al. "Absorbent Article With Activatable Material." EP3426214A1. 2017.

[124] Hanjia Chen et al. "Surface modification of polypropylene. I. Surface enrichment of poly(ethylene glycol) on polypropylene/poly(ethylene glycol) blends." *Journal of Vinyl and Additive Technology* 14.1 (2008), pp. 28–33.

[125] Franz Fourné. *Synthetic Fibers*. München: Carl Hanser Verlag GmbH & Co. KG, 1999.

[126] A. Weidinger and P. H. Hermans. "On the determination of the crystalline fraction of isotactic polypropylene from x-ray diffraction." Vol. 50, pp. 98–115.

[127] M. van Drongelen, T. B. van Erp, and G.W.M. Peters. "Quantification of non-isothermal, multi-phase crystallization of isotactic polypropylene: The influence of cooling rate and pressure." *Polymer* 53.21 (2012), pp. 4758–4769.

[128] V. La Carrubba, S. Piccarolo, and V. Brucato. "Crystallization kinetics of iPP: Influence of operating conditions and molecular parameters." *Journal of Applied Polymer Science* 104.2 (2007), pp. 1358–1367.

[129] Franz J. Lanyi et al. "A method to reveal bulk and surface crystallinity of Polypropylene by FTIR spectroscopy - Suitable for fibers and nonwovens." *Polymer Testing* 71 (2018), pp. 49–55.

[130] Franz J. Lanyi et al. "On the Determination of the Enthalpy of Fusion of α-Crystalline Isotactic Polypropylene Using Differential Scanning Calorimetry, X-Ray Diffraction, and Fourier-Transform Infrared Spectroscopy: An Old Story Revisited." *Advanced Engineering Materials* 31 (2019), p. 1900796.

[131] Annamaria Fichera and Roberto Zannetti. "Thermal properties of isotactic polypropylene quenched from the melt and annealed." *Die Makromolekulare Chemie* 176.6 (1975), pp. 1885–1892.

[132] Jiaxing Chen and Joseph A. Gardella. "Quantitative ATR FT-IR Analysis of Surface Segregation of Polymer Blends of Polystyrene/Poly(Dimethylsiloxane)-co-polystyrene." *Applied spectroscopy* 52.3 (1998), pp. 361–366.

[133] David R. Burfield and Patrick S. T. Loi. "The use of infrared spectroscopy for determination of polypropylene stereoregularity." *Journal of Applied Polymer Science* 36.2 (1988), pp. 279–293.

[134] Trinh An Huy et al. "Molecular deformation mechanisms of isotactic polypropylene in α- and β-crystal forms by FTIR spectroscopy." *Journal of Polymer Science Part B: Polymer Physics* 42.24 (2004), pp. 4478–4488.

[135] Ali Kilic et al. "Surface crystallinity of meltspun isotactic polypropylene filaments." *Macromolecular Research* 24.1 (2016), pp. 25–30.

[136] R. G. Quynn et al. "Density, crystallinity, and heptane insolubility in isotactic polypropylene." *Journal of Applied Polymer Science* 2.5 (1959), pp. 166–173.

[137] Hiroyuki Tadokoro et al. "Normal Vibrations of the Polymer Molecules of Helical Conformation. V. Isotactic Polypropylene and Its Deuteroderivatives." *The Journal of Chemical Physics* 42.4 (1965), pp. 1432–1449.

[138] Peter Böckh and Thomas Wetzel. *Wärmeübertragung: Grundlagen und Praxis*. 5., überarb. und erw. Aufl. 2014. Berlin, Heidelberg: Springer Berlin Heidelberg, Imprint, and Springer Vieweg, 2014.

[139] W. Heinen. "Infrared determination of the crystallinity of polypropylene." *Journal of Polymer Science* 38.134 (1959), pp. 545–547.

[140] Lei Li et al. "Effect of compressed CO2 on the melting behavior and βα-recrystallization of β-form in isotactic polypropylene." *The Journal of Supercritical Fluids* 60 (2011), pp. 137–143.

[141] M. Aboulfaraj et al. "Spherulitic morphology of isotactic polypropylene investigated by scanning electron microscopy." *Polymer* 34.23 (1993), pp. 4817–4825.

[142] Md. Arifur Rahman, Mubarak A. Khan, and Shafi M. Tareq. "Preparation and characterization of polyethylene oxide (PEO)/gelatin blend for biomedical application: Effect of gamma radiation." *Journal of Applied Polymer Science* 117.4 (2010), pp. 2075–2082.

[143] Zhi Chen et al. "Preparation and thermal properties of n-octadecane / molecular sieve composites as form-stable thermal energy storage materials for buildings." *Energy and Buildings* 49 (2012), pp. 423–428.

[144] D. J. Greenhalgh et al. "Solubility parameters as predictors of miscibility in solid dispersions." *Journal of pharmaceutical sciences* 88.11 (1999), pp. 1182–1190.

[145] Paul J. Flory. "Thermodynamics of High Polymer Solutions." *The Journal of Chemical Physics* 9.8 (1941), p. 660.

[146] Charles M. Hansen. "Polymer additives and solubility parameters." *Progress in Organic Coatings* 51.2 (2004), pp. 109–112.

[147] Peter B. Rim and James P. Runt. "Melting point depression in crystalline/compatible polymer blends." *Macromolecules* 17.8 (1984), pp. 1520–1526.

[148] T. Nishi and T. T. Wang. "Melting Point Depression and Kinetic Effects of Cooling on Crystallization in Poly(vinylidene fluoride)-Poly(methyl methacrylate) Mixtures." *Macromolecules* 8.6 (1975), pp. 909–915.

[149] Lubomir Simek, Jiri Dostal, and Miloslav Bohdanecky. "Morphological factor in the melting point depression of polypropylene by alkanes." *Polymer* 42.21 (2001), pp. 8897–8900.

[150] E. G. Lezcano, C. Salom Coll, and M. G. Prolongo. "Melting behaviour and miscibility of poly(epsilon-caprolactone) + poly(4-hydroxystyrene) blends." *Polymer* 37.16 (1996), pp. 3603–3609.

[151] Fang Chen and Michael P. Wolcott. "Miscibility studies of paraffin / polyethylene blends as form-stable phase change materials." *European Polymer Journal* 52 (2014), pp. 44–52.

[152] G. Defieuw, G. Groeninckx, and H. Reynaers. "Miscibility, crystallization and melting behaviour, and morphology of binary blends of polycaprolactone with styrene-co-maleic anhydride copolymers." *Polymer* 30.12 (1989), pp. 2158–2163.

[153] Vishal Bansal and Robert L. Shambaugh. "On-Line determination of density and crystallinity during melt spinning." *Polymer Engineering & Science* 36.22 (1996), pp. 2785–2798.

[154] Cao Jinan et al. "Nonisothermal orientation-induced crystallization in melt spinning of polypropylene." *Journal of Applied Polymer Science* 37.9 (1989), pp. 2683–2697.

[155] Rakesh K. Gupta and Kim F. Auyeung. "Crystallization in polymer melt spinning." *Journal of Applied Polymer Science* 34.7 (1987), pp. 2469–2484.

[156] P. Y.-F. Fung and S. H. Carr. "Morphology and deformation of melt-spun polyethylene fibers." *Journal of Macromolecular Science, Part B* 6.4 (1972), pp. 621–633.

[157] Joni Hautojärvi and Antti Leijala. "A morphological study of melt-spun polypropylene filaments by atomic force microscopy." *Journal of Applied Polymer Science* 74.5 (1999), pp. 1242–1249.

[158] J. R. Dees and J. E. Spruiell. "Structure development during melt spinning of linear polyethylene fibers." *Journal of Applied Polymer Science* 18.4 (1974), pp. 1053–1078.

[159] Qixiong Zhou et al. "Shish–kebab-like cylindrulite structures resulted from periodical shear-induced crystallization of isotactic polypropylene." *Polymer* 52.13 (2011), pp. 2970–2978.

[160] Peng-wei Zhu and Graham Edward. "Distribution of Shish-Kebab Structure of Isotactic Polypropylene under Shear in the Presence of Nucleating Agent." *Macromolecules* 37.7 (2004), pp. 2658–2660.

[161] Hari P. Nadella et al. "Melt spinning of isotactic polypropylene: Structure development and relationship to mechanical properties." *Journal of Applied Polymer Science* 21.11 (1977), pp. 3003–3022.

[162] Hari P. Nadella, Joseph E. Spruiell, and James L. White. "Drawing and annealing of polypropylene fibers: Structural changes and mechanical properties." *Journal of Applied Polymer Science* 22.11 (1978), pp. 3121–3133.

[163] V. B. Gupta, P. N. Khanna, and T. H. Somashekar. "Orientation-dependence of the Young's modulus of high-density polyethylene filaments." *Colloid and Polymer Science* 252.4 (1974), pp. 288–293.

[164] Hilmar Fuchs and W. Albrecht. *Vliesstoffe: Rohstoffe, Herstellung, Anwendung, Eigenschaften, Prüfung / herausgegeben von Hilmar Fuchs und Wilhelm Albrecht*. 2., vollständig überarbeitete Aufl. Weinheim: Wiley-VCH, 2012.

[165] Karsten Leucker. "Influence of the calender pattern on the mechanical properties of polypropylene spunbond nonwovens." Dissertation. Friedrich-Alexander-Universität Erlangen-Nürnberg, 2020.

[166] Jie Qiu et al. "Deformation-induced highly oriented and stable mesomorphic phase in quenched isotactic polypropylene." *Polymer* 48.23 (2007), pp. 6934–6947.

[167] Joni Hautojärvi and Heidi Niemi. "Surface Morphologies of Polypropylene Fibers Studied by Atomic Force Microscopy." *Textile Research Journal* 70.9 (2000), pp. 820–827.

[168] Milton J. Rosen and Joy T. Kunjappu. *Surfactants and interfacial phenomena*. 4th ed. Hoboken N.J.: Wiley, 2012.

[169] Nitin Kumar, Stephen Garoff, and Robert D. Tilton. "Experimental Observations on the Scaling of Adsorption Isotherms for Nonionic Surfactants at a Hydrophobic Solid–Water Interface." *Langmuir* 20.11 (2004), pp. 4446–4451.

[170] Rudolf Beck. "Benetzende Wirkung von Tensidlösungen an harten Oberflächen." *Seifen Öle Fette Wachse* 108 (1982), pp. 496–501.

[171] J. M. Corkill, J. F. Goodman, and J. R. Tate. "Adsorption of non-ionic surface-active agents at the Graphon/solution interface." *Transactions of the Faraday Society* 62 (1966), p. 979.

[172] R. H. Ottewill and T. Walker. "The influence of non-ionic surface active agents on the stability of polystyrene latex dispersions." *Kolloid-Zeitschrift & Zeitschrift für Polymere* 227.1-2 (1968), pp. 108–116.

[173] J. M. Corkill, J. F. Goodman, and J. R. Tate. "Adsorption of alkylsulphinylalkanols on Graphon." *Transactions of the Faraday Society* 63 (1967), p. 2264.

[174] Lachlan M. Grant, Thomas Ederth, and Fredrik Tiberg. "Influence of Surface Hydrophobicity on the Layer Properties of Adsorbed Nonionic Surfactants." *Langmuir* 16.5 (2000), pp. 2285–2291.

[175] Thilo Bauer et al. "Phosphonate- and carboxylate-based self-assembled monolayers for organic devices: a theoretical study of surface binding on aluminum oxide with experimental support." *ACS applied materials & interfaces* 5.13 (2013), pp. 6073–6080.

[176] Linda Rockmann. "Einfluss der Molekulararchitektur von Tensiden auf die Beschichtungs- und Benetzungseigenschaften verschiedener mittels Spincoating beschichteter Substrate." Bachelor thesis. Friedrich-Alexander-Universität Erlangen-Nürnberg, 2018.

[177] Enikő Földes. "Study of the effects influencing additive migration in polymers." *Die Angewandte Makromolekulare Chemie* 261-262.1 (1998), pp. 65–76.

[178] Khushdeep Sharma. "Influence of polymer morphology and crystallinity on the migration behaviour of additives in polypropylene produced via fibre spinning, injection moulding and cast film extrusion." Master thesis. Friedrich-Alexander-Universität Erlangen-Nürnberg, 2018.

[179] Shohei Horike et al. "Thermodynamics and kinetics of polyoxyethylene alkyl ether evaporation from inkjet-printed carbon nanotube thin films by vacuum annealing." *Flexible and Printed Electronics* 3.2 (2018), p. 025006.

[180] Annika Kleebauer. "Einfluss von Temperatur und der molekularen Architektur von Additiven auf das Migrationsverhalten in spritzgegossenene Polypropylenplatten." Bachelor thesis. Friedrich-Alexander-Universität Erlangen-Nürnberg, 2018.

[181] Kenneth Möller and Thomas Gevert. "An FTIR solid-state analysis of the diffusion of hindered phenols in low-density polyethylene (LDPE): The effect of molecular size on the diffusion coefficient." *Journal of Applied Polymer Science* 51.5 (1994), pp. 895–903.

[182] J. Y. Moisan. "Diffusion des additifs du polyethylene—IV." *European Polymer Journal* 17.8 (1981), pp. 857–864.

[183] M. Dubini et al. "Diffusion of thiodipropionic esters and hydroxybenzophenones in isotactic polypropylene." *European Polymer Journal* 3.3 (1967), pp. 473–479.

[184] J. Koszinowski. "Diffusion and solubility of n -alkanes in polyolefines." *Journal of Applied Polymer Science* 32.5 (1986), pp. 4765–4786.

[185] Stefan Hiemer. "Evaluation of the Migration Behaviour of Surfactants in Polypropylene with Molecular Dynamics Simulation." Masterarbeit. Erlangen: Friedrich-Alexander-Universität Erlangen-Nürnberg, 5.2019.

[186] Peter F. Green and Edward J. Kramer. "Matrix effects on the diffusion of long polymer chains." *Macromolecules* 19.4 (1986), pp. 1108–1114.

[187] J. Klein. "Effect of matrix molecular weight on diffusion of a labeled molecule in a polymer melt." *Macromolecules* 14.2 (1981), pp. 460–461.

[188] Julian Kattinger. "Einfluss der Molmasse und ausgewählter Prozessparameter auf das Migrationsverhalten von Additiven in schmelzgesponnenen Polypropylenfasern." Master thesis. Friedrich-Alexander-Universität Erlangen-Nürnberg, 2018.

[189] A. Nogales et al. "Shear-induced crystallization of isotactic polypropylene with different molecular weight distributions: In situ small- and wide-angle X-ray scattering studies." *Polymer* 42.12 (2001), pp. 5247–5256.

[190] C. Duplay. "Shear-induced crystallization of polypropylene: Influence of molecular weight." *Journal of Materials Science* 35.24 (2000), pp. 6093–6103.

[191] Milliken. *Millad NX10 Concentrate*.

[192] J. M. G. Cowie, B. G. Devlin, and I. J. McEwen. "Surface enrichment in polystyrene/poly(vinyl methyl ether) blends. 3. An analysis of the near-surface composition profile." *Macromolecules* 26.21 (1993), pp. 5628–5632.

[193] Eugene Kim et al. "Surface segregation in blends of styrene-acrylonitrile copolymers." *Polymer* 36.12 (1995), pp. 2427–2433.

[194] Human & Environmental Risk Assessment. *Alcohol Ethoxylates*. 2009.

[195] I. Cooper and P. A. Tice. "Migration studies on fatty acid amide slip additives from plastics into food simulants." *Food additives and contaminants* 12.2 (1995), pp. 235–244.

[196] J. Comyn, ed. *Polymer Permeability*. Dordrecht: Springer Netherlands, 1985.

[197] Paul J. Flory. "Thermodynamics of Crystallization in High Polymers. IV. A Theory of Crystalline States and Fusion in Polymers, Copolymers, and Their Mixtures with Diluents." *The Journal of Chemical Physics* 17.3 (1949), pp. 223–240.

Melt additives are low molar mass molecules which are added to polymers during processing. If the molecules migrate to the surface, the properties of the polymer surface can be tailored. Therefore, melt additives offer an easy to implement method to hydrophilize hydrophobic polymers, such as polypropylene. For reproducible product quality, it is necessary to control and understand the complex migration process, influenced by diffusion, surface segregation, miscibility or polymer morphology.

Various commercially available surfactants (ethoxylated alcohols, PEO-PPO block copolymers, sorbitan esters) are investigated to determine which requirements have to be met by molecules to be utilized as hydrophilic melt additives. In order to correlate polymer morphology and additive migration, a method was developed which determines the degree of crystallinity and the additive concentration at the surface and in the bulk of samples using Fourier-transform infrared spectroscopy (FTIR).

It is demonstrated, that the hydrophilization of the surface is a function of the additive surface concentration and the ability of the additive to enable wetting. Ethoxylated alcohols with a low molar mass, a long hydrophobic and a short hydrophilic part of the surfactant impart the highest hydrophilicity. Novel models for structure formation during injection molding, film casting and fiber spinning are developed using a combination of X-ray diffraction (XRD) and FTIR. The migration of additives with varying molecular architectures was determined over a period of 1000 hours and described using a semiempirical migration equation. Coefficients characterizing the kinetics and thermodynamics of migration are described as a function of the most relevant process parameters and the associated change in polymer morphology.

The experiments revealed that migration depends on the packing density of polymer chains given by molecular orientation and (post-)crystallization of the polymer. Besides polymer morphology, the miscibility and molecular dimensions of the additive as well as the storage conditions after production (time and temperature) affect migration. Within the scope of the work, permanent and durable melt additives for polypropylene as well as methods for the selective activation of hydrophilicity were found.

ISBN 978-3-96147-360-1

9 783961 473601

FAU UNIVERSITY PRESS 2020